

July 2019

# FINITE ELEMENT SIMULATION OF BONDED AND MECHANICALLY ANCHORED SHEAR INTERFACES OF EXTERNALLY APPLIED FRP SHEETS TO CONCRETE AND WOOD-CONCRETE COMPOSITES

Alaa Al-Sammari

Follow this and additional works at: [https://scholarworks.umass.edu/dissertations\\_2](https://scholarworks.umass.edu/dissertations_2)



Part of the [Civil Engineering Commons](#), [Engineering Mechanics Commons](#), [Mechanics of Materials Commons](#), [Structural Engineering Commons](#), and the [Structural Materials Commons](#)

---

## Recommended Citation

Al-Sammari, Alaa, "FINITE ELEMENT SIMULATION OF BONDED AND MECHANICALLY ANCHORED SHEAR INTERFACES OF EXTERNALLY APPLIED FRP SHEETS TO CONCRETE AND WOOD-CONCRETE COMPOSITES" (2019). *Doctoral Dissertations*. 1620.  
<https://doi.org/10.7275/3c40-gj78> [https://scholarworks.umass.edu/dissertations\\_2/1620](https://scholarworks.umass.edu/dissertations_2/1620)

This Open Access Dissertation is brought to you for free and open access by the Dissertations and Theses at ScholarWorks@UMass Amherst. It has been accepted for inclusion in Doctoral Dissertations by an authorized administrator of ScholarWorks@UMass Amherst. For more information, please contact [scholarworks@library.umass.edu](mailto:scholarworks@library.umass.edu).

**FINITE ELEMENT SIMULATION OF BONDED AND MECHANICALLY  
ANCHORED SHEAR INTERFACES OF EXTERNALLY APPLIED FRP  
SHEETS TO CONCRETE AND WOOD-CONCRETE COMPOSITES**

A Dissertation Presented

by

ALAA TAWFIQ AHMED AL-SAMMARI

Submitted to the Graduate School of the  
University of Massachusetts Amherst in partial fulfillment  
of the requirements for the degree of

DOCTOR OF PHILOSOPHY

May 2019

Civil and Environmental Engineering

© Copyright by Alaa Tawfiq Ahmed Al-Sammari 2019

All Rights Reserved

**FINITE ELEMENT SIMULATION OF BONDED AND MECHANICALLY  
ANCHORED SHEAR INTERFACES OF EXTERNALLY APPLIED FRP  
SHEETS TO CONCRETE AND WOOD-CONCRETE COMPOSITES**

A Dissertation Presented

by

ALAA TAWFIQ AHMED AL-SAMMARI

Approved as to style and content by:

---

Sergio F. Breña, Chair

---

Alan J. Lesser, Member

---

Peggi L. Clouston, Member

---

Simos Gerasimidis, Member

---

Richard N. Palmer, Department Head  
Civil and Environmental Engineering Department

## **DEDICATION**

*This dissertation is dedicated to my parents Tawfiq and Faten, my mother in law Sajida, my wife Huda, my wonderful children Dalya and Hasan, my brothers Ahmed,*

*Ziad, and Waleed, and my sister Nadia.*

*To all of you, thank you for your support, encouragement, sacrifices, and helping me to achieve my dreams.*

*I am truly grateful for having all of you in my life.*

## **ACKNOWLEDGMENTS**

I would like to express my appreciation to all of those with whom I have had the pleasure to work during the stages of my doctoral dissertation.

I am extremely grateful to my advisor, Professor Dr. Sergio F. Brena from the Department of Civil and Environmental Engineering (Structural Engineering and Mechanics program), for his guidance, encouragement and support he has provided throughout this research work.

Special thanks should also be given to the members of my dissertation committee from the University of Massachusetts Amherst, Professor Dr. Alan J. Lesser from the Polymer Science and Engineering Department, Associate Professor Dr. Peggi L. Clouston from the Department of Environmental Conservation (Building and Construction Technology program), and Assistant Professor Dr. Simos Gerasimidis from the Department of Civil and Environmental Engineering (Structural Engineering and Mechanics program) for their guidance and recommendations.

I would like to thank my family for their unconditional love and encouragement. My parents, my mother in law, my wife, my children, my brothers, and my sister, I am grateful for your support and being my motive to overcome all life challenges.

Finally, I extend my sincere gratitude and acknowledgements to the Higher Committee for Education Development in Iraq (HCED) for their financial support and I wish my country all the best and development.

## **ABSTRACT**

### **FINITE ELEMENT SIMULATION OF BONDED AND MECHANICALLY ANCHORED SHEAR INTERFACES OF EXTERNALLY APPLIED FRP SHEETS TO CONCRETE AND WOOD-CONCRETE COMPOSITES**

MAY 2019

ALAA TAWFIQ AHMED AL-SAMMARI

B.S., UNIVERSITY OF TIKRIT

M.S., UNIVERSITY OF TIKRIT

Ph.D., UNIVERSITY OF MASSACHUSETTS AMHERST

Directed by: Professor Sergio F. Breña

Composite construction is prevalent in advanced structural systems where components of different materials are combined in the same structure to improve the performance of strong and economic structural sections. Maintaining continuity between the different structural components to produce monolithic structural behavior is challenging because of differences in the mechanical properties of these materials in terms of stiffness, strength, and ductility. The different components of the composite section are typically joined using adhesives and/or mechanical anchors to produce partial or full composite action. This dissertation discusses two types of shear interfaces intended to result in structural composite behavior. The first type of interface that is part of this dissertation focuses on bonded and mechanically anchored externally applied FRP sheets used in concrete structure for rehabilitation of concrete structures. The second type of connection is a new wood-concrete composite that includes a perforated steel connector bonded to engineered wood elements to transfer shear stresses to cast-in-place concrete.

Fiber reinforced polymer (FRP) materials have been confirmed as an excellent option for strengthening existing or even newly constructed concrete structures. However, FRP

sheets may debond before reaching a high level of FRP stress. This behavior adversely affects the efficiency of using FRP materials for strengthening concrete structures. FRP anchors have been added to the bonded joints to delay or avoid debonding and allow FRP sheets to reach their ultimate strength. Yet, the behavior of carbon fiber anchors is not well understood, particularly the effect of the dimensional and geometric properties of the anchors on the total strength of FRP-concrete joints. Therefore, the influence of key anchor parameters on joint behavior were examined in this research through analytical simulations. The parameters investigated were; the number of anchors used in the joint, the distance between anchors, anchor shaft depth, anchor shaft diameter, anchor splay angle, and anchor splay diameter. A general-purpose finite element software (ABAQUS) was used to study the behavior of the anchored FRP-concrete joints having different anchor configurations and geometries.

Different three-dimensional finite element models were used to describe the different components of the FRP-concrete joint. These different components were categorized based on the different materials, geometric shapes and functional roles of each part or component. Consequently, five different components were considered in the finite element models to represent the FRP-concrete joint. These components are the concrete substrate, the FRP sheet, the adhesive layer, the FRP anchor, and the adhesive envelopes around the anchors (for modeling the interface between concrete, FRP sheet, and the FRP anchors).

Based on this study, design recommendations for fiber reinforced polymer anchors were developed to determine the number of anchors, distance between anchors, anchor shaft depth, anchor shaft diameter, anchor splay angle, and anchor splay diameter



required to achieve a goal strength. The finite element analysis can be extended to model full-scale structural members strengthened with fiber-reinforced material under different loading conditions building on the findings from this research.

The second type of composite application included in this dissertation focuses on new structural deck systems that benefit from the use of wood as a lightweight, sustainable substructure and concrete as a wear-resistant, vibration damping top element. These systems employ metallic connectors to transfer shear stresses between the wood and the concrete leading to full or partial composite action for strength and stiffness benefits. Results of finite element analysis and a parametric investigation are presented for one type of connector similar to those available commercially: a perforated steel plate of which half is epoxied into a groove in the wood member while the other half is embedded in a concrete slab. The analysis was first validated against experimental push-out tests performed on a commercial product and then employed to examine the effect of several parameters of the connection: thickness of plate; insulation gap between concrete and wood; depth of embedment in concrete; and depth of embedment in wood. The results showed that thickness predictably affects shear capacity as well as ductility and stiffness (slip moduli) of the connector.

This dissertation highlights the importance of including parameters that affect the response of joints between dissimilar materials in order to properly capture their behavior through numerical models. The detailed parametric studies presented in this research can form the basis for development of design recommendations for these types of connections. Given the expense associated with laboratory experimentation, the tools used in this research provide an inexpensive complement to physical testing in the

development of robust and reliable equations that can be incorporated into design standards.

Keywords: fiber reinforced polymer sheets (FRP-sheets); fiber reinforced polymer anchors (FRP-anchors); FRP-concrete joints; anchor splay; strengthening of concrete structures; cohesive elements; debonding propagation; Shear connector; wood-concrete composite; timber-concrete; finite element analysis.

## TABLE OF CONTENTS

	Page
ACKNOWLEDGMENTS .....	v
ABSTRACT .....	vi
LIST OF TABLES .....	xiii
LIST OF FIGURES .....	xiv
CHAPTER	
1. INTRODUCTION .....	1
1.1 General .....	1
1.2 Externally FRP strengthened concrete in the literature .....	2
1.2.1 Bond-slip behavior in the literature .....	4
1.2.2 Anchored fiber-reinforced polymer sheets in the literature .....	16
1.3 Wood-concrete composites in the literature .....	21
2. FRP-CONCRETE SYSTEM: MATERIAL CONSTITUTIVE RELATIONSHIPS .....	26
2.1. Introduction .....	26
2.2. Parts and materials used .....	26
2.3. Modeling of concrete material .....	28
2.3.1 Tensile behavior of concrete .....	28
2.3.2 Compressive behavior of concrete .....	32
2.3.3 Damage variable for multiaxial stress condition .....	34
2.3.4 Crack formation and crack propagation .....	35
2.3.5 Stress invariants .....	36
2.3.6 The flow rule .....	36
2.3.7 Yield condition .....	37
2.4. Modeling of fiber-reinforced polymer material .....	40
2.4.1 Undamaged stage .....	40
2.4.2 Damage initiation stage .....	41
2.4.3 Damage evolution stage .....	43
2.5. Modeling of adhesive material .....	45
2.5.1 Linear elastic stage of adhesive material .....	45
2.5.2 Damage initiation stage of adhesive material .....	46
2.5.3 Damage evolution stage of cohesive material .....	46
3. FRP-CONCRETE SYSTEM: FINITE ELEMENT MODELING .....	49
3.1. Introduction .....	49
3.2. Finite element modeling of CFRP-concrete joints .....	49
3.2.1 Finite element modeling of the concrete .....	50
3.2.2 Finite element modeling of the CFRP sheet .....	50
3.2.3 Finite element modeling of the adhesive layer .....	51
3.2.4 Finite element modeling of the CFRP Anchor .....	54
3.2.5 Finite element modeling of the adhesive envelope around the anchor .....	55
3.3. Analysis procedure .....	56
4. FRP-CONCRETE SYSTEM: VERIFICATION OF THE PROPOSED MODEL .....	60

4.1 Calibration and verification process .....	60
4.2 CFRP-concrete joints without anchors .....	61
4.3 CFRP-concrete joints with anchors .....	81
4.4 Summary of the verification of the finite element model .....	93
4.4.1 Model verification using CFRP-concrete bond tests .....	93
4.4.2 Model verification using tests of FRP-anchored sheets.....	98
<b>5. FRP-CONCRETE SYSTEM: PARAMETRIC STUDY ON THE BEHAVIOR</b>	
<b>OF ANCHORED FRP SHEETS .....</b>	<b>101</b>
5.1 Introduction.....	101
5.2 Effect of the number of anchors.....	102
5.3 Effect of anchor longitudinal spacing .....	103
5.4 Effect of anchor length.....	104
5.5 Effect of anchor shaft diameter.....	108
5.6 Effect of anchor splay diameter .....	108
5.7 Effect of anchor splay angle .....	109
5.8 Effect of FRP sheet thickness .....	111
<b>6. DEVELOPMENT AND APPLICATION OF FRP ANCHORAGE</b>	
<b>EFFICIENCY FACTOR.....</b>	<b>113</b>
6.1 Introduction.....	113
6.2 FRP strain limits .....	117
6.3 Debonding strain of unanchored FRP sheets .....	119
6.4 Debonding strain of anchored FRP sheets .....	120
6.5 Proposed anchorage efficiency factor.....	122
6.6 Observations on the results of the FE model parametric analyses.....	123
6.7 Normalization of FE modeling results .....	131
6.8 Anchorage efficiency formula .....	135
6.9 Simplified Formula for Anchorage Strain Efficiency Factor .....	141
6.10 Application of anchorage efficiency factor to flexural strengthening	
of beams and slabs .....	145
6.11 Description of design procedure using anchorage efficiency factor.....	145
6.12 FRP strength estimator.....	149
<b>7. FINITE ELEMENT ANALYSIS AND PARAMETRIC STUDY OF</b>	
<b>PERFORATED STEEL PLATE SHEAR CONNECTORS FOR WOOD-</b>	
<b>CONCRETE COMPOSITES.....</b>	<b>156</b>
7.1 Introduction.....	156
7.2 Previous experimental work .....	158
7.3 Finite element modeling .....	159
7.3.1 Constitutive model for concrete.....	161
7.3.2 Constitutive model for wood .....	162
7.3.3 Constitutive model for steel.....	162
7.3.4 Constitutive model for adhesive .....	163
7.4 Finite element model validation.....	165
7.5 Parametric Study.....	168
7.5.1 Effect of embedment depth of steel connector .....	168
7.5.2 Effect of steel plate thickness .....	173
7.5.3 Effect of the gap between concrete and wood .....	175

8. CONCLUSIONS AND DESIGN RECOMMENDATIONS .....	177
8.1 Bonded and mechanically anchored externally applied FRP to concrete .....	177
8.2 Development of strain efficiency factor for anchored FRP sheets .....	178
8.3 Bonded and mechanically anchored wood-concrete composites.....	179
APPENDIX: SUPPLEMENTAL INFORMATION.....	181
REFERENCES .....	248

## LIST OF TABLES

Table	Page
Table 4.1: Given data of the experimental specimen tested by Mazzotti et al. 2008 .....	62
Table 4.2: Given data of the experimental specimen tested by Ueda et al. 1999. ....	65
Table 4.3: Values required to define materials of the model (base units = N, mm) .....	65
Table 4.4: Given data of the experimental specimen tested by Breña and McGuirk 2013.....	75
Table 4.5: Properties obtained from the specification of the manufacturer (FYFE Tyfo Fiberware Systems).....	76
Table 4.6: Values required to define materials of the model (base units = N, mm) .....	77
Table 4.7: Properties of selected laboratory specimens.....	94
Table 4.8: Comparison between measured peak loads and finite element analyses.....	96
Table 6.1: Properties of the experimental specimens used in the regression analysis.....	127
Table 6.2: Parameters and summary of results from the regression analysis .....	139
Table 6.3: Comparison of simplified form of $K\epsilon a$ with test data .....	144
Table 6.4: Environmental reduction factor for various FRP systems and exposure conditions [Table 9.4 of the ACI 440.2R-17] .....	146
Table 7.1: Test and FEM results .....	166

## LIST OF FIGURES

Figure	Page
Figure 1.1: Typical FRP-concrete joint subjected to a single tensile force .....	5
Figure 1.2: Different bond test setups.....	6
Figure 1.3: Different types of FRP anchors .....	17
Figure 1.4: Method of application of FRP anchors.....	19
Figure 1.5. The John W. Olver Design Building at the University of Massachusetts under Construction in May 2016 (Photo credit: Alexander C. Schreyer).....	22
Figure 1.6. Typical HBV-shear connector .....	24
Figure 2.1: Parts of a CFRP-concrete joint.....	27
Figure 2.2: An assembled CFRP-concrete joint .....	28
Figure 2.3: Concrete under uniaxial tensile stress state.....	29
Figure 2.4: Uniaxial tensile stress-plastic strain curve .....	31
Figure 2.5: Concrete under uniaxial compressive stress state .....	32
Figure 2.6: Uniaxial compressive stress-plastic strain curve.....	33
Figure 2.7: Post failure stress-displacement curve .....	35
Figure 2.8: Hyperbolic Drucker-Prager .....	37
Figure 2.9: Yield surface in plane stress.....	39
Figure 2.10: Yield surfaces in the deviatoric plane for different values of $K_c$ .....	39
Figure 2.11: Damage variable as a function of equivalent displacement .....	44
Figure 2.12: Equivalent stress versus equivalent displacement.....	44
Figure 2.13: Linear damage model .....	47
Figure 3.1: A concrete block with four holes for the CFRP anchors.....	50
Figure 3.2: A CFRP sheet with four holes for the CFRP anchors. ....	51
Figure 3.3: An adhesive layer with four holes for the CFRP anchors. ....	52

Figure 3.4: Cohesive elements sharing nodes with elements of other components.....	53
Figure 3.5: Tie constraints connect surfaces of cohesive elements to surrounding elements of other parts .....	53
Figure 3.6: Contact interactions to connect cohesive elements to the surrounding components .....	54
Figure 3.7: Three-dimensional solid hexahedral elements used to model a CFRP anchor.....	55
Figure 3.8: The adhesive envelope used around each CFRP anchor.....	56
Figure 4.1: Distribution of strains at the top surface along the centerline of the CFRP sheet for the first replicated specimen tested by Mazzotti et al. 2008.....	64
Figure 4.2: Force-slip diagram at the loaded end of the CFRP sheet for the first replicated specimen tested by Mazzotti et al. 2008 .....	64
Figure 4.3: Distribution of strains at the top surface along the centerline of the CFRP sheet for the second replicated specimen tested by Ueda et al. 1999.....	69
Figure 4.4: Force-slip diagram at the end of the CFRP sheet for the second replicated specimen tested by Ueda et al. 1999 .....	70
Figure 4.5: Shear retention factors SR-0.2-0.01 .....	71
Figure 4.6: Shear retention factors SR-0.2-0.015 .....	71
Figure 4.7: Shear retention factors SR-0.4-0.005 .....	72
Figure 4.8: Shear retention factors SR-0.4-0.01 .....	72
Figure 4.9: Shear retention factors SR-0.4-0.02 .....	73
Figure 4.10: Force-slip diagram at the loaded end of the CFRP sheet for the first replicated specimen tested by Mazzotti et al. 2008 using the explicit analysis procedure.....	74
Figure 4.11: Force-slip diagram at the loaded end of the CFRP sheet for the second replicated specimen tested by Ueda et al. 1999 using the explicit analysis procedure.....	75
Figure 4.12: Force-slip diagram at the loaded end of the CFRP sheet for the third replicated specimen tested by Breña and McGuirk 2013 using the explicit analysis procedure.....	80



Figure 4.13: Dimensions of the CFRP anchor .....	81
Figure 4.14: Beginning of debonding propagation (Mises stress = 1025 MPa) .....	82
Figure 4.15: Debonding propagation at the CFRP anchors (Mises stress = 1425 MPa).....	82
Figure 4.16: Debonding propagation between the CFRP anchors (Mises stress = 1784 MPa).....	83
Figure 4.17: Debonding propagation between the CFRP anchors (Mises stress = 2135 MPa).....	83
Figure 4.18: Debonding propagation at the loaded end of the CFRP anchors (Mises stress = 2470 MPa).....	84
Figure 4.19: Debonding propagation far from the CFRP anchors (Mises stress = 2793 MPa).....	84
Figure 4.20: Debonding propagation far from the CFRP anchors (Mises stress = 3163 MPa).....	85
Figure 4.21: Debonding propagation far from the CFRP anchors (Mises stress = 3448 MPa).....	85
Figure 4.22: Debonding propagation before fully separation (Mises stress = 3585 MPa).....	86
Figure 4.23: Stress distribution in the CFRP anchor .....	87
Figure 4.24: Stress distribution in the adhesive envelope around the anchor.....	87
Figure 4.25: Stress distribution in the CFRP sheet before failure .....	87
Figure 4.26: Stress distribution in the adhesive layer before failure .....	88
Figure 4.27: Cracking propagation in concrete-FRP interface and corresponding longitudinal stress distributions in the CFRP sheet and anchors for different load stages .....	89
Figure 4.28: Stress distribution at the ultimate force before the failure of the CFRP-concrete joint.....	90
Figure 4.29: Strain distribution at the ultimate force before the failure of the CFRP-concrete joint.....	90
Figure 4.30: Calculated force-slip diagram for the CFRP-anchored joint (Breña and McGuirk, 2013; Specimen F1-4a-1-24).....	91

Figure 4.31: Comparison of measured and calculated strains on the top surface of the CFRP sheet centerline (Specimen F1-4a-1-24 tested by Breña and McGuirk, 2013).....	92
Figure 4.32: Comparison of measured and calculated strain diagrams along FRP sheet centerline.....	98
Figure 5.1: Effect of the number of FRP anchors on peak force .....	103
Figure 5.2: Effect of FRP anchor longitudinal spacing on peak force.....	104
Figure 5.3: Effect of FRP anchor depth on peak force .....	106
Figure 5.4: Stress distribution on the shaft of the CFRP anchor .....	106
Figure 5.5: Deformed shape of the anchor (shaft depth = 20 mm).....	107
Figure 5.6: Effect of anchor shaft diameter on peak force .....	107
Figure 5.7: Effect of anchor splay diameter on peak force.....	108
Figure 5.8: Different anchor splay shapes: (a) and (b) (Smith 2011); (c) (Breña and McGuirk 2013).....	109
Figure 5.9: Splay angle .....	110
Figure 5.10: Effect of splay angle.....	110
Figure 5.11: Effect of FRP sheet thickness on applied tensile force .....	112
Figure 6.1: Compatibility of axial strains in an FRP-strengthened concrete beam under flexure .....	118
Figure 6.2: Ratios of ultimate tensile force of anchored to unanchored FRP sheets ( $T_{u\text{ anc}}/T_{u\text{ unanc}}$ ) due to change in thickness $t_f$ .....	124
Figure 6.3: Ratios of ultimate tensile force of anchored to unanchored FRP sheets ( $T_{u\text{ anc}}/T_{u\text{ unanc}}$ ) due to change in longitudinal spacing between anchors $s_a$ .....	129
Figure 6.4: Influence of anchor shaft diameter ( $a_d$ ) on ultimate tensile force ratio ( $T_{u\text{ anc}}/T_{u\text{ unanc}}$ ).....	129
Figure 6.5: Influence of anchor fan diameter ( $f_d$ ) on ultimate tensile force ratio ( $T_{u\text{ anc}}/T_{u\text{ unanc}}$ ).....	130
Figure 6.6: Influence of number of anchor rows along debonding path ( $n_a$ ) on strength factor .....	130

Figure 6.7: Influence of FRP sheet thickness ( $t_f$ ) on the standardized strength factor ( $S_t$ ) .....	132
Figure 6.8: Influence of the center-to-center spacing between anchors ( $S_a$ ) on the standardized strength factor ( $S_s$ ).....	132
Figure 6.9: Influence of the anchor shaft diameter ( $a_d$ ) on the standardized strength factor ( $S_{ad}$ ) .....	133
Figure 6.10: Influence of the normalized anchor splay diameter ( $f_d$ ) on the standardized strength factor ( $S_{fd}$ ).....	133
Figure 6.11: Comparison between anchorage strain factors obtained from tests to regression analysis (Equations 6.14 or 6.15) .....	141
Figure 6.12: Comparison between anchorage strain factors from tests to simplified formula (Equation 6.16).....	143
Figure 6.13: Flow chart.....	155
Figure 7.1: Typical HBV-shear connector.....	156
Figure 7.2: Test configuration.....	158
Figure 7.3: Model with mesh and boundary conditions .....	160
Figure 7.4: Stress-strain relationships adopted for (a) concrete and (b) steel materials (see section A4 of the Appendix for values).....	163
Figure 7.5: Load-displacement curves obtained from finite element model and experimental tests reported by Clouston et al. (2005) .....	165
Figure 7.6: Von Mises stress distribution in the steel connector .....	167
Figure 7.7: Interfacial stresses developed in concrete cross section around the steel connector, MPa.....	169
Figure 7.8: Stress distribution in the direction of the applied force developed at the surface of concrete around the steel connector, MPa.....	170
Figure 7.9: Distribution of longitudinal stresses in the direction of the applied force developed in the wood, MPa .....	171
Figure 7.10: Shear stress distribution around the connector in the wood, MPa .....	172
Figure 7.11: Interfacial von Mises stresses developed in the adhesive, MPa.....	172

Figure 7.12: Load-displacement curves of the HBV shear connector corresponding to different steel connector thicknesses (t).....	174
Figure 7.13: Variation in slip modulus with change in steel connector thickness.....	174
Figure 7.14: Effect of the insulation gap (g) between concrete and wood .....	176
Figure 7.15: Deformed shape of the plate with 25 mm insulation gap.....	176
Figure A1: Anchored FRP sheet .....	181
Figure A2: A simply supported beam with external FRP reinforcement .....	183
Figure A3: Proposed application of the anchors (dimensions are not to scale).....	184
Figure A4: User interface.....	188
Figure A5: Estimation of flexural strength .....	189
Figure A6: Estimating required anchorage length .....	191
Figure A7: Assigning anchorage system properties .....	192
Figure A8: Input data for the tested specimen and the obtained results .....	195

## **CHAPTER 1**

### **INTRODUCTION**

#### **1.1 General**

Modern structural systems employ components of different materials in the same structure to ensure the acquisition of strong and economic structural sections. Wood, concrete, steel, fiber reinforced polymers (FRP), and many other materials are combined to produce these sections either during construction or after buildings are constructed where new materials are added to the original members for rehabilitation purposes. The selection of the appropriate materials depends on strength, sustainability, and workability factors of these materials. However, maintaining continuity between the different components to enhance composite action is challenging because of differences in mechanical properties of these materials, specifically differences in stiffness, strength, and ductility. Structural members subjected to bending moments, such as beams and slabs, require shear forces generated along the interfaces to be transferred between the components of the composite section and provide full or partial composite action. The different components of the composite section are typically bonded using adhesives or connected using mechanical anchors (in some cases bonding and mechanical anchors are used together). This dissertation focuses on identifying and studying, through finite element simulations calibrated using laboratory data, the parameters that influence the behavior of two types of shear interfaces. The first type of connection studied in the dissertation discusses bonded and mechanically anchored externally applied FRP sheets to concrete used for rehabilitation of concrete structures. The second type of connection studied is a new wood-concrete composite that is composed of a steel connector bonded

into a groove made in engineered wood composite beams, which is subsequently cast into a concrete topping slab. This steel connector is used to transfer shear stresses between the wood and the concrete slab to promote composite behavior.

## **1.2 Externally FRP strengthened concrete in the literature**

Strengthening concrete elements using fiber-reinforced polymer (FRP) sheets is a recognized and widely used method. The weight advantages of FRP materials over steel, high tensile strength, resistance to corrosion and ability to increase the durability of the strengthened component have made them the material of choice in many strengthening applications. It is difficult, however, to reach the strength of FRP materials when sheets are externally bonded to the surface of the concrete because of debonding (Garden et al. 1998; Nguyen et al. 2001; Breña et al. 2003; Camata et al. 2007). The importance of the FRP-concrete bond to reliably develop high tensile stresses in the FRP materials has prompted a significant amount of research to understand better and improve bond performance. Debonding typically initiates within a thin layer near the surface of concrete at much lower loads than those corresponding to the strength of the FRP sheet. The effective (limiting) strain in an FRP sheet at debonding is found by invoking strain compatibility at a cross section as detailed in the ACI Committee 440 Guide (2008). Debonding, therefore, hinders the development of high interfacial stresses in the FRP-concrete joint and thereby limits the efficiency of this strengthening system. The magnitude of interfacial shear stresses increases only throughout the effective bond length (also termed the stress transfer zone); beyond this region, the force in a bonded FRP sheet does not increase substantially as a consequence of stress transfer between the

concrete surface and FRP sheet. FRP-anchors have been used in the past to supplement the strength provided by bonding FRP sheets to concrete, therefore allowing FRP sheets to develop their ultimate strength.

Past researchers have used FRP-anchors in experimental studies involving FRP-concrete strengthening schemes (Niemitz et al. 2010; Smith 2011; Breña and McGuirk 2013). However, a comprehensive evaluation of factors that govern the behavior of the FRP anchors has not been reported in the literature to date. A better understanding of the behavior of FRP anchors and their influence on FRP-concrete joints is needed to develop design guidance for these systems.

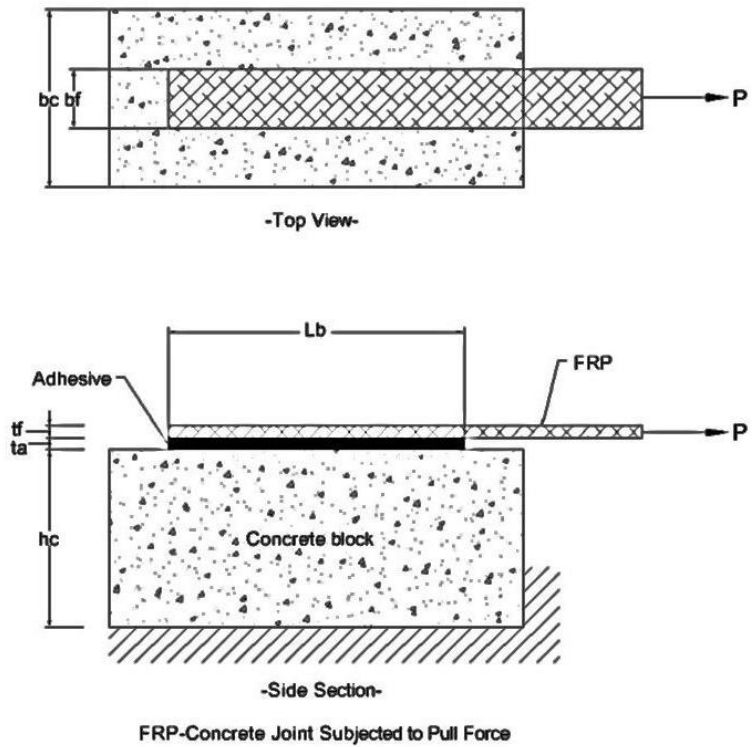
In this research work, the behavior of anchored FRP sheets was studied using a detailed finite element model of the system. The finite element model was constructed to represent concrete elements strengthened using carbon FRP (CFRP) composite sheets. The different components that integrate the CFRP-concrete joint system were modeled using appropriate material models, physically consistent geometric shapes, and establishing explicitly the function of each component. Most previous studies that have focused on studying FRP-concrete bond have concentrated on two-dimensional models of the system (Lu et al. 2005; Martinelli et al. 2011). Two-dimensional models are useful when only the average response over the width of the FRP sheet is of interest, but they fail to capture variations across the width of the sheets. Furthermore, it is impossible to study the influence of FRP anchors on the stress-strain behavior of the FRP system in the vicinity of anchor locations with two-dimensional models. Therefore, three-dimensional modeling was chosen in this research to be able to determine the strain and stress fields generated in the FRP-concrete joint system in detail. The fidelity of the three-dimensional

model results is compared with laboratory tests available in the literature, first of FRP-concrete bonded systems without supplemental anchors, and subsequently of FRP-concrete systems containing anchors. After the accuracy of the proposed modeling technique is verified, several dimensional parameters of the anchors are varied within reasonable limits (distance between anchors, anchor depth, anchor diameter, anchor splay angle, and anchor splay diameter) to identify the influence of anchorage in behavior of the system with the ultimate goal of developing guidance for design of FRP-concrete anchored sheets.

### **1.2.1 Bond-slip behavior in the literature**

The bond-slip behavior of FRP-concrete joints has been observed and extensively studied in many experimental tests in the past (see Figure 1.1 for a typical FRP-concrete joint). These tests are primarily adopted to investigate the strength of different structural members after reinforcing them with FRP plates. Therefore, different experimental test arrangements have been considered to better-representing the failure of these members. Double shear pull tests, double shear push tests, single shear pull tests, single shear push tests, and beam flexural tests are different test sets that can be carried out to identify bond-slip behavior (Yuan et al. 2004, Yao et al. 2005, Chen et al. 2001) (see Figure 1.2). Basically, choosing one of these test arrangements depends on the type of the actual structural member and the method of reinforcing.





- Notation
- bc: width of concrete block
  - bf: width of FRP plate
  - hc: height of concrete block
  - Lb: bond length
  - P: applied pull force
  - ta: thickness of adhesive
  - tf: thickness of FRP plate

**Figure 1.1: Typical FRP-concrete joint subjected to a single tensile force**

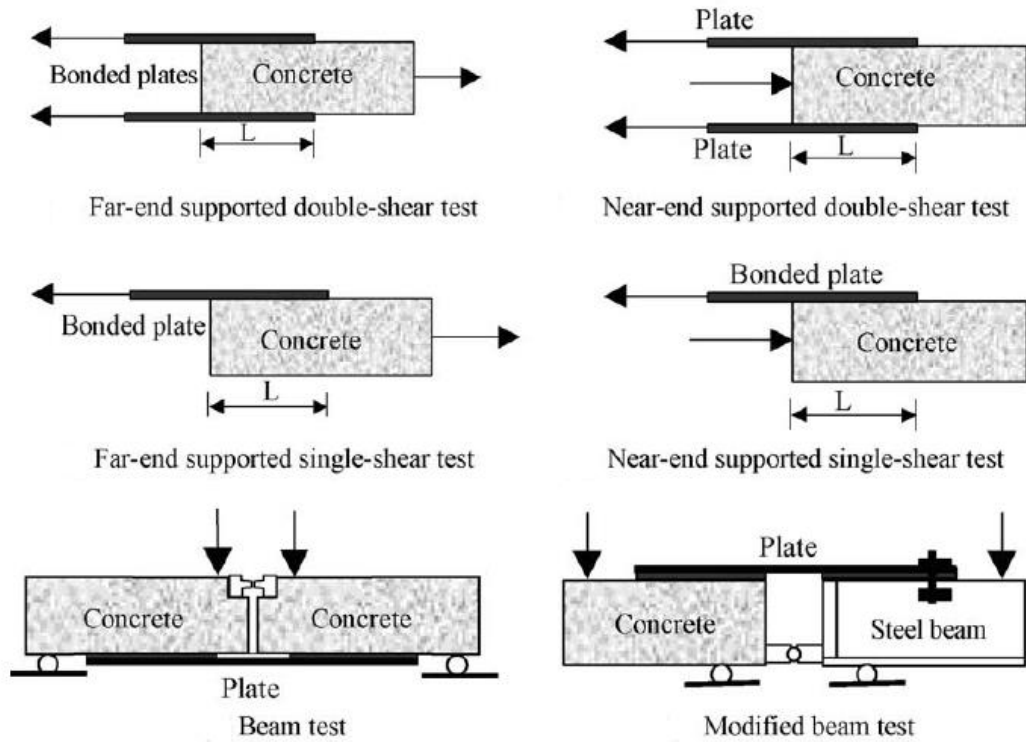


**Figure 1.2: Different bond test setups**

(Reported in Yao et al. 2005 from Chen et al. 2001)

Many bond-slip experimental tests were conducted in the past (Chajes et al. 1995, Bizindaviyi and Neale 1999, Sebastian 2001, Yao et al. 2005, Dai et al. 2005, Czaderski et al. 2010). Yao et al. (2005) introduced the results of 72 specimens tested, under the single-shear configuration, to identify the bond-slip behavior of FRP plated concrete prisms. This experimental work shows that even though concrete cover separation was the primary failure mode, other failure modes may occur as well. These failure modes are debonding at the adhesive-concrete interface and concrete prism failure. It was also found that increasing the bond length more than the effective length would not lead to any significant increase in bond strength since debonding propagates along the interface after developing peak stresses within the effective length.

In addition to experimental studies, finite element analysis and fracture mechanics theoretical investigations are methods that have been conducted to predict the bond-slip behavior (2005). Previous researchers have also developed a mixed analytical method that introduces fracture mechanics to finite element analysis.

Lu et al. (2005) presented a bond-slip model that is based on finite element analysis. This study focused on the debonding of FRP plated concrete joints occurring within the concrete in a thin layer adjacent to the adhesive-concrete interface. This debonding behavior represents the most common debonding failure observed during experimental tests. The FRP-concrete joint was modeled as a plane stress problem in this study. The width of the FRP plate was represented to be equal to the width of the concrete prism used. This representation is not necessarily the arrangement for all FRP plated-concrete joints. Therefore, a width factor was introduced to take into consideration the effect of the difference in the width of different FRP-to-concrete joints. In this study, two sets of (0.25 and 0.5mm) square shaped finite elements, mesoscale elements, were considered. These elements were adopted to capture precisely concrete cracking. Nevertheless, it should be noted that this study is a mesoscale finite element study rather than a meso-mechanical study since concrete is still treated as a homogeneous material.

Lu et al. (2005) reviewed several bond-slip models that were obtained based on previous experimental work of the other researchers and the model presented in (2005). They compared these models with the outcome of pull-out experimental work on similar FRP-concrete joints specimens. According to previous studies reviewed by the researchers, six parameters were considered paramount to represent bond-slip models, including concrete strength, bond length, FRP stiffness, FRP-concrete joint width ratio,

adhesive stiffness, and adhesive strength. However, among these parameters, it was observed that the effect of the shear stiffness of the adhesive material is negligible, especially for regular adhesive FRP-concrete joints. It was found that the mesoscale finite element model introduced in (2005) was the most accurate model to represent the bond-slip behavior compared with the other reviewed models. Two other models were also established based on the mesoscale finite element model to simplify it. The first simplified model consists of just a plastic part since it is based on assuming infinite initial stiffness for practical considerations. The second simplified model was even simpler by introducing bilinear behavior. This model consists of both a linear ascending elastic part and a linear descending plastic part. All Three models were tested, and it was shown that the outcome was in good agreement with experimental results. However, it is noteworthy that the two simplified models are not realistic since the observed bond-slip behavior in the experimental tests is nonlinear even within the elastic part (Chajes et al. 1995, Bizindavyi and Neale 1999).

Wang J. (2006) examined the effect of the bond-slip curve shape in a study to analyze debonding in the FRP-plated concrete beam with flexural cracks. It was found that the softening zone increases as the elastic stiffness of the FRP-concrete interface increases whereas the ultimate load and moment are not affected by the change in this value. Therefore, a linear bond-slip model with just an elastic stage was proposed to substitute the real bilinear model. The linear model provides an easier formulation for both ultimate load and bending moment. This simplification for the bond-slip behavior leads to approximate results that are not necessary right for all debonding problems.

Wu et al. (2010) provide two formulas to represent two failure modes of externally bonded FRP-concrete joints. These failure modes are the interface debonding and concrete cover separation. This formulation is based on avoiding all empirical bond-slip parameters that were adopted in previous studies except the width parameter. Rather than the empirical parameters, new derived bond-slip formulas were presented based on fracture mechanics principles. The first model consists of a two-layer structure with a semi-infinite crack at the interface, which leads to interface debonding. The second model is based on assuming a three-layer structure with a semi-infinite crack at the interface between concrete and the cohesive material. Hence, this study shows a new formulation that has a stronger physical background based on fracture mechanics and distinguishes between the two failure modes: the interface debonding and concrete cover separation. Furthermore, a finite element simulation with cohesive zone elements between the concrete and the FRP layers to simulate crack propagation by determining the fracture energy of the interface was considered to validate the proposed models.

It is worth noting that the derived formula for interface debonding defines fracture energy in terms of the FRP stiffness that is represented by the FRP thickness and modulus of elasticity. In fact, cracking in this failure mode was assumed to occur in the adhesive layer, not the FRP layer. Therefore, the fracture energy is supposed to be in term of the adhesive stiffness. In addition, the derived fracture energy formula for the case of concrete cover separation includes coefficients that are related to the concrete and FRP-plate; nevertheless, it does not include any parameter to represent the adhesive material. The reason behind the miss representation of the adhesive might be due to the assumption

used that the property of the adhesive material is constant, and it is included within fracture energy value.

Martinelli et al. (2011) introduced a modeling approach for the bond-slip behavior of FRP-concrete joints. This approach is different from most existing studies as it includes both in-plane and out of plane displacement fields and based on the experimental results presented in (2010). The theoretical modeling was established by representing the FRP plate as a Bernoulli beam over a layer of elastic springs. A bilinear model was first adopted as the base model then the nonlinear behavior incorporated to represent crack propagation. This study was able to illustrate the distribution of normal stresses in the adhesive-concrete interface. However, this study shows that shearing stresses are the main factor that affects FRP-concrete joints debonding. The finite difference approach was adopted to identify an expression for the boundary conditions in terms of vertical displacement and slip. Accordingly, a relationship between vertical displacement and slip was obtained in a matrix form. Then, the previous expression was developed to include the fracture effect that leads to nonlinear behavior. As a result, relationships between shear stiffness and slip were derived, and an iterative process was considered to reach final results. Briefly, this study demonstrates a new formulation that takes into consideration both in-plane and out of plane stresses.

Cornetti and Carpinteri (2011) argue that the widely used bilinear model is not able to accurately represent the realistic behavior of the bond-slip of externally bonded FRP-concrete joints. In fact, when bond strength is reached; the bond-slip curve behaves nonlinearly. Nevertheless, most existing studies consider the bilinear model since it is easier to achieve an approximated solution for bond-slip problems. Consequently, this

study attempts to achieve an analytical solution that is based on the linear-exponential model presented in (2006). A formula for Mode II fracture energy was derived to represent the area under the bond-slip curve. This formula is a function of the bond strength, elastic slip, and a factor that represents the ratio between the areas of the elastic part of the bond-slip curve to the area of the plastic part. As the value of the elastic-plastic area factor approaches infinity, it was found that the interface will act as an elastic-perfectly brittle material. On the other hand, when the value of the elastic-plastic area factor approaches zero, the interface will act as an elastic-perfectly plastic material. Accordingly, two more models were considered based on the elastic-plastic area factor in addition to the bilinear and linear-exponential models.

All four models were compared with existing experimental tests, and it was proved that the linear-exponential model provides the best fit to the experimental data. Furthermore, the other models overestimate the maximum bonding force of the FRP-concrete joints, and hence the actual debonding may occur before reaching this force. Therefore, an extensive parametric study was adopted focusing on the exponential model. The effect of bond length, the FRP stiffness, the shape of the cohesive law, and size-scale effect were all investigated in this study.

Hence, this research provides a more acceptable model than the bilinear model since it captures the nonlinear behavior of the softening part of the bond-slip curve. In addition, this study provides a detailed description of the behavior of FRP-concrete joints under a variety of studied parameters that affect bond-slip behavior.

It has been observed in many existing bond-slip experimental tests that the maximum shearing strength is not constant over the bonded length of the FRP-plate since the local

bond strength decreases as the bonded length increases. Not only does shear strength decrease but also the entire bond-slip curve changes as debonding propagates. Existing bond-slip models, however, do not take into consideration the effect of shear stress variation along the bonded FRP-plate length. To address this issue, Abdel Baky et al. (2012) introduced a new nonlinear FRP-concrete bond-slip model. This model was derived using micromechanics-finite elements analysis-based results.

In this study, a few steps were considered to build up the new nonlinear bond-slip model. First, the micromechanics finite element based results (2008) were used to find out the relationship between shear and normal stresses. As a result, an expression of the local bond strength was derived as a function of the normal stress and tensile stress. Then, the variation of the normal stress along the FRP-concrete interface was studied and defined. Finally, the bond-slip model was established based on the previous steps, and the Mohr-Coulomb failure criterion was adopted to identify failure limits in concrete. Furthermore, both normal and shear stresses were investigated with particular attention to the top 1-mm layer of concrete below the adhesive-concrete interface.

In general, this study presents an investigation for slip values in the FRP, adhesive and concrete layers separately rather than jointly. In addition, the researchers found that the slip represents 1.0%, 60.0%, 39.0% at the FRP, adhesive, and concrete layers, respectively. Therefore, through the estimated fracture energy, the bond-slip relations of each layer were derived to define the total bond-slip model precisely. This model was compared with other existing models. This comparison shows that some differences were observed since the existing models do not take into consideration the adhesive as a



separate material. However, these models include the adhesive in the general fracture energy formula.

Notably, the proposed model reflects a general formulation that is applicable for all variations in material properties since it represents each material separately and then combines all properties of the material used in a single model. In addition, this model takes into consideration the nonlinear behavior of the bonded FRP-concrete joints through including the effect of the normal stresses, which makes the presented model more precise than the other existing models.

Wu and Jiang (2013) conducted a study to quantify bond-slip parameters based on a database of existing FRP shear tests in addition to new experimental tests. Furthermore, an analytical investigation was adopted to develop a closed-form solution that can introduce a precise definition of some of the bond-slip parameters. Both FRP to concrete width ratio and concrete strength were considered to derive a new model for width factor. This model is expected to be accurate because it does not depend on the previous discontinuous bond-slip relationships, and also it does not assume infinite bond length contrary to the previous studies. Hence, the obtained closed-form solution can be used for joints that have arbitrary bond lengths.

Shear-displacement curves of externally bonded FRP pull-off tests were analyzed to derive two forms of pull strength. The first type depends on bond length approaches infinity. On the other hand, the second type depends on an arbitrary length and restates the first form but after multiplying it by a coefficient that is related to the arbitrary bond length. As a consequence, the effective bond length can be indicated as the value of the second form of the bond strength approaches the value of the first form. Through this

formulation, it was observed that the active bond length relies only on FRP stiffness, which is represented by the FRP elastic modulus multiplied by FRP-plate thickness and concrete strength.

As the researchers reviewed previous analytical solutions, they noticed that most existing studies, FRP bond-slip analytical studies, were based on assuming the FRP strip width equal to the width of the concrete block. In fact, all these studies used data of experimental tests in which the FRP strip width was smaller than the concrete block, and this affects results significantly. Therefore, a width correction factor was proposed to correct any 2D strength formula that depends on an equal FRP strip-concrete block width. This correction considers the 3D width effect that takes into account the difference in width between FRP-plate and concrete block. Studying a database of 80 test specimens, the researchers found that width effect varies due to concrete strength when the FRP-plate to concrete block width ratio is constant. Based on this study, the parameters of the bond-slip model were developed by suggesting two factors to correct length and width effects. These parameters were compared with the existing models and experimental data, and they showed a better representation of the bond-slip behavior.

The studies by Abdel Baky et al. (2012) and Wu and Jiang (2013) represent two different approaches in the field of externally bonded CFRP-concrete joints. Whereas a fracture mechanics approach was introduced to finite elements in the first study, the second is considered an analytical study that is based on previously existing models and experimental data observations. Equally important to demonstrate that the first study is considered comprehensive in representing all materials included within the FRP-concrete joint that permits the tracking of all possible failure modes. In contrast, the second is

considered applicable to the cases where concrete cover separation is the main reason behind debonding.

The study of Obaidat et al.(2013) introduces a finite element model that is capable of solving debonding problems using three-dimensional representation. This three-dimensional modeling is necessary to improve accuracy by eliminating dimensional correction parameters. These correction parameters have been used in the literature with two-dimensional models to simulate three-dimensional behavior. However, in this study with a three-dimensional model, there is no need to consider dimensional parameters, and rather this research focusses on material parameters.

A number of relevant material parameters, such as initial stiffness, fracture energy, and shear strength of the interface between FRP plate and concrete, were considered in this study. The FRP plate was considered as an elastic isotropic material since no failure was expected to occur in FRP. On the other hand, a plastic-damage model was considered for concrete. The properties of the interface were mainly controlled by the tensile strength of concrete and the shear stiffness of the cohesive material. A quadratic traction function was utilized to represent damage initiation in the FRP-concrete interface. This function is defined by introducing the tensile strength of concrete and shear strength of the interface.

Obaidat et al. assumed the interface properties to be influenced by concrete, FRP and the cohesive materials. Subsequently, a cohesive zone model was adopted to identify three parameters that characterize the cohesive behavior of the interface. These parameters are initial stiffness, fracture energy, and shear strength of the interface.

The initial stiffness was investigated by introducing several stiffness values to find the value that represents the best fit to experimental results reported in the literature. This

investigation shows that the transfer of stress to the concrete increases with the increase of the interfacial stiffness. This increase in the transferred stresses will decrease the stress transfer length along the FRP-concrete joint. Furthermore, shear stresses increase at the interface. In addition to the previous results, shear stiffness of the interface was defined in terms of the shear modulus of the cohesive material and thickness of the adhesive.

Interfacial fracture energy and shear strength were investigated similar to the interfacial stiffness. Several combinations of fracture energies and shear strengths were examined and compared with experimental results. Consequently, both fracture energy and shear strength of the interface were related to shear modulus of the adhesive and tensile strength of the concrete material.

Finally, the obtained relationships were examined by introducing them through different bond-slip relations to the finite element models. Bilinear, trilinear and exponential bond-slip relations were all considered in the investigation. However, load-slip results showed that the shape of the bond-slip curve has a minimum effect on debonding behavior. Therefore, a simple bilinear bond-slip curve was suggested to be considered in debonding problems.

### **1.2.2 Anchored fiber-reinforced polymer sheets in the literature**

Breña and McGuirk (2013) presented the results of a series of laboratory experiments conducted to study the possibility of strengthening FRP-concrete joints by applying FRP anchors (see Figure 1.3 for the different types of FRP anchors). The purpose of using these anchors was to preclude debonding of bonded CFRP joints (see Figure 1.4) to allow development of the FRP sheet strength. In general, FRP-concrete joints debond before

reaching a significant level of FRP strength. This behavior adversely affects the efficiency of using FRP material for strengthening concrete structures. Consequently, to avoid debonding issues and allow FRP sheets to reach their ultimate strength, the researchers proposed applying FRP-anchors to the bonded joints to increase the total strength of the joints.

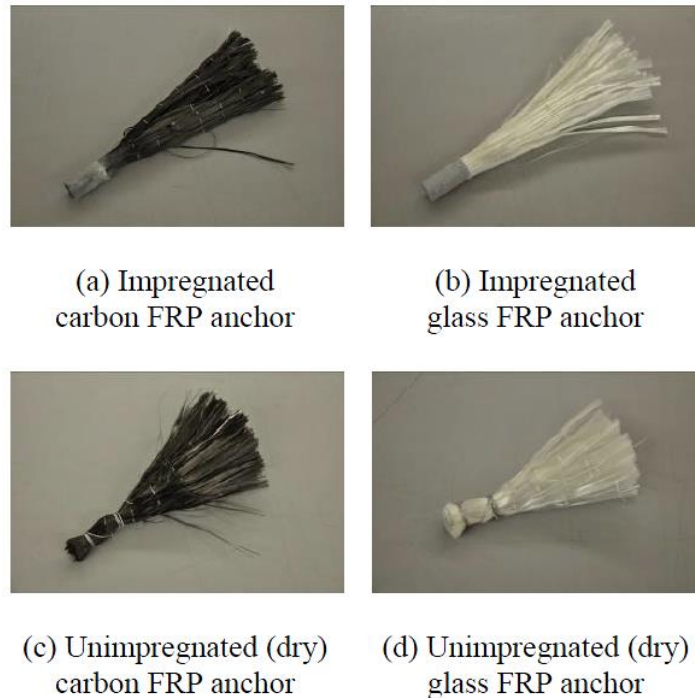


**Figure 1.3: Different types of FRP anchors**

(Smith 2009)

Specimens of concrete blocks with FRP-sheets attached to the top surfaces of the concrete blocks using an adhesive material were tested. Specimens were different in bonded lengths, the number of FRP anchors, and anchor placement. Test results were compared with the results of specimens tested by Niemitz et al. (2010) and showed similar behavior in terms of observed failure modes. These failure modes were shear

rupture, splay delamination, and pull out of FRP anchors. Based on the experimental work of Niemitz et al. (2010) it was recommended that the FRP-anchor splay diameter cover the entire width of the FRP sheet to avoid longitudinal splitting of the unidirectional FRP sheet. Therefore, a splay width effect was considered in this study. Other parameters were also discussed, including the effect of anchor longitudinal spacing and the effect of the number of FRP sheet plies. Anchors that do not lie within the stress transfer zone of the debonded FRP-sheet were found to not contribute to the strength of FRP sheets until the debonding front reached the anchor location (anchors within or in front of the stress transfer zone). On the other hand, FRP sheets with multiple plies require more anchors to develop their strengths because of the increase in the total thickness of FRP material. The most important finding of this experimental work was to prove that increasing the number of anchors within the stress transfer zone improves the strength of FRP-concrete joints significantly. This improvement in strength belongs to the use of anchors that help to develop strains and reach ultimate strengths in FRP sheets.

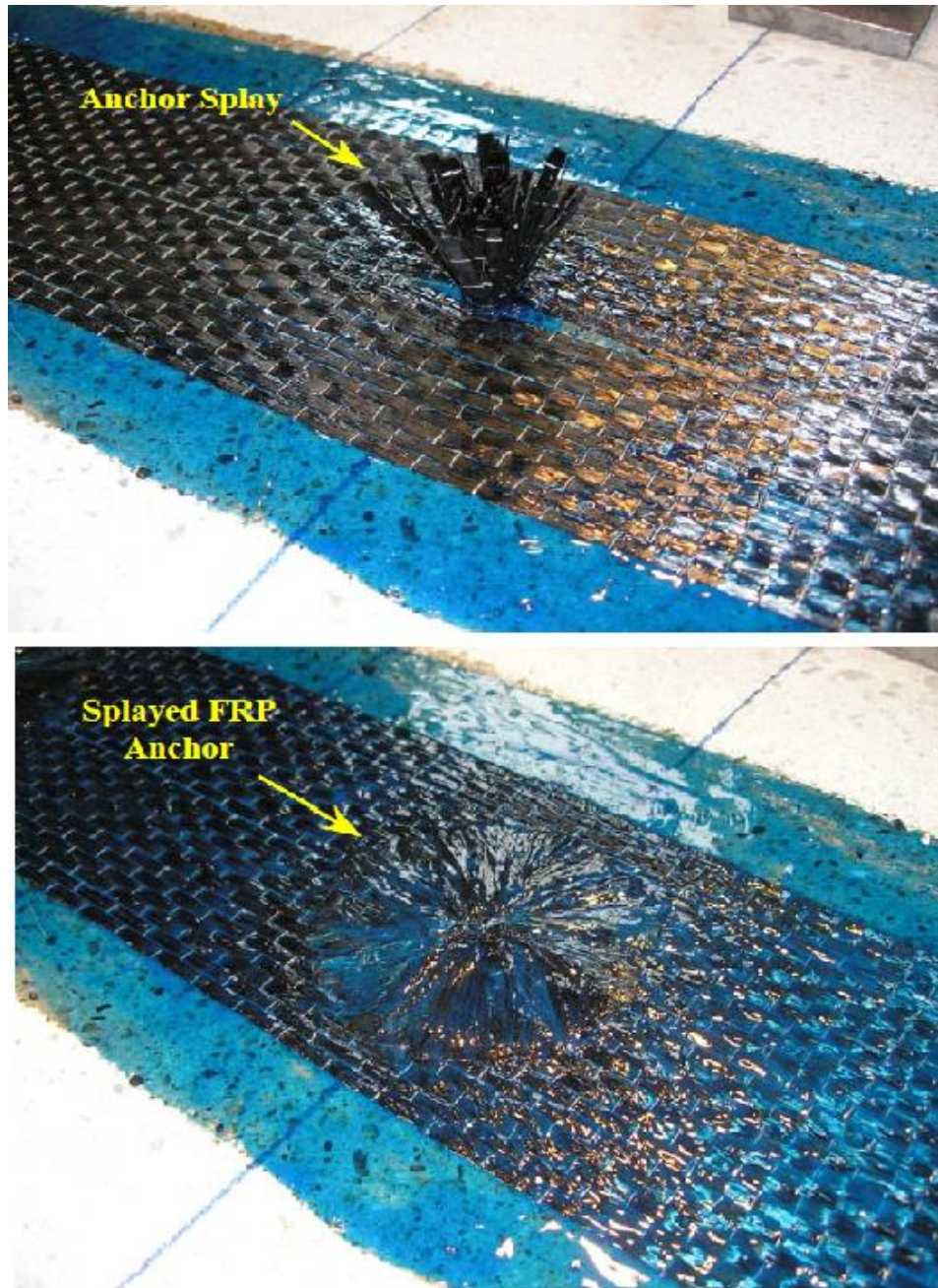


**Figure 1.4: Method of application of FRP anchors**

(Breña and McGuirk 2013)

Finite element modeling was also performed by Breña and McGuirk (Breña and McGuirk 2013) to characterize the effect of anchors on the debonding behavior and distribution of strains on FRP sheets. This modeling consisted of thin shell elements with

orthotropic linear elastic material to characterize the FRP sheet. These shell elements are connected to springs that represent the interface. These springs are fixed from the other end to represent the connection of the interface to the rigid concrete that was assumed 5 mm from the interface. Anchored regions were also modeled using similar springs, but with higher rigidity. The behavior of springs was also calibrated to correspond with experimental results. Force-deformation relationships were used to represent the behavior of anchors. Both transverse and longitudinal strain distributions at the top of the FRP sheet were studied. All these results in addition to the peak loads were compared with the experimental results in the literature and showed that they provide a good agreement.

Smith et al. (2011) conducted experimental work of several FRP strengthened slabs under bending forces. The primary objective of this study was to investigate the effect of applying FRP anchors to the strengthened members. These FRP anchors were used to delay or prevent debonding of FRP sheets. Eight simply supported slabs were constructed from reinforced concrete and experimentally tested.

The first slab was tested without applying FRP sheets or anchors to investigate its resistance without adding any FRP strengthening. The second slab was reinforced with FRP sheets without anchors. The six other slabs were reinforced with both FRP sheets and anchors. Different types of anchors were investigated. The difference between these anchors was the amount of FRP fibers used to form each type of anchors. Furthermore, the spacing between applied anchors was different for each slab to study the effect of anchors placement.

Different failure modes for the anchors were observed during the experimental tests. These failure modes are; Pull-out from the concrete substrate, Partial rupture, and



complete rupture at bending regions. The propagation of cracks was much slower in the slabs where FRP anchors exist. Furthermore, larger displacements and strengths were achieved. Having closer spaced anchors at the edges of the slabs at the regions of maximum shear stresses increased the deflection, but no improvement in strength was made. The debonding behavior of the anchored slabs showed that FRP plates debonded before the failure of the anchors. This behavior provides signals of warning since FRP anchors prevent direct plate separation after debonding of FRP sheets. The distributions of strains were also investigated. These distributions showed that smaller values of strains were detected in the anchored regions. This reduction in strains was due to the added fibers of the anchor-splays. Generally, the main achievement of both strength and deflection was obtained by positioning the anchors of the densest fiber content close to the maximum bending moment region in the middle of the slab. Furthermore, by applying closely spaced anchors with less dense fibers at the free ends of FRP sheets close to the regions of maximum shear stress.

### **1.3 Wood-concrete composites in the literature**

Wood-concrete composite systems are gaining in popularity for large-scale construction applications such as floors, roofs, and bridge decks (Clouston and Schreyer 2008, Dias et al. 2016). State-of-the-art timber buildings, such as the new UMass Design Building, showcase this technology as a way to improve floor performance while minimizing the environmental impact of building (see Figure 1.5).



**Figure 1.5. The John W. Olver Design Building at the University of Massachusetts under Construction in May 2016 (Photo credit: Alexander C. Schreyer)**

The hybrid system is made up of a concrete slab that is integrally connected to a substructure of structural wood beams or panels forming high-performance composite panels. Incorporating wood elements in large-scale construction in this way has the environmental benefits of using renewable materials while also lowering embodied energy during manufacture and reducing the overall carbon footprint of the built environment due to carbon sequestration of wood (Oliver et al. 2014). Other advantages of using wood include the reduction in construction time and cost due to wood functioning as permanent formwork and reduced foundation costs because of the high strength-to-weight ratio of wood (Yeoh et al. 2010a). For the same reason that shear studs

are utilized in steel-concrete systems, shear connectors are incorporated in wood-concrete systems. They are needed to effectively produce composite behavior between the concrete slab and wood elements by transferring shear stresses that control slippage between the two materials. Lower slip induces a higher level of composite action and consequently, improved overall structural performance of the composite floor system in terms of stiffness and strength. The challenge for wood-concrete floor systems is that wood, being a soft material, is inherently susceptible to slip, reducing the level of composite action. Therefore, the type of shear connector between the wood element and the concrete slab and its rigidity, are critical factors in the design of these systems.

Many different wood-concrete shear connectors have been proposed and used in practice. They come in the form of nails and screws; steel tubes or plates; shear keys with steel anchors; and glued-in metal plates (Yeoh et al. 2010b, Gutkowski et al. 2008, Tannert et al. 2017). It is generally accepted that glued-in metal plates provide the best performance in terms of strength and stiffness (Clouston et al. 2005, Tannert et al. 2017). For this connector type, a portion of a metal plate or mesh is embedded into a slot cut in the wood along the length of the structural member. The slot is pre-filled with epoxy to glue the connector to the wood. The protruding portion of the connector is embedded in the concrete slab at the time of casting the floor. Figure 1.6 shows a typical shear connector where part of the concrete is removed from the figure to reveal a part of the perforated steel plate. A layer (or layers) of insulation is often placed horizontally between the concrete and the wood for sound attenuation and also to inhibit moisture from transferring into the wood after the concrete is placed and has not yet hardened.

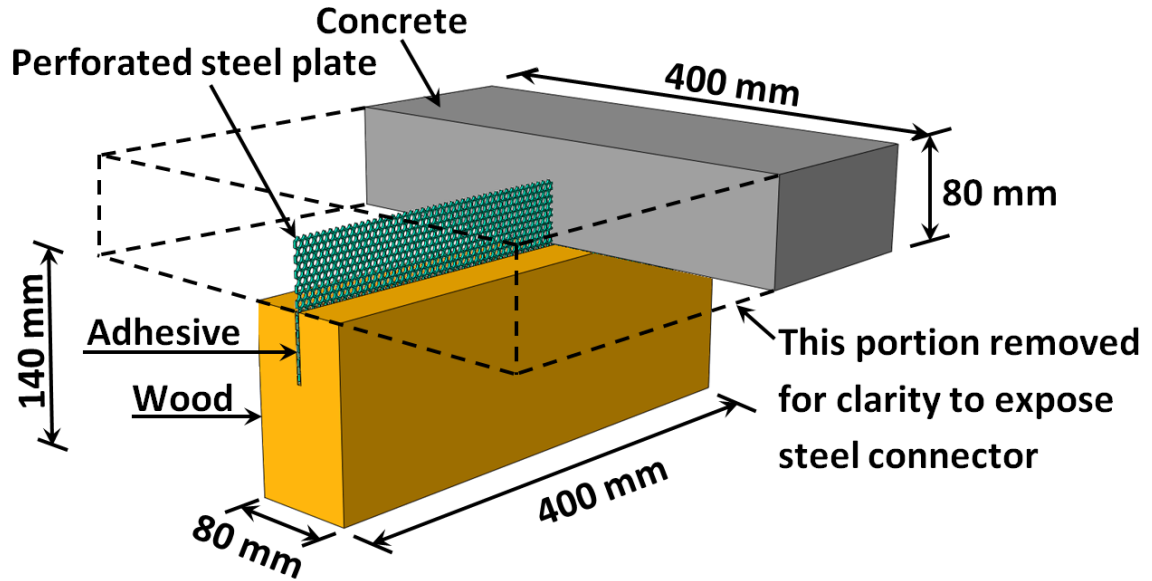


**Figure 1.6. Typical HBV-shear connector**

**(dimensions for specimen reported in Clouston et al. 2005)**

One particular glued-in metal plate connector, known as the HBV® (Figure 1.6), was developed in 1992 by Leander Bathon at Hochschule RheinMain University, in Wiesbaden, Germany (Technical Dossier HBV-Systems 2014; Clouston et al. 2005). This connector holds European code approval (Nr. Z-9.1-557), is produced by Zang and Bahmer GmbH, and has been implemented in many public buildings and bridges in Europe and also recently in North America (Clouston and Schreyer 2016; McKnight 2017). The connector was designed to be used specifically in wood-concrete composites as per its name HBV® (or Holz-Beton-Verbund) which means wood-concrete-connector in German.

The design philosophy of the HBV® is based on enhancing stiffness in the service load range while ensuring ductility of the system in the post-yield stress range. The steel plate

connector is perforated and acts as a fuse element with a perfectly-plastic failure mechanism (Clouston et al. 2005).

In this research, results are presented of finite element (FE) analyses and a parametric investigation for one type of connector: a perforated steel plate of which half is epoxied into a route in the wood member while the other half is embedded in a concrete slab. The FE model was first validated against experimental push-out tests performed on a commercial product and then employed to examine the effect of several parameters of the connection: thickness of plate; insulation gap between concrete and wood; depth of embedment in concrete; and depth of embedment in wood.

## CHAPTER 2

### FRP-CONCRETE SYSTEM: MATERIAL CONSTITUTIVE RELATIONSHIPS

#### 2.1. Introduction

The objective of this research is to study the behavior of anchored FRP sheets applied to different structural members and identify critical parameters that affect the behavior. These structural members were made from concrete as the main material and reinforced with steel bars in addition to carbon fiber reinforced polymer (CFRP) sheets. Therefore, four materials were used and modeled to represent all structural members considered in this study. These materials are concrete, carbon fibers, a cohesive material, and steel reinforcement. Each material was modeled independently considering both elastic and plastic behavior to characterize the real behavior of the materials used. Interfaces between materials were also considered to characterize contacts between their surfaces. Yield and fracture criteria were introduced and defined for the materials used so that the failure of these materials could be characterized more realistically. Moreover, different parts with different geometries were used to represent the various structural elements considered. Therefore, even though some of the parts used had the same material, different behaviors were proposed for the same material to accommodate the representation of these components with the requirements of finite element material modeling. Further details are presented clearly to describe the proposed behaviors and properties of the used materials in this chapter.

#### 2.2. Parts and materials used

Different structural elements were considered in this study. These structural elements or parts were modeled in different ways to provide a suitable characterization of these

elements based on geometrical, material, and functional requirements. Consequently, five different parts were considered to represent the FRP-concrete joint. These parts were the concrete block, a layer or layers of an adhesive, a ply or plies of CFRP, CFRP anchors, and adhesive envelopes for the interface between concrete and the CFRP anchors (see Figures 2.1 and 2.2).

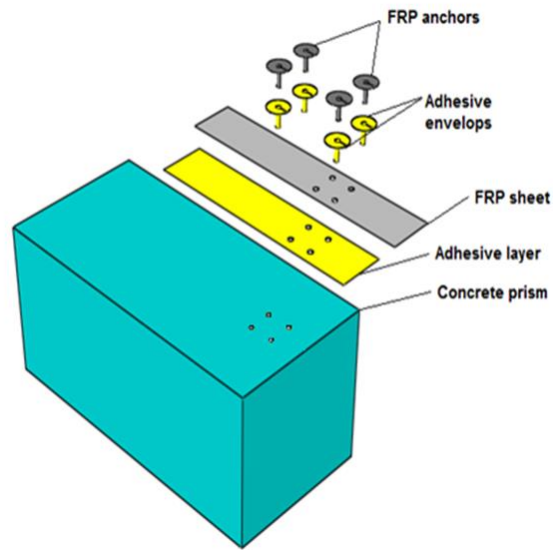


**Figure 2.1: Parts of a CFRP-concrete joint**

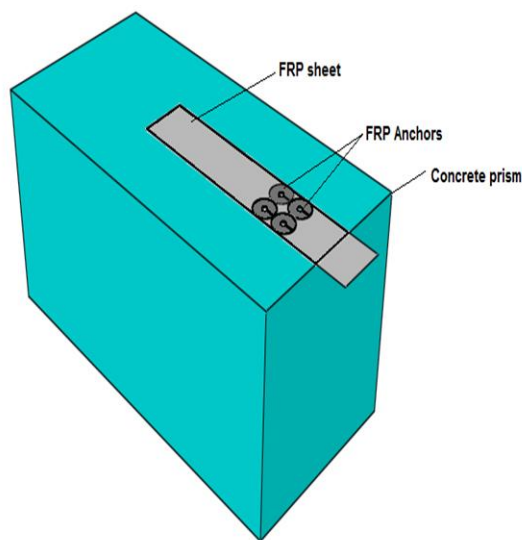


**Figure 2.2: An assembled CFRP-concrete joint**

### **2.3. Modeling of concrete material**

The concrete material was modeled essentially based on the plastic-damage model proposed by Lubliner et al. (Lubliner et al. 1989) and adopted in ABAQUS software (Simulia Abaqus 6.13 2014). This model takes into consideration the representation of both the elastic and plastic behaviors of concrete. The description of the formation and propagation of cracks was based on the model proposed by Hillerborg et al. (Hillerborg et al. 1976). This model depends on both fracture mechanics principals and finite element analysis.

#### **2.3.1 Tensile behavior of concrete**

The plastic-damage model available in ABAQUS software (Simulia Abaqus 6.13 2014) was used to represent the concrete material. The behavior of concrete under the uniaxial tensile stress state consists of two parts; elastic and softening (damage) region. Figure 2.3 shows that concrete under tension was considered linear elastic until the tensile strength  $\sigma_{t0}$  was reached.

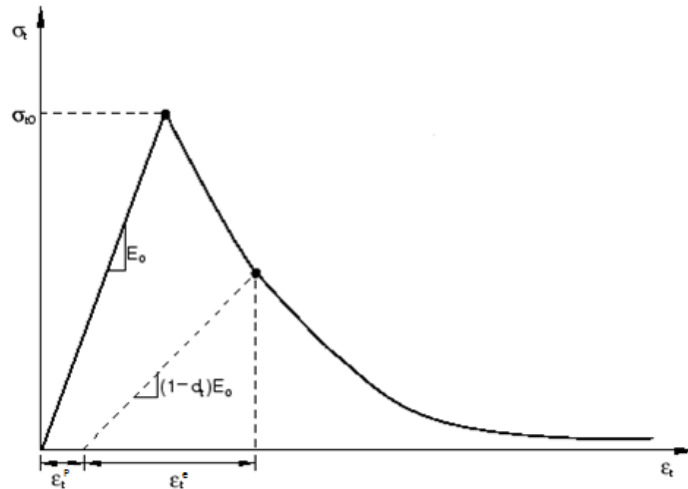




### Figure 2.3: Concrete under uniaxial tensile stress state

(Adapted from Simulia Abaqus 6.13 2014)

The stress-strain relationship within elasticity was based on Hook's law;

$$\sigma = E_o \epsilon \quad (2.1)$$

where  $E_o$  represents the modulus of elasticity,  $\epsilon$  is the strain, and  $\sigma$  denotes the stress in concrete.

The biaxial behavior of concrete was assumed isotropic. Therefore, the constitutive relation for linear elastic concrete in three dimensions was represented by

$$\begin{Bmatrix} \sigma_{11} \\ \sigma_{22} \\ \sigma_{33} \\ \sigma_{12} \\ \sigma_{13} \\ \sigma_{23} \end{Bmatrix} = D_o \begin{Bmatrix} \epsilon_{11} \\ \epsilon_{22} \\ \epsilon_{33} \\ \gamma_{12} \\ \gamma_{13} \\ \gamma_{23} \end{Bmatrix} \quad (2.2)$$

and

$$D_o = \frac{E_o}{(1+\nu)(1-2\nu)} \begin{bmatrix} 1-\nu & \nu & \nu & 0 & 0 & 0 \\ \nu & 1-\nu & \nu & 0 & 0 & 0 \\ \nu & \nu & 1-\nu & 0 & 0 & 0 \\ 0 & 0 & 0 & (1-2\nu)/2 & 0 & 0 \\ 0 & 0 & 0 & 0 & (1-2\nu)/2 & 0 \\ 0 & 0 & 0 & 0 & 0 & (1-2\nu)/2 \end{bmatrix} \quad (2.3)$$

Equation 2.2 represents the general form of all linear elastic isotropic materials. In Equation 2.3,  $\nu$  is poison's ratio, and  $\gamma$  is the shear strain.

The softening part of Figure 2.1 is based on introducing a damage parameter  $d_t$  to the modulus of elasticity  $E_o$ . The value of this parameter varies between zero for undamaged material and one for completely degraded material. Consequently, the loading and unloading behavior of concrete after yielding is affected by this parameter. The reduction of the modulus of elasticity was determined based on the following formula;

$$E = (1 - d_t)E_0 \quad (2.4)$$

Therefore, the stress-strain relationship under uniaxial tension was represented by;

$$\sigma_t = (1 - d_t)E_0(\varepsilon_t - \varepsilon_t^P) \quad (2.5)$$

where  $\varepsilon_t$  is the tensile strain, and  $\varepsilon_t^P$  is the plastic tensile strain.

Similarly, the general three-dimensional stress-strain relationship under tension was represented by substituting  $E_0$  with  $D_0$  of Equation 2.3.

$$\sigma_t = (1 - d_t)D_0(\varepsilon_t - \varepsilon_t^P) \quad (2.6)$$

The damage parameter  $d_t$  in the previous formulas was defined as a function of the damage variable  $\tilde{k}_t$  ( Lubliner et al. 1989, Lee and Fenves 1998). Therefore, Equation 2.6 can be written as;

$$\sigma_t = (1 - d_t(\tilde{k}_t))D_0(\varepsilon_t - \varepsilon_t^P) \quad (2.7)$$

The damage variable  $\tilde{k}_t$  is determined based on the relationship between the tensile stress and the plastic strain of concrete (see Figure (2.4))

$$\tilde{k}_t = \frac{1}{g_t} \int_0^{\varepsilon_t^P} \sigma_{te} d\varepsilon^P \quad (2.8)$$

where  $g_t$  is the “dissipated energy density” in tension and it is equal to  $G_t/l$  and  $G_t$  is the fracture energy and  $l$  is a characteristic length related to the adopted finite element size and represents the width of the damage localization zone (Lubliner et al. 1989).

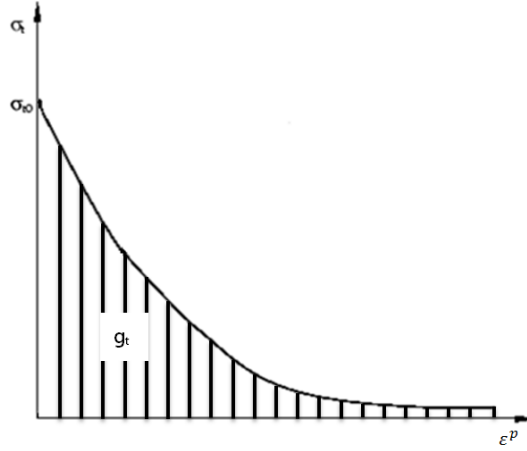


**Figure 2.4: Uniaxial tensile stress-plastic strain curve**

The value of  $g_t$  is determined from the following ( Lubliner et al. 1989, Lee and Fenves 1998);

$$g_t = \frac{\sigma_{t0}}{b_t} \left(1 + \frac{a_t}{2}\right) \quad (2.9)$$

where  $a_t$  and  $b_t$  are dimensionless constants, and  $\sigma_{t0}$  is the initial yield stress.

The value of  $\sigma_{te}$  is determined from

$$\sigma_{te} = \sigma_{t0} [(1 + a_t) \exp(-b_t \varepsilon^P) - a_t \exp(-2b_t \varepsilon^P)] \quad (2.10)$$

The damage parameter  $d_t(k_t)$  is defined as;

$$d_t(\tilde{k}_t) = 1 - \left[ \left(\frac{1}{a_t}\right) (1 + a_t - \sqrt{1 + (2 + a_t) a_t \tilde{k}_t}) \right]^{(n_t/b_t)} \quad (2.11)$$

where  $n_t$  is a constant.

Equation 2.7 can be represented in terms of the “effective cohesion stress”:

$$\sigma_t = (1 - d_t(\tilde{k}_t)) \bar{\sigma}_t \quad (2.12)$$

where  $\bar{\sigma}_t = D_0(\varepsilon_t - \varepsilon_t^P)$  is the effective tensile cohesion stress that identifies the yield surface.

### 2.3.2 Compressive behavior of concrete

The behavior of concrete under uniaxial compression stress state is elastic until reaching the initial yielding stress  $\sigma_{c0}$  (see Figure 2.5). The constitutive relationship is similar to that in tension (see Equation 2.1 and 2.2). Beyond the initial yielding stress, a stress hardening behavior was proposed. The hardening behavior continues until reaching the ultimate stress  $\sigma_{cu}$ . Post the ultimate stress, a softening behavior was considered to characterize the degradation in concrete stiffness. The reduction of the modulus of elasticity was determined based on the following formula;

$$E = (1 - d_c)E_0 \quad (2.13)$$

where  $d_c$  is the damage parameter of the modulus of elasticity  $E_0$  in compression. The value of this parameter varies, similar to that in tension, between zero for undamaged material and one for completely degraded material.

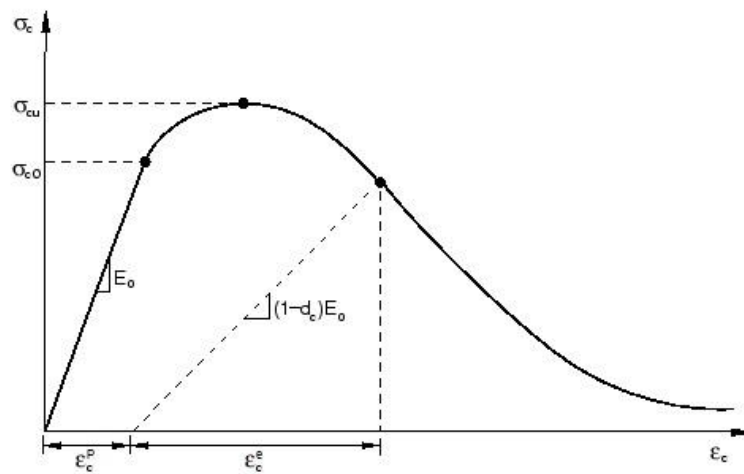


**Figure 2.5: Concrete under uniaxial compressive stress state**

(Adapted from Simulia Abaqus 6.13 2014).

The general stress-strain relationship under uniaxial compression was represented by;

$$\sigma_c = (1 - d_c)E_0(\varepsilon_c - \varepsilon_c^P) \quad (2.14)$$

where  $\varepsilon_c$  is the compressive strain, and  $\varepsilon_c^P$  is the plastic compressive strain.

The general three-dimensional stress-strain relationship under compression was represented by substituting  $E_0$  with  $D_0$  of Equation 2.3.

$$\sigma_c = (1 - d_c)D_0(\varepsilon_c - \varepsilon_c^P) \quad (2.15)$$

The damage parameter  $d_c$  is defined as a function of the damage variable  $k_c$  (Lee and Fenves 1998). Therefore, Equation 2.15 can be written as;

$$\sigma_c = (1 - d_c(\tilde{k}_c))D_0(\varepsilon_c - \varepsilon_c^P) \quad (2.16)$$

The damage variable  $k_c$  is determined based on the relationship between tensile stress and the plastic strain of concrete (see Figure (2.6)).

$$\tilde{k}_c = \frac{1}{g_c} \int_0^{\varepsilon^p} \sigma_{ce} d\varepsilon^P \quad (2.17)$$

where  $g_c$  is the dissipated energy in compression and it is equal to  $G_c/l$ . Here,  $G_c$  is the fracture energy, and  $l$  is the characteristic length.

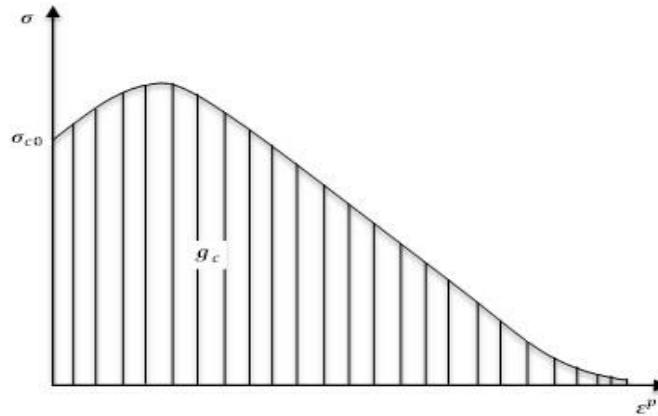


**Figure 2.6: Uniaxial compressive stress-plastic strain curve**

(Lubliner et al. 1989).

The value of  $g_c$  can be determined from the following (Lee and Fenves 1998);

$$g_c = \frac{\sigma_{c0}}{b_c} \left(1 + \frac{a_c}{2}\right) \quad (2.18)$$

where  $a_c$  and  $b_c$  are constants, and  $\sigma_{c0}$  is the initial yield stress.

The value of  $\sigma_{ce}$  is determined from

$$\sigma_{ce} = \sigma_{c0} [(1 + a_c) \exp(-b_c \varepsilon^P) - a_c \exp(-2b_c \varepsilon^P)] \quad (2.19)$$

The damage parameter  $d_c(k_c)$  is defined as;

$$d_c(\tilde{k}_c) = 1 - \left[ \left( \frac{1}{a_c} \right) (1 + a_c - \sqrt{1 + (2 + a_c) a_c \tilde{k}_c}) \right]^{(n_c/b_c)} \quad (2.20)$$

where  $n_t$  is a constant.

Equation 2.16 can be represented in terms of the “effective cohesion stress”:

$$\sigma_c = (1 - d_c(\tilde{k}_c)) \bar{\sigma}_c \quad (2.21)$$

where  $\bar{\sigma}_c = D_0(\varepsilon_c - \varepsilon_c^P)$  is the effective compressive cohesion stress that identifies the yield surface.

### 2.3.3 Damage variable for multiaxial stress condition

The damage variable for multiaxial stress state can be defined based on Equation 2.8 and 2.17 by introducing the following rate Equation (Lubliner et al. 1989).

$$\dot{k} = \frac{r(\sigma)}{g_t} \sigma_t \varepsilon_1^P - \frac{1-r(\sigma)}{g_c} \sigma_c \varepsilon_3^P \quad (2.22)$$

where  $\dot{k}$  is the rate or derivative of  $\tilde{k}$ ,  $\varepsilon_1^P$  is the rate of change in plastic strain in 1-direction,  $\varepsilon_3^P$  is the rate of change in plastic strain in 3- direction,  $r(\sigma)$  is a scale factor that depends on the stress  $\sigma$ .

$$r(\sigma) = \frac{\sum_{i=1}^3 \left( \frac{1}{2} (|\sigma_i| + \sigma_i) \right)}{\sum_{i=1}^3 |\sigma_i|} \quad (2.23)$$

The values of  $r(\sigma)$  in Equation 2.21 vary between 0 for  $\sigma_i \leq 0$  and 1 for  $\sigma_i \geq 0$ .

### 2.3.4 Crack formation and crack propagation

The representation of crack formation and crack propagation is based on the cracking model proposed by Hillerborg et al. (Hillerborg et al. 1976). This model depends on both fracture mechanics principals and finite element analysis. Crack propagation is characterized based on the energy balance approach. This approach assumes that crack propagation occurs when energy released rates (because of cracking) are equal or greater than stored energy that is required to form a crack surface. Consequently, this method permits the use of relatively large elements in the finite element mesh because it depends only on energy balance. In addition, it does not require tiny elements to be close to the crack tip like the stress intensity factor and other approaches in fracture mechanics.

The proposed behavior of this model for the stress-displacement curve after passing the failure stress  $\sigma_{to}$  is linear (see Figure 2.7).

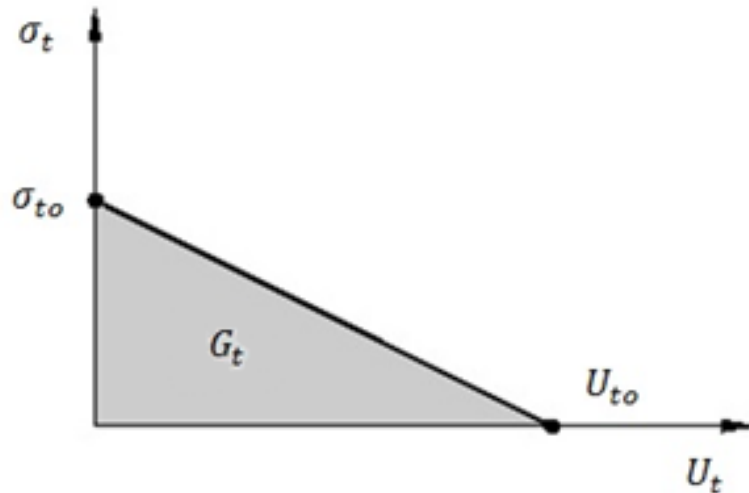


**Figure 2.7: Post failure stress-displacement curve**

(Adapted from Simulia Abaqus 6.13 2014)

The area under the stress-displacement curve of Figure 2.7 represents the fracture energy  $G_t$ . The final displacement  $U_{t0}$  at the complete cracking of concrete where no more strength can be obtained is defined as

$$U_{t0} = 2 G_t / \sigma_{t0} \quad (2.24)$$

### 2.3.5 Stress invariants

Two stress invariants are considered to represent the yield function (Simulia Abaqus 6.13 2014). The first is the hydrostatic stress invariant.

$$\bar{p} = \frac{1}{3}(\bar{\sigma}_1 + \bar{\sigma}_2 + \bar{\sigma}_3) \quad (2.25)$$

The second is the Mises stress invariant.

$$\bar{q} = \sqrt{\frac{3}{2}(\bar{s} : \bar{s})} \quad (2.26)$$

where  $\bar{s} = \bar{\sigma} + \bar{p}I$  is the effective stress deviator,  $I$  is the identity matrix, and  $\bar{\sigma} = D_0(\varepsilon - \varepsilon^P)$  is the effective stress.

### 2.3.6 The flow rule

In the plastic damage model, nonassociated flow rule is considered. The Drucker-Prager hyperbolic function is used to define the potential plastic flow  $G$  (see Figure 2.8).

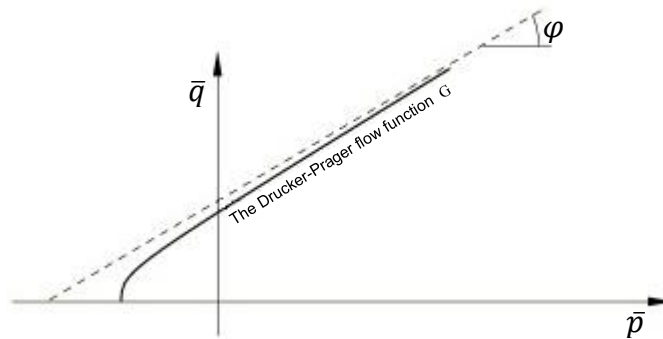




## Figure 2.8: Hyperbolic Drucker-Prager

(Adapted from Simulia Abaqus 6.13 2014)

The potential plastic flow  $G$  is defined as

$$G = \sqrt{(\epsilon \sigma_{t0} \tan \varphi)^2 + \bar{q}^2} - \bar{p} \tan \varphi \quad (2.27)$$

where  $\epsilon$  is the eccentricity parameter that represents the degree of linearity closer of Drucker-Prager function,  $\sigma_{t0}$  is the uniaxial tensile stress at failure, and  $\varphi$  is the dilation angle formed by the yield surface at high confining pressure.

### 2.3.7 Yield condition

The yield condition considered in this study stands in the yield function that was reported in ABAQUS documentation (Simulia Abaqus 6.13 2014). The formulation of the yield condition was based on the proposed model of Lubliner et. al. (Lubliner et al. 1989) and the modifications of Lee and Fenves (Lee and Fenves 1998) (see Figure 2.9).

$$F = \frac{1}{1-\alpha} (\bar{q} - 3\alpha\bar{p} + \beta \epsilon^p \hat{\sigma}_{max} + \gamma \hat{\sigma}_{max}) - \bar{\sigma}_c \epsilon_c^p = 0 \quad (2.28)$$

where,

$$\alpha = \frac{(\sigma_{b0}/\sigma_{c0})-1}{2(\sigma_{b0}/\sigma_{c0})-1} \quad (2.29)$$

$$\beta = \frac{\bar{\sigma}_c}{\bar{\sigma}_t} (1 - \alpha) - (1 + \alpha) \quad (2.30)$$

$$\gamma = \frac{3(1-K_c)}{2K_c-1} \quad (2.31)$$

Here,  $\hat{\sigma}_{\max}$  is the maximum principal effective stress,  $\sigma_{b0}$  is the initial equibiaxial compressive yield stress,  $\sigma_{c0}$  is the initial uniaxial compressive yield stress, and  $K_c = \frac{\sqrt{\bar{q}}_{\text{for } \sigma_1 > \sigma_2 = \sigma_3}}{\sqrt{\bar{q}}_{\text{for } \sigma_1 = \sigma_2 > \sigma_3}}$  for any given value of the hydrostatic stress invariant  $\bar{p}$ . It should be noted that  $K_c$  values vary between 0.5 and 1.0 (see Figure 2.10 for the yield surface corresponding to different values of  $K_c$ ).

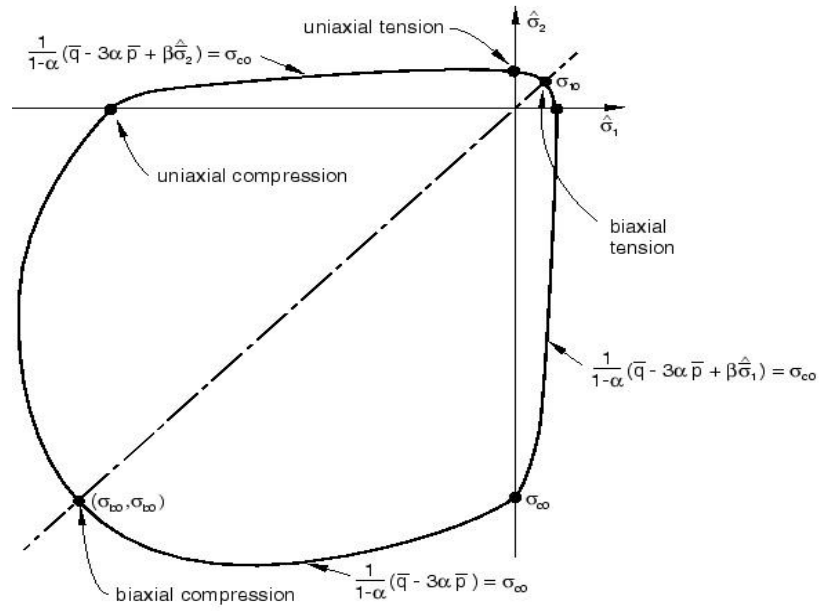


**Figure 2.9: Yield surface in plane stress**

(Simulia Abaqus 6.13 2014)

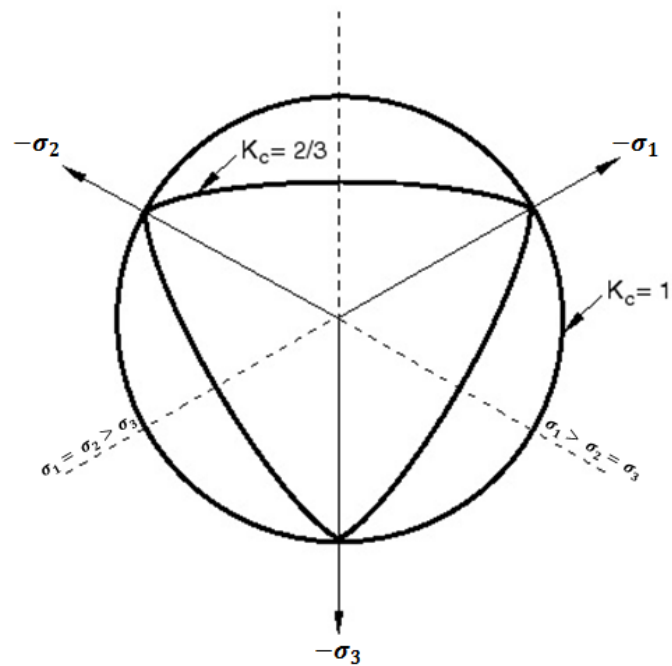


**Figure 2.10: Yield surfaces in the deviatoric plane for different values of  $K_c$**

(Adapted from Simulia Abaqus 6.13 2014)

## 2.4. Modeling of fiber-reinforced polymer material

The general behavior of fiber reinforced polymers is elastic-brittle. Two main regions can be identified in fiber-reinforced composites: fiber and matrix regions. The behaviors of these regions are different since their materials are different. Tensile strength under uniaxial tension along fiber direction depends on the fibers in that direction. On the other hand, compressive strength under uniaxial compression in the direction of fibers does not depend just on the fibers in that direction but also on the stiffness of the matrix (Matzenmiller et al. 1995).

In this research, Hashin model was considered to represent damage and failure of carbon fiber-reinforced composite material. This model is available in ABAQUS software (Simulia Abaqus 6.13 2014) and based on the progressive work of different researchers (Hashin and Rotem 1973b) (Z Hashin 1980) (Matzenmiller et al. 1995) (Camanho and Dávila 2002). This module describes the behavior of fiber-reinforced composites in three stages: undamaged, damage initiation and damage evolution stages.

### 2.4.1 Undamaged stage

The strain-stress relationships of Fiber-reinforced polymer are based on considering the moduli of elasticity, poison's ratios and the shear moduli in the three principal directions.

$$\begin{Bmatrix} \varepsilon_{11} \\ \varepsilon_{22} \\ \varepsilon_{33} \\ \gamma_{12} \\ \gamma_{13} \\ \gamma_{23} \end{Bmatrix} = \begin{bmatrix} 1/E_1 & -v_{21}/E_2 & -v_{31}/E_3 & 0 & 0 & 0 \\ -v_{12}/E_1 & 1/E_2 & -v_{32}/E_3 & 0 & 0 & 0 \\ -v_{13}/E_1 & -v_{23}/E_2 & 1/E_3 & 0 & 0 & 0 \\ 0 & 0 & 0 & 1/G_{12} & 0 & 0 \\ 0 & 0 & 0 & 0 & 1/G_{13} & 0 \\ 0 & 0 & 0 & 0 & 0 & 1/G_{23} \end{bmatrix} \begin{Bmatrix} \sigma_{11} \\ \sigma_{22} \\ \sigma_{33} \\ \sigma_{12} \\ \sigma_{13} \\ \sigma_{23} \end{Bmatrix} \quad (2.32)$$

However, an elastic-orthotropic behavior in-plane stress will be used in the following formulation to simplify the description of the general modeling theory.

Therefore,

$$\begin{Bmatrix} \sigma_{11} \\ \sigma_{22} \\ \tau_{12} \end{Bmatrix} = \frac{1}{1-\nu_{12}\nu_{21}} \begin{bmatrix} E_1 & \nu_{21}E_1 & 0 \\ \nu_{12}E_2 & E_2 & 0 \\ 0 & 0 & G_{12} \end{bmatrix} \begin{Bmatrix} \varepsilon_1 \\ \varepsilon_2 \\ \gamma_{12} \end{Bmatrix} \quad (2.33)$$

#### 2.4.2 Damage initiation stage

In fiber-reinforced composites, damage initiation occurs in either the reinforcement fibers or the matrix of the composite lamina or both together. The studies of Hashin and Rotem (Hashin and Rotem 1973b) and Hashin (Z Hashin 1980) introduced four failure mechanisms to represent damage behavior. These failure mechanisms are fiber tension, fiber compression, matrix tension, and matrix compression. All these failure criteria are considered in ABAQUS software (Simulia Abaqus 6.13 2014) to represent the damage initiation stage of fiber reinforced composites.

In tension, the tensile strength of the composite lamina is affected mainly by the strength of fibers because of the high strength of the reinforcement fibers compared to the surrounding matrix. Consequently, damage initiates when the damage initiation variable  $F_f^t$  reaches and exceeds a value of one.

$$F_f^t = \left(\frac{\bar{\sigma}_{11}}{X^T}\right)^2 + \alpha \left(\frac{\bar{\tau}_{12}}{S^L}\right)^2 \quad \text{when } \bar{\sigma}_{11} \geq 0 \quad (2.34)$$

Where  $X^T$  is the longitudinal tensile strength,  $S^L$  is the longitudinal shear strength and  $\alpha$  is a coefficient for shear stress contribution.

In compression, fibers suffer buckling and kinking. Therefore, transverse tensile stresses are generated due to the effect of the difference in Poisson's ratios of the fibers and the matrix (Hahn and Williams 1984) (Matzenmiller et al. 1995). In general, damage

initiation in fibers can be detected when the value of the variable  $F_f^c$  reaches and exceeds a value of one.

$$F_f^c = \left( \frac{\bar{\sigma}_{11}}{X^c} \right)^2 \quad \text{when} \quad \bar{\sigma}_{11} < 0 \quad (2.35)$$

where  $X^c$  is the longitudinal compressive strength.

Other failure modes (mechanisms) in tension and compression can be observed in the matrix region of the composite lamina. These failure modes are governed by the longitudinal and transverse shear strengths as well as the transverse tensile and compressive strengths. Similar to the damage initiation in fibers, two damage variables are used to detect the initiation of damage in the matrix region. These variables ( $F_m^t$  and  $F_m^c$ ) indicate damage initiation if they reach and exceed a value of one.

$$F_m^t = \left( \frac{\bar{\sigma}_{22}}{Y^T} \right)^2 + \left( \frac{\bar{\tau}_{12}}{S^L} \right)^2 \quad \text{when} \quad \bar{\sigma}_{22} \geq 0 \quad (2.36)$$

For the matrix in tension and

$$F_m^c = \left( \frac{\bar{\sigma}_{22}}{2S^T} \right)^2 + \left[ \left( \frac{Y^c}{2S^T} \right)^2 - 1 \right] \frac{\bar{\sigma}_{22}}{Y^c} + \left( \frac{\bar{\tau}_{12}}{S^L} \right)^2 \quad \text{when} \quad \bar{\sigma}_{22} < 0 \quad (2.37)$$

For the matrix in compression.

Here,  $Y^T$  and  $Y^c$  is the transverse tensile and compressive strengths respectively, and  $S^T$  is the transverse shear strength.

The effective stress tensor can be calculated from

$$\begin{Bmatrix} \bar{\sigma}_{11} \\ \bar{\sigma}_{22} \\ \bar{\tau}_{12} \end{Bmatrix} = \begin{bmatrix} \frac{1}{(1-d_f)} & 0 & 0 \\ 0 & \frac{1}{(1-d_m)} & 0 \\ 0 & 0 & \frac{1}{(1-d_s)} \end{bmatrix} \begin{Bmatrix} \sigma_{11} \\ \sigma_{22} \\ \tau_{12} \end{Bmatrix} \quad (2.38)$$

where  $d_f$  and  $d_m$  are damage variables related to the effective normal stress for fibers and matrix respectively.  $d_s$  is a damage variable related to the effective shear stress. It should be noted that the behavior of the first two parameters differs in tension compared to compression.

### 2.4.3 Damage evolution stage

Post the initiation of damage, the damage evolution stage can be characterized by introducing the damage variables  $d_f$ ,  $d_m$ , and  $d_s$  to the stress- strain relationship defined in 2.31.

$$\begin{Bmatrix} \sigma_{11} \\ \sigma_{22} \\ \tau_{12} \end{Bmatrix} = \frac{1}{D} \begin{bmatrix} (1-d_f)E_1 & (1-d_f)(1-d_m)v_{21}E_1 & 0 \\ (1-d_f)(1-d_m)v_{12}E_2 & (1-d_m)E_2 & 0 \\ 0 & 0 & (1-d_s)DG_{12} \end{bmatrix} \begin{Bmatrix} \varepsilon_1 \\ \varepsilon_2 \\ \gamma_{12} \end{Bmatrix} \quad (2.39)$$

where  $D = 1 - (1 - d_f)(1 - d_m)v_{12}v_{21}$ .

Each damage variable was calculated based on the following general relationship that is considered in ABAQUS software;

$$d = \frac{\delta_{eq}^f(\delta_{eq} - \delta_{eq}^0)}{\delta_{eq}(\delta_{eq}^f - \delta_{eq}^0)} \quad (2.40)$$

Here,  $\delta_{eq}^0$  is the equivalent displacement where damage starts to initiate, and  $\delta_{eq}^f$  is the equivalent displacement where complete damage of the material is reached (see Figures 2.11 and 2.12).

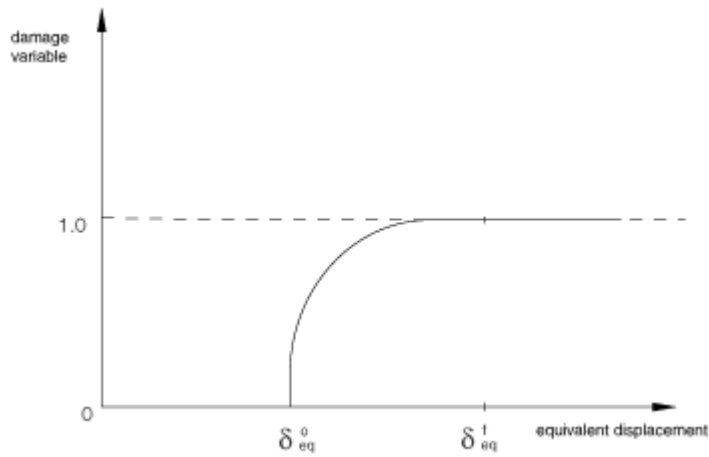


**Figure 2.11: Damage variable as a function of equivalent displacement**

(Simulia Abaqus 6.13 2014)

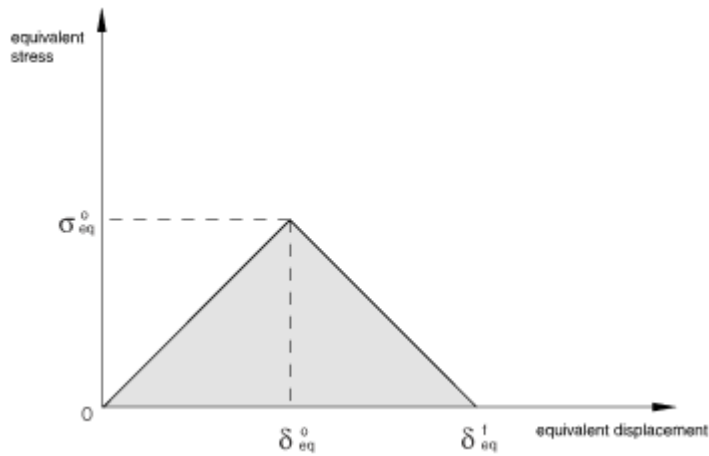


**Figure 2.12: Equivalent stress versus equivalent displacement**

(Simulia Abaqus 6.13 2014)

The values of the equivalent displacement are calculated by ABAQUS through involving a characteristic length in the formulation to reduce the effect of mesh dependency. This characteristic length depends on the type of element used (Simulia Abaqus 6.13 2014).



## 2.5. Modeling of adhesive material

The constitutive relationships that describe the behavior of the cohesive material considered in this research were based on the traction-separation model that is available in ABAQUS software. This model is more appropriate for modeling the cases that thin layers of the adhesive are used. Therefore, the traction-separation model is adopted here to characterize the behavior of the thin layer of the adhesive between the concrete and the fiber reinforced polymer sheet.

The traction-separation model proposes three stages of material behavior: a linear elastic stage, a damage initiation stage, and a damage evolution stage.

### 2.5.1 Linear elastic stage of adhesive material

ABAQUS software (Simulia Abaqus 6.13 2014) provides both coupled and uncoupled traction-separation modeling options. The coupled traction-separation model represents the general case where all stiffness components are included in the stiffness matrix.

$$\begin{Bmatrix} t_n \\ t_s \\ t_s \end{Bmatrix} = \begin{bmatrix} E_{nn} & E_{ns} & E_{nt} \\ E_{ns} & E_{ss} & E_{st} \\ E_{nt} & E_{st} & E_{tt} \end{bmatrix} \begin{Bmatrix} \varepsilon_n \\ \varepsilon_s \\ \varepsilon_t \end{Bmatrix} \quad (2.41)$$

On the other hand, the uncoupled traction-separation stiffness matrix consists only of the diagonal stiffness components while other stiffness components are zero.

$$\begin{Bmatrix} t_n \\ t_s \\ t_s \end{Bmatrix} = \begin{bmatrix} E_{nn} & 0 & 0 \\ 0 & E_{ss} & 0 \\ 0 & 0 & E_{tt} \end{bmatrix} \begin{Bmatrix} \varepsilon_n \\ \varepsilon_s \\ \varepsilon_t \end{Bmatrix} \quad (2.42)$$

The argument for considering coupled or uncoupled traction-separation law was discussed in (Liu et al. 2014). The uncoupled traction-separation was considered sufficient to achieve accuracy based on the studies referenced in (Liu et al. 2014);

therefore, the relationship described in Equation 2.42 was used in this research. In Equation 2.42, each diagonal component of the stiffness matrix should not be zero to satisfy stability.

### 2.5.2 Damage initiation stage of adhesive material

Many methods are available in ABAQUS software to define damage initiation. One of these, the maximum nominal strain criterion, will be used to model damage initiation of the adhesive in this research. This model assumes the initiation of damage when the maximum nominal strain ratio reaches a value of one.

$$\max \left\{ \frac{\varepsilon_n}{\varepsilon_n^o}, \frac{\varepsilon_s}{\varepsilon_s^o}, \frac{\varepsilon_t}{\varepsilon_t^o} \right\} = 1 \quad (2.43)$$

where  $\varepsilon_n^o$  is the maximum nominal strain normal to the interface that is greater than or equal to zero,  $\varepsilon_s^o$  is the maximum nominal strain in the longitudinal direction, and  $\varepsilon_t^o$  is the maximum nominal strain in the transverse direction.

### 2.5.3 Damage evolution stage of cohesive material

Camanho and Dávila (Camanho and Dávila 2002) reported a formulation for a linear model to represent the damage evolution stage of the cohesive material. This model is available in ABAQUS software and it is based on introducing a damage variable  $D$  to the traction-separation law (see Figure 2.13).

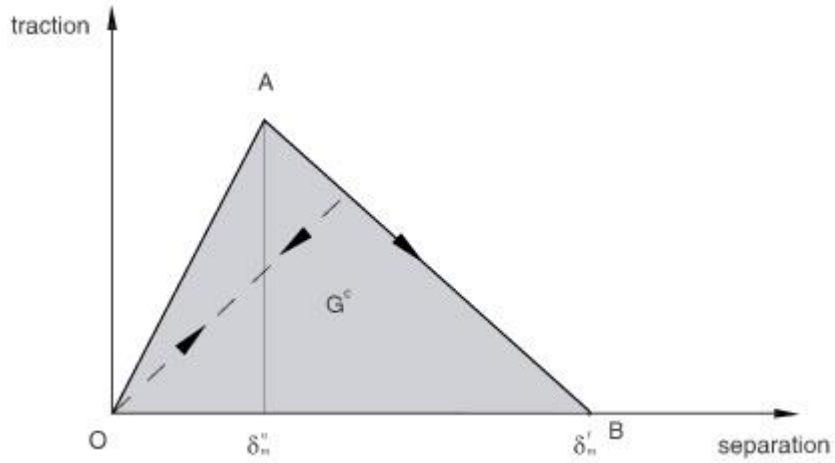


**Figure 2.13: Linear damage model**

(Simulia Abaqus 6.13 2014)

The damage variable values vary between one and zero and it can be calculated as follows:

$$D = \frac{\delta_m^f (\delta_m^{max} - \delta_m^o)}{\delta_m^{max} (\delta_m^f - \delta_m^o)} \quad (2.44)$$

where  $\delta_m^o$  is the separation value when the maximum traction value is reached,  $\delta_m^f$  is the final separation value before losing strength entirely, and  $\delta_m^{max}$  the maximum value of the effective displacement.

The general value of  $\delta_m$  can be represented by;

$$\delta_m = \sqrt{\delta_n^2 + \delta_s^2 + \delta_t^2} \quad (2.45)$$

where  $\delta_n$  is the separation normal to the interface that is greater than or equal to zero,  $\delta_s$  is the separation in the longitudinal direction, and  $\delta_t$  is the separation in the transverse direction.

The traction values are calculated considering the introduced damage variable.

$$t_n = (1 - D)\bar{t}_n \quad (2.46)$$

$$t_s = (1 - D)\bar{t}_s \quad (2.47)$$

$$t_t = (1 - D)\bar{t}_t \quad (2.48)$$

where  $\bar{t}_n$ ,  $\bar{t}_s$ , and  $\bar{t}_t$  are the stress components before damage.

It should be noted that the damage variable in Equation (2.46) is used only when  $\bar{t}_n$  is greater than or equal to zero. The reason is that no damage is assumed by this model under compression in the normal direction to the interface.

## CHAPTER 3

### FRP-CONCRETE SYSTEM: FINITE ELEMENT MODELING

#### 3.1. Introduction

From its early beginnings, the finite element method has approved its usefulness in getting approximated solutions for different engineering problems. Its ability to solve complex problems that have very complicated geometries, boundary conditions, and loading make it suitable in substituting full-scale experimental tests with inexpensive numerical modeling. The continuous progress in studying and exploring the behavior of different materials under various types of excitations helped to improve finite element results significantly. One of the aspects that finite element analysis has greatly contributed to is the field of composite materials and hybrid sections. This contribution belongs to the ability of the finite element analysis to represent the complicated behavior of the interface between the different materials. In this research, ABAQUS finite element software was used to study the behavior of anchored fiber-reinforced polymer sheets. Different finite element methods were used to describe the different materials and the geometric parts that were considered in this study. The purpose of the diversity of the finite element methods is to get a better and more realistic solution of the problem under investigation. However, great calibration effort is needed to overcome the approximated nature of the finite element solution.

#### 3.2. Finite element modeling of CFRP-concrete joints

The finite element modeling of CFRP-Concrete joints conducted in this study was based on categorizing the different components that form these joints based on the different materials, geometrical shapes and functional roles of each part or component.

Five different parts were considered to represent each joint. These parts are the concrete part, the CFRP sheet, the adhesive layer, the CFRP anchor, and the adhesive envelope around the anchor (see Figures 2.1 and 2.2 in chapter 2).

### 3.2.1 Finite element modeling of the concrete

Three-dimensional solid hexahedral elements were used to model the concrete part. Each brick element has 8 nodes and is based on the linear interpolation concept (first-order interpolation). Furthermore, a reduced integration scheme with hourglass control was used to overcome shear locking and avoid possible distortion of the elements. In this study, the concrete substrate consists of a concrete block with or without the cylindrical holes for the CFRP anchors (see Figure 3.1). The concrete block is supported as shown in Figure 1.1 to prevent rigid body motion.

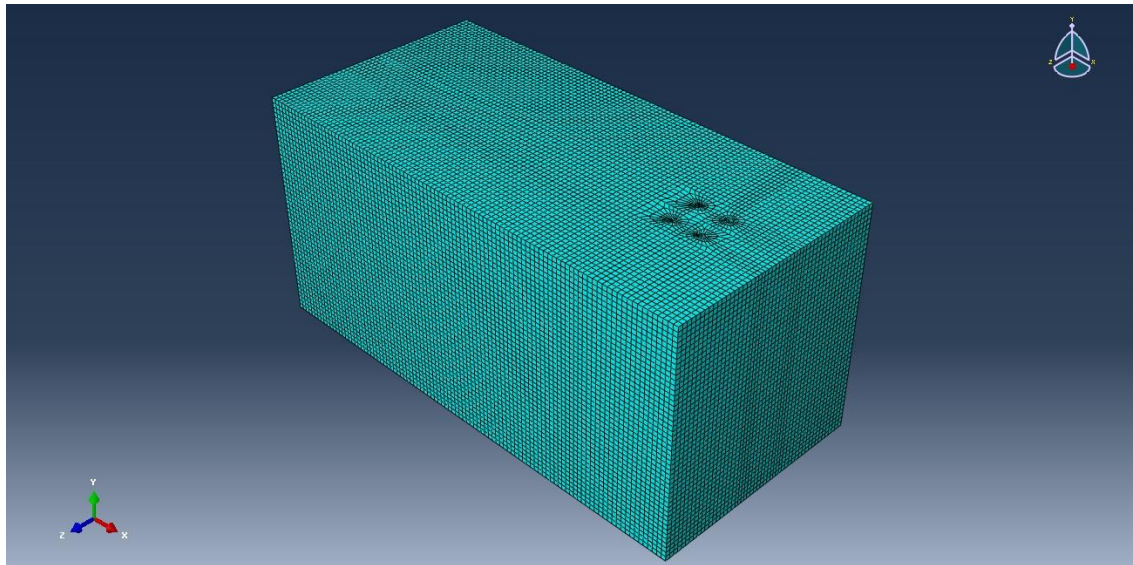


**Figure 3.1: A concrete block with four holes for the CFRP anchors**

### 3.2.2 Finite element modeling of the CFRP sheet

The CFRP sheet has been modeled using 8-node hexahedron continuum-shell elements. For this type of elements, distortion is expected because of the high aspect ratio.

Therefore, the reduced integration scheme with hourglass control is considered in ABAQUS software by default for this type of elements (see Figure 3.2).

Regarding the constitutive response, ABAQUS provides Hashin damage model for defining the behavior of these elements (see section 2.4).

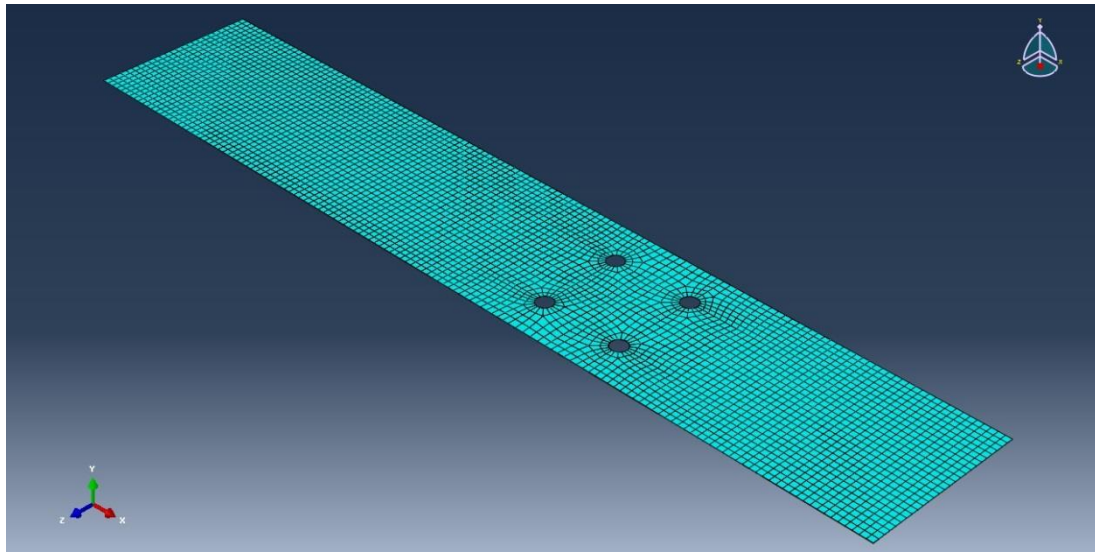


**Figure 3.2: A CFRP sheet with four holes for the CFRP anchors.**

### **3.2.3 Finite element modeling of the adhesive layer**

The adhesive material between the concrete and the CFRP was modeled using cohesive elements available in ABAQUS finite element software. These elements are useful in representing interfaces of composites and adhesive joints (see Figure 3.3). Assuming a thin layer of the adhesive at the bonded interface, the constitutive response of the cohesive zone was defined based on the traction-separation model (see section 2.5).

Based on the built-in algorithms of ABAQUS, cohesive elements can be connected to other components by sharing nodes with other elements, by using surface-based tie constraints, or by using contact interactions between cohesive elements and the other components.

When the cohesive elements and their neighboring parts have matched meshes, sharing nodes is possible. In this case, it is better to refine the cohesive elements more than the surrounding elements by creating more nodes in the thickness direction of the cohesive layer (see Figure 3.4).

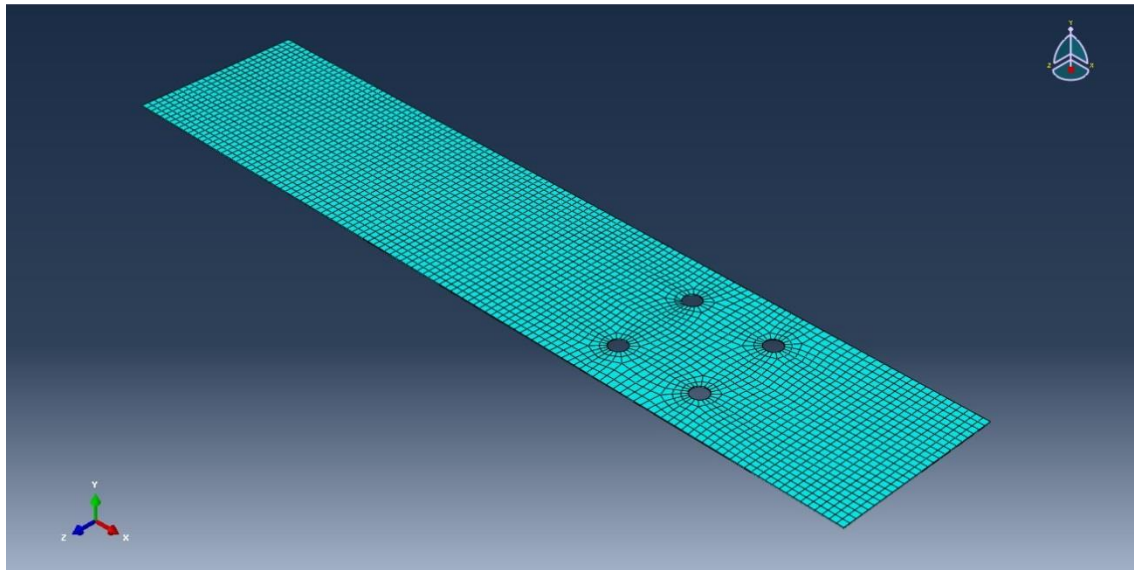


**Figure 3.3: An adhesive layer with four holes for the CFRP anchors.**

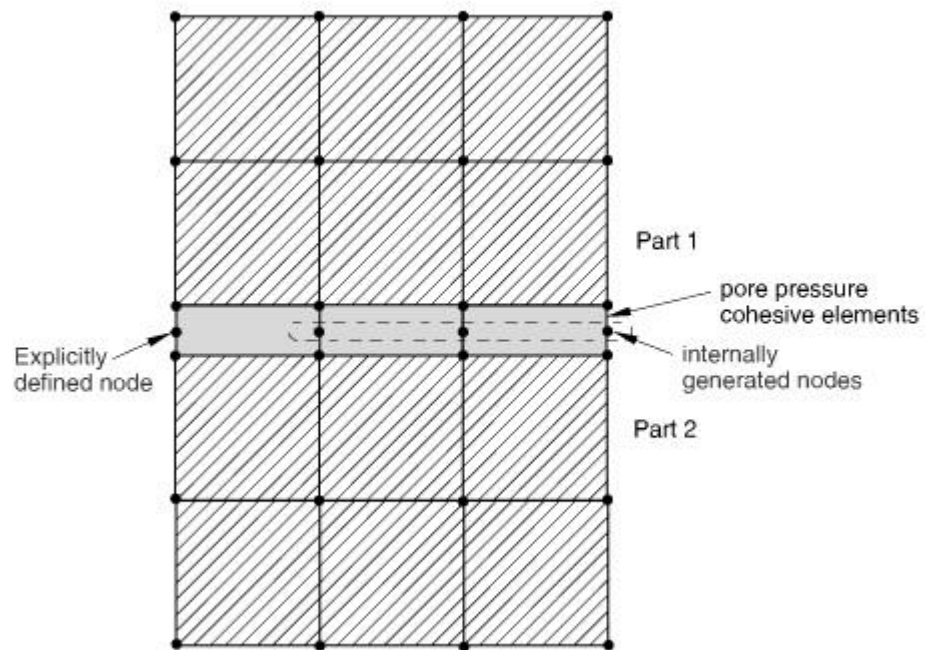




**Figure 3.4: Cohesive elements sharing nodes with elements of other components.**

(Simulia Abaqus 6.13 2014)

In the cases where meshes do not match, tie constraints can be used to connect surfaces of cohesive elements to surrounding elements of other parts. Consequently, tie constraints help in making changes in mesh density within the model without needing any mesh matching (see Figure 3.5).

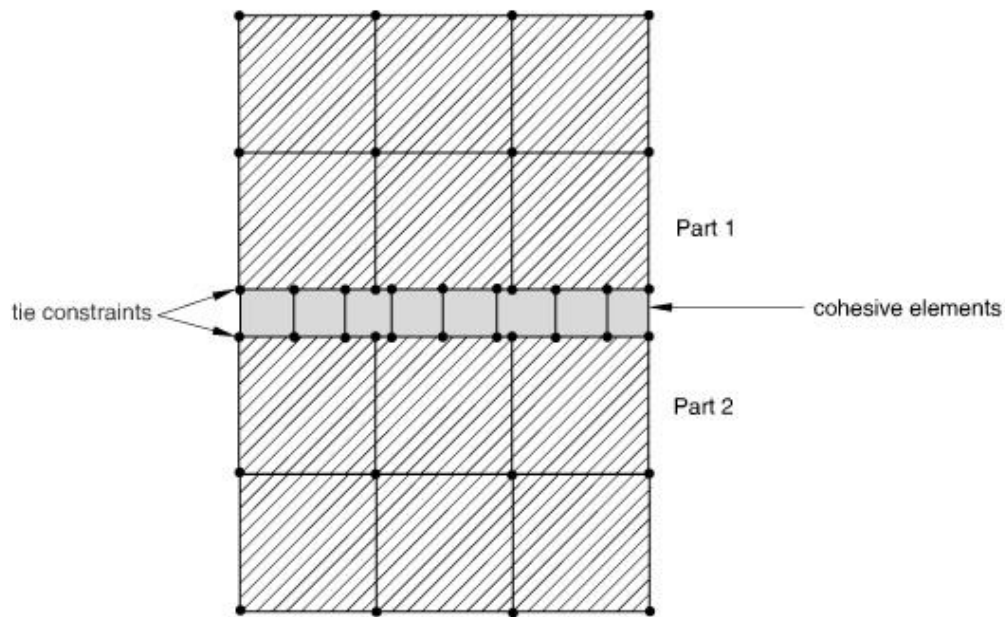


**Figure 3.5: Tie constraints connect surfaces of cohesive elements to surrounding elements of other parts**

(Simulia Abaqus 6.13 2014)

Another technique to connect cohesive elements to the surrounding components is the method of contact interactions. This method includes connecting surfaces of cohesive elements to surfaces of other components by creating surface-to-surface interactions (see Figure 3.6).

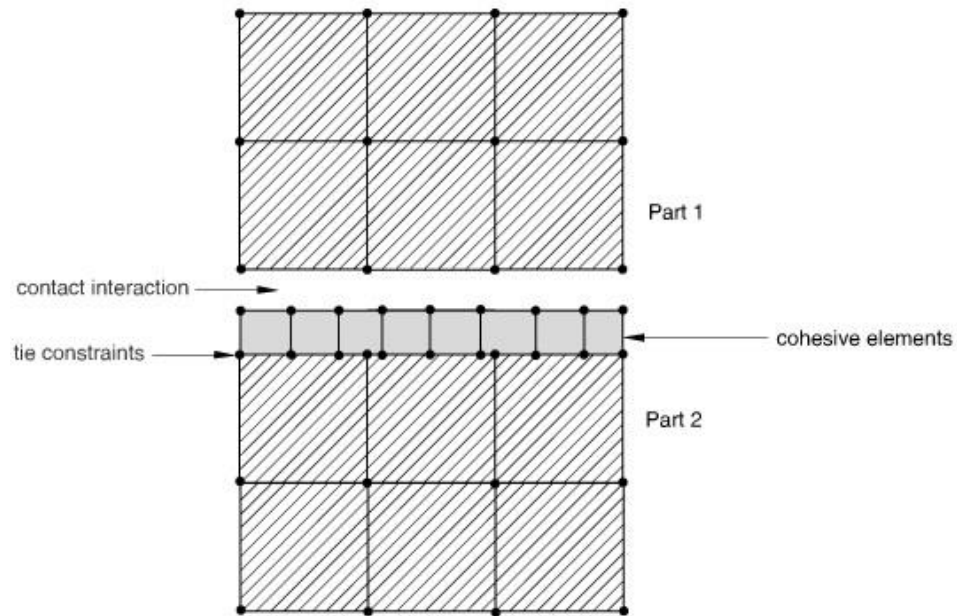


**Figure 3.6: Contact interactions to connect cohesive elements to the surrounding components**

(Simulia Abaqus 6.13 2014)

In this study, all the previously mentioned methods are used to achieve an accurate connection between cohesive elements and other elements of the other parts.

### 3.2.4 Finite element modeling of the CFRP Anchor

CFRP anchors are used in the CFRP – concrete joints to provide more fixity to the CFRP sheet. Different from the CFRP sheet, three-dimensional solid hexahedral elements were used to model the CFRP anchor (see Figure 3.7). Each brick element has 8 nodes and is based on the linear interpolation concept (first-order interpolation). The constitutive behavior of these elements was based on the plasticity model in conjunction with the potential option available in ABAQUS to define stress ratios for anisotropic

yield. Material orientations were also defined to illustrate local fiber directions of the CFRP anchors.

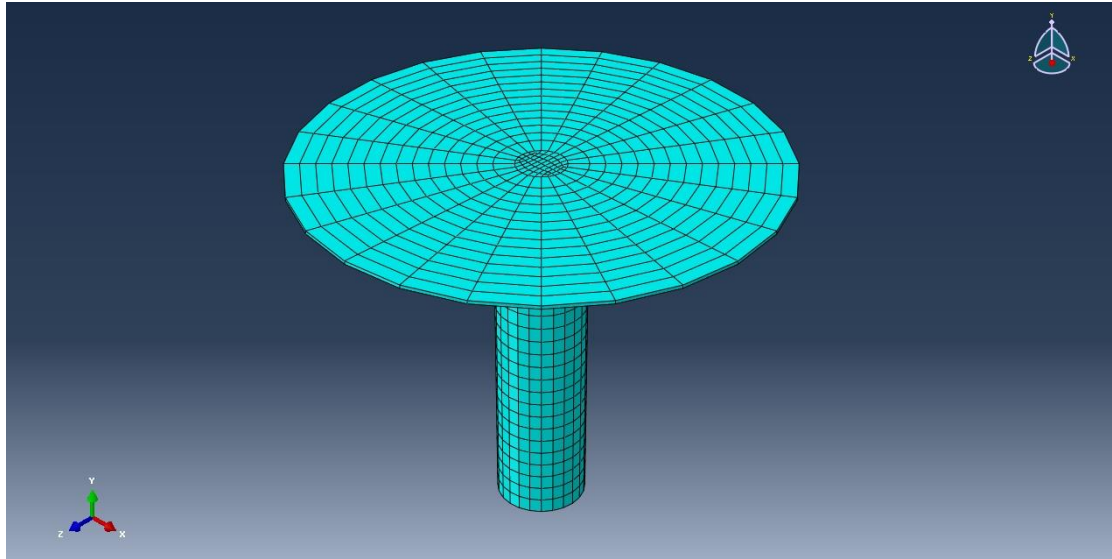


**Figure 3.7: Three-dimensional solid hexahedral elements used to model a CFRP anchor.**

### **3.2.5 Finite element modeling of the adhesive envelope around the anchor**

The adhesive layer that forms an envelope around each anchor and connects the anchors to the concrete was modeled using three-dimensional solid hexahedral elements (see Figure 3.8). This approach is different from the modeling approach of the adhesive layer between the CFRP sheet and the concrete since more complicated geometry is involved in this part. Therefore, 8-node first-order brick elements were used to model the adhesive envelopes around the anchors. The constitutive response of these elements was similar to that defined in section 2.5. However, the quadratic nominal strain criterion has been considered to model the damage initiation of the adhesive envelope rather than the maximum nominal strain criterion that is described in section 2.5 to model the adhesive layer.

The quadratic nominal strain criterion assumes initiation of damage when a quadratic function of the nominal strain ratios reaches a value of one.

$$\left\{ \frac{\varepsilon_n}{\varepsilon_n^0} \right\}^2 + \left\{ \frac{\varepsilon_s}{\varepsilon_s^0} \right\}^2 + \left\{ \frac{\varepsilon_t}{\varepsilon_t^0} \right\}^2 = 1 \quad (3.1)$$

where  $\varepsilon_n^0$  is the maximum nominal strain normal to the interface that is greater than or equal to zero,  $\varepsilon_s^0$  is the maximum nominal strain in the longitudinal direction, and  $\varepsilon_t^0$  is the maximum nominal strain in the transverse direction.

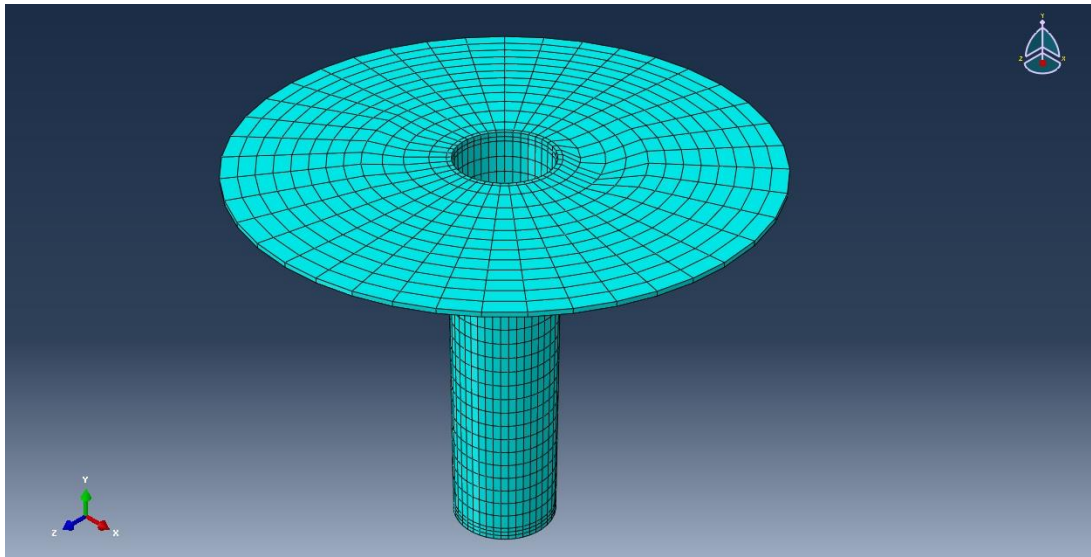


**Figure 3.8: The adhesive envelope used around each CFRP anchor.**

### 3.3. Analysis procedure

In this research, static, implicit quasi-static, and explicit quasi-static analysis procedures were examined to look into the method that provides the best results with the minimum computational cost. Static analysis procedure solves the following formula;

$$F_{t+\Delta t} = K_{t+\Delta t} \cdot U_{t+\Delta t} \quad (3.2)$$

Where  $F$ ,  $K$ , and  $U$  are the force, stiffness, and displacement of the system. Here, the displacement is unknown at  $t+\Delta t$  and it is determined from;

$$U_{t+\Delta t} = U_t + \Delta U \quad , \text{ and } \quad \Delta U = K^{-1} \cdot (F - I)_{t+\Delta t}$$

Where  $I$  is the internal force determined from  $I = \int B^T K_t B \, dU$ , and  $B$  is the strain – displacement matrix.

The static analysis procedure was able to capture deformations of the CFRP sheet to the point where the first debonding occurred. After that point, no more convergence has been obtained because of losing elastic stability. The loss of elastic stability belongs to the generation of large deformations and oscillations (snapping and buckling) that leads to singularity problems. Singularity problems can be described as the creation of singular points at the locations that affect the undeformed state of the structure (the boundaries of the CFRP sheet in this case) (more details can be found in Riks, 1979, Gao and Bower, 2004 Matouš and Maniatty, 2004, Lu, Ye, Teng, and Jiang, 2005, Ten Thije, Akkerman, and Huétink, 2007 and Simulia Abaqus 6.13, 2014). Consequently, the captured load-deformation history was limited within the elastic range of the problem between the beginning of loading and the instant of the first debonding.

To study the behavior of the CFRP anchors that are placed at relatively distant locations, it is important to have a complete debonding propagation of the CFRP sheet and a complete load-deformation history. Therefore, an implicit quasi-static analysis scheme was tested as an alternative to the static analysis method.

Implicit analysis solves the following formula;

$$F_{t+\Delta t} = (K \cdot U + C \cdot \dot{U} + M \cdot \ddot{U})_{t+\Delta t} \quad (3.2)$$

Where  $C$ ,  $M$ ,  $\dot{U}$  and  $\ddot{U}$  are the damping, mass, velocity and acceleration of the system.

Here, the displacement is unknown at  $t+\Delta t$  and it is determined by inverting the stiffness matrix as in the static analysis.

The results obtained from performing implicit quasi-static analysis were better than the previous outcomes of the static analysis. A complete debonding propagation was achieved with a complete load-deformation history. However, this analysis procedure is expensive in terms of computational time, especially when using large numbers of elements (dense mesh) to represent the interfaces of the CFRP-concrete joint. Hence, modeling full-scale models based on this approach seems impossible regarding the required computational resources.

The next alternative to be examined for its computational efficiency compared to the previously tested methods was the explicit quasi-static analysis scheme. In terms of the computational efficiency, the explicit method is more efficient than the implicit quasi-static scheme since the later requires doing iterations for force equilibrium at each loading increment and update the stiffness matrix. Therefore, convergence checking is needed for each iteration. On the contrary, the explicit quasi-static analysis procedure requires no iterations within the increments. In addition, the stiffness matrix is updated once at the end of each increment. Therefore, no convergence checking is required within load increments. The explicit analysis procedure solves the following formula;

$$F_{t+\Delta t} = (K \cdot U + C \cdot \dot{U} + M \cdot \ddot{U})_{t+\Delta t} \quad (3.2)$$

Here, the displacement is known at  $t+\Delta t$  since it is determined by integrating the acceleration using the central difference method to get the velocity and then the velocity

is integrated to get the displacement; therefore, no need to invert the stiffness matrix as in the previous examined methods.

The results obtained from performing explicit quasi-static analysis were better than the static and implicit analysis results (see chapter four for the obtained results). A complete debonding propagation was achieved using large numbers of elements (dense mesh) to represent the interfaces of the CFRP-concrete joint. Furthermore, the computational time was more reasonable compared to the other methods. Accordingly, modeling full-scale debonding problems using the explicit quasi-static analysis procedure is possible.

## **CHAPTER 4**

### **FRP-CONCRETE SYSTEM: VERIFICATION OF THE PROPOSED MODEL**

#### **4.1 Calibration and verification process**

The behavior of FRP-concrete joints has been studied for many years to investigate all factors that affect this type of structural strengthening. Both experimental results and computer modeling have provided a great deal of information about this behavior. However, some material and dimensional parameters are still hard to measure, which makes it difficult to achieve high accuracy. These uncertain parameters create a great challenge especially when trying to create a model that represents sensitive experimental results. The recent development in computer modeling creates another challenge since new modeling programs require many parameters that might be difficult to measure. This difficulty in quantifying parameters comes from requiring expensive testing machines or performing complicated procedures to measure these quantities. Therefore, many calibration processes are required to identify unknown parameters and validate proposed models. In addition, the calibrated models should be verified by comparing them with experimental results.

Two stages were adopted to verify the proposed model in this research. The first stage includes replicating three experimental specimens of CFRP-concrete joints without anchors, which were reported in the literature, based on the proposed model. Then, the results of the finite element analysis were compared with the experimental results from the literature.



The second verification stage includes introducing CFRP anchors to the previously calibrated and validated model and comparing the results with the experimental outcomes of a correspondent anchored specimen in the literature.

#### 4.2 CFRP-concrete joints without anchors

Three experimental specimens of CFRP-concrete joints without anchors were replicated to verify the proposed modeling. The first specimen was analyzed based on the modeling approach described in (Obaidat et al. 2013). This modeling is based on determining the initial stiffness, fracture energy, and shear strength of the interface between the CFRP sheet and concrete by introducing the tensile strength of concrete and shear strength of the interface to previously calibrated formulas in the literature (Obaidat et al. 2013). These formulas are:

$$K = 0.16 \frac{G_a}{t_a} + 0.47 \quad (4.1)$$

$$G_F = 0.52 f_{ct}^{0.26} G_a^{-0.23} \quad (4.2)$$

$$\tau_{max} = 1.46 f_{ct}^{1.033} G_a^{0.165} \quad (4.3)$$

Where  $K$  is the initial stiffness,  $G_F$  is the fracture energy,  $\tau_{max}$  is the shear strength of the interface,  $G_a$  is the shear modulus of the adhesive,  $t_a$  is the thickness of the adhesive, and  $f_{ct}$  is the concrete tensile strength.

This method does not consider the adhesive layer as an explicit interfacial part of the model. Rather, a quadratic interaction function was utilized to represent the damage initiation of the interface. Therefore, the model consists of concrete and CFRP sheet parts only.

The quadratic nominal stress criterion assumes initiation of damage when a quadratic function of the nominal stress ratios reaches a value of one (Simulia Abaqus 6.13 2014).

$$\left\{\frac{\tau_n}{\tau_n^o}\right\}^2 + \left\{\frac{\tau_s}{\tau_s^o}\right\}^2 + \left\{\frac{\tau_t}{\tau_t^o}\right\}^2 = 1 \quad (4.4)$$

Where  $\tau_n^o$  is the maximum nominal stress normal to the interface that is greater than or equal to zero,  $\tau_s^o$  is the maximum nominal stress in the longitudinal direction, and  $\tau_t^o$  is the maximum nominal stress in the transverse direction.

As shown in Equations 4.1 to 4.3, the properties of the interface were mainly controlled by the tensile strength of concrete and the shear stiffness of the cohesive material.

The CFRP sheet was considered as an elastic isotropic material since no failure was assumed to occur in it. Table 4.1 shows the details of an experimental specimen tested by (Mazzotti et al. 2008), studied and reported in (Obaidat et al. 2013), and replicated in this study.

**Table 4.1: Given data of the experimental specimen tested by Mazzotti et al. 2008**

CFRP sheet			
Thickness (mm)	Width (mm)	Bond Length (mm)	Elastic Modulus (GPa)
1.2	50	100	195.2
Concrete prism			
Width (mm)	Height (mm)	Length (mm)	Elastic Modulus (GPa)
150	200	600	30.7
Compressive strength $f'_c$ (MPa)		Tensile Strength $f_{ct}$ (MPa)	
52.6		3.81	
Adhesive layer			
Shear Modulus (GPa)		Layer Thickness (mm)	
4.65		1.5	

Based on Equations 4.1 to 4.3 and the given data in table 4.3, the values of the initial stiffness, fracture energy, and shear strength of the interface were 0.966 GPa/mm, 0.517 kJ/m<sup>2</sup> (N/mm), and 7.49 MPa, respectively. The tensile strength of the interface in the normal direction was assumed to equal the tensile strength of concrete.

Figure (4.1) and (4.2) shows that the results of the proposed model are close to both Obaidat et al. modeling and the experimental data.

However, when applying CFRP anchors to the model the behavior of the anchors, which is the goal of this study, was not captured since the model seems to force failure to occur only at the interface between the concrete and the CFRP sheet without considering the failure of the other parts. Therefore, independent material modeling was developed as an alternative to the previous approach.

A specimen tested by (Ueda et al. 1999) and reported in (Lu, Ye, et al. 2005) was analyzed considering definite material representation with the possibility of studying the failure of each material independently. The following table shows the reported details of this specimen.

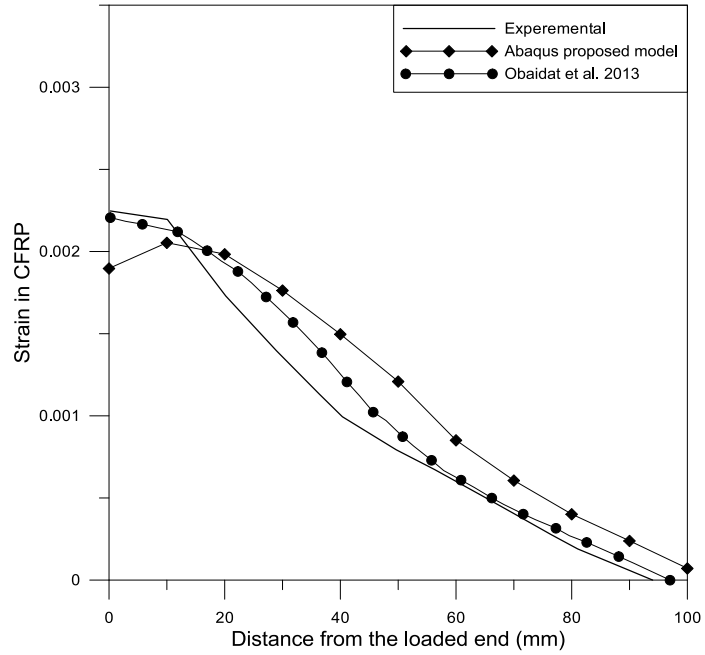


**Figure 4.1: Distribution of strains at the top surface along the centerline of the CFRP sheet for the first replicated specimen tested by Mazzotti et al. 2008**

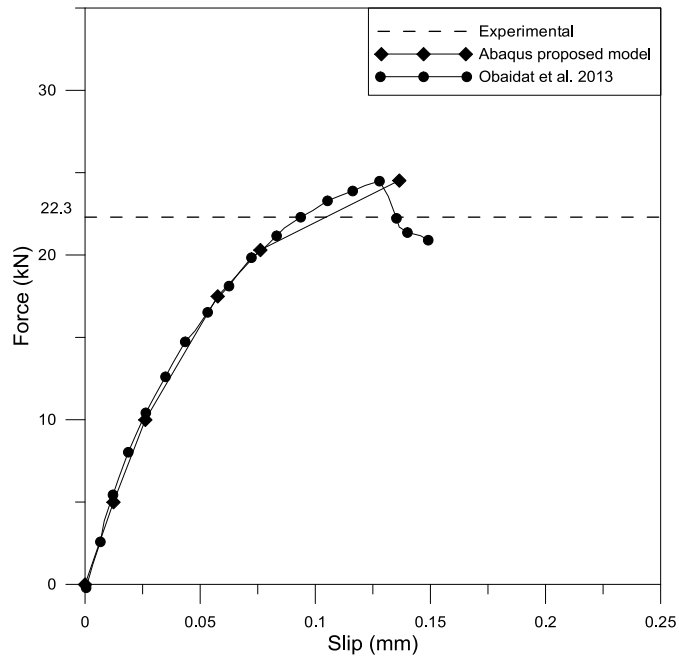


**Figure 4.2: Force-slip diagram at the loaded end of the CFRP sheet for the first replicated specimen tested by Mazzotti et al. 2008**

**Table 4.2: Given data of the experimental specimen tested by Ueda et al. 1999.**

CFRP sheet				Concrete prism		$P_u$ (kN)
Thickne ss (mm)	Width (mm)	Bond Length (mm)	Elastic Modulus (GPa)	Compressi ve Strength $f'_c$ (MPa)	Width (mm)	
0.33	100	200	230	45.9	500	38

Other parameters were required to define properties of each material based on their representative models described previously in chapter two. The values of these parameters were not measured or reported in the experimental work. Therefore, these values were estimated proportionally based on properties that are reported in other standards. Furthermore, some other effective parameters were estimated by conducting calibration processes implicitly through this study. All these parameters are reported in the following Table.

**Table 4.3: Values required to define materials of the model (base units = N, mm)**

Material	Property	Assumed Value	Assumption
Concrete (Smear Cracking Model)  (it should be noted that the concrete model used for the first specimen is different from the concrete model discussed in section 2.3. For more information about this model see (Simulia Abaqus 6.13 2014))	Compressive stress – Plastic strain	13.77 – 0 45.9 - 0.003348	Plastic behavior of concrete starts at 30% of the maximum compressive strength
	Failure ratios	1.16 0.078 1.28 0.333	All default values reported in (Simulia Abaqus 6.13 2014) except the second value was assumed to be 0.078 for the uniaxial tensile stress at the failure to the uniaxial

			compressive stress at failure.
	Cracked shear retention	Shearing modulus of cracked concrete = 0.4 Maximum strain before losing shear strength = 0.015	Reported in (Lu, Ye, et al. 2005) based on a calibration process.
	Tension stiffening	Ultimate displacement of 0.06	Proportional value to the values reported in (Simulia Abaqus 6.13 2014)
	Young's modulus	32000	$4700\sqrt{f'_c}$
	Poisson's ratio	0.2	Typical value
Carbon Fiber Reinforced Polymer (Hashin Damage Model)	Longitudinal tensile strength	3479	Proportional value to previously reported properties in the literature.
	Longitudinal compressive strength	2790	Proportional value to previously reported properties in the literature.
	Transverse tensile strength	3479	Proportional value to previously reported properties in the literature.
	Transverse compressive strength	2790	Proportional value to previously reported properties in the literature.
	Longitudinal shear strength	560	Proportional value to previously reported properties in the literature.
	Transverse shear strength	560	Proportional value to previously reported properties in the literature.
	Longitudinal tensile fracture energy	21.5	Proportional value to previously reported properties in the literature.

	Longitudinal Compressive fracture energy	21.5	Proportional value to previously reported properties in the literature.
	Transverse tensile fracture energy	21.5	Proportional value to previously reported properties in the literature.
	Transverse compressive fracture energy	21.5	Proportional value to previously reported properties in the literature.
	$E_1$	230000	Reported ( see Table 4.1)
	$E_2$	230000	Proportional value to previously reported properties in the literature.
	$E_3$	230000	Proportional value to previously reported properties in the literature.
	$\mu_{12}$	0.25	Proportional value to previously reported properties in the literature.
	$\mu_{13}$	0.25	Proportional value to previously reported properties in the literature.
	$\mu_{23}$	0.25	Proportional value to previously reported properties in the literature.
	$G_{12}$	6849	Proportional value to previously reported properties in the literature.
	$G_{13}$	6849	Proportional value to previously reported properties in the literature.
	$G_{23}$	6849	Proportional value to previously

			reported properties in the literature.
Adhesive ( Traction- Separation Model)	Nominal strain; Normal – only mode	0.062	Reported as technical data.
	Nominal strain; Shear – only mode First direction	0.062	Reported as technical data.
	Nominal strain; Shear – only mode Second direction	0.062	Reported as technical data.
	Damage evolution-type; Displacement- Traction	0.062	Based on the nominal strain value and a one unit constitutive thickness of the adhesive.
	Elastic – type; Traction E	3160	Reported as technical data.
	Elastic – type; Traction G <sub>1</sub>	3160	Reported as technical data.
	Elastic – type; Traction G <sub>2</sub>	3160	Reported as technical data.

Based on the given information in table 4.2 and the assumed values in table 4.3, ABAQUS finite element software was used to model the CFRP-concrete joint. The obtained results were compared with the experimental and ABAQUS modeling results reported in (Lu, Ye, et al. 2005) ( see Figure 4.3).



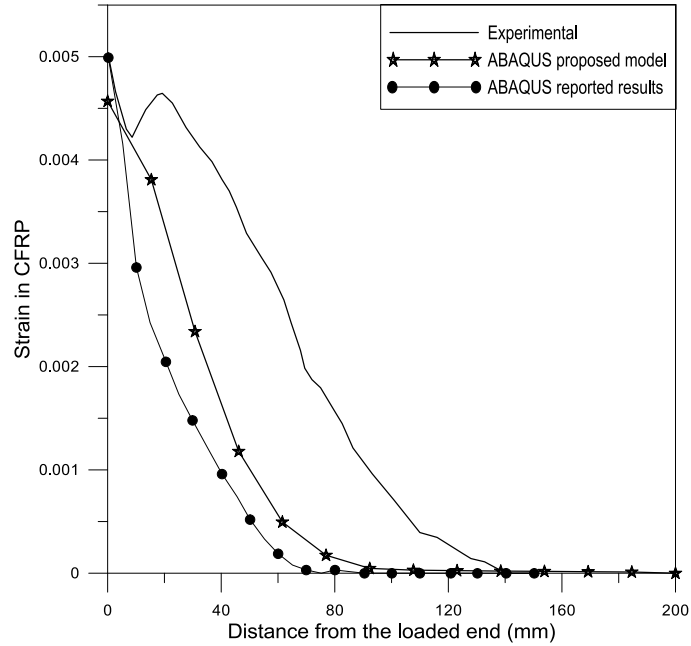


**Figure 4.3: Distribution of strains at the top surface along the centerline of the CFRP sheet for the second replicated specimen tested by Ueda et al. 1999**

Figure 4.3 shows that the results of the proposed model were slightly better than the reported modeling results. Further, Figure 4.4 shows that the maximum load obtained was very close to the value obtained from the reported experimental results.

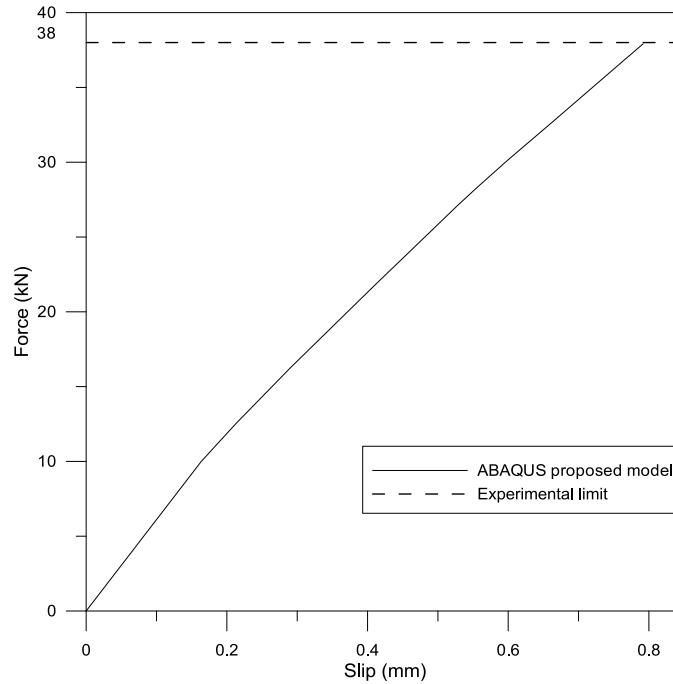


**Figure 4.4: Force-slip diagram at the end of the CFRP sheet for the second replicated specimen tested by Ueda et al. 1999**

However, an investigation was conducted to look for better results by examining the effect of shear retention factors.

Table 4.3 shows that the values of the cracked shear retention factors (Shearing factor of cracked concrete and the maximum strain before losing shear strength) considered in (Lu, Ye, et al. 2005) modeling were equal to 0.4 for the shearing factor and 0.015 for the maximum strain. Hence, other values were tested to study the effect of shear retention factors. Figure (4.5) to Figure (4.9) show the strain distribution along the CFRP sheet for different values of the shear retention factors.

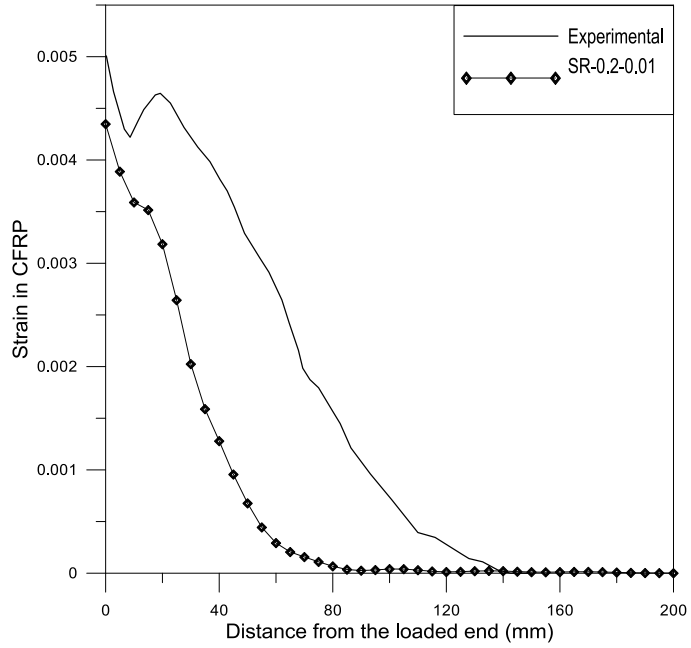


**Figure 4.5: Shear retention factors SR-0.2-0.01**

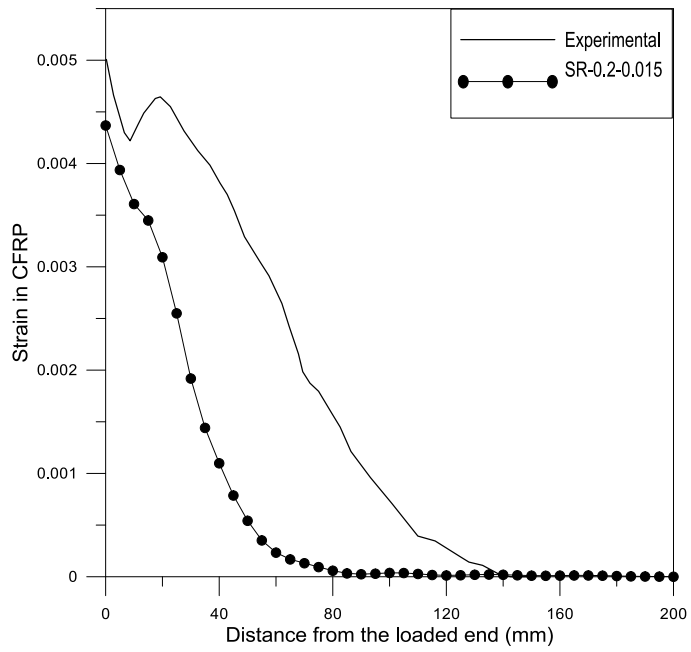


**Figure 4.6: Shear retention factors SR-0.2-0.015**

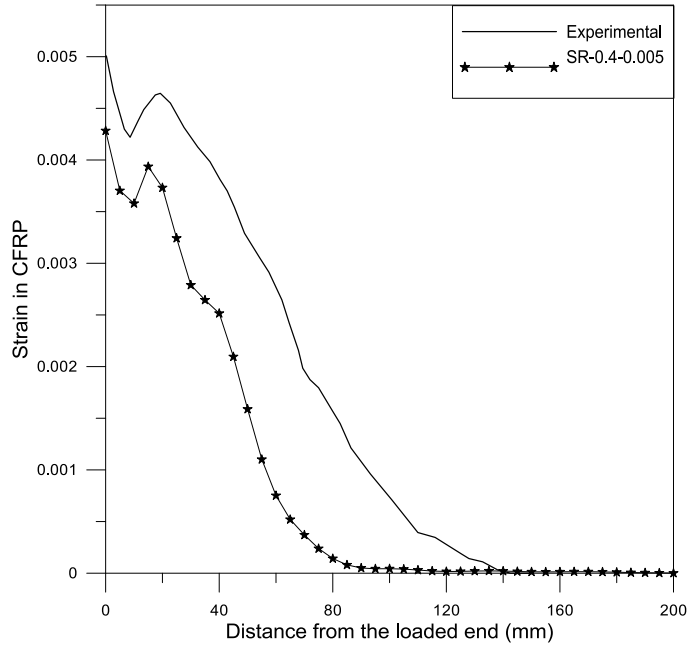


**Figure 4.7: Shear retention factors SR-0.4-0.005**

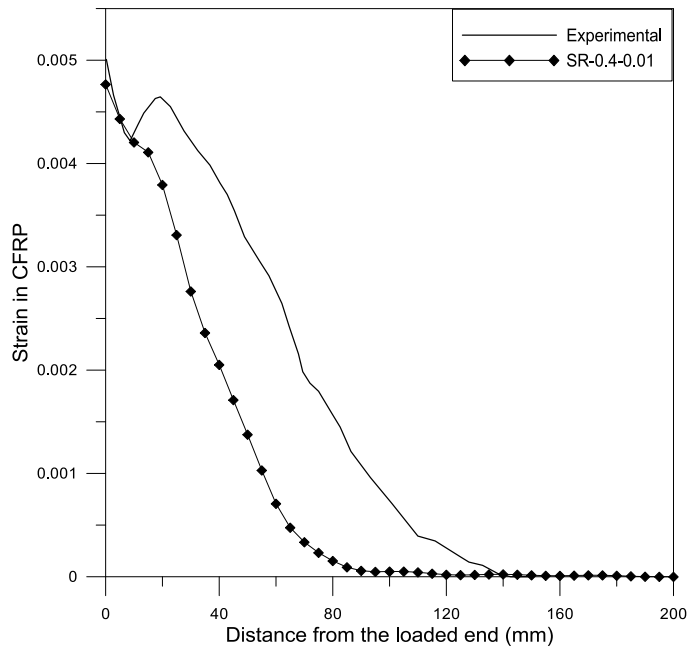


**Figure 4.8: Shear retention factors SR-0.4-0.01**

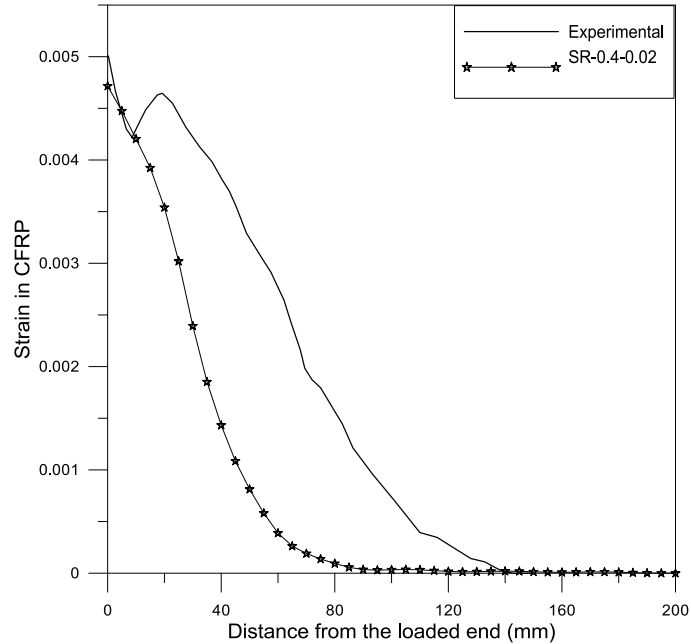


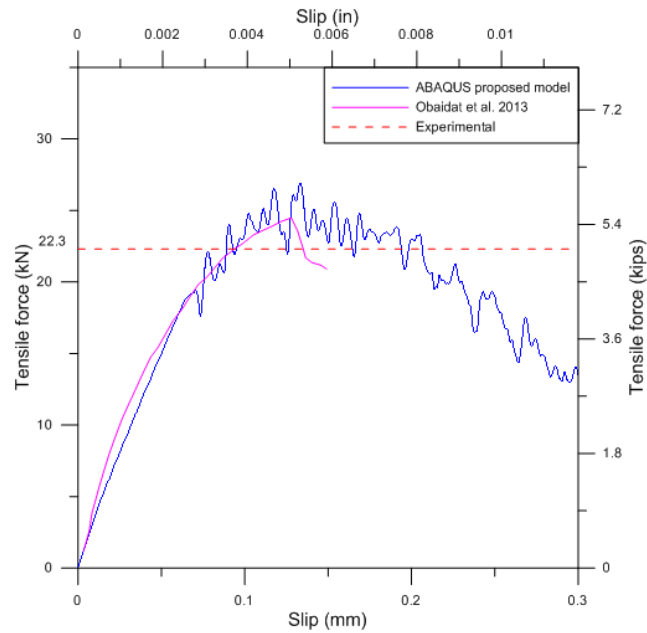
**Figure 4.9: Shear retention factors SR-0.4-0.02**

In each of these Figures, the symbol SR represents the shear retention parameters and the following numbers are the first parameter (the shearing factor) and the second parameter (the maximum strain before losing shear strength). Figure (4.7) represents the best result considering a shear factor of 0.4 and a maximum strain of 0.005. However, this modeling is successful in representing just the first debonding event of the CFRP sheet. After the first debonding of the CFRP sheet, the model fails in representing debonding propagation since no more convergence can be achieved because of losing elastic stability.

As described before in section 3.3, it is difficult to study the behavior of the CFRP anchors placed far from the first effective debonding length without having a complete debonding propagation. Therefore, the explicit analysis scheme was considered to investigate if full propagation could be achieved rather than the static analysis scheme

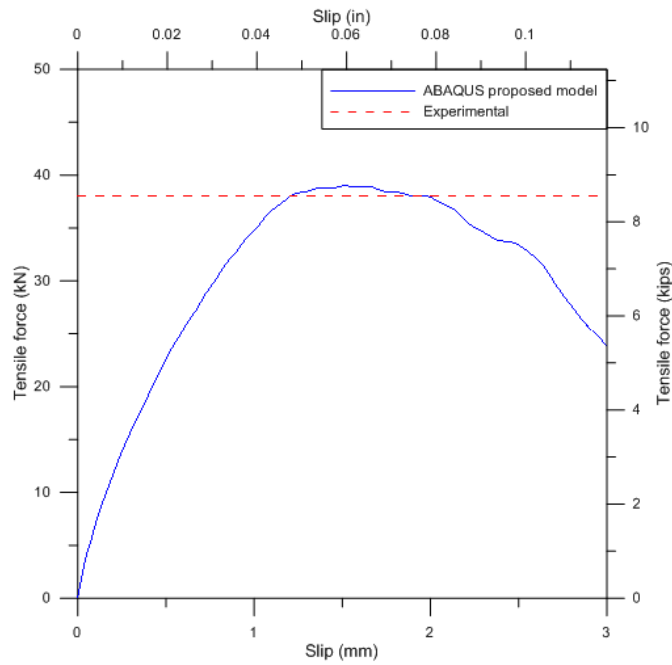
that was used in the previous modeling. Hence, ABAQUS Explicit was used rather than ABAQUS Standard to perform the analysis.

Figure (4.10) shows that the results of the proposed model are close to both Obaidat et al. finite element modeling and the experimental data obtained by Mazzotti et al.



**Figure 4.10: Force-slip diagram at the loaded end of the CFRP sheet for the first replicated specimen tested by Mazzotti et al. 2008 using the explicit analysis procedure**

Figure (4.11) shows that the ultimate tensile force obtained is close to the value obtained from the reported experimental results.



**Figure 4.11: Force-slip diagram at the loaded end of the CFRP sheet for the second replicated specimen tested by Ueda et al. 1999 using the explicit analysis procedure**

A third experimental specimen that was tested by ( Breña and McGuirk 2013) has been analyzed based on the new modeling approach. The following table shows the reported details of this specimen.

**Table 4.4: Given data of the experimental specimen tested by Breña and McGuirk 2013**

CFRP sheet (cured lamina)					
Cured Thickness (mm)	Width (mm)	Bond Length (mm)	Elastic Modulus (GPa)	Rupture Strain (%)	Tensile Strength (MPa)
1	127	610	72.4	1.2	875
Concrete prism					
Width (mm)		Height (mm)	Length (mm)		

480	480	1000
Compressive strength $f'_c$ (MPa)		Tensile Strength $f_{ct}$ (MPa)
35.2		3.4
Adhesive layer		
Shear Modulus (GPa)		
3.18		

Other properties were not available at the main reference; therefore, the missing properties were obtained from the specifications of the original manufacturer of these materials (FYFE Tyfo Fiberware Systems). See table 4.5 for these properties.

**Table 4.5: Properties obtained from the specification of the manufacturer (FYFE Tyfo Fiberware Systems)**

CFRP sheet (uncured)			
Thickness (mm)	Elastic Modulus (GPa)	Rupture Strain (%)	Tensile Strength (GPa)
Weight for each $m^2$ / Density= $393 (g/m^2) / (1.8(g/cm^3) \times 1000) =$ 0.218 mm	230	1.7	3.79
Adhesive layer			
Elongation (%)			
5.0			

Other properties were required to complete the proposed model. These values were estimated by either considering proportional values to similar material properties reported in the literature or by calibrating missing values. See table 4.6 for these properties.

Shear connector, wood-concrete composite, timber-concrete, finite element analysis.



**Table 4.6: Values required to define materials of the model (base units = N, mm)**

Material	Property	Assumed Value	Assumption
Concrete (Plastic Damage Model)  (See section 2.3. For more information about this model)	Dilation angle	15	Typical concrete properties (calibrated values).
	Eccentricity	0.1	
	$f_{b0} / f_{c0}$	1.16	
	K	0.66	
	Viscosity parameter	1E-005	
	Yield Stress	26.0	Proportional values to the values reported in (Simulia Abaqus 6.13 2014)
		31.75	
		34.43	
		35.20	
		34.51	
32.98			
30.98			
23.77			
Inelastic Strain	0	Proportional values to the values reported in (Simulia Abaqus 6.13 2014)	
	0.0004		
	0.0008		
	0.0012		
	0.0016		
	0.002		
	0.0024		
	0.0036		
Tensile behavior:	Yield stress	3.4	Given (see table 4.4),
	Fracture energy	0.05	
	Young's modulus	27885	$4700\sqrt{f'_c}$
	Poisson's ratio	0.18	Typical value
Carbon Fiber Reinforced Polymer (Hashin Damage Model)	Longitudinal tensile strength	3790	Given (see table 4.5)
	Longitudinal compressive strength	3040	Proportional value to previously reported properties in the literature.
	Transverse tensile strength	3790	Proportional value to previously reported properties in the literature.

	Transverse compressive strength	3040	Proportional value to previously reported properties in the literature.
	Longitudinal shear strength	605	Proportional value to previously reported properties in the literature.
	Transverse shear strength	605	Proportional value to previously reported properties in the literature.
	Longitudinal tensile fracture energy	21.5	Proportional value to previously reported properties in the literature.
	Longitudinal Compressive fracture energy	21.5	Proportional value to previously reported properties in the literature.
	Transverse tensile fracture energy	21.5	Proportional value to previously reported properties in the literature.
	Transverse compressive fracture energy	21.5	Proportional value to previously reported properties in the literature.
	$E_1$	230000	Reported ( see Table 4.5)
	$E_2$	230000	Proportional value to previously reported properties in the literature.
	$E_3$	230000	Proportional value to previously reported properties in the literature.
	$\mu_{12}$	0.25	Proportional value to previously reported properties in the literature.
	$\mu_{13}$	0.25	Proportional value to previously

			reported properties in the literature.
	$\mu_{23}$	0.25	Proportional value to previously reported properties in the literature.
	$G_{12}$	6849	Proportional value to previously reported properties in the literature.
	$G_{13}$	6849	Proportional value to previously reported properties in the literature.
	$G_{23}$	6849	Proportional value to previously reported properties in the literature.
Adhesive ( Traction- Separation Model)	Nominal strain; Normal – only mode	0.05	Reported ( see Table 4.4).
	Nominal strain; Shear – only mode First direction	0.05	Reported ( see Table 4.4).
	Nominal strain; Shear – only mode Second direction	0.05	Reported ( see Table 4.4).
	Damage evolution-type; Displacement- Traction	0.05	Based on the nominal strain value and a one unit constitutive thickness of the adhesive.
	Elastic – type; Traction E	3180	Reported ( see Table 4.4)
	Elastic – type; Traction $G_1$	1200	Proportional value to previously reported properties in the literature.
	Elastic – type; Traction	1200	Proportional value to previously

	$G_2$		reported properties in the literature.
--	-------	--	-------------------------------------------

Figure (4.12) shows that the results of the proposed model are close to the experimental results obtained by (McGuirk 2011). Furthermore, Full propagation with a complete force-deformation history was achieved based on the explicit analysis approach. Therefore, CFRP anchors were applied to this model, and the obtained results were compared with the experimental outcomes of a corresponding anchored experimental specimen tested by (McGuirk 2011).

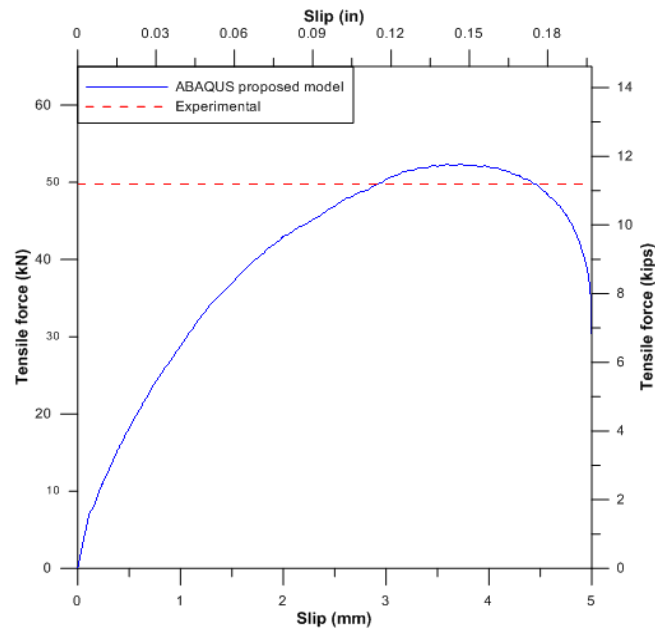


**Figure 4.12: Force-slip diagram at the loaded end of the CFRP sheet for the third replicated specimen tested by Breña and McGuirk 2013 using the explicit analysis procedure**

### 4.3 CFRP-concrete joints with anchors

An experimental specimen tested by (Breña and McGuirk 2013) was replicated by applying CFRP-anchors to the previous model and compare the results with the corresponding experimental tests. The properties of this specimen are similar to that of the third replicated unanchored specimen reported in table 4.5 and its other estimated properties in table 4.6. Five different parts were considered to represent the joint. These parts are the concrete part, the CFRP sheet, the adhesive layer, the CFRP anchor, and the adhesive envelope around the anchor (see Figures 2.1 and 2.2 in chapter two). The dimensions of the anchors used in this specimen were 50 mm for the height of the anchor, 13 mm for the diameter of the shaft of the anchor, and 64 mm for the diameter of the splays of the anchor (see Figure 4.13). Modeling of the materials used was based on the constitutive relationships that were described in chapter two.

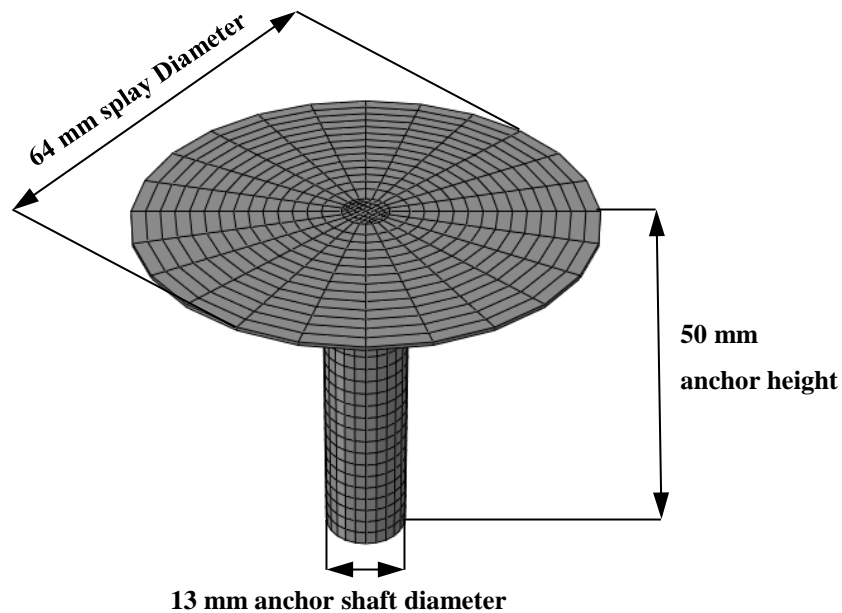


**Figure 4.13: Dimensions of the CFRP anchor**

Based on this modeling approach, a complete debonding propagation was achieved. Figures (4.14) to (4.22) show debonding propagation stages until the final failure of the joint.

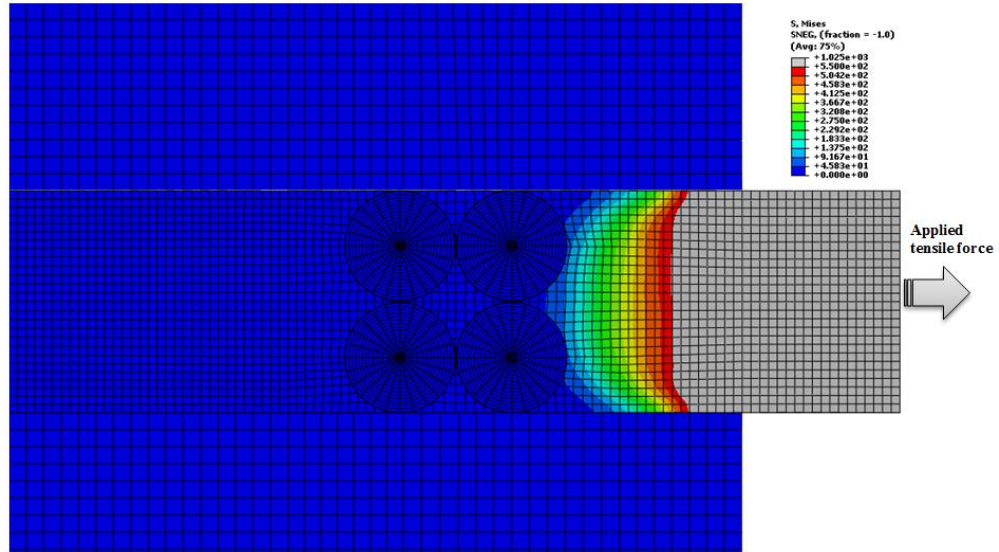


**Figure 4.14: Beginning of debonding propagation (Mises stress = 1025 MPa)**

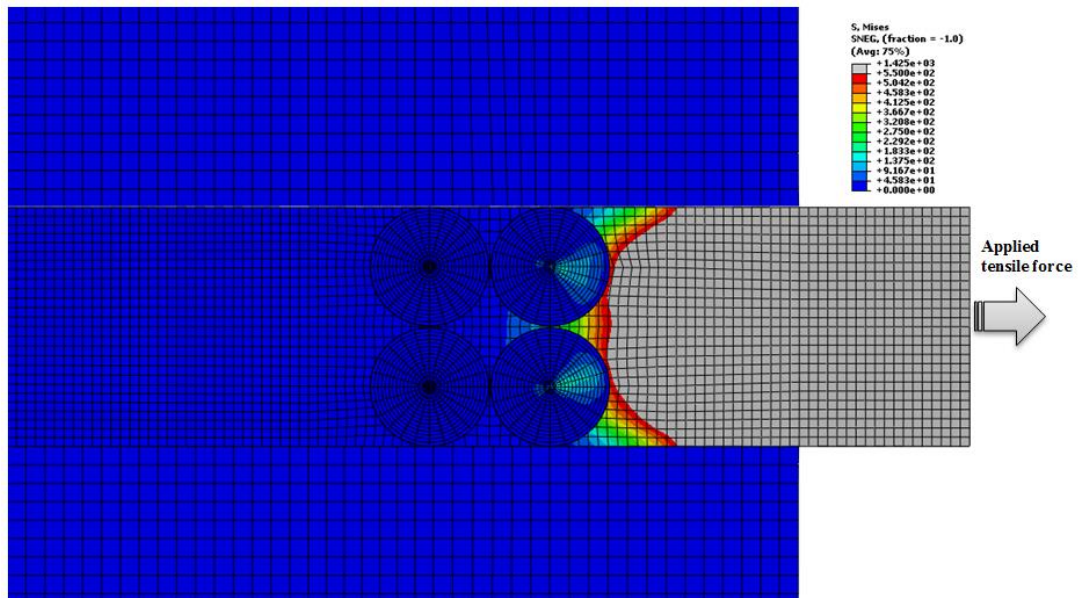


**Figure 4.15: Debonding propagation at the CFRP anchors (Mises stress = 1425**

**MPa)**

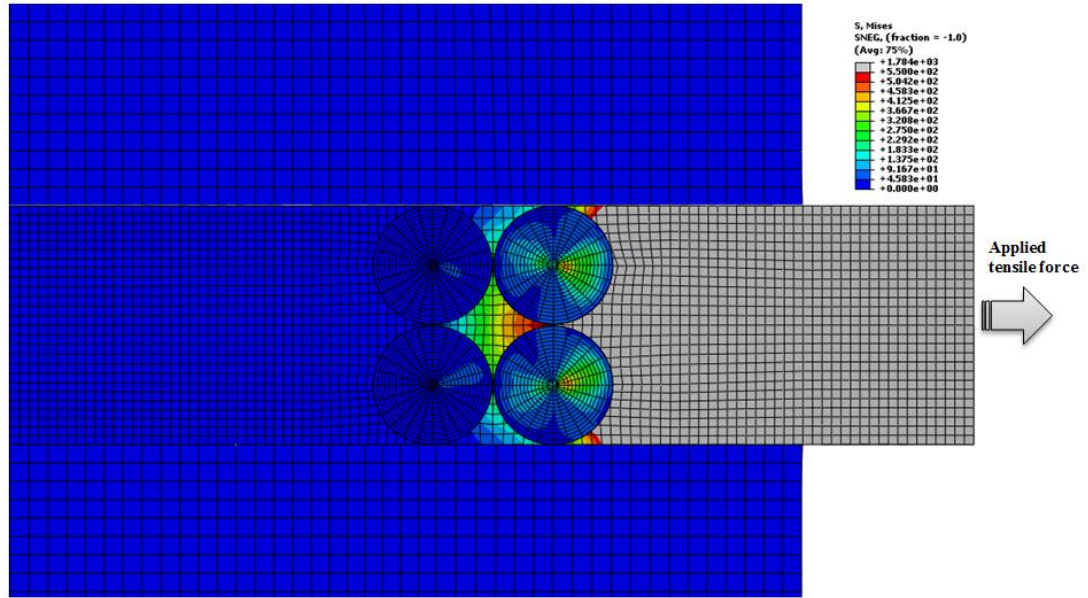


Figure 4.16: Debonding propagation between the CFRP anchors (Mises stress = 1784 MPa)

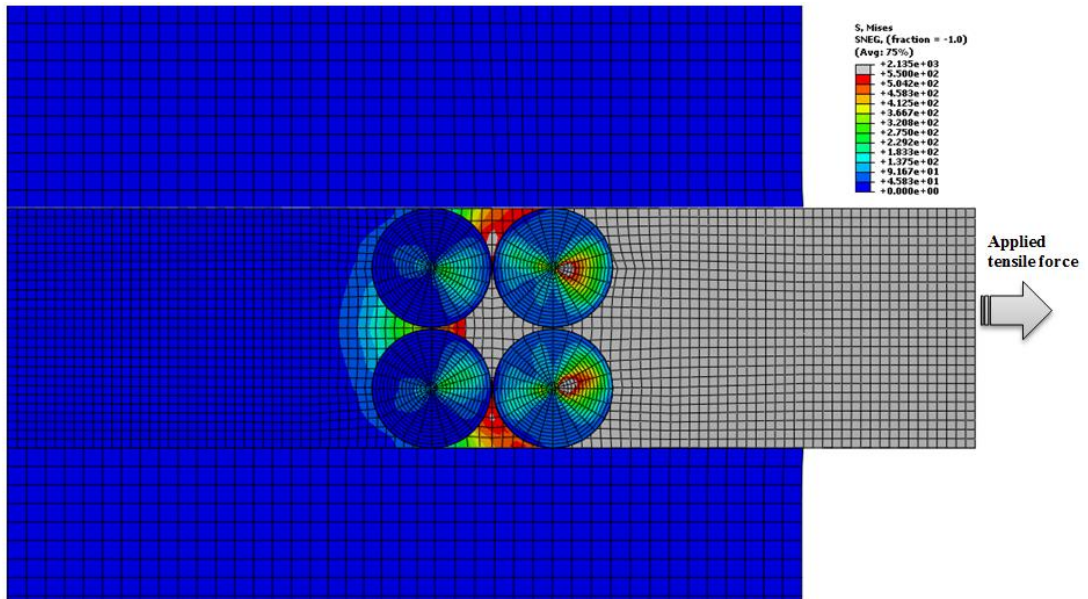


Figure 4.17: Debonding propagation between the CFRP anchors (Mises stress = 2135 MPa)

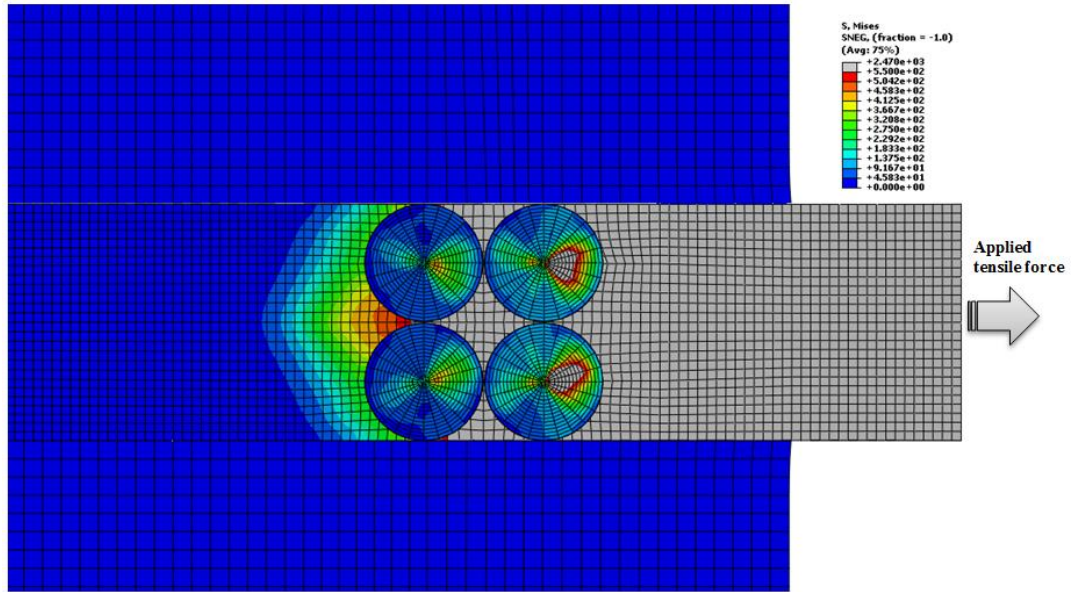


Figure 4.18: Debonding propagation at the loaded end of the CFRP anchors

(Mises stress = 2470 MPa)

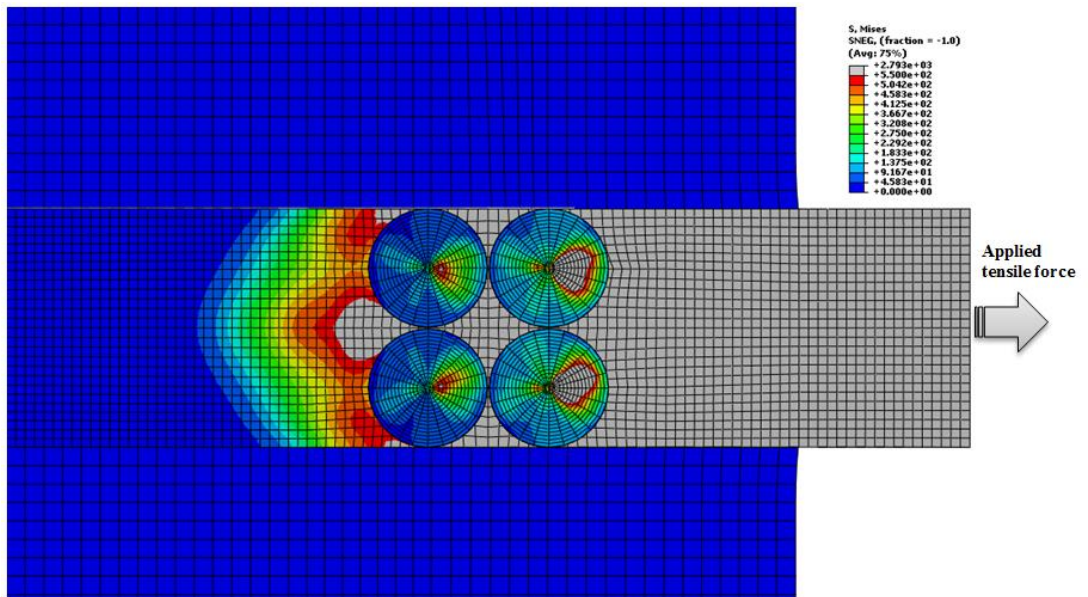
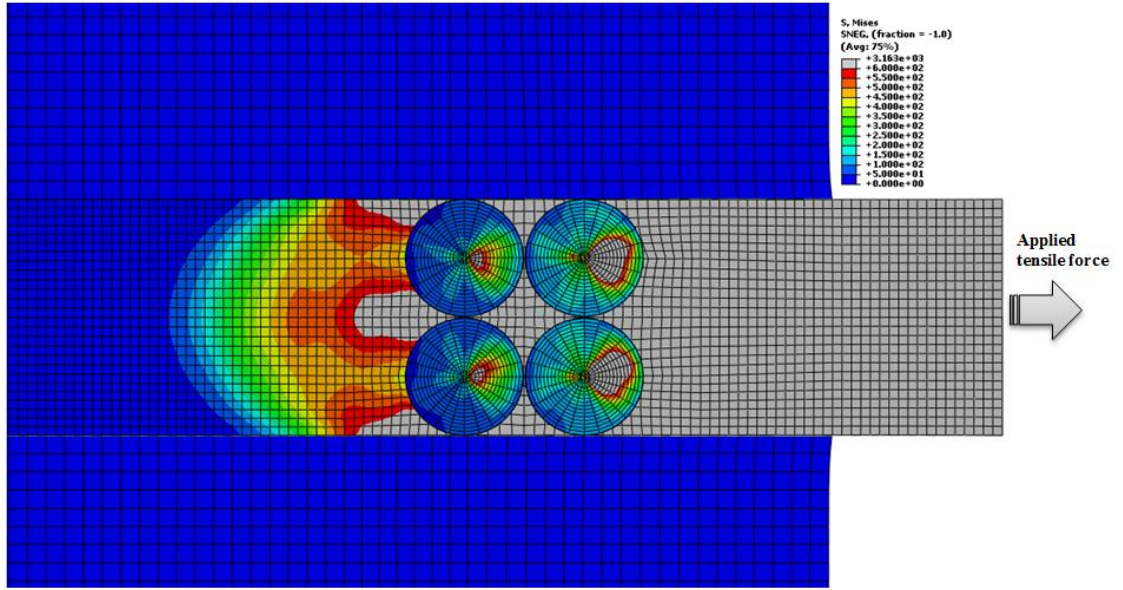


Figure 4.19: Debonding propagation far from the CFRP anchors (Mises stress =

2793 MPa)





**Figure 4.20: Debonding propagation far from the CFRP anchors (Mises stress = 3163 MPa)**

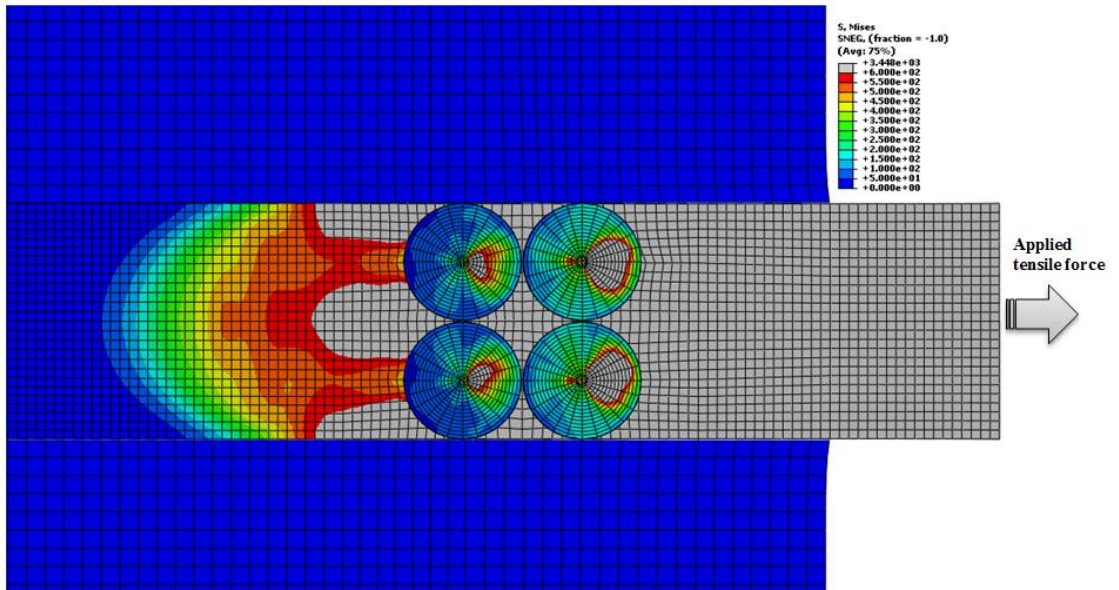


**Figure 4.21: Debonding propagation far from the CFRP anchors (Mises stress = 3448 MPa)**

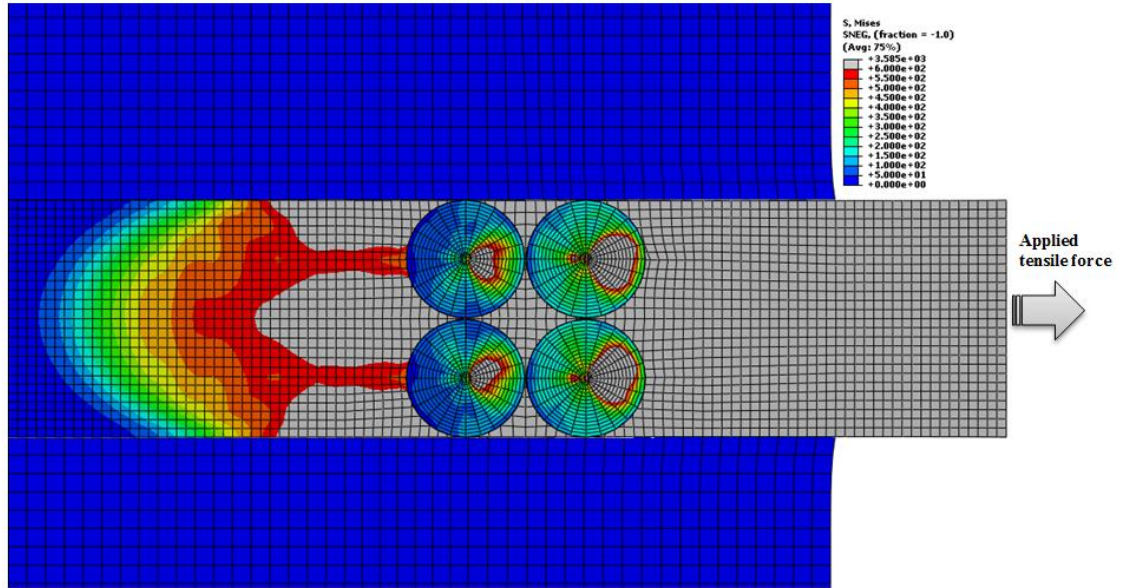


**Figure 4.22: Debonding propagation before fully separation (Mises stress = 3585 MPa)**

Figure (4.23) shows stress distribution in the CFRP anchor while Figure (4.24) shows stress distribution in the adhesive envelope around the anchor.

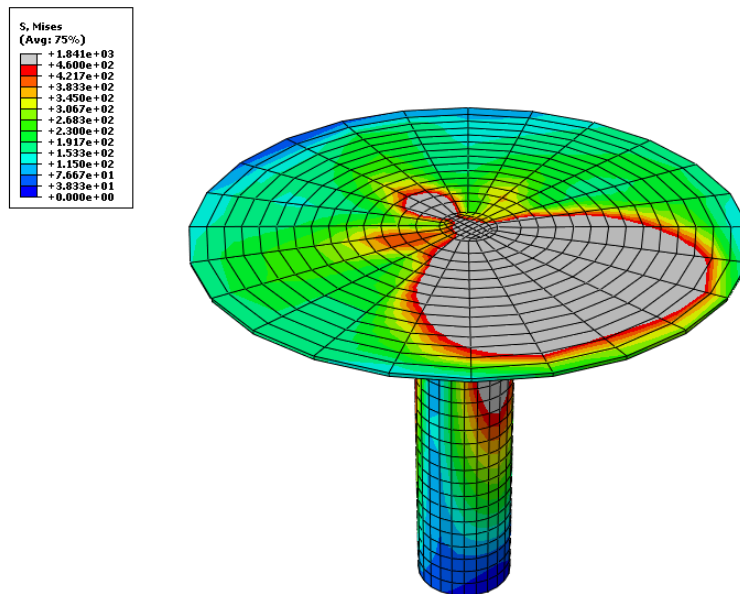


**Figure 4.23: Stress distribution in the CFRP anchor**

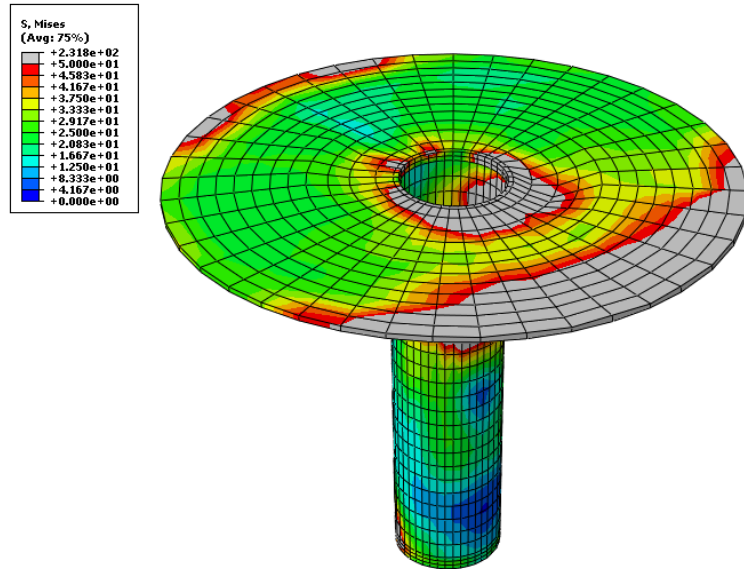


**Figure 4.24: Stress distribution in the adhesive envelope around the anchor**

Figure (4.25) shows stress distribution in the CFRP sheet and Figure (4.26) shows stress distribution in the adhesive layer, while Figure (4.27) shows stress distribution in the concrete part.

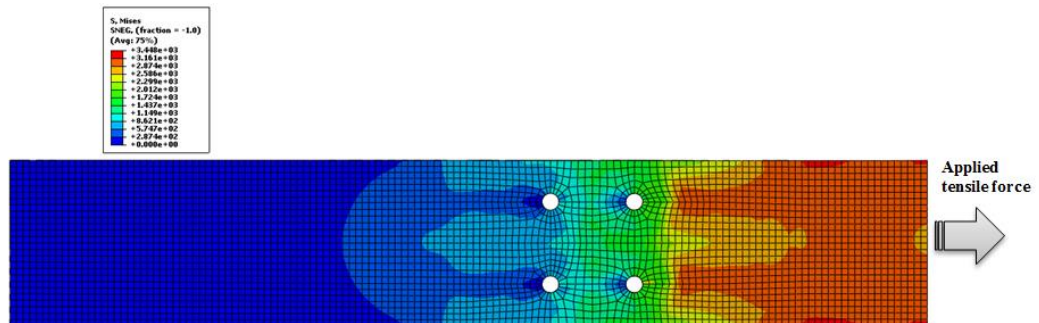


**Figure 4.25: Stress distribution in the CFRP sheet before failure**

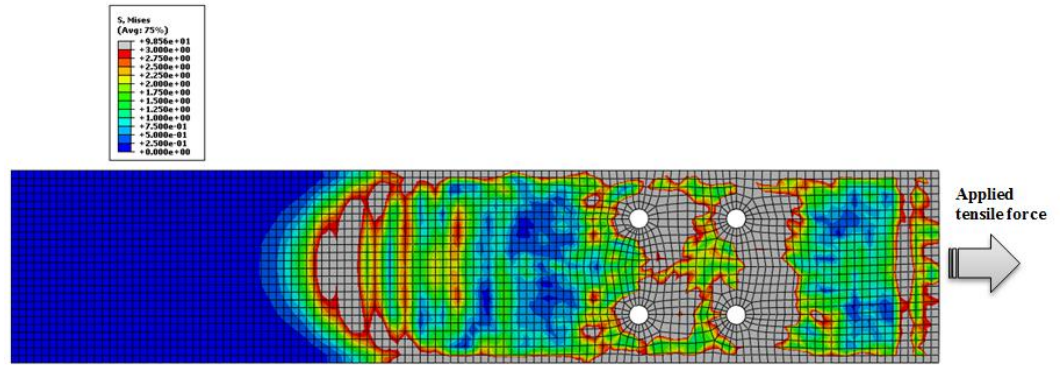


**Figure 4.26: Stress distribution in the adhesive layer before failure**

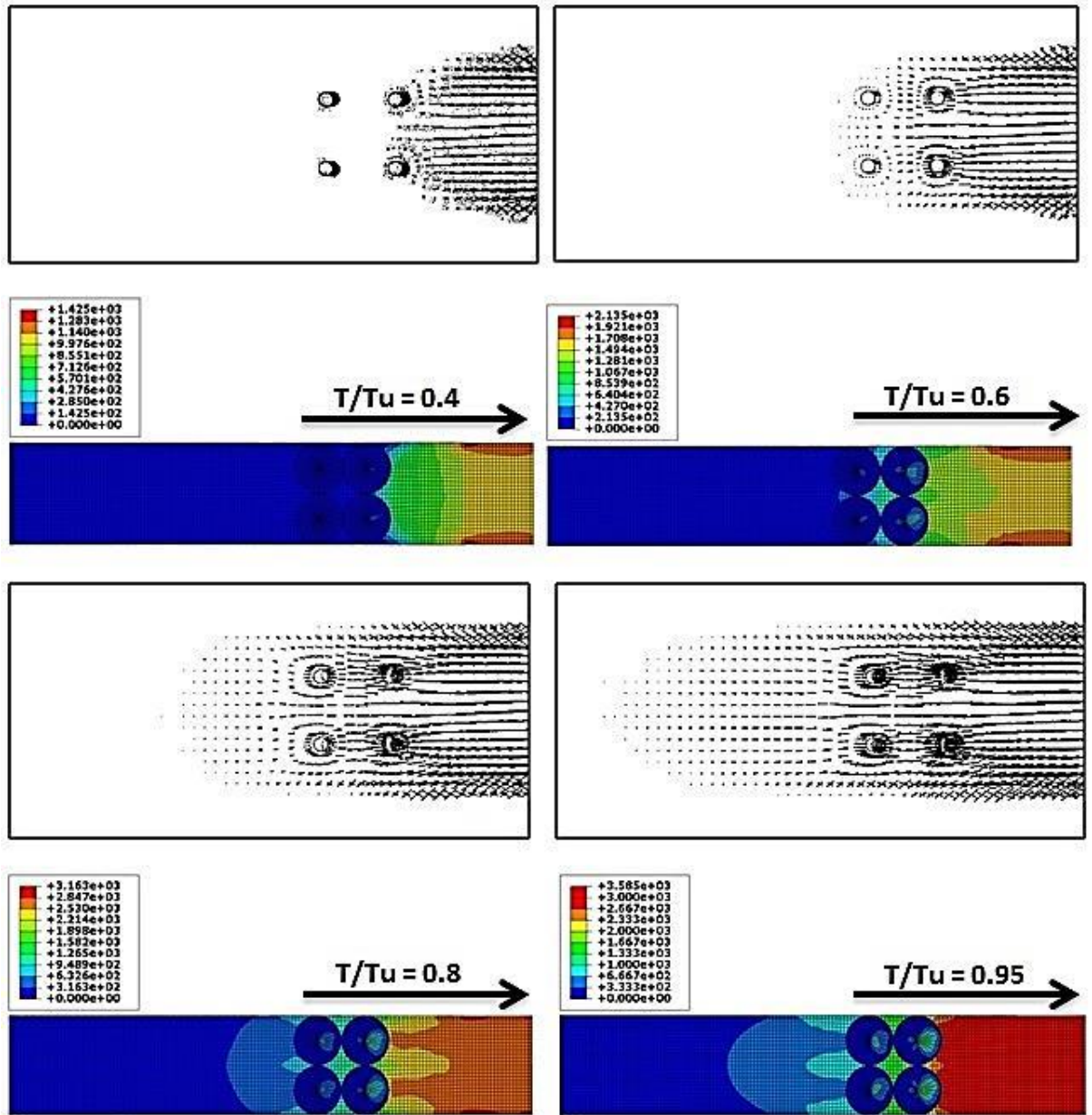


**Figure 4.27: Cracking propagation in concrete-FRP interface and corresponding longitudinal stress distributions in the CFRP sheet and anchors for different load stages**

Figure (4.28) shows the stress distribution at the failure of the CFRP-concrete joint while Figure (4.29) shows the strain distribution at the failure of the CFRP-concrete joint.

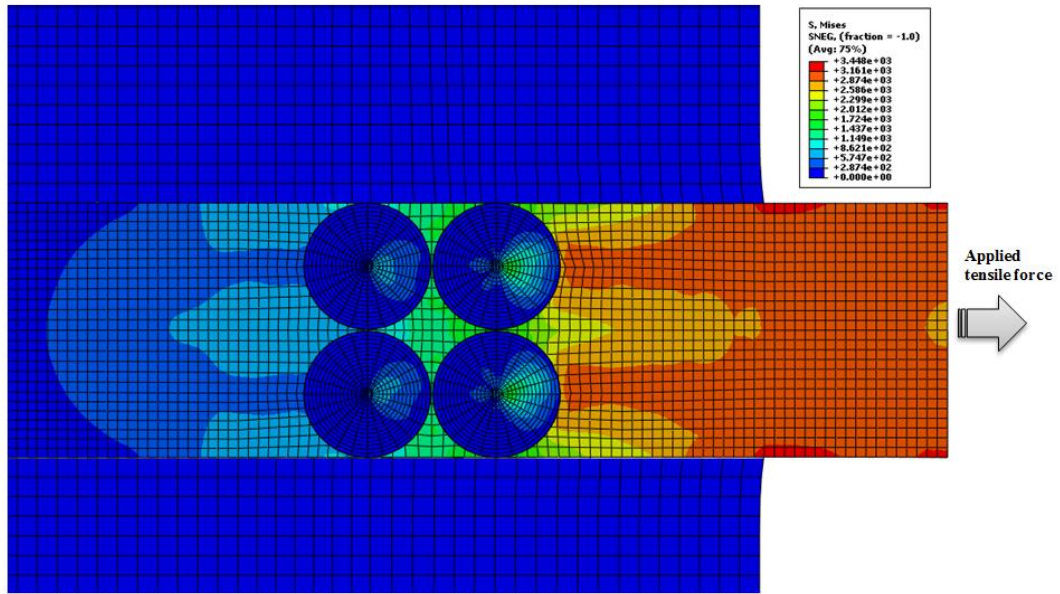


**Figure 4.28: Stress distribution at the ultimate force before the failure of the CFRP-concrete joint**

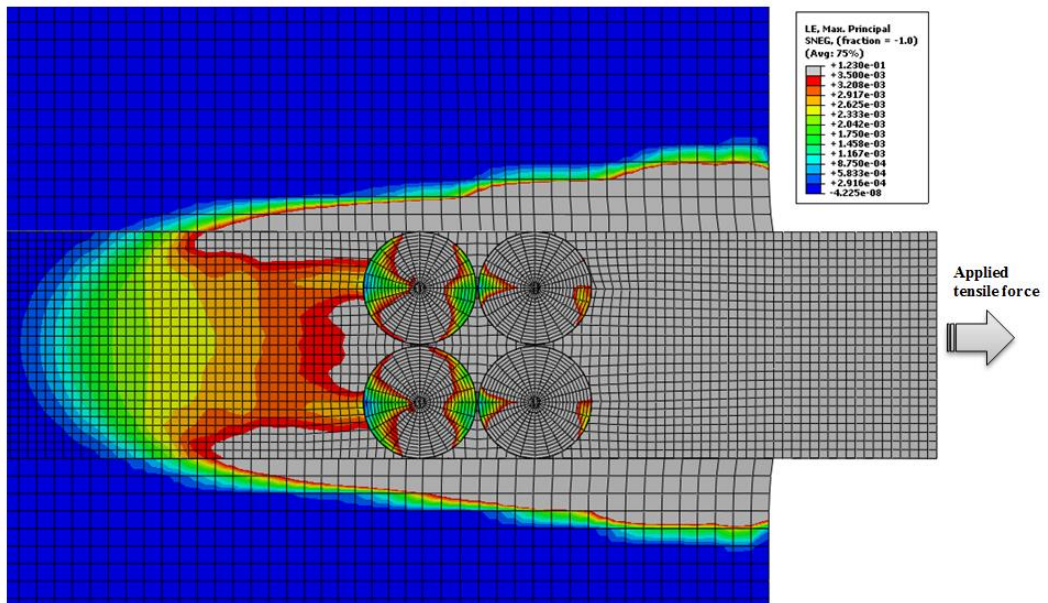


**Figure 4.29: Strain distribution at the ultimate force before the failure of the CFRP-concrete joint.**

Figure (4.29) shows the Force-slip diagram at the end of the CFRP sheet for the anchored joint. Figure (4.30) shows the distribution of strains at the top surface of the CFRP sheet for the anchored joint. These Figures show that the results of the proposed model are close to the experimental results obtained by (McGuirk 2011).

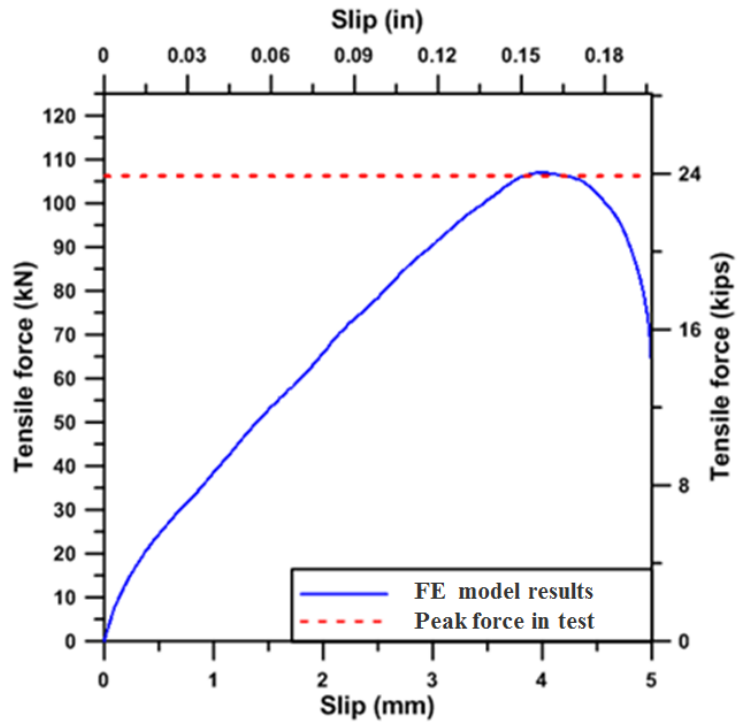


**Figure 4.30: Calculated force-slip diagram for the CFRP-anchored joint (Breña and McGuirk, 2013; Specimen F1-4a-1-24)**

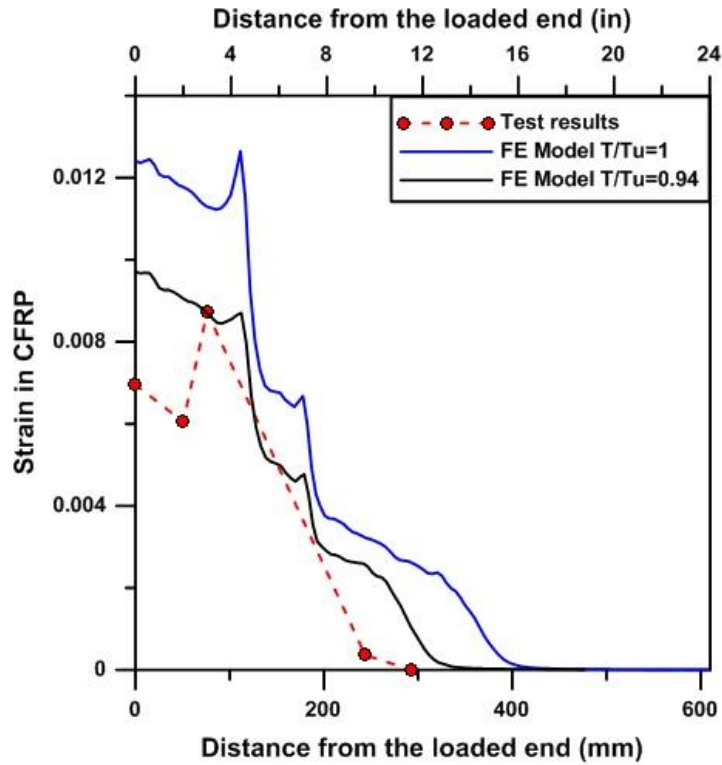


**Figure 4.31: Comparison of measured and calculated strains on the top surface of the CFRP sheet centerline (Specimen F1-4a-1-24 tested by Breña and McGuirk, 2013)**

It is clear from the previous Figures that the proposed model has achieved all the characteristics that represent the physical behavior of the CFRP-concrete joint under applied forces. A complete debonding propagation of the CFRP sheet and a full load-deformation history has been obtained by adopting this modeling approach. Therefore, the last modeling method will be considered as the main modeling procedure throughout the rest of this research.



#### **4.4 Summary of the verification of the finite element model**

Calibration and verification of the accuracy of the finite element model were conducted in two stages. The model was initially calibrated by considering the FRP-concrete joint exclusively bonded using adhesives. This case has been studied extensively by past researchers, both numerically and experimentally, so it provided a means by which results from the proposed model could be evaluated against experimental results. Verification of the proposed finite element modeling technique was then extended to the case of FRP sheets attached to concrete through bond and supplemental FRP anchors. Fewer experimental and analytical studies have been conducted to date for this second condition, but a few of the available laboratory results were used to verify the accuracy of the model after calibration had been conducted using the FRP-concrete bonded condition.

##### **4.4.1 Model verification using CFRP-concrete bond tests**

Laboratory tests conducted by three different research groups (Ueda et al. 1999; Mazzotti et al. 2008; and Breña and McGuirk 2013) were used to verify the accuracy of the proposed finite element model in cases where the FRP sheets were attached to concrete blocks exclusively by bonding. The three selected bond strength studies were conducted using a similar test setup that was designed to generate direct shear stresses along the interface between concrete and FRP sheets. Key properties of the materials used for the experiments in these three research programs are listed in Table 4.7. The FRP composite sheet and adhesive properties listed in the table were either measured and reported directly by the researchers or, if not reported, obtained from the literature provided by the manufacturer of the different composite systems.

**Table 4.7: Properties of selected laboratory specimens**

Property	Unit	Specimen properties					
		Breña and McGuirk (2013)		Mazzoti et al. (2008)		Ueda et al. (1999)	
		F1-0a-24	S1-0a-24	BL100 b <sub>p</sub> 50	BL50 b <sub>p</sub> 50	B-2	B-1
CFRP laminate properties:							
CFRP thickness	mm (in)	1.0 (0.039)		1.2 (0.05)		0.33 (0.013)	0.11 (0.004)
CFRP sheet width	mm (in)	127 (5)		50 (2)		100 (4)	
CFRP bonded length	mm (in)	610 (24)		100 (4)	50 (2)	200 (8)	
CFRP elastic modulus (fibers)	GPa (ksi)	230 (33359)	230 (33359)	195.2 (28311)		230 (33359)	
CFRP elastic modulus (laminate)		72.4 (10500)	70.5 (10225)	—		—	
CFRP rupture strain	%	1.2	1.12	—		—	
CFRP tensile strength (fibers)	MPa (ksi)	3793 (550)		—		—	
CFRP tensile strength (laminate)		875 (127)	849 (123)	—		—	
Adhesive layer properties:							
Adhesive thickness	mm (in)	—		1.5 (0.06)		—	
Shear modulus	GPa (ksi)	3.18 (461)		4.65 (674)		—	
Maximum elongation	%	—		—		—	
Concrete block properties:							
Dimensions (width x height x length)	mm (in)	480 x 480 x 1000 (19 x 19 x 39)		150 x 200 x 600 (6 x 8 x 23.6)		500 (20)	
Concrete compressive strength	MPa (ksi)	35.2 (5)	34 (4.93)	52.6 (7.63)		45.9 (6.66)	
Concrete tensile strength	MPa (ksi)	3.4 (0.5)	2.8 (0.4)	3.81 (0.55)		—	
Elastic modulus	GPa (ksi)	—		30.7 (4453)		—	

The tests conducted by Mazzotti et al. (2008), and Breña and McGuirk (2013) consisted of CFRP sheets of two different widths and various thicknesses bonded to concrete blocks that were fixed to a stiff reaction frame. The tests by Ueda et al. (1999) consisted of two concrete blocks joined using CFRP sheets with loading applied concentrically onto the blocks to generate interfacial stresses in the CFRP sheets. The leading end of the FRP sheets in all tests was intentionally debonded from the concrete blocks over the initial 100 mm (4 in.) so that the concrete corner would not experience spalling because of stress concentrations. The load in all tests was applied monotonically to the end of the CFRP sheet (Mazzotti et al., 2008; and Breña and McGuirk, 2013) or through the concrete blocks (Ueda et al., 1999) to generate interfacial shear stresses between the composite sheet and the concrete surface. Longitudinal strains were typically measured along the sheet centerline, although sometimes strains were also measured at various points across the sheet width.

Comparisons between the peak force computed through finite element modeling of each of the laboratory tests and the maximum measured tensile force applied prior to bond failure are listed in Table 4.8. Plots that illustrate comparisons between computed and measured strains along the FRP sheet centerline are presented in Figure 4.32. The comparisons show that the load reached during the tests was predicted within 12% using the finite element model. Furthermore, the measured and calculated distribution of longitudinal strains along the sheet centerline compare reasonably well. These results gave confidence in the calibrated values used for material model parameters in the finite element model simulations. Therefore, these calibrated values for the parameters were

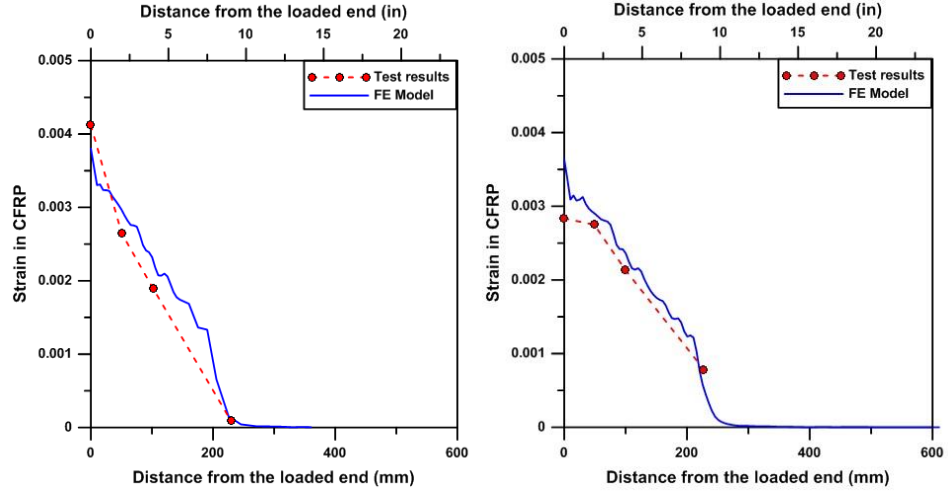
used to model the more complex condition of CFRP sheets containing supplemental FRP anchors.

**Table 4.8: Comparison between measured peak loads and finite element analyses**

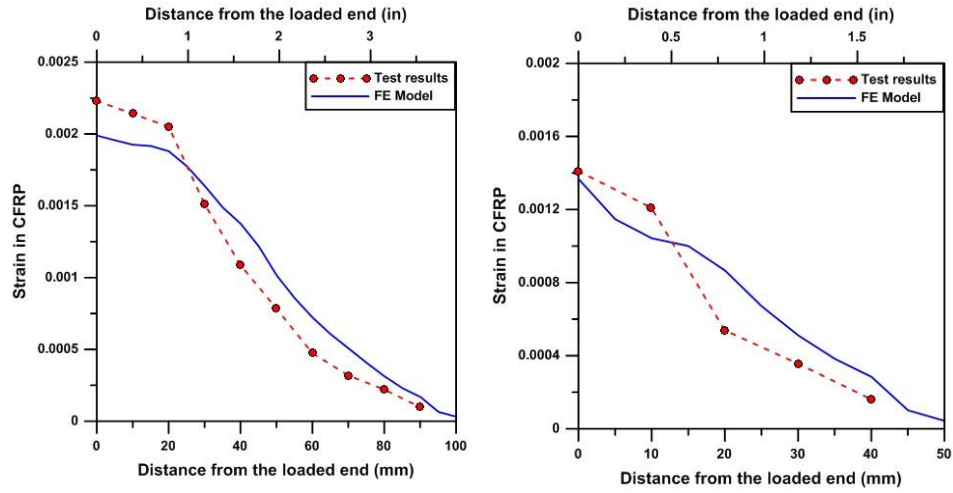
<b>Specimen</b>	<b>Ultimate load from test <math>T_{test}</math></b>	<b>Ultimate load from FEM <math>T_{FEM}</math></b>	<b><math>T_{FE}</math> M/ <math>T_{test}</math></b>
F1-0a-24	49.8	52.3	1.05
S1-0a-24	43.4	47.2	1.09
BL 100 b <sub>p</sub> 50	22.3	24.5	1.10
BL 50 b <sub>p</sub> 50	14.0	15.7	1.12
B-2	38.0	39.0	1.03
B-1	20.6	20.1	0.98

The finite element model was developed with the goal of accurately capturing the propagation of debonding by using an explicit analysis solution. Because of the highly nonlinear behavior of the debonding process, debonding propagation is a feature that has not been captured consistently by other models developed in the past. Experimental studies have confirmed that once FRP debonding occurs over a length known as the stress transfer zone, debonding propagates toward the unloaded end of the FRP sheet without a notable increase in force applied to the FRP sheet. Capturing this characteristic of the failure propagation process was fundamental to allow us to study the effect of anchors on the behavior of the FRP-concrete system during debonding. The calibrated model used to simulate the tests conducted only by Breña and McGuirk (2013) was extended to incorporate the influence of CFRP anchors in the system since this is one of the few experimental studies that compared the performance of adhesively bonded-only sheets with that of bonded sheets plus supplemental FRP anchors. Comparison of results

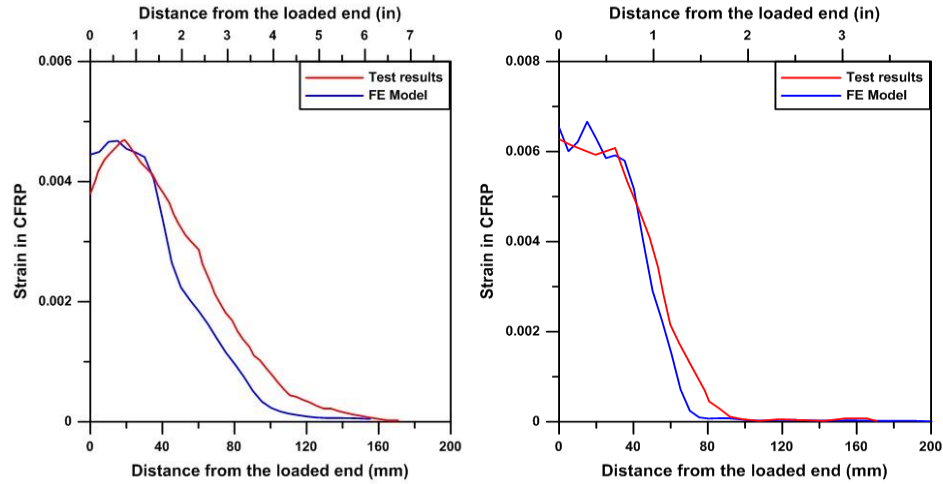
between the finite element models, including detailed modeling of the FRP anchors, and available laboratory experiments are presented in the following section.



(a) Specimen tested by Breña and McGuirk 2013: F1-0a-24, S1-0a-24



(b) Specimens tested by Mazzotti et al. 2008: BL 100, BL 50



(c) Specimens tested by Ueda et al. (1999): B-2, B-1

**Figure 4.32: Comparison of measured and calculated strain diagrams along FRP sheet centerline**

#### 4.4.2 Model verification using tests of FRP-anchored sheets

The main objective of developing a robust finite element model that explicitly included the different components of the FRP sheet-to-concrete bond was to allow it to be extended to complex conditions such as those encountered when supplemental anchors are provided to delay debonding of the FRP sheets. The stress and strain fields developed in the FRP sheet in the vicinity of the FRP anchors are complex. Furthermore, the influence of anchor parameters needed to develop design recommendations (depth, diameter, location, and grouping) on the behavior of the FRP-concrete joint system has not been reported in the existing literature. A detailed examination of these parameters on system behavior, as presented and discussed in the following section, would not be possible without having a reliable finite element model that has been calibrated through experimental testing.

Tests reported by Breña and McGuirk (2013) were used to compare the measured response of FRP anchored sheets with the finite element model presented in this research. The previously validated model using tests of FRP sheets bonded to concrete was extended to include CFRP-anchors. The five different components that constitute the FRP-concrete joint were modeled, including a concrete substrate, CFRP sheet, an adhesive layer, CFRP anchor, and adhesive envelope around the anchor, using the material properties summarized in Table 4.7 (specimens F1-0a-24 and S1-0a-24). The specimen selected for the comparison (F1-4a-1-24) included a single CFRP sheet bonded to concrete and containing four CFRP anchors with a 50 mm (2 in.) depth, a 13 mm (0.5 in.) anchor shaft diameter, and a 64 mm (2.5 in.) circular anchor splay diameter. The same constitutive relationships described for the models with FRP bonded-only sheets were used to model the response of this specimen.

A plot illustrating the calculated force-slip diagram at the end of the CFRP sheet determined from the finite element simulation and the maximum measured force in the laboratory experiment is depicted in Figure 4.30. Slip between the CFRP sheet and the concrete surface was not measured in the laboratory test, so it was only possible to compare the maximum measured force with the maximum force determined in the model. The figure shows that the comparison is quite favorable, with a ratio of measured to calculated peak force of approximately 0.99.

Strains were measured at discrete points on the top surface along the CFRP sheet using strain gauges attached along the center of the sheet. These strains are compared with strains determined using the finite element model along the sheet centerline in Figure 4.31. As shown, although the general trend is captured reasonably well in the finite

element model, the differences in measured to calculated strains are significant at the peak load step in the model. The finite element model predicted a stress transfer zone of approximately 400 mm (15.7 in.) compared with 300 mm (11.8 in.) that was determined in the laboratory using measured strains. It is notable, however, that the measured and computed strains are much closer if one uses a load near failure ( $T/T_u = 0.94$  in this case) instead of the peak load. The strain differences may have been caused by the inability of recording strains precisely at the instant that failure occurred in the specimen. Note that the stress transfer zone determined from the finite element model and the laboratory test at a load equal to 94% of the failure load was 340 and 300 mm (13.6 and 12 in.), respectively.



## CHAPTER 5

### FRP-CONCRETE SYSTEM: PARAMETRIC STUDY ON THE BEHAVIOR OF ANCHORED FRP SHEETS

#### 5.1 Introduction

Design provisions for fiber-reinforced polymer (FRP) strengthening systems recognize the inability of FRP sheets to reach their ultimate strength because of debonding from the concrete substrate. These provisions, therefore, limit the maximum strain of the FRP sheet that can be used for design. To increase the design efficiency of FRP sheets, past researchers have proposed anchoring the sheets to the concrete substrate instead of relying solely on bond to transfer stresses between concrete and FRP materials. Yet, the effect of applying anchors to FRP sheets has not been well understood. This research work presents the results of a detailed finite element simulation of the FRP-concrete joint system that includes all the components of the system explicitly. The model was then used to investigate the effect of several parameters of the anchor on the ultimate strength of the FRP system.

The parametric study included several anchor parameters that were considered influential in the debonding behavior of the CFRP-concrete joint system. The parameters that were studied are: (1) the number of anchors used in the sheet; (2) the distance between anchors; (3) anchor depth; (4) anchor shaft diameter; (5) anchor splay angle, (6) anchor splay diameter, and (7) FRP sheet thickness. Each parameter was studied independently while other parameters were held constant to isolate the effect of each parameter on behavior. Except for the case investigating the effect of the number of anchors on behavior, the base model for comparison consisted of an FRP-concrete joint

with four anchors positioned in a two-by-two pattern. The longitudinal spacing of anchors was kept constant in most cases except when examining the spacing effect.

## **5.2 Effect of the number of anchors**

Based on the modeling approach described in the previous chapters of this dissertation and the experimental tests conducted by (Breña and McGuirk 2013), Figure 5.1 compares finite element model and laboratory results of unanchored and anchored CFRP sheets. The anchored sheets used two to ten anchors to investigate the influence of the number of anchors on behavior. When two anchors were used, they were placed laterally spaced at 64 mm (2.5 in.) such that anchor splays on adjacent anchors came in contact. When more than two anchors were used, pairs of anchors had a longitudinal spacing equal to  $1.0D$ , where  $D$  represents the diameter of the anchor splay. The tensile strength of the specimens was accurately predicted using the finite element model described in previous sections of this research. For the number and geometry of anchors presented in the figure, there seems to be a linear increase in the tensile strength of the system as the number of anchors increases from zero to four anchors. However, the observed increase in strength does not continue linearly with an increasing number of anchors when more than four anchors are simulated as presented in Figure 5.1.

The sheet anchored using two anchors experienced a tensile strength increase of about 60% compared with the unanchored (bonded only) sheet. The tensile strength of the anchored system increased by more than 100% when a group of four anchors or more was placed in adjacent rows using a pattern as illustrated in the figure. With this pattern, the strength of the CFRP sheet was reached at maximum load.

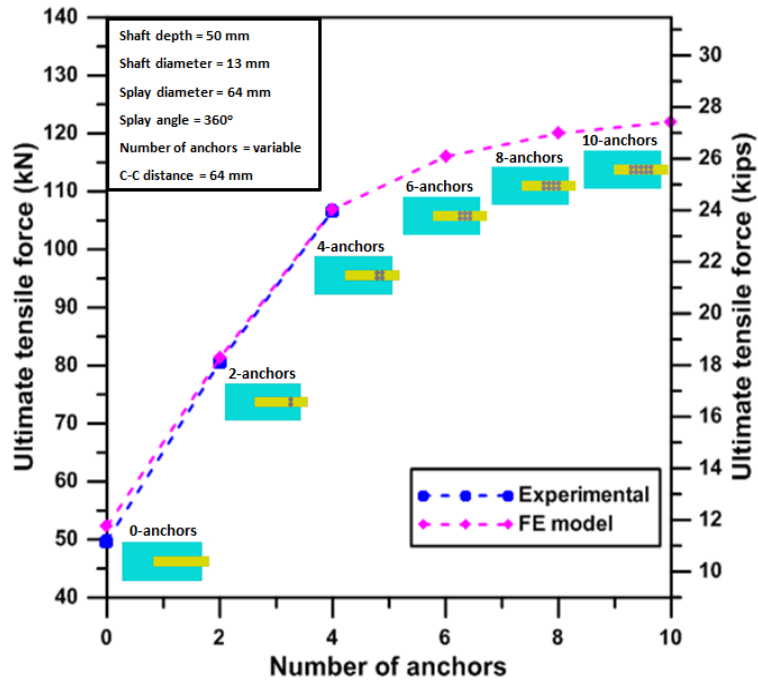


**Figure 5.1: Effect of the number of FRP anchors on peak force**

### 5.3 Effect of anchor longitudinal spacing

The results presented in Figure 5.2 show that placing anchors in rows that are distant from each other reduces the anchor effectiveness in developing higher tensile strength above the baseline strength of a CFRP sheet anchored with a single row of anchors (2 anchors in this case). The reduced effectiveness can be explained by considering the length of the stress transfer zone, the length over which stresses are transferred between the CFRP sheet and the underlying concrete. Anchors are most efficient when placed in rows that lie within the stress transfer zone.

The different points in Figure 5.2 are marked by indicating longitudinal anchor spacing as a multiple of splay diameter,  $D$ . A second row of anchors at distance  $5D$  from the first row led to a considerable reduction in tensile strength compared with anchors placed at a

longitudinal spacing of  $D$ . When comparing the ultimate tensile force obtained in the system anchored with four anchors spaced longitudinally at  $5D$  to the force obtained by a system containing a single row of two anchors (see Figure 5.1), similar strength values were obtained (82.3 kN for the system with four anchors at  $5D$  compared to 81.2 for the system with two anchors only). This comparison shows that anchors placed far from the stress transfer zone have little-to-no effect on the strength of the joint. The major benefit that might be obtained from placing anchors at large longitudinal separations is to increase the ductility of the joint.

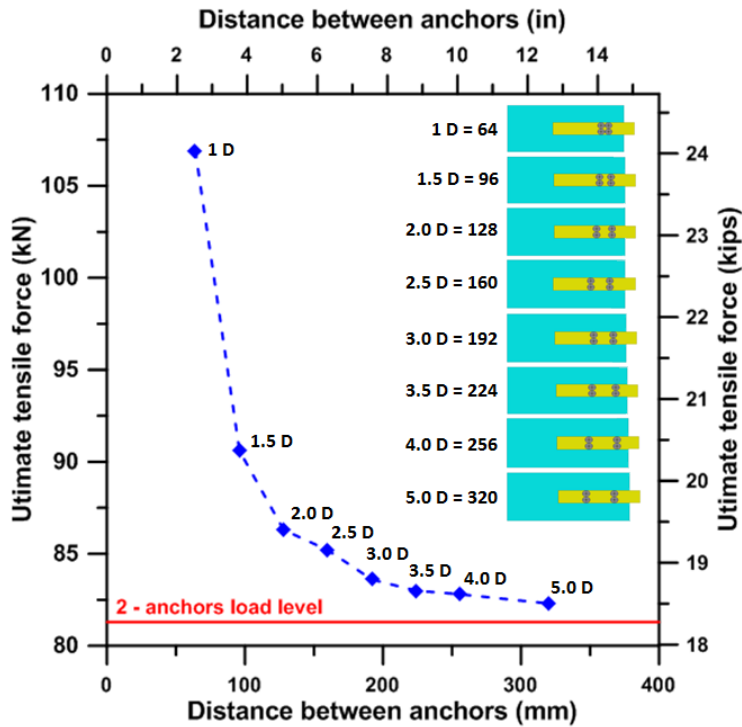


Figure 5.2: Effect of FRP anchor longitudinal spacing on peak force

#### 5.4 Effect of anchor length

Anchor length is considered a key parameter that affects the strength of the FRP-concrete joint. This effect belongs to anchor length that may increase the tensile capacity

of anchors when loaded normal to the anchored surface by preventing pullout failures and promoting the development of a concrete cone failure. For flexible anchors, such as those formed using FRP materials, it is not clear what anchor depth is needed to develop the tensile strength of a CFRP sheet when subjected to loading parallel to the bond surface (shear loading). Results of the finite element models show that reducing the depth of the CFRP anchor leads to a reduction in joint interface strength (Figure 5.3). The results also show that the contribution of 4 shallow anchors with an embedment of only 10 mm (0.4 in.) is sufficient to develop a strength comparable with a CFRP sheet anchored using two deeper anchors as shown in Figure 5.3. The increase in strength for deeper anchor embedment is not linear as can be observed in Figure 5.3. Interfacial shear loading generates stresses near the top of the anchor shaft as shown in Figure 5.4, just below the anchor splay. The generation of these stresses implies that most of the in-plane force that is transferred from the sheet is resisted by the anchor approximately within the top half of the anchor shaft.

When anchors with shaft depth of 30 mm (1.2 in) were used, the finite element results indicated that only 73% of the strength of the CFRP sheet (fiber tensile stress equal to 2770 MPa [402 ksi]) was developed before debonding occurred. For comparison, the system with 50 mm (1.2 in.) deep anchors developed the full strength of the FRP sheet. It should also be noted that the failure of the system without anchors occurred at approximately 62% of the tensile strength of the fibers.

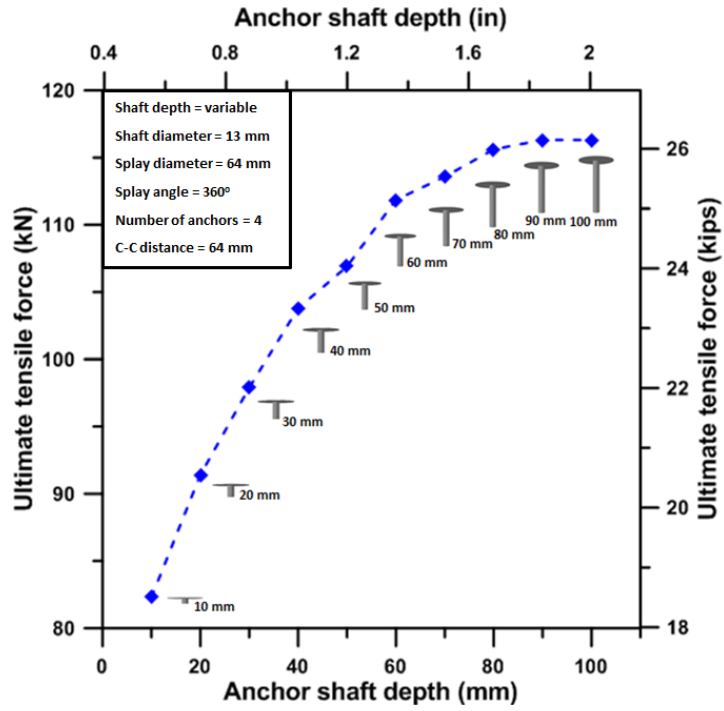


Figure 5.3: Effect of FRP anchor depth on peak force

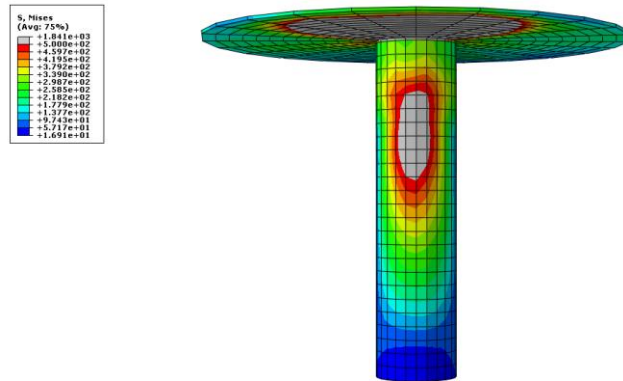


Figure 5.4: Stress distribution on the shaft of the CFRP anchor

In the analyses, failure of sheets containing anchors with a shaft depth of 30 mm (1.2 in.) or less occurred by anchor pullout and cover separation of concrete rather than

anchor fiber rupture. Therefore, anchors with less than 30 mm (1.2 in.) depth should not be recommended for design (see Figure 5.5).

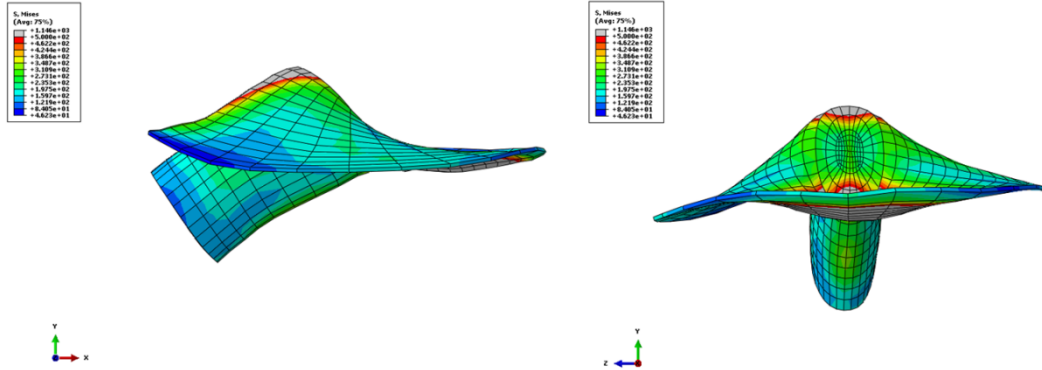


Figure 5.5: Deformed shape of the anchor (shaft depth = 20 mm)

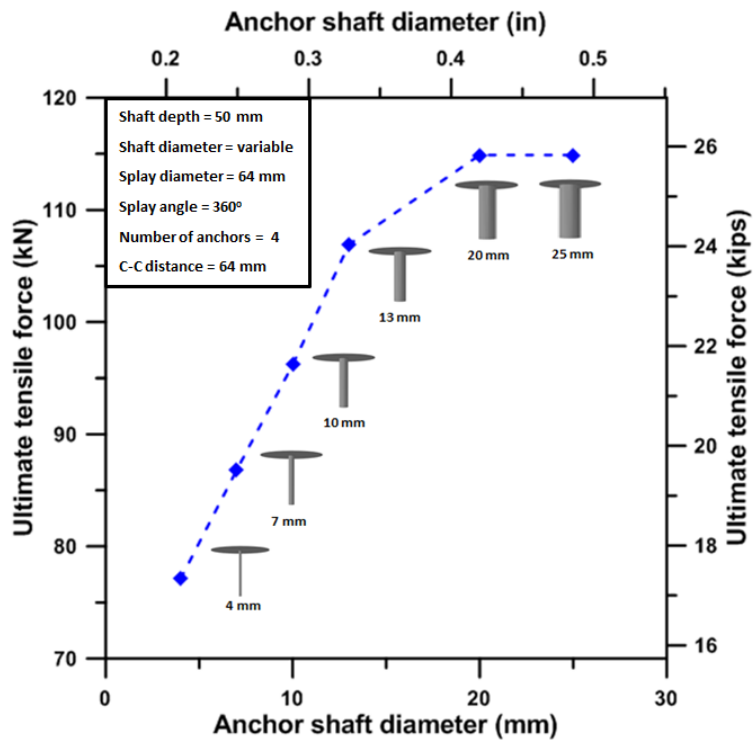


Figure 5.6: Effect of anchor shaft diameter on peak force

### 5.5 Effect of anchor shaft diameter

Figure 5.6 shows that increasing the diameter of the anchor shaft increases the strength of the joint. By increasing anchor diameter the contact area between the shaft of the anchor and concrete hole becomes larger, increasing shear strength. However, no further increase in strength was observed for anchor diameters exceeding 20 mm (0.80 in.).

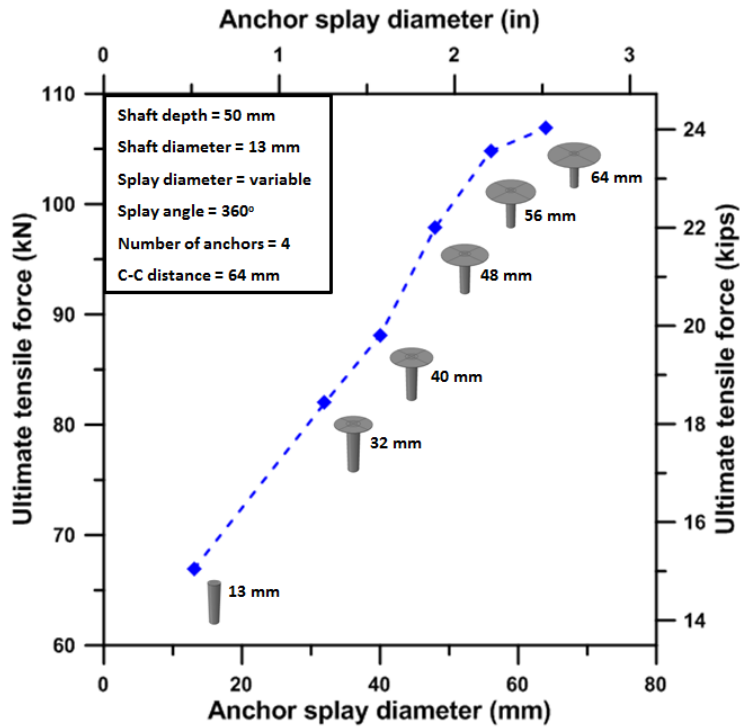


Figure 5.7: Effect of anchor splay diameter on peak force

### 5.6 Effect of anchor splay diameter

Modeling of CFRP-concrete joints that have anchors with different splay diameters shows that the ultimate strength of the joint is obtained when the splay of the anchor covers the entire width of the FRP sheet (Figure 5.7). This result is in agreement with the experimental observation of Niemitz et al. (2010), who observed that unidirectional FRP



sheets split longitudinally into regions between anchors because of the comparatively low tensile strength of the epoxy matrix.

### 5.7 Effect of anchor splay angle

Different shapes of the splayed part of the anchor have been observed in the literature (see Figure 5.8). However, no clear explanation of the reason behind using these shapes has been reported in any of the previous studies.

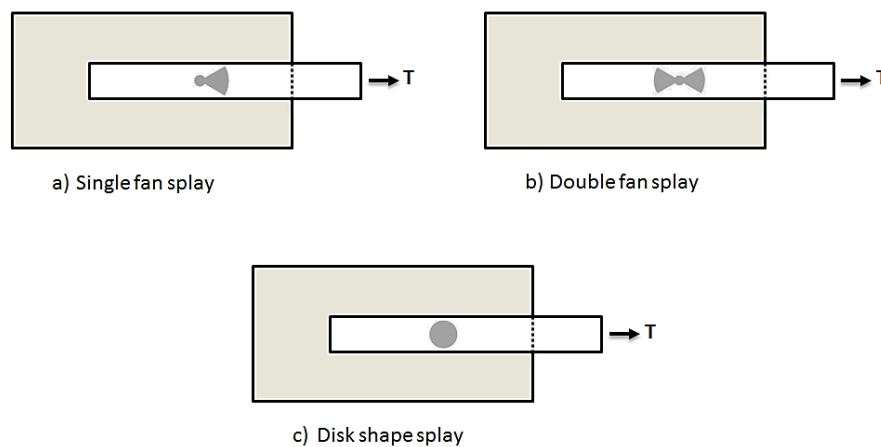


**Figure 5.8: Different anchor splay shapes: (a) and (b) (Smith 2011); (c) (Breña and McGuirk 2013)**

On the other hand, stress distribution in the CFRP anchor (see Figure 4.24 in chapter four) shows that stresses concentrated in front of the anchor in the direction of the tensile force forming the shape of a butterfly wing. This observation led to a new investigation to test the effect of using different anchors that have different splay or fan angles (see Figure 5.9). The results obtained from the finite element analysis of the anchored CFRP-concrete joint using different splay angles are shown in Figure 5.10.

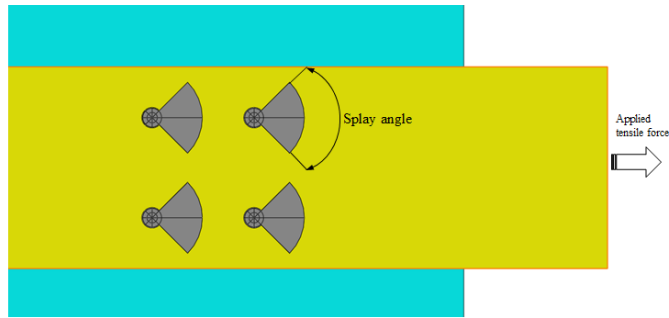


**Figure 5.9: Splay angle**

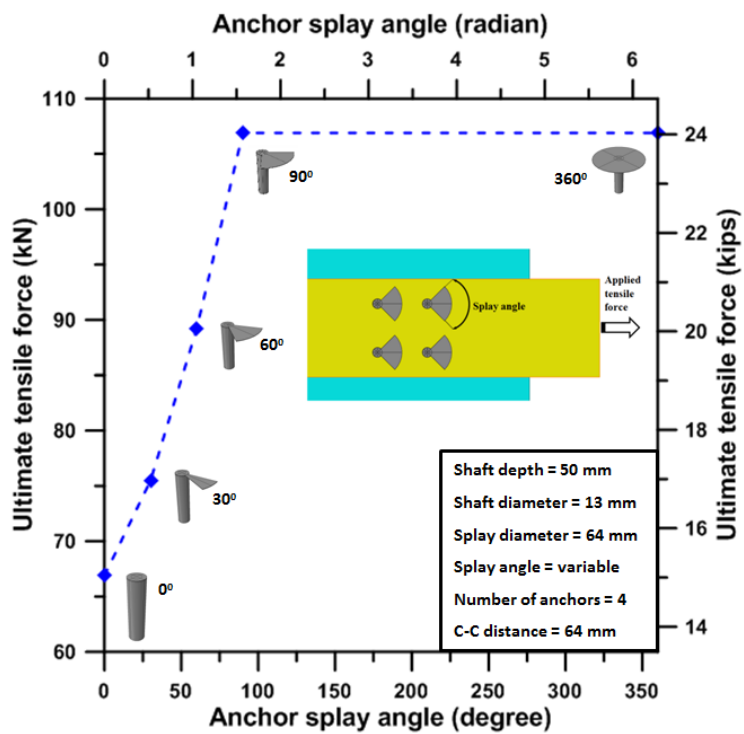


**Figure 5.10: Effect of splay angle**

Figure 5.10 shows that no more strength was obtained when using a CFRP anchor that has a splay angle of more than 90 degrees. This finding agrees with the observed distribution of tensile stresses in Figure 4.24 in chapter four where stresses concentrate on just a part of the splay.

### **5.8 Effect of FRP sheet thickness**

A 1-mm thick FRP sheet (cured thickness including adhesive), corresponding to Specimen F1-4a-1-24 tested by Breña and McGuirk (2013) was considered as the reference model. Because the tests reported by Breña and McGuirk (2013) used a wet-layup system, including the effect of FRP thickness in a model that explicitly considers the FRP sheet separately from the adhesive thickness was challenging.

To construct the model for Specimen F1-4a-1-24 (Breña and McGuirk 2013), the dry FRP fiber thickness was set equal to the value of 0.22 mm reported by the manufacturer of the composite system. Dry fiber thickness is defined as the ratio between area density to the volumetric density of dry fibers. The dry fiber thickness was subtracted from the cured FRP laminate thickness to obtain an adhesive thickness of 0.78 mm. for the interface between concrete and FRP sheet in the reference specimen. This adhesive thickness of 0.78 mm. was used in all other models regardless of the cured FRP laminate thickness. Different dry fiber thicknesses were used as a parameter to investigate the effect of the sheet thickness while keeping all other properties of the FRP system constant and equal to the properties of the reference specimen. The FE model results presented in Figure 5.11 show that the maximum tensile force developed in the FRP sheet increases approximately linearly with a corresponding increase in the thickness of the FRP sheet.

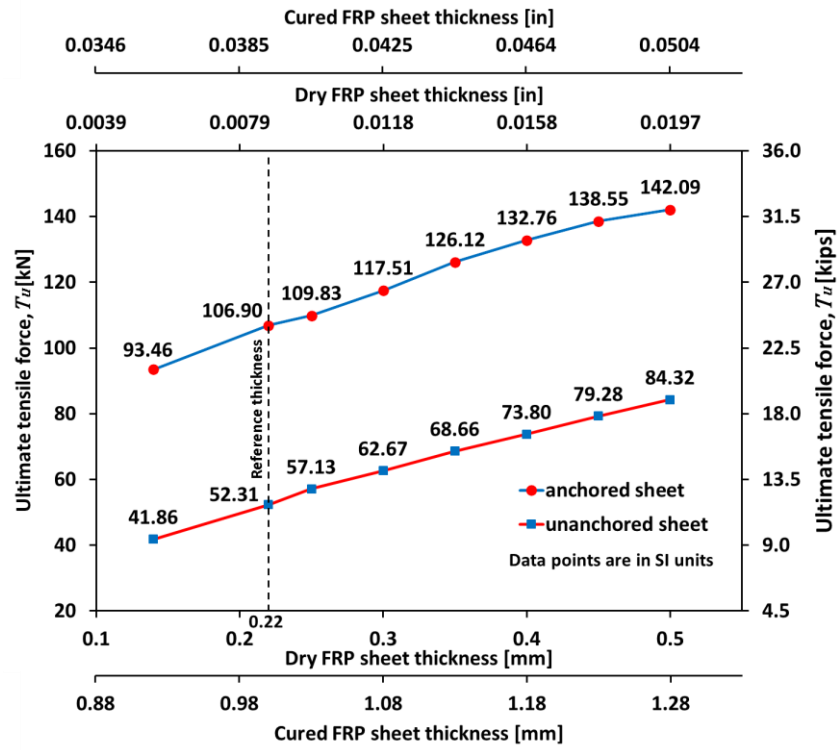


Figure 5.11: Effect of FRP sheet thickness on applied tensile force

## CHAPTER 6

### DEVELOPMENT AND APPLICATION OF FRP ANCHORAGE EFFICIENCY FACTOR

#### 6.1 Introduction

Several design guides are available to assist engineers in design, installation, and maintenance of externally bonded FRP systems (e.g., ACI 440.2R-17; AASHTO 2012, ISIS Canada 2007; fib technical report 2001; CNR-DT 200 2013; AFGC 2011; and JSCE 2001). These design guides take into consideration different strengthening scenarios such as strengthening for flexural, shear, and torsion; strengthening of members under axial or combined forces; strengthening for seismic and fatigue.

Debonding prior to reaching the FRP material ultimate strength is an important failure mode for externally bonded FRP sheets (Garden et al. 1998; Minh et al. 2001; Breña et al. 2003; Camata et al. 2007). To address this potential failure mode, design guides in general use empirically based factors that limit the maximum design strain that can be used in the FRP sheet to account for the potential of debonding, limiting the peak strain to a fraction of the useable strain.

Debonding behavior of FRP-to-concrete joints has been observed and extensively studied in many experimental programs in the past (Chajes et al. 1995; Bizindavyi and Neale 1999; Sebastian 2001; Yao et al. 2005; Dai et al. 2005; Czaderski et al. 2010). These tests also identified the different failure modes of the bonded FRP-to-concrete joints. The primary observed failure modes were concrete cover separation, debonding at the adhesive-concrete interface, and rupture of the FRP plate. It was also found that increasing the bond length beyond the effective stress transfer zone would not lead to any

significant increase in bond strength because once debonding initiates; it propagates along the interface without a notable increase in peak stresses within the stress transfer zone.

Propagation of cracks along the adhesive/concrete interface is the common failure mode for plates bonded on beam sides for shear strengthening and in flexurally strengthened beams where debonding starts at a major crack and propagates toward the plate ends (Teng et al. 2000; Smith et al. 2001).

In flexural applications, debonding failure modes of fiber reinforced polymer (FRP) sheets externally bonded to reinforced concrete beams are classified into debonding failure due to stress concentration near the end of the bonded plate and debonding failure due to flexural or flexural-shear crack away from the plate ends (Teng et al. 2003).

Chen and Teng (2001), for example, developed a bond strength model based on simple shear tests to predict the critical stress level in bonded plates due to intermediate flexural crack debonding in reinforced concrete beams. The model was then modified through calibration with other tests (Teng et al. 2003).

Techniques to allow development of higher stresses in the FRP-concrete interface have also been developed so that increased efficiency of the materials may be achieved. Experimental and theoretical studies have been conducted by researchers to investigate the change in debonding behavior that results from the application of FRP anchors that supplement epoxy bonding of FRP sheets (Niemitz et al. 2010; Smith et al. 2011; Breña and McGuirk 2013; Zhang et al. 2017). Niemitz et al. (2010) and Breña and McGuirk (2013) presented the results of a series of laboratory experiments conducted to study the possibility of strengthening FRP-concrete joints by applying FRP-anchors. The purpose

of using these anchors was to preclude debonding of bonded CFRP joints to allow reaching the FRP sheet strength. Specimens consisting of concrete blocks with FRP-sheets attached to the top surfaces of the concrete blocks using an epoxy adhesive material were tested in the laboratory. The laboratory specimens were designed to study the effect of changes in bond length, the number of FRP anchors, and anchor placement, among other parameters. These experiments also identified failure modes of FRP anchored sheets, which included shear rupture of the FRP anchors, anchor splay delamination, and anchor pull out. Based on the experimental work of Niemitz et al. (2010) it was recommended that the FRP-anchor splay diameter cover the entire width of the FRP sheet to avoid longitudinal splitting of the unidirectional FRP sheet. Other parameters were also investigated, including the effect of anchor longitudinal spacing and the effect of the number of FRP sheet plies. The researchers found that anchors that are not within the stress transfer zone of the debonded FRP-sheet minimally contributed to increases in strength of the FRP-concrete system, although increases in ductility were observed that resulted from a delay in debonding propagation. The most important finding of this experimental work was to prove that increasing the number of anchors within the stress transfer zone improves the strength of FRP-concrete joints significantly, but that additional anchors lying outside the stress transfer zone are not significantly efficient.

Smith et al. (2011) conducted laboratory experiments that included several FRP strengthened slabs subjected to bending. The primary objective of these tests was to investigate the effect of applying FRP anchors to the strengthened members. These FRP anchors were used to delay or prevent debonding of FRP sheets from the concrete surface

of the strengthened slabs. Differences in anchor properties included the volume of FRP fibers used to form each type of anchor and the spacing between anchors. As a result of these tests, the failure modes were documented including pullout from the concrete substrate, partial rupture of FRP sheets, and complete rupture of the FRP sheets within the slab constant moment region. The tests demonstrated that debonding crack propagation was partially arrested in slabs where FRP anchors were applied, specifically in the shear span where closer spaced anchors were provided. Furthermore, larger displacements and higher strengths were achieved. Debonding of the FRP sheets still occurred prior to FRP anchor failure; anchors delayed complete separation of the FRP sheets from the concrete substrate. Strength and deflection were increased by positioning the anchors with densest fiber content near the region of maximum bending in the middle of the slab.

Zhang et al. (2017) developed a load-slip model for FRP anchors that the investigators derived from several laboratory tests of FRP-concrete joints anchored with FRP anchors. This model has been found to be useful to conduct detailed debonding simulations of externally-bonded FRP sheets containing supplemental FRP anchors. A practical formulation that can be used for the design of FRP anchorage systems, however, is still lacking.

Laboratory experiments have demonstrated that anchored FRP sheets achieve higher strengths compared with FRP bonded-only sheets. Currently, the effective strain of the bonded FRP sheet determined from ACI 440.2R-17 or other similar guides is limited to the strain at which FRP debonding may occur. This strain level does not account for the



beneficial effect of FRP anchors on the system, and therefore the efficiency of the FRP sheets is not fully utilized.

The strain level at which debonding of anchored FRP sheet may occur is difficult to be quantified analytically because of the mixed failure modes of the different materials and the different geometric parts in the FRP-concrete joint system. Therefore, a semi-empirical approach based on both finite element analysis and previous laboratory tests is presented in this research with the goal of developing a method to estimate the debonding strain of anchored FRP sheets.

The proposed formulation is based on an anchorage efficiency factor that accounts for the increase in strength that FRP anchors provide. This formulation is presented in a format that could be incorporated into design guidelines such as ACI 440.2R-17 by introducing a modification factor in existing debonding strain equations to estimate the maximum strain that an FRP sheet can develop before debonding. The introduction of this modification factor allows the effect of FRP anchors in developing higher strains in FRP sheets to be estimated within the current framework of existing design guides.

## **6.2 FRP strain limits**

For design, the ACI 440.2R-17 Guide considers three limiting strain values that need to be considered in design of externally bonded FRP sheets used to strengthen existing concrete elements. These limits are the FRP rupture strain  $\epsilon_{fu}$ , the debonding strain  $\epsilon_{fd}$ , and the effective strain  $\epsilon_{fe}$  (Figure 6.1). For flexural strengthening, the strain at rupture,  $\epsilon_{fu}$ , of the FRP sheet is assumed to occur at a value equal to 90% of the rupture strain determined from tensile testing of FRP coupons. Debonding of the FRP sheet from the

concrete surface typically takes place before FRP sheets reach their rupture strain and therefore strains developed in the FRP sheet are limited to a strain associated with debonding  $\epsilon_{fd}$ . (debonding strain limit in the ACI 440.2R-17 Guide).

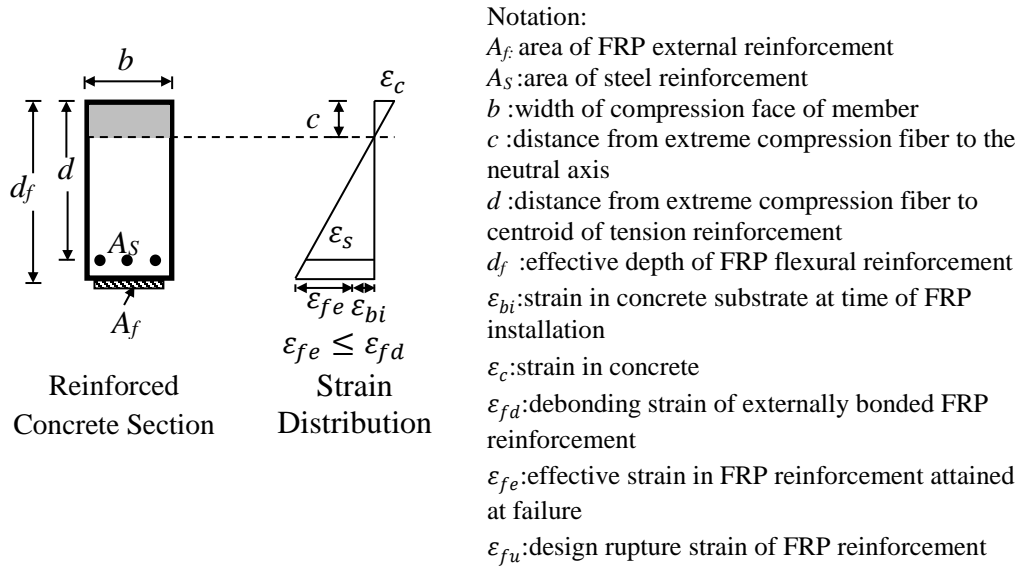


**Figure 6.1: Compatibility of axial strains in an FRP-strengthened concrete beam under flexure**

In addition to the debonding limit, the ACI 440.2R-17 Guide sets a limit on the maximum strain that can develop in an FRP sheet bonded to the tension face of a concrete element at the onset of concrete crushing in compression. This limit, for members dominated by flexure, is determined assuming a linear distribution of strains along the cross-sectional depth as is commonly done in the design of reinforced concrete members (Figure 6.1). Following the linear strain distribution assumption, the strain in the FRP sheet at concrete crushing ( $\epsilon_{cu}=0.003$ ) can be determined from:

$$\epsilon_{fe} = \epsilon_{cu} \left( \frac{d_f - c}{c} \right) - \epsilon_{bi} \leq \epsilon_{fd} \quad (6.1)$$

Where  $\varepsilon_{fe}$  is the effective strain developed in FRP sheets attained at the crushing of concrete and  $\varepsilon_{bi}$  is the substrate (concrete) strain that exists due to dead loads acting in the flexural member before strengthening. Therefore, the effective strain represents the maximum strain that could be developed in the FRP sheet if debonding were not to occur prior to reaching concrete crushing in compression.

The three preceding strain limits can be expressed using a single equation as:

$$\varepsilon_{fe} \leq \varepsilon_{fd} \leq 0.9 \varepsilon_{fu} \quad (6.2)$$

The highest efficiency in a strengthening application is obtained by increasing the debonding strain value  $\varepsilon_{fd}$  in Equation 6.2 if debonding is delayed or eliminated. One way of achieving higher debonding strains is to provide supplemental anchorage of the FRP sheet as research has demonstrated and summarized in the Introduction Section (Smith et al. 2011; Niemitz et al. 2010; Orton et al. 2008). Current design guidelines of FRP-strengthening systems, however, lack information for the design of anchored FRP sheets primarily due to the paucity of both experimental and analytical research related to this topic. This research seeks to fill this information void.

### 6.3 Debonding strain of unanchored FRP sheets

The debonding strain formula proposed by Teng et al. (2003; 2004) was used in modified form for inclusion in the ACI 440.2R-17 Guide. In ACI 440.2R-17, the calculated strain at which FRP debonds from the surface of concrete is estimated using:

$$\varepsilon_{fd} = 0.083 \sqrt{\frac{f'_c}{nE_f t_f}} \leq 0.9 \varepsilon_{fu} \text{ in in.-lb. units} \quad (6.3)$$

$$\varepsilon_{fd} = 0.41 \sqrt{\frac{f'_c}{nE_f t_f}} \leq 0.9 \varepsilon_{fu} \text{ in SI units}$$

Where  $\varepsilon_{fd}$  is the debonding strain of externally bonded FRP sheets,  $f'_c$  is the compressive strength of concrete (in psi for in-lb. units or MPa for SI units),  $n$  is the number of plies (layers) of FRP material,  $E_f$  is the tensile modulus of elasticity of the FRP laminate,  $t_f$  represents the nominal thickness of one ply of FRP sheet, and  $\varepsilon_{fu}$  is the tension rupture strain of the FRP material.

Application of Equation 6.3 in common design situations results in a significant reduction in the maximum strain that can be considered in FRP materials for design before debonding. The goal of providing supplemental anchors is to enable larger strains to develop prior to debonding of the FRP sheet resulting in a more efficient application of FRP materials as a strengthening material for reinforced concrete structures. Supplemental anchorage of FRP sheets results in higher strains developed in FRP sheets, but a formulation that includes the effect of anchors on the maximum developed strain and corresponding strength of the FRP sheets is needed. The following sections describe the methodology used in this research to develop a formula that includes the effect of anchorage of FRP sheets in maximum strain developed.

#### **6.4 Debonding strain of anchored FRP sheets**

Results from laboratory tests and finite element analyses suggest that FRP sheets debond at higher strains when FRP anchors are used in addition to epoxy bonding the materials to the surface of concrete elements (Garden et al. 1998; Minh et al. 2001; Niemitz et al. 2010; Breña and McGuirk 2013; Smith et al. 2011). The magnitude of strains developed depends on the anchorage method and the properties of the anchors. Although the beneficial effect of anchoring FRP sheets has been demonstrated, little has

been done to develop a rational method to quantify the strength increase of FRP-anchored sheets. The method proposed herein is based on a modification of the current debonding strain equation included in the ACI 440.2R-17 Guide (Equation 6.3), which was developed for epoxy-bonded FRP sheets. The ratio between the strength of a bonded-plus-anchored FRP sheet to the strength of a bonded-only FRP sheet can be used to develop a modification factor, denoted here as  $K_{\epsilon a}$  and defined as the anchorage efficiency factor, that can be included in the debonding strain equation  $\epsilon_{fd}$  of the ACI 440.2R-17 Guide, such that:

$$\epsilon_{fd(anchored)} = K_{\epsilon a} \cdot \epsilon_{fd} \quad (6.4)$$

Where,  $\epsilon_{fd}$  is the debonding strain of externally bonded FRP sheets, and  $K_{\epsilon a}$  is the proposed anchorage efficiency factor that increases the strain of anchored FRP sheets over the respective values for bonded-only (unanchored) FRP sheets.

For consistency with current strain limits of bonded sheets contained in ACI 440.2R-17, It is proposed that the limits be also applied to the design strain of anchored FRP sheets ( $\epsilon_{fd(anchored)}$ ), namely,

$$\epsilon_{fd(anchored)} \leq 0.9\epsilon_{fu} \quad (6.5)$$

and

$$\epsilon_{fe} \leq \epsilon_{fd(anchored)} \quad (6.6)$$

Consequently, when using FRP anchors in design, only the design strain of externally applied FRP sheets would need to be modified from  $\epsilon_{fd}$  for bonded-only applications to  $\epsilon_{fd(anchored)}$  for bonded-anchored applications.

## 6.5 Proposed anchorage efficiency factor

Debonding behavior of anchored-externally bonded FRP sheets involves complex and combined failure modes. To develop an anchorage efficiency factor, an approach was developed to include the effect of those parameters that have been found to affect the behavior of FRP anchored systems. This approach is based on experimental results reported previously in the technical literature and finite element analyses of bonded FRP sheets containing supplemental FRP anchors.

As stated in chapter five, a parametric study was conducted based on a finite element (FE) model calibrated using research results obtained from previous tests that involved FRP-sheets bonded onto the surface of concrete blocks tested in a direct shear configuration. These simulated FRP-concrete joints mimic debonding failure due to crack propagation along the adhesive/concrete interface. This failure mode is common in reinforced concrete beams strengthened for shear with externally bonded FRP sheets and beams strengthened for flexure when debonding of the FRP sheet propagates at the adhesive/concrete interface starting from major flexural cracks (Teng et al. 2000; Smith et al. 2001). The parameters included in the study were the number of anchors applied to the FRP sheet, the distance between anchors, anchor shaft diameter, anchor shaft depth, anchor fan angle, and anchor fan diameter.

Results from this parametric study were used to develop an equation to estimate the anchorage efficiency factor ( $K_{\epsilon a}$ ) to incorporate as a modifier in the current debonding strain equation (Equation 6.3) and account for the effect of anchors. To accomplish this, the FE analysis results were processed in two stages as described in the following section to develop a general formulation that considers anchor geometries and configurations not

included in the simulations by adopting results from regression analysis and determined using best fitting curves.

To produce standard strength factors so that strength can be determined for any number of anchors along the debonding path (FRP sheet longitudinal direction), The values from the parametric study were first normalized to the strength of unanchored sheet. Then, the normalized values from the first stage were divided by the normalized strength ratio of the sheet with four anchors of a reference specimen (Specimen F1-4a-1-24, Breña and McGuirk 2013). The resulting standardized values for all parameters were multiplied by the strength ratio due to the change in number of anchors to determine the proposed anchorage efficiency factor. This procedure is described in more detail in the following two sections.

## **6.6 Observations on the results of the FE model parametric analyses**

Strength values of anchored FRP sheets obtained in the parametric study were divided by the calculated strength of the reference unanchored sheet (0.22 mm. dry fiber thickness) to determine the strength gain obtained by using FRP anchors with different configurations. The strength ratio between models with anchored FRP sheets and models with unanchored FRP sheets decreased from a maximum of 2.23 to a minimum of 1.69 (Figure 6.2) for FRP dry fiber thicknesses of 0.14 to 0.5 mm., respectively (FRP sheets having between one and three layers, respectively).

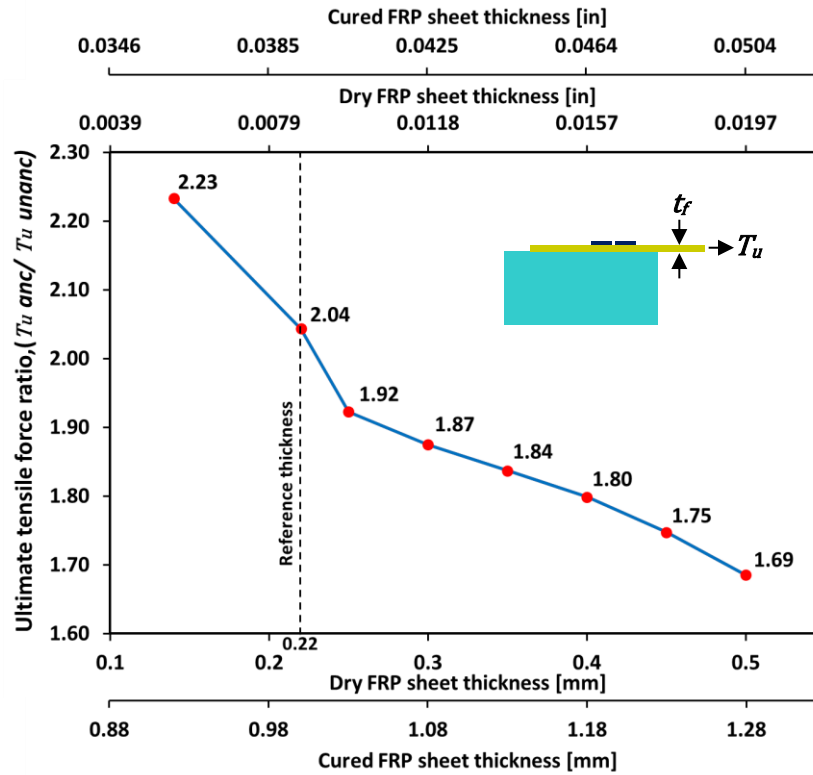


**Figure 6.2: Ratios of ultimate tensile force of anchored to unanchored FRP sheets ( $T_u \text{ anc} / T_u \text{ unanc}$ ) due to change in thickness  $t_f$**

The reference FRP-anchored model corresponds to an FRP sheet with a 0.22 mm. dry fiber thickness and four anchors arranged in a 2 by 2 pattern as was tested in the laboratory. The FE model gave a tensile strength equal to 2.04 times the companion FE model constructed for unanchored bonded FRP sheets, which is close to the strength ratio of 2.14 that is determined from the test results of Breña and McGuirk (2013). Maintaining the FRP sheet thickness constant, other parameters specific to the FRP anchors were varied to focus on the effect of anchors on strength gain including: (1) spacing between anchors, (2) anchor shaft diameter, (3) anchor fan diameter, and (4) number of anchors along the debonding path.



As stated in chapter five, strength gain achieved by embedding anchors deeper than 50 mm into the concrete was found negligible in the experiments and simulations, and that forming an anchor fan angle of at least  $90^\circ$  splayed in the direction of tensile force resulted in the maximum gain in strength. However, the anchor fan angle of  $360^\circ$  and the anchor shaft depth of 50 mm were selected in this research and maintained constant in all models to be consistent with the reference model and the laboratory testing.

It should be noted that the anchor fan diameter considered in this research is given as the ratio of splay diameter divided by the FRP sheet times the number of anchors across the FRP sheet. Therefore, the results obtained from this parametric study are considered applicable for different number of anchors along the width of the FRP sheet that is within the FRP anchor fan diameter (see Table 6.1 for the values of anchor fan diameters / [FRP sheet width/number of anchors across width] considered in this research).

Figure 6.3 presents ratios of calculated tensile force of anchored to unanchored FRP sheet (0.22 mm dry fiber thickness) as longitudinal spacing between anchors ( $s_a$ ) increases. This figure shows that, as spacing increases, anchor efficiency decreases exponentially and asymptotically approaches a minimum value of approximately 1.55, which corresponds to the strength gain provided by a single row of anchors (see Figure 6.6). The largest reduction in strength ratio was observed as spacing increased from 64 mm. to approximately 200 mm. This result indicates that anchors placed outside of the effective stress transfer zone are ineffective, which in this case was between 200 and 300 mm. Figure 6.4 presents strength ratios of anchored to unanchored FRP sheets as a function of anchor shaft diameter ( $a_d$ ). The figure illustrates that increasing anchor shaft

diameter from 13 mm. to 20 mm. increased the strength ratio. An increase in  $a_d$  beyond 20 mm. had no additional effect on strength gain, indicating that beyond this diameter the failure mode was directly related to anchor diameter. A reduction in  $a_d$  from 13 mm. had a consequent decrease in strength gain ratio.

**Table 6.1: Properties of the experimental specimens used in the regression analysis**

Research group	Specimen Notation	Number of anchors ( $n_a$ )	Thickness of the FRP sheet ( $t_f$ )	Spacing between anchors ( $s_a$ )	Anchor shaft diameter ( $a_d$ )	Anchor fan diameter <sup>1</sup> ( $f_d$ )	$T_u$ without anchors, kN	$T_u$ with anchors, kN
Niemitz et al. (2010)	BI-13-0.6-5	2	0.22	254	6	0.4	35.6	45.4
	BI-13-1.3-5	2	0.22	254	13	0.4	35.6	53
	BIIs-25-1.9-10	1	0.22	----	19	0.8	50.9	87.6
	BI-13-1.3-10	2	0.22	254	13	0.8	35.6	49
	BI-13-1.9-10	2	0.22	254	19	0.8	35.6	58.2
Brena and McGuirk (2013)	F1-4a-1-24	2	0.22	64	13	1	49.8	106.7
	F2-4a-1-24	2	0.44	64	13	1	69.9	182.5
	F1-2a-24	1	0.22	----	13	1	49.8	80.6
	F2-2a-24	1	0.44	----	13	1	69.9	150.5
Zhang and Smith (2012)	1FA	1	0.262	----	14	1	15.53	31.13
	2FA100	2	0.262	100	14	1	15.53	37.94
	2FA125	2	0.262	125	14	1	15.53	33.08
	2FA150	2	0.262	150	14	1	15.53	26.86
	3FA75	3	0.262	75	14	1	15.53	42.89

<sup>1</sup> Normalized value (anchor splay diameter/ (FRP sheet width /number of anchors along the width)).

Figure 6.5 presents the effect of anchor fan diameter ( $f_d$ ) on the strength gain ratio of anchored FRP sheets. The figure, where anchor fan diameter is normalized with respect to width of the FRP sheet, highlights the importance of covering the entire FRP sheet width within the fan diameter  $f_d$  since the maximum strength is obtained when the  $f_d$  is equal to the FRP sheet width.

Figure 6.6 presents the strength factor ratio  $S_n$  as a function of number of anchors along the debonding path such that the anchor fans do not overlap and are just in contact. As shown in the figure, only the number of anchor rows was used to define this parameter regardless of number of anchors placed across the sheet width because each anchor is only effective in engaging the area of FRP sheet within its corresponding fan diameter. This figure shows that increasing the number of anchors along the debonding path increases the strength ratio, but up to a limit. For the reference model used in this study, however, no significant increase in strength ratio was obtained for more than four anchor rows along the debonding path, corresponding to a sheet length equal to 256 mm., in this case. This result is consistent with the observation that anchors are only effective when placed inside the effective stress transfer zone, although higher ductility might be obtained by placing anchors outside this region. The figure also includes a best-fit curve for  $S_n$  based on number of anchor rows. The curve clearly illustrates that the increase in strength beyond four rows is negligible.

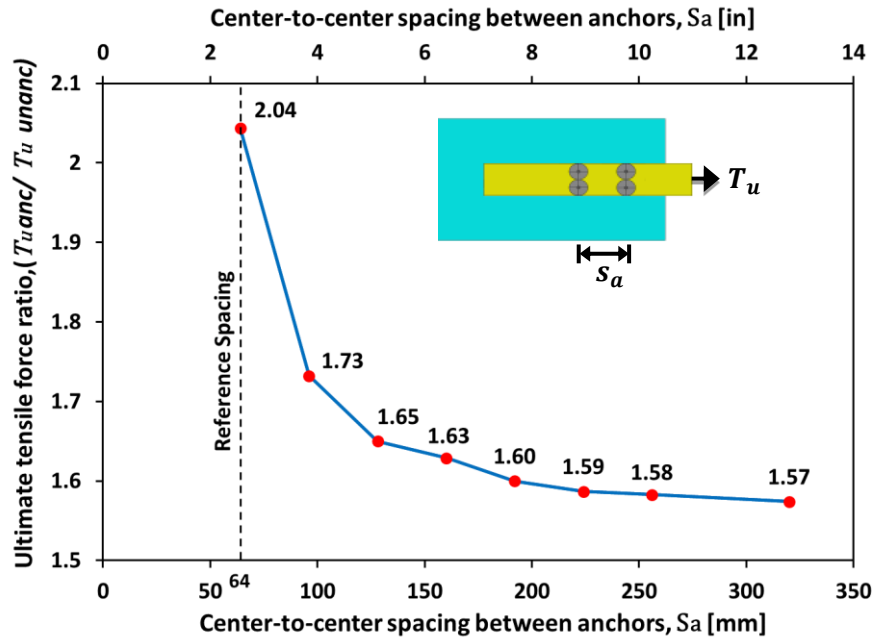


Figure 6.3: Ratios of ultimate tensile force of anchored to unanchored FRP sheets

$(T_{u\text{ anc}} / T_{u\text{ unanc}})$  due to change in longitudinal spacing between anchors  $s_a$

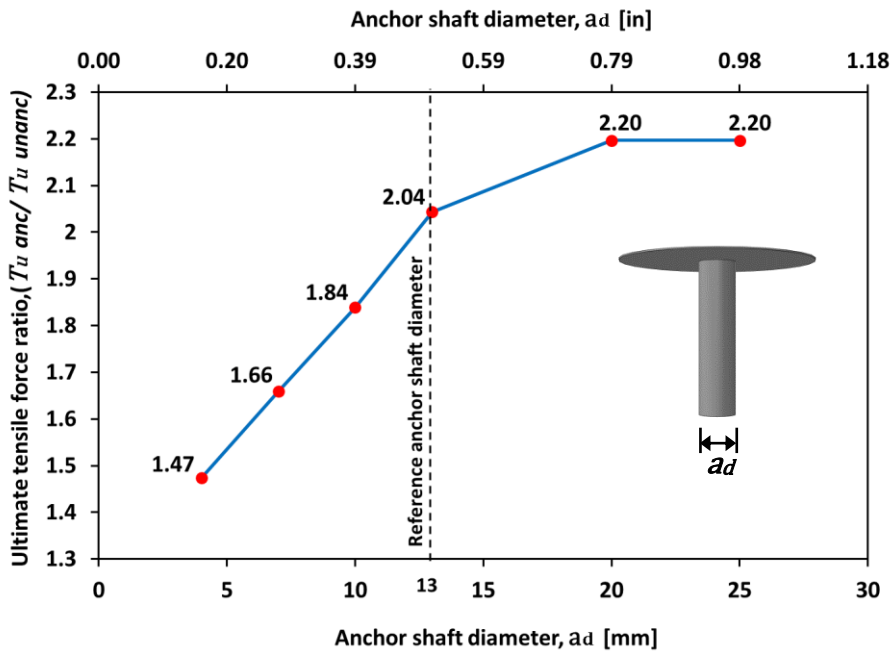


Figure 6.4: Influence of anchor shaft diameter ( $a_d$ ) on ultimate tensile force ratio

$(T_{u\text{ anc}} / T_{u\text{ unanc}})$

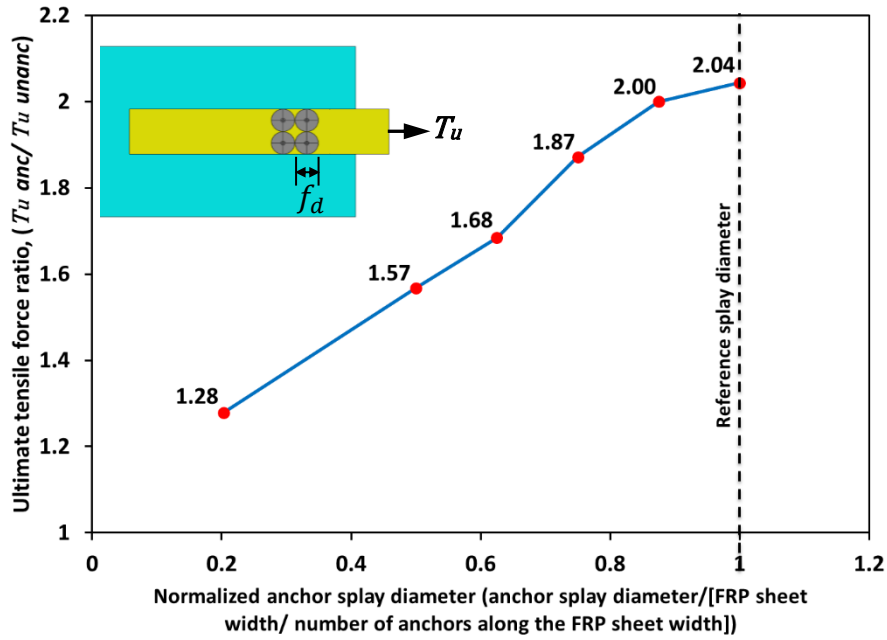


Figure 6.5: Influence of anchor fan diameter ( $f_d$ ) on ultimate tensile force ratio ( $T_u\text{ anc} / T_u\text{ unanc}$ )

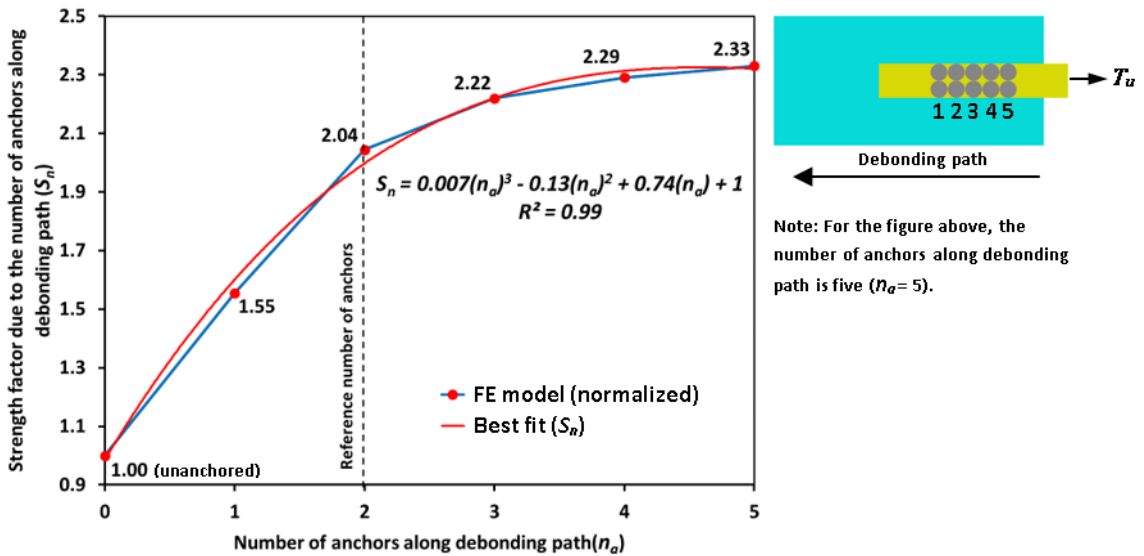


Figure 6.6: Influence of number of anchor rows along debonding path ( $n_a$ ) on strength factor

## 6.7 Normalization of FE modeling results

Each strength ratio factor obtained in the parametric analysis as discussed in the previous section was divided by the factor calculated for the reference specimen (four anchors arranged in a two-by-two pattern). The resulting standardized strength factors along with best-fit curves were calculated for each normalized parameter tested as presented in Figures 6.7 through 6.10.

Figure 6.7 presents the data along with the best-fit curve that captures the effect of FRP sheet thickness on standardized anchorage strength gain ( $S_t$ ). Similarly, Figure 6.8 depicts the data and best-fit curve for the anchorage strength gain factor  $S_s$  corresponding to a change in spacing between anchors. Figures 6.9 and 6.10 present results for the two remaining parameters that were studied and that were considered relevant in the behavior of anchored FRP sheets, anchor shaft diameter ( $S_{ad}$ ) and anchor fan diameter ( $S_{fd}$ ), respectively.

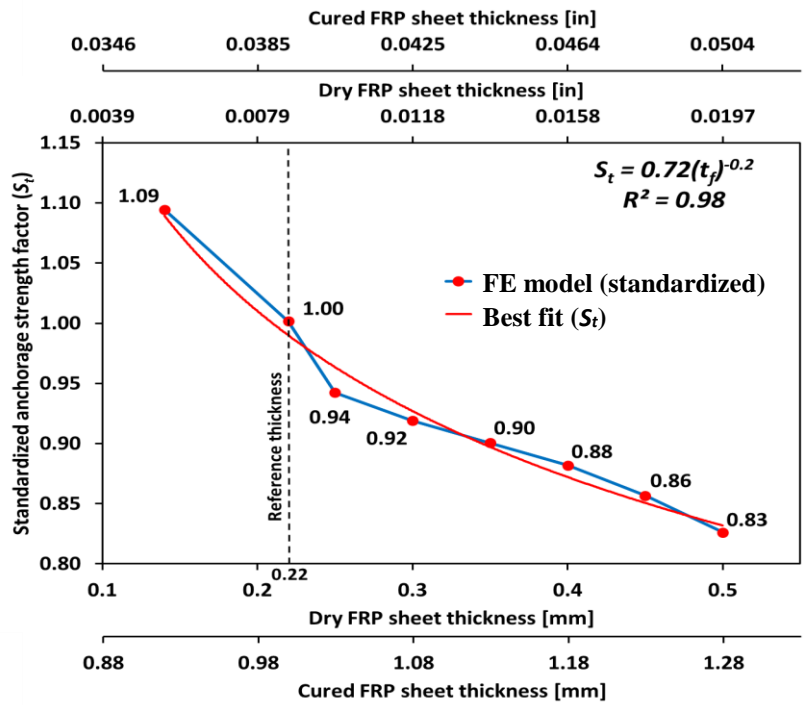


Figure 6.7: Influence of FRP sheet thickness ( $t_f$ ) on the standardized strength factor

( $S_t$ )

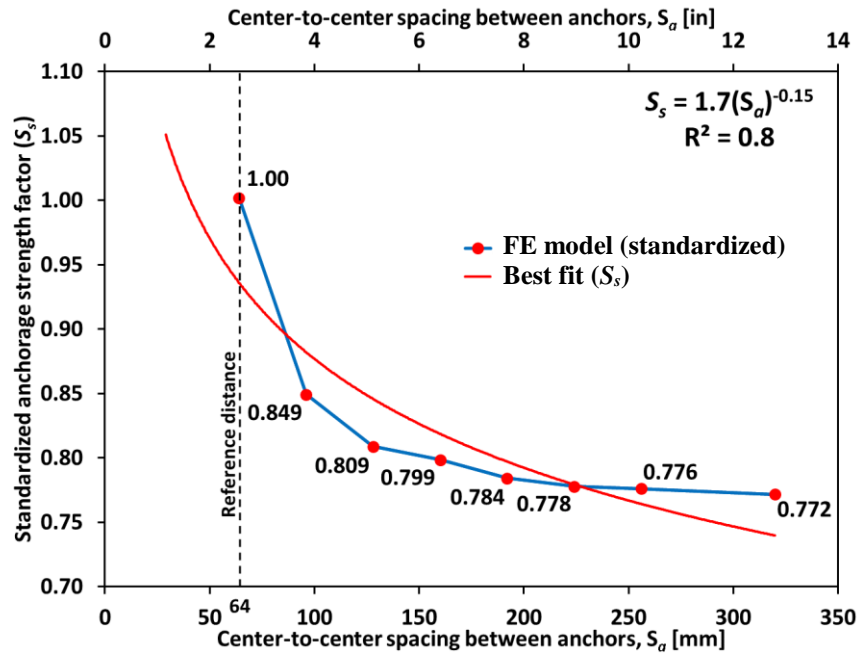


Figure 6.8: Influence of the center-to-center spacing between anchors ( $S_a$ ) on the standardized strength factor ( $S_s$ )



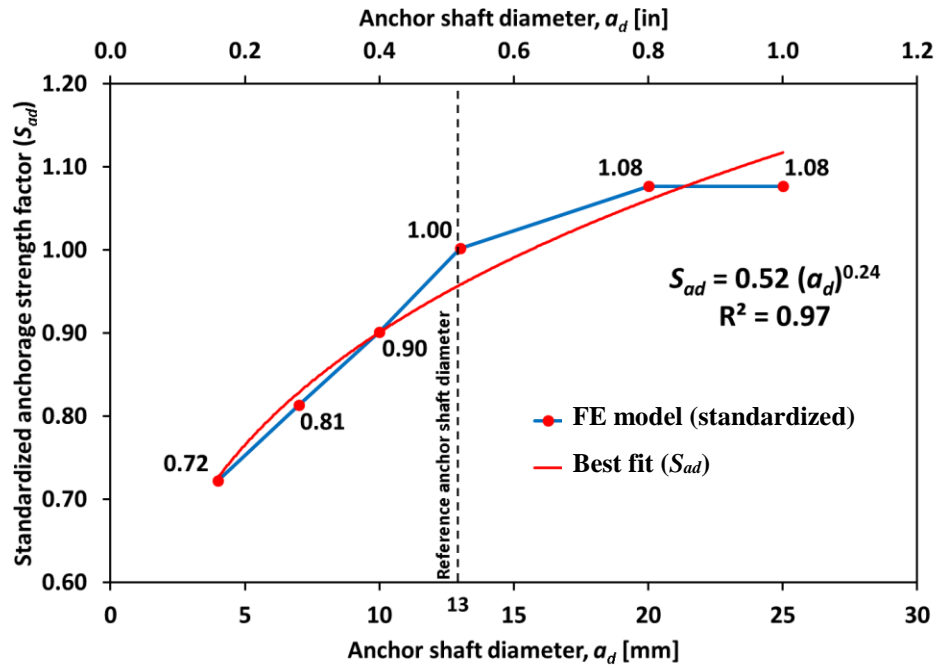


Figure 6.9: Influence of the anchor shaft diameter ( $a_d$ ) on the standardized strength factor ( $S_{ad}$ )

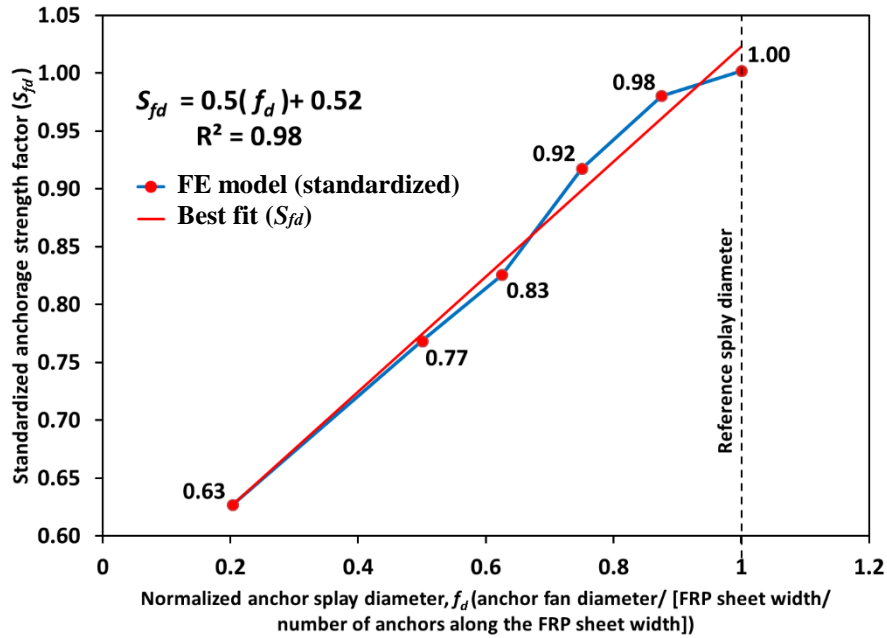


Figure 6.10: Influence of the normalized anchor splay diameter ( $f_d$ ) on the standardized strength factor ( $S_{fd}$ )

Because the stress-strain relationship of FRP materials is linear, the standardized strength gain factors were combined to calculate a unique anchorage strain efficiency factor ( $K_{\epsilon a}$ ) that represents the increase in strain that is developed in an anchored FRP sheet with respect to an unanchored sheet for different values of the modeled parameters. The product of the standardized best-fit strength efficiency factors, elevated to exponents  $a$  through  $e$ , result in the overall strain efficiency factor for a given number of FRP anchors, anchor dimensions, and anchor arrangement:

$$K_{\epsilon a} = S_n^a \cdot S_t^b \cdot S_s^c \cdot S_{ad}^d \cdot S_{fd}^e \geq 1.0 \quad (6.7)$$

The exponential formula (Equation 6.7) is based on a segmented model in which exponents  $a$  through  $e$  are determined through nonlinear regression analysis (conditional logic) conducted using IBM SPSS software package. Laboratory tests conducted by three different research groups (Niemitz et al. 2010; Zhang and Smith 2012; Breña and McGuirk 2013) were used in the regression analysis. Properties of the laboratory specimens used in the regression analysis are shown in Table 6.1. The anchorage strain efficiency factor is considered as the dependent variable while the other factors are considered independent.

The proposed segmented model (Equation 6.7), is based on the product of the various standardized strength gain factors that correspond to each of the parameters that influence anchored sheet behavior ( $S_i$ ) and the strength factor due to change in number of anchors ( $S_n$ ). The values of exponents  $a$  through  $e$  for each of the strength gain factors were determined through the nonlinear regression analysis that is based on previous laboratory tests to develop the anchorage strain efficiency formula represented by Equation 6.7.

The anchorage strain efficiency factor  $K_{\varepsilon a}$  from Equation 6.7 could then be used to increase the debonding strain  $\varepsilon_{fd}$  obtained from Equation 6.3 to account for the effect of FRP anchorage. Therefore, the strain that an anchored FRP sheet can potentially develop,  $\varepsilon_{fd(anchored)}$ , can be estimated by combining Eqs. 6.3 and 6.4 as:

$$\varepsilon_{fd(anchored)} = K_{\varepsilon a} \cdot 0.083 \sqrt{\frac{f'_c}{nE_f t_f}} \leq 0.9 \varepsilon_{f\mu} \quad \text{in . in - lb units} \quad (6.8)$$

$$\varepsilon_{fd(anchored)} = K_{\varepsilon a} \cdot 0.41 \sqrt{\frac{f'_c}{nE_f t_f}} \leq 0.9 \varepsilon_{f\mu} \quad \text{in SI units}$$

The expressions for strength gain factors obtained through regression analysis that were incorporated for calculation of a general anchorage efficiency factor  $K_{\varepsilon a}$  are presented in the following section.

### 6.8 Anchorage efficiency formula

Each of the best-fit curves corresponding to normalized strength dependent on number of anchors ( $S_n$ ) and the standardized anchorage strength gain factors ( $S_t$ ,  $S_s$ ,  $S_{ad}$ ,  $S_{fd}$ ) are presented in Figures 6.6 through 6.10. The resulting best-fit equations for each of the normalized (Equation 6.9) or standardized anchorage strength gain factors (Equations 6.10 through 6.13) are:

$$S_n = 0.007(n_a)^3 - 0.13(n_a)^2 + 0.74(n_a) + 1 \quad (6.9)$$

$$S_t = 0.72(t_f)^{-0.2} \quad (6.10)$$

$$S_s = 1.7 (s_a)^{-0.15} \quad (6.11)$$

$$S_{ad} = 0.52(a_d)^{0.24} \quad (6.12)$$

$$S_{fd} = 0.5(f_d) + 0.52 \quad (6.13)$$

Where  $n_a$  represents the number of anchors along the debonding path,  $t_f$  is the FRP sheet fiber thickness (mm),  $s_a$  is the center to center spacing between anchors along the debonding path (mm),  $a_d$  represents the anchor shaft diameter (mm), and  $f_d$  is the normalized anchor fan (or splay) diameter (mm), defined as the fan diameter divided by FRP sheet width and the number of FRP anchors across the sheet. The resulting exponents  $a$  through  $e$  of the proposed segmented model discussed in the previous section for the strain efficiency factor (Equation 6.7) were  $a = 1.6$ ,  $b = -1$ ,  $c = 2.35$ ,  $d = 1$ , and  $e = 0.1$ , giving:

$$K_{\varepsilon a} = S_n^{1.6} \cdot S_t^{-1} \cdot S_s^{2.35} \cdot S_{ad}^1 \cdot S_{fd}^{0.1} \geq 1.0 \quad (6.14)$$

Development of Equation 6.14 was based on laboratory experiments where FRP anchors covered at least 40% of the width of the FRP sheet, so this formulation is only applicable for the case where the normalized anchor splay diameter is 0.4 or more.

When FRP anchors have a longitudinal spacing exceeding 200 mm (8 in.) along the debonding path, the second row of anchors lies close to the end of the effective stress transfer zone so no significant strength gain is achieved by adding more rows of anchors. In this case, only one anchor should be considered along the debonding path in Equation 6.9 and exponent  $a$  should be set equal to 1.0 in Equation 6.14. Therefore, for this case and when only one anchor is placed along debonding path, Equation 6.14 becomes:

$$K_{\varepsilon a} = 1.617 \cdot S_t^{-1} \cdot S_{ad}^1 \cdot S_{fd}^{0.1} \geq 1.0 \quad (6.15)$$

The strain efficiency factors calculated using Equations 6.14 or 6.15 were compared with laboratory data of specimens tested by three research groups (Niemitz et al. 2010; Breña and McGuirk 2013; Zhang and Smith 2012). The strain efficiency factor from

laboratory experiments was defined as the strength of specimens tested with anchored FRP sheets divided by the strength of companion specimen containing unanchored (bonded) FRP sheets. A comparison of strain efficiency factors calculated from the parametric analysis ( $K_{\varepsilon a}$  regression) and strain efficiency factors determined from laboratory results ( $K_{\varepsilon a}$  test) is presented in Table 6.2. The values of regression to test ratios ranged from a minimum of 0.79 to a maximum of 1.15, with an average of 0.99 and a standard deviation of 0.11. It should be noted that the minimum ratio of 0.79 was obtained in a replicate specimen tested by Zhang and Smith (2012), for which the ratios of strain efficiency factors in the two other specimens in the replicate series were 0.85 and 0.89. The variation of these values might be due to material variabilities and inherent variations in the application of FRP sheets and anchors of the tested specimens.

As listed in Table 6.2 and shown in Figure 6.11, the anchorage strain efficiency factor predictions using either Equation 6.14 or 6.15 fall within +/-15% bands when compared with results obtained from the laboratory experiments of the three different research groups that were included in the comparison (Niemitz et al. 2010; Breña and McGuirk 2013; Zhang and Smith 2012). The accuracy obtained by the strain efficiency factor from Eqs. 6.14 or 6.15 seems reasonable given the complexity of the problem and the typical variations that exist in the application of the FRP materials.

The primary failure mode that was reported in the laboratory specimens was cracking propagation within the concrete substrate close to the FRP-concrete interface. This failure mode was followed by rupture of the FRP anchors or rupture of the FRP sheet in the neighborhood of the anchors. Although Equations 6.14 and 6.15 gave reasonably accurate

results compared with test data, it was felt that the format of the equations was not particularly amenable for design. Therefore, a simplification of the equations is presented in the next section to more easily incorporate the anchorage efficiency factor into design guides such as ACI 440.2R-17.

**Table 6.2: Parameters and summary of results from the regression analysis**

Research group	Specimen Notation	$S_n$	$S_t$	$S_s$	$S_{ad}$	$S_{fd}$	$K_{\epsilon a}$ test <sup>1</sup>	$K_{\epsilon a}$ regression <sup>2</sup>	$K_{\epsilon a}$ regression/ $K_{\epsilon a}$ test
Niemitz et al. (2010)	BI-13-0.6-5	2.016	0.975	0.741	0.799	0.72	1.275	1.283	1.01
	BI-13-1.3-5	2.016	0.975	0.741	0.962	0.72	1.488	1.545	1.04
	BIIs-25-1.9-10	1.617	0.975	----	1.054	0.92	1.721	1.734	1.01
	BI-13-1.3-10	2.016	0.975	0.741	0.962	0.92	1.376	1.583	1.15
	BI-13-1.9-10	2.016	0.975	0.741	1.054	0.92	1.634	1.734	1.06
Breña and McGuirk (2013)	F1-4a-1-24	2.016	0.975	0.911	0.962	1	2.142	2.435	1.14
	F2-4a-1-24	2.016	0.848	0.911	0.962	1	2.610	2.797	1.07
	F1-2a-24	1.617	0.975	----	0.962	1	1.618	1.597	0.99
	F2-2a-24	1.617	0.848	----	0.962	1	2.153	1.834	0.85
Zhang and Smith(2012)	1FA-1	1.617	0.941	----	0.979	1	2.136	1.683	0.79
	1FA-2	1.617	0.941	----	0.979	1	1.894	1.683	0.89
	1FA-3	1.617	0.941	----	0.979	1	1.984	1.683	0.85
	2FA100-1	2.016	0.941	0.852	0.979	1	2.583	2.194	0.85
	2FA100-2	2.016	0.941	0.852	0.979	1	2.303	2.194	0.95
	2FA125-1	2.016	0.941	0.824	0.979	1	2.374	2.028	0.85
	2FA125-2	2.016	0.941	0.824	0.979	1	1.885	2.028	1.08
	2FA150-1	2.016	0.941	0.802	0.979	1	1.751	1.901	1.09
	2FA150-2	2.016	0.941	0.802	0.979	1	1.708	1.901	1.11
3FA75-1	2.239	0.941	0.890	0.979	1	2.916	2.871	0.98	

	3FA75-2	2.239	0.941	0.890	0.979	1	2.607	2.871	1.10
								<b>Average</b>	<b>0.99</b>
								<b>Standard deviation</b>	<b>0.11</b>

1  $K_{ea}$  test: determined from laboratory experiments ( $K_{ea}$  test =Ultimate force of specimen with anchored sheet/Ultimate force of companion specimen with unanchored sheet).

2  $K_{ea}$  regression: proposed anchorage efficiency factor based on formulas in Equations 6.14 or 6.15 (regression analysis).



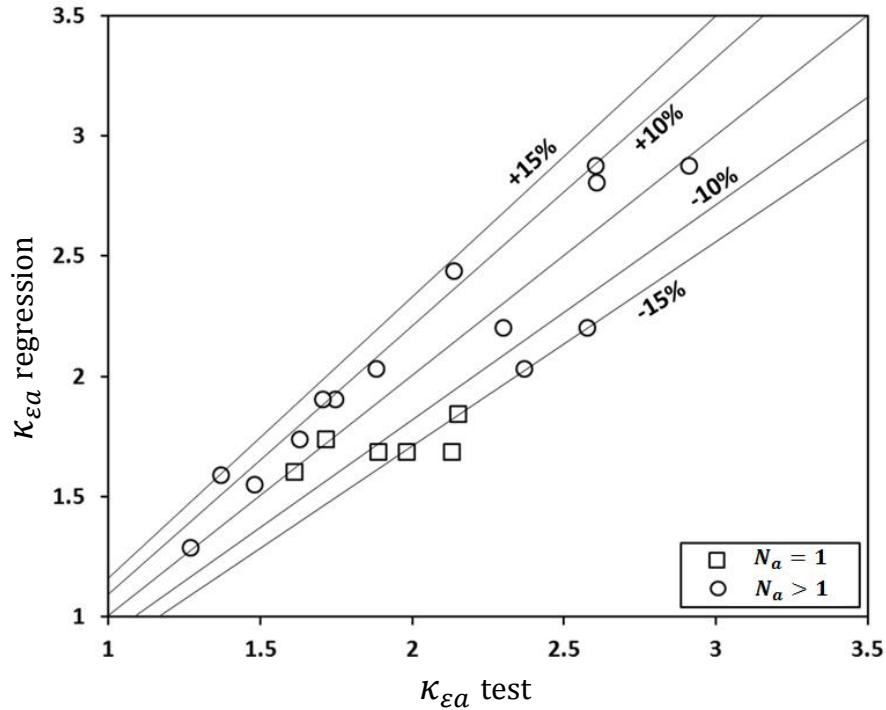


**Figure 6.11: Comparison between anchorage strain factors obtained from tests to regression analysis (Equations 6.14 or 6.15)**

### 6.9 Simplified Formula for Anchorage Strain Efficiency Factor

The anchorage strain efficiency presented in Equation 6.14 or Equation 6.15 was simplified to provide a formula that could be more easily applied for design. It was considered important to have the form of this equation be similar to the current form of the debonding equation contained in ACI 440.2R-17, Equation 6.3, so that the design engineer would not have to determine many additional parameters of the FRP system. An additional factor  $\alpha_c$  was introduced and calibrated using test data shown in Table 6.3 so that the calculated anchorage strain efficiency factor maintained similar accuracy with test data to what was obtained when using Equations 6.14 or 6.15. The use of this calibration factor also allowed combining Equations 6.14 and 6.15 into one equation that captures the difference in behavior when  $s_a$  approaches the length of the effective stress

transfer zone. The simplified formula includes the main three parameters that primarily governed the behavior of anchored FRP sheets, namely the number of FRP anchors  $n_a$ , the FRP sheet thickness  $t_f$  (mm), the center-to-center spacing between anchors along the debonding path  $s_a$  (mm), and anchor shaft diameter  $a_d$  (mm). The anchor splay diameter is recommended to be large enough to cover the entire width of the FRP sheet an anchor is engaging, so this parameter was eliminated from the simplified formulation. The simplified formula proposed is:

$$K_{\varepsilon a} = 1 + \alpha_c \cdot \sqrt{\frac{t_f a_d}{3s_a}} \cdot n_a^2 \quad (6.16)$$

Where;

$$\alpha_c = \frac{3}{8} \quad \text{and} \quad s_a = 1/3 \quad \text{when} \quad n_a = 1$$

and

$$\alpha_c = \frac{15}{8} \quad \text{when} \quad n_a > 1$$

It should be noted that this formula is recommended when the number of anchors along the debonding path does not exceed three anchors. If more than three anchors are applied to the FRP sheet, Equation 6.14 or 6.15 should be used. A comparison of results obtained when using the simplified formula (Equation 6.16) for  $K_{\varepsilon a}$  ( $K_{\varepsilon a}$  sim) with experimental data from the three previously used references (Niemitz et al. 2010; Breña and McGuirk 2013; Zhang et al. 2017) are presented in Table 6.3 and illustrated in Figure 6.12. The average ratio of calculated-to-test anchorage strain efficiency factor ( $K_{\varepsilon a}$ ) obtained applying Equation 6.16 was observed to decrease slightly when compared with results from using Equations 6.14 or 6.15 (Table 6.2 and Table 6.3), but the standard deviation

remained approximately equal. Although a slight loss of accuracy was observed, a reduction of calculated anchorage strain efficiency factors is conservative. A comparison between Figures 6.11 and 6.12 also reveals that using Equation 6.16 caused calculated points that fell on the +10% or +15% lines to get within +5% of values determined experimentally. Furthermore, application of a strength reduction factor as is commonly done in strength-based design would increase the margin of safety to within acceptable levels. Figure 6.13 shows a flowchart that describes the steps that should be considered for designing an FRP sheet system containing FRP anchors. To illustrate this approach, illustrative examples are given in the Appendix in practical situations.

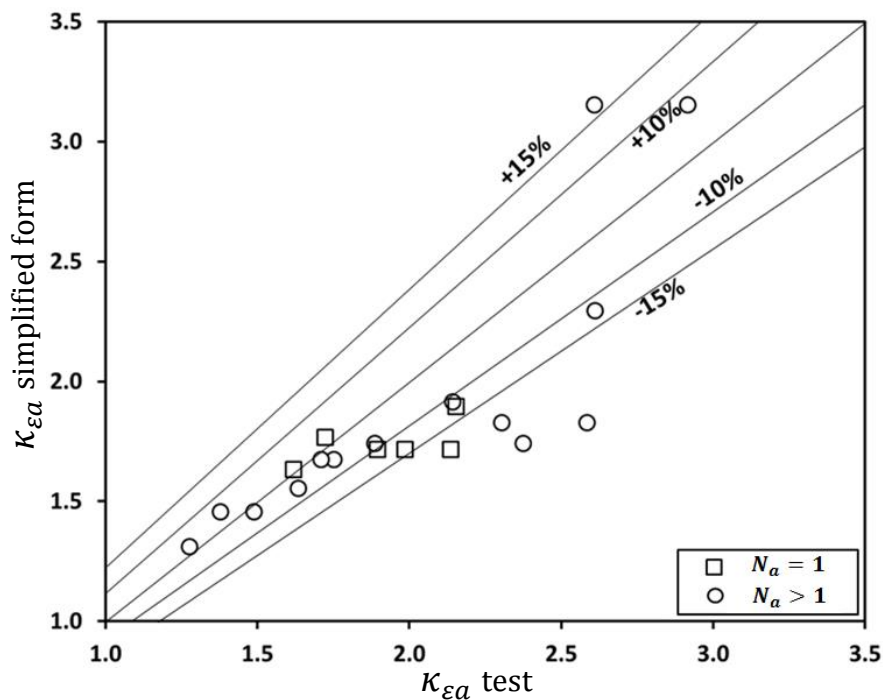


**Figure 6.12: Comparison between anchorage strain factors from tests to simplified formula (Equation 6.16)**

**Table 6.3: Comparison of simplified form of  $K_{\epsilon a}$  with test data**

Research group	Specimen Notation	Number of anchors ( $n_a$ )	Thickness of the FRP sheet ( $t_f$ )	Spacing between anchors ( $s_a$ )	Anchor shaft diameter ( $a_d$ )	$K_{\epsilon a}$ test <sup>1</sup>	$K_{\epsilon a}$ sim <sup>2</sup>	$K_{\epsilon a}$ sim/ $K_{\epsilon a}$ test
Niemitz et al. (2010)	BI-13-0.6-5	2	0.22	254	6	1.275	1.312	1.03
	BI-13-1.3-5	2	0.22	254	13	1.488	1.459	0.98
	BIIs-25-1.9-10	1	0.22	----	19	1.721	1.767	1.03
	BI-13-1.3-10	2	0.22	254	13	1.376	1.459	1.06
	BI-13-1.9-10	2	0.22	254	19	1.634	1.555	0.95
Brena and McGuirk (2013)	F1-4a-1-24	2	0.22	64	13	2.142	1.915	0.89
	F2-4a-1-24	2	0.44	64	13	2.610	2.295	0.88
	F1-2a-24	1	0.22	----	13	1.618	1.634	1.01
	F2-2a-24	1	0.44	----	13	2.153	1.897	0.88
Zhang and Smith (2012)	1FA-1	1	0.262	----	14	2.136	1.718	0.80
	1FA-2	1	0.262	----	14	1.894	1.718	0.91
	1FA-3	1	0.262	----	14	1.984	1.718	0.87
	2FA100-1	2	0.262	100	14	2.583	1.829	0.71
	2FA100-2	2	0.262	100	14	2.303	1.829	0.79
	2FA125-1	2	0.262	125	14	2.374	1.742	0.73
	2FA125-2	2	0.262	125	14	1.885	1.742	0.92
	2FA150-1	2	0.262	150	14	1.751	1.677	0.96
	2FA150-2	2	0.262	150	14	1.708	1.677	0.98
	3FA75-1	3	0.262	75	14	2.916	3.155	1.08
3FA75-2	3	0.262	75	14	2.607	3.155	1.21	
							<b>Average</b>	<b>0.93</b>
							<b>Standard deviation</b>	<b>0.12</b>

1  $K_{\epsilon a}$  test: determined from experimental tests ( $K_{\epsilon a}$  test =Ultimate force of specimen with anchored sheet/Ultimate force of companion specimen with unanchored sheet).

2  $K_{\epsilon a}$  sim: Simplified form of the anchorage efficiency factor (Equation 6.16).

## **6.10 Application of anchorage efficiency factor to flexural strengthening of beams and slabs**

Concrete beams and slabs have been strengthened in flexure through bonding FRP reinforcement externally to the tension face. FRP sheets have been applied as U-wraps in beams to provide anchorage of sheets applied to the tension face and as a way to increase shear strength. However, if the goal is to increase flexural strength, FRP anchors provide another alternative to U-wraps to delay debonding of FRP sheets. Even though several design guides have specified procedures to determine the flexural strength of beams and slabs, none of them have considered the anchorage effect of FRP anchors and their contribution to strength. Therefore, the proposed anchorage efficiency factor developed in this chapter was introduced to the design procedure included in the *ACI 440.2R-17 Guide for the Design and Construction of Externally Bonded FRP Systems for Strengthening Concrete Structures*. This design guide includes a debonding limit state that must be used in design of FRP strengthening systems that limits the stress developed in FRP sheets and therefore limits its efficiency. It is not uncommon for the debonding stress of FRP sheets to be about 40-50% of the rupture stress of the material, resulting in somewhat inefficient designs.

## **6.11 Description of design procedure using anchorage efficiency factor**

A procedure to include the anchorage efficiency factor in flexural strengthening applications is proposed in this section. The following steps illustrate how to introduce the proposed modification to the design procedure that is reported in the ACI 440.2R-17 (2017) to include the effect of integrated FRP anchors;

1. Follow the procedure in the ACI 440.2R-17 (2017) Guidelines and start with determining the appropriate environmental reduction factor  $C_E$  of the FRP material for the application using values listed in Table 6.4 (taken from ACI 440.2R-17, Table 9.4). Determine the design ultimate tensile strength  $f_{fu}$  and design rupture strain  $\varepsilon_{fu}$  of FRP reinforcement using:

$$f_{fu} = C_E f_{fu}^* \quad (6.17)$$

$$\varepsilon_{fu} = C_E \varepsilon_{fu}^* \quad (6.18)$$

Where;  $f_{fu}^*$  and  $\varepsilon_{fu}^*$  are the ultimate tensile strength and rupture strain of the FRP reported by the manufacturer of the FRP system.

**Table 6.4: Environmental reduction factor for various FRP systems and exposure conditions [Table 9.4 of the ACI 440.2R-17]**

Exposure conditions	Fiber type	Environmental reduction factor $C_E$
Interior exposure	Carbon	0.95
	Glass	0.75
	Aramid	0.85
Exterior exposure (bridges, piers, and unenclosed parking garages)	Carbon	0.85
	Glass	0.65
	Aramid	0.75
Aggressive environment (chemical plants and wastewater treatment plants)	Carbon	0.85
	Glass	0.50
	Aramid	0.70

Then, determine the existing state of strain at the surface of concrete  $\varepsilon_{bi}$  based on dead load moments acting on the beam prior to application of FRP sheets and assuming cracked section analysis:

$$\varepsilon_{bi} = \frac{M_{DL}(d_f - k d)}{I_{cr} E_c} \quad (6.19)$$

Where:  $k$  is the ratio between neutral axis depth and effective depth to interior steel reinforcement ;  $I_{cr}$  moment of inertia of cracked section;  $M_{DL}$  = dead-load moment;  $d_f$  is the effective depth of FRP sheet;  $d$  is the distance from extreme compression fiber to centroid of internal tension reinforcement;  $E_c$  is the modulus of elasticity of concrete.

2. Determine the effective level of strain in the FRP reinforcement using Equation 6.1 and the debonding strain in the FRP reinforcement using Equation 6.3 then check the strain limits stated in Equation 6.2.

3. Determine FRP strain assuming perfect bond between concrete and FRP sheet. FRP strain assuming perfect bond can be calculated with the aid of a numerical method developed by Breña et al. (2001) that determines moment capacity and curvature of FRP reinforced concrete beams. This method is summarized by setting a maximum compression strain in the concrete to a value between zero and the maximum usable concrete strain and then estimating the initial neutral axis position. The strain profile is calculated based on the extreme compression fiber strain and the position of the neutral axis. Then, equilibrium is checked and the neutral axis depth is adjusted if equilibrium is not satisfied. The moment and curvature for that strain profile is calculated and the previous steps are repeated for another point in the moment-curvature response.

4. If strain values determined using step 3 (calculated assuming perfect bond between FRP and concrete) are larger than the strain value obtained from step 2 (calculated based on the debonding strain limit), identify the longitudinal distance along the FRP sheet where strains assuming perfect bond exceed debonding strain. This distance represents the part of the sheet that needs to be anchored (see Figure A8 of the Appendix).

5. Based on step 4, Identify the expected debonding region where the maximum strain in the FRP sheet occurs. As several experimental tests have reported, the maximum measured strains were close to mid-span in the tested beams (Guadagnini et al. 2006; Teng et al. 2009; Loo et al. 2012). Therefore, two debonding regions around mid-span should be assumed in the case of a simply supported beam under uniformly distributed loading (see Figure A3 and section A1.2 of the Appendix).

6. Determine the number of anchors that are expected to be applied for one of the regions in step 5 based on the width of the FRP sheet and a proposed anchor fan diameter (count the number of anchors across the width of the FRP sheet and the number of anchors along the debonding region).

7. Calculate the anchorage efficiency factor  $K_{ea}$  from Equation 6.14; Equation 6.15; or Equation 6.16.

8. Determine the design strain of the anchored FRP system using Equation 6.8.

9. Follow the procedure in the ACI 440.2R-17 (2017) Guidelines to determine the strain level in concrete and steel reinforcement, and the stress in FRP and steel by assuming an initial value for the distance from extreme compression fiber to the neutral axis  $c$ .

$$\varepsilon_c = (\varepsilon_{fe} + \varepsilon_{bi}) \left( \frac{c}{d_f - c} \right) \quad (6.20)$$

$$\varepsilon_s = (\varepsilon_{fe} + \varepsilon_{bi}) \left( \frac{d - c}{d_f - c} \right) \quad (6.21)$$

$$f_s = E_s \varepsilon_s \leq f_y \quad (6.22)$$

$$f_{fe} = E_f \varepsilon_{fe} \quad (6.23)$$



Where:  $\varepsilon_c$  is the strain in concrete;  $f_s$  and  $\varepsilon_s$  are the stress and strain in steel reinforcement, respectively;  $f_{fe}$  and  $E_f$  are the effective strain and modulus of elasticity of FRP material, respectively.

The estimated value of  $c$  is adjusted and checked until force equilibrium is satisfied.

$$c = \frac{A_s f_s + A_f f_{fe}}{\alpha_1 f'_c \beta_1 b} \quad (6.24)$$

Where:  $A_s$ ,  $A_f$  are steel and FRP cross-sectional areas, respectively;  $\alpha_1$  is a multiplier on the compressive strength of concrete  $f'_c$  to determine the intensity of equivalent rectangular stress distribution.  $\beta_1$  is the ratio of depth of equivalent rectangular stress block to the depth of the neutral axis.  $b$  is the width of the compression face of the member.

The design flexural strength is determined using:

$$M_{ns} = A_s f_s \left( d - \frac{\beta_1 c}{2} \right) \quad (6.25)$$

$$M_{nf} = A_f f_{fe} \left( d - \frac{\beta_1 c}{2} \right) \quad (6.26)$$

$$\phi M_n = \phi [M_{ns} + \psi_f M_{nf}] \quad (6.27)$$

Where:  $M_{ns}$ ,  $M_{nf}$  are the contribution of steel and FRP reinforcement to nominal flexural strength;  $\psi_f$  is an FRP strength reduction factor (0.85 for flexure).  $\phi$  is the strength reduction factor.

## 6.12 FRP strength estimator

A software program named “FRP Strength Estimator” was developed to facilitate calculations and to determine the flexural strength of concrete beams and one-way slabs

containing externally applied FRP sheets. This software also includes the capability to determine flexural strength including FRP anchors to the strengthening system. This application is based on the formulation reported in the ACI 440.2R-17 (2017), with the needed modifications to include the effect of FRP anchors that were included in the development of the anchorage efficiency factor.

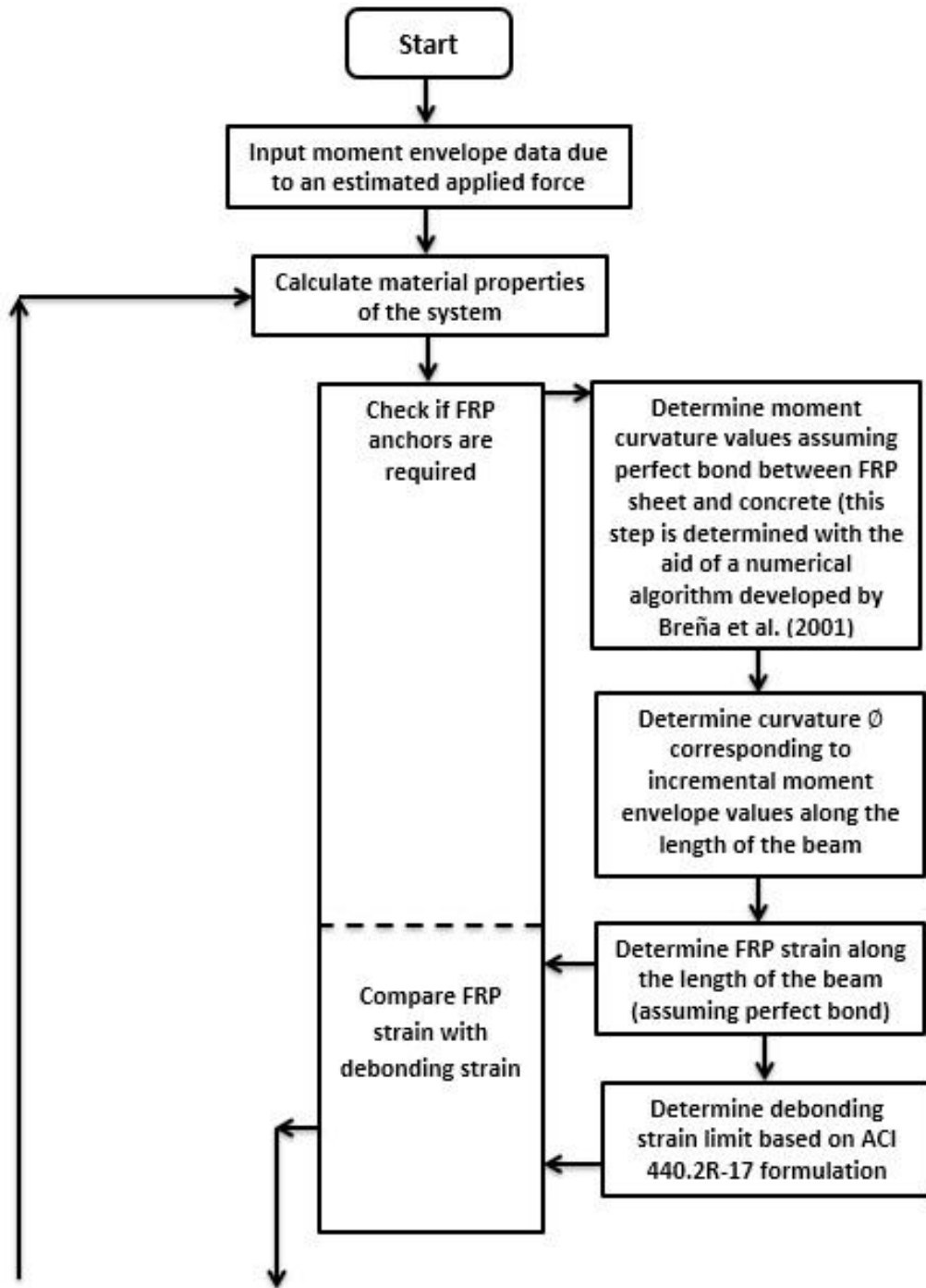
The program calculates the following:

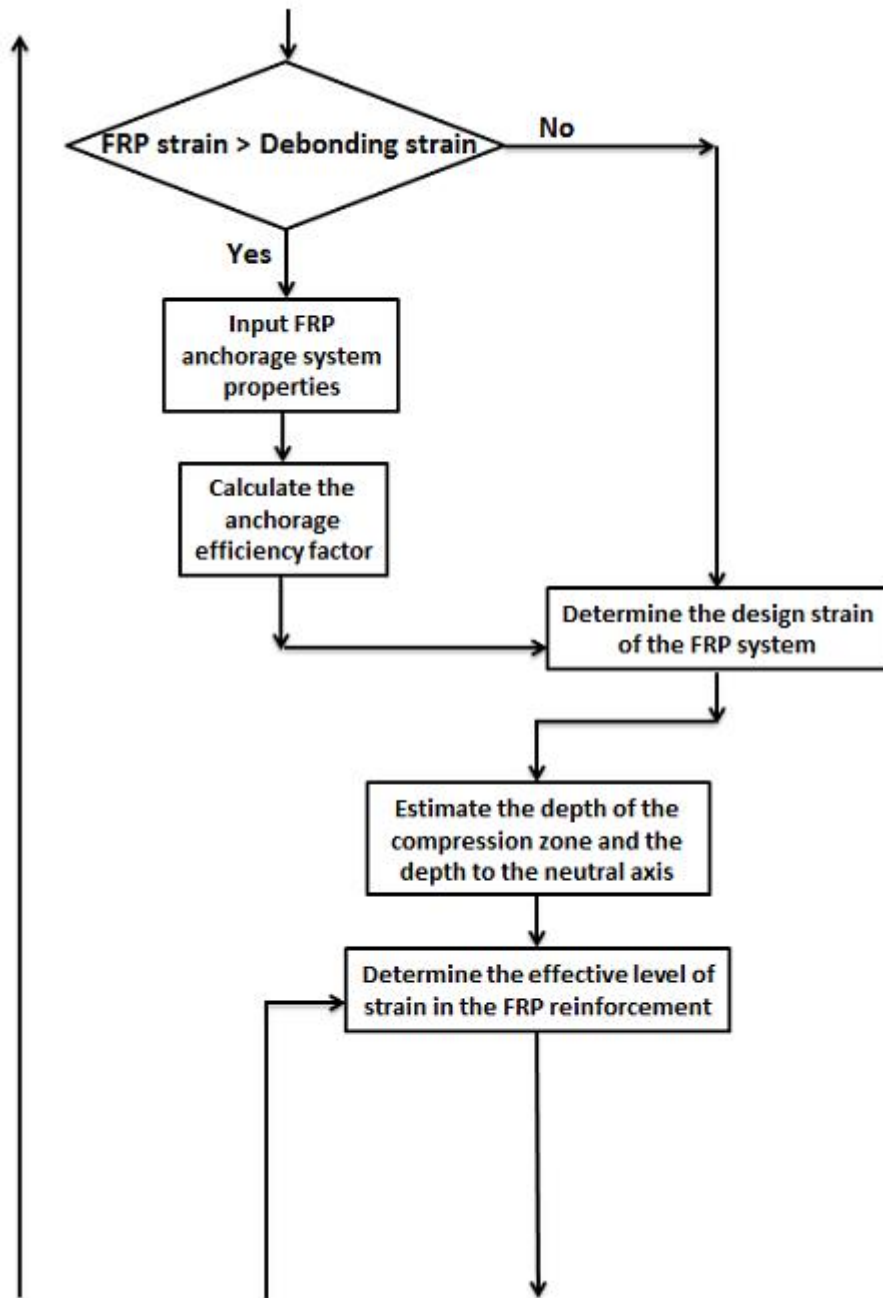
1. Flexural strength of FRP reinforced concrete beams and one-way slabs.
2. Estimate if mechanical anchors are required to achieve a target flexural strength.
3. Determine the required anchored length of the FRP plate along the length of the beam.
4. Determine the required dimensional properties and spacing of the anchors.
5. Conduct a cracked section analysis, moment capacity check, service stress check, creep rupture check, and optimize the thickness of the FRP plate.

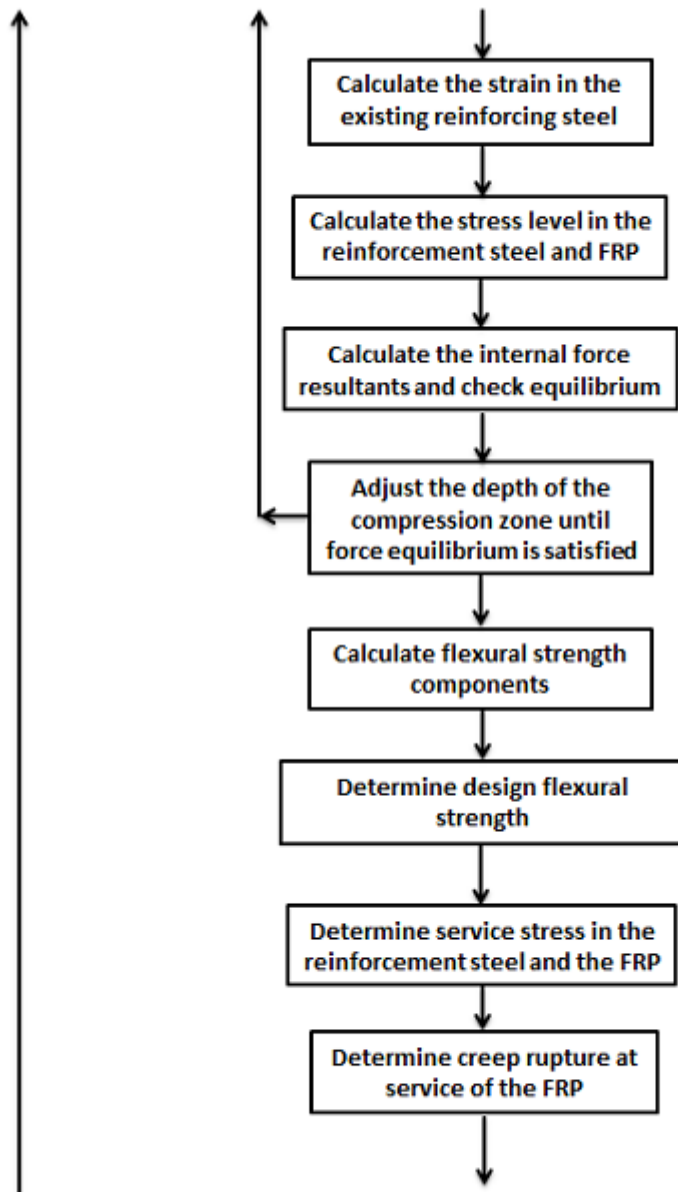
Anchorage length algorithm was developed by comparing debonding strain limit with FRP strain determined assuming perfect bond between concrete and FRP sheet (as stated before in section 6.11 step 3).

The software developed in this research introduces moment envelope data to the calculated moment-curvature response of the cross-section to estimate the corresponding curvature at a section along the beam. The FRP sheet strain, assuming perfect bond, is determined based on the obtained curvature data. The debonding strain limit is determined from Equation 6.4 and then compared with the FRP strain assuming perfect bond. If the FRP sheet strain is higher than the debonding strain, FRP anchorage is required at that section and along the region where FRP sheet strains exceed the debonding strain limit (see Example 3.4 in section A.3.4 of the Appendix).

The software determines the strength of the anchored system based on user-introduced properties of the anchors and performs cracked section analysis, moment capacity check, service stress check, creep rupture check, and optimize the thickness of the FRP plate if required by the user. The complete source code used to develop the software is reported in section A.5.2 of the Appendix. The following flow chart describes the main steps of the algorithm that was used to develop the software. Further details on the operation and a description of menus to input data for this software are given in section A.2 of the Appendix.







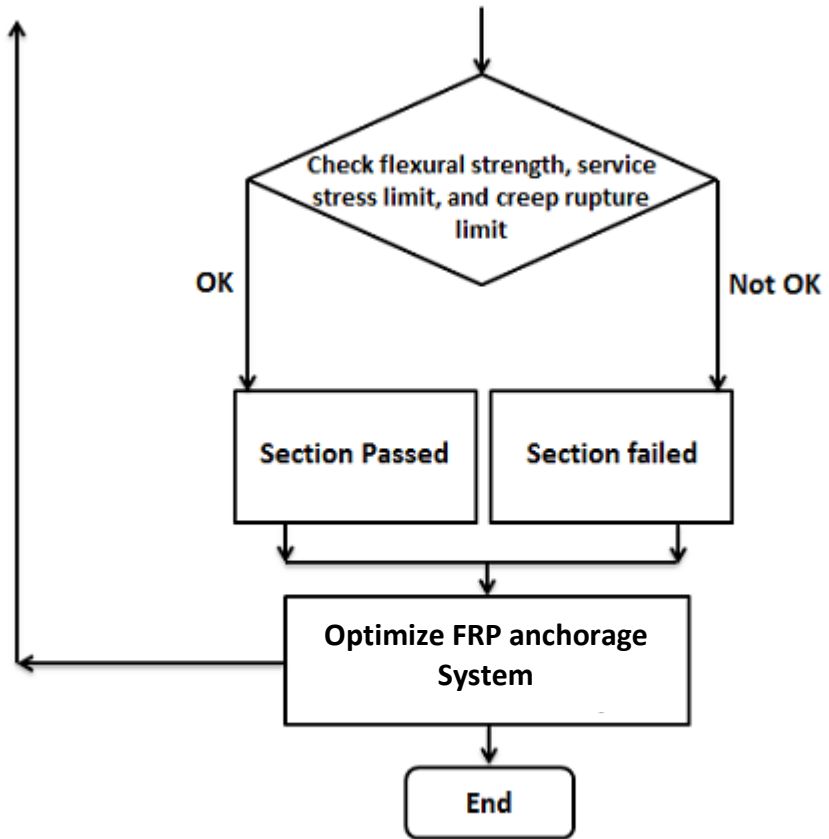


**Figure 6.13: Flow chart**

## CHAPTER 7

### FINITE ELEMENT ANALYSIS AND PARAMETRIC STUDY OF PERFORATED STEEL PLATE SHEAR CONNECTORS FOR WOOD- CONCRETE COMPOSITES

#### 7.1 Introduction

Wood-concrete composites are structural deck systems that benefit from the use of wood as a lightweight, sustainable substructure and concrete as a wear-resistant, vibration-damping top element. These systems employ shear connectors to transfer shear stresses between the wood and the concrete leading to full or partial composite action for strength and stiffness benefits.

Figure 7.1 shows a typical shear connector where part of the concrete is removed from the figure to reveal a part of the perforated steel plate. A layer (or layers) of insulation is often placed horizontally between the concrete and the wood for sound attenuation and also to inhibit moisture from transferring into the wood after the concrete is placed and has not yet hardened.

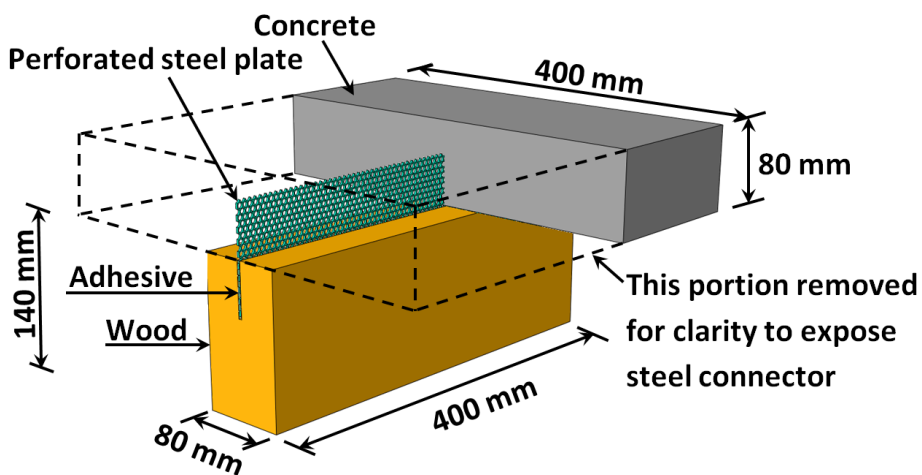


Figure 7.1: Typical HBV-shear connector

(dimensions for specimen reported in Clouston et al. 2005)



This connector is known as the HBV® and it was developed in 1992 by Leander Bathon at Hochschule RheinMain University, in Wiesbaden, Germany (Technical Dossier HBV-Systems 2014; Clouston et al. 2005). The connector was designed to be used specifically in wood-concrete composites as per its name HBV® (or Holz-Beton-Verbund) which means wood-concrete-connector in German.

The design philosophy of the HBV® is based on enhancing stiffness in the service load range while ensuring ductility of the system in the post-yield stress range. The steel plate connector is perforated and acts as a fuse element with a perfectly-plastic failure mechanism (Clouston et al. 2005). Finite element (FE) models have been presented in the literature to study the behavior of the HBV® (Bathon et al. 2006, Bathon and Bletz-Mühldorfer 2014), and similar steel plate connectors (Yeoh et al. 2010a; Miotto and Dias 2012). These models, however, only capture the general behavior of the connectors without providing information on how connector parameters, such as plate thickness or gap height, influence the performance of the connector.

The objective of this study is, therefore, to employ a three-dimensional FE analysis to investigate the detailed effect of manipulating several parameters of perforated steel plate connectors on shear stresses and strains in wood-concrete composite systems. A similar approach was adopted by Bedon and Fragiacommo (2017) to model notched connections for timber-concrete composite beams.

The physical properties of the HBV® are used as a baseline for comparison in performance with an existing connector. The parameters studied are: thickness of plate; insulation gap between concrete and wood; depth of embedment in concrete; and depth of

embedment in wood. The investigation enables the development of design criteria for perforated steel plate type connectors so that optimized designs can be achieved.

## 7.2 Previous experimental work

The characteristic shear strength and slip moduli were evaluated for the HBV<sup>®</sup> by Clouston et al. (2005). The study conducted push-out tests (see Figure 7.2) to measure ultimate failure load, corresponding displacement, corresponding shear stress, and slip modulus (i.e., the slope of the linear elastic portion of the load-displacement curve).

Test results showed that the slip modulus varied between 331.13 kN/mm to 657.42 kN/mm with an average of 415.46 kN/mm while average shear stresses varied between 2.56 MPa to 3.02 MPa, with an average value of 2.79 MPa (see Table 7.1 for test data). In all of the tested specimens, the failure mode initiated by yielding followed by rupture of the steel shear connector. These experimental results were used to calibrate the FE model presented in the following section for the HBV<sup>®</sup>.

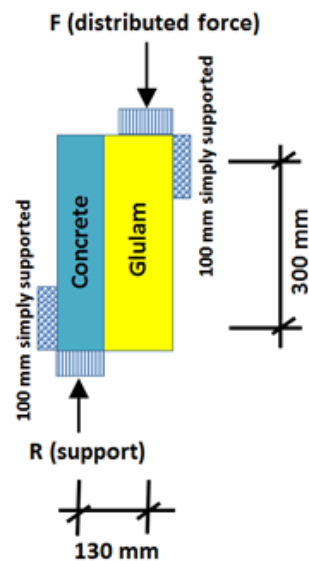


Figure 7.2: Test configuration

### 7.3 Finite element modeling

A general-purpose FE software (ABAQUS™) was employed to perform 3D simulations to study the impact of varying different parameters of the concrete-wood system. Four separate components of the system were modeled: concrete, wood, the steel connector plate, and the adhesive between the plate and wood beam (see Figure 7.1). Three-dimensional solid hexahedral brick elements were used to model the concrete slab and the wood beam. Each brick element has eight nodes with linear (first-order) interpolation of displacement between nodes. The steel plate was modeled using 8-node hexahedral continuum-shell elements and cohesive elements were used to model the adhesive between plate and wood beam.

The push-out tests that Clouston et al. (2005) conducted were used to calibrate the FE model. Figure 7.2 and Figure 7.3 illustrate the push-out test configuration and the corresponding discretized model and boundary conditions used in the model. The simulation was conducted by controlling displacement of a reference point that was constrained to all other nodes lying on the face corresponding to the surface loaded during the laboratory tests (i.e., displacement control). Then, the corresponding forces required for equilibrium at a given displacement (applied forces) were determined at the reference point. Embedded constraints were used to model the contact between the perforated steel plate and both concrete and adhesive of the shear connector. This type of constraint is available in ABAQUS™ where guest elements (elements of the steel connector) are embedded in host elements (concrete elements or elements of the adhesive). The response of the host elements is used to constrain the translational degrees of freedom of the embedded nodes (Simulia Abaqus documentation 2016). In addition,

surface-based tie constraints were used to connect surfaces of the adhesive elements to the adjacent wood elements. With this type of constraint two parallel surfaces are joined by defining a slave surface (adhesive elements in contact with wood elements) and a master surface (wood elements in contact with adhesive elements). Nodes on the slave surface are constrained to the master surface to achieve equal displacements.

The FE model has a large number of elements and nodes, and it involves contact interactions between different parts that result in response nonlinearity. For these reasons, an explicit quasi-static analysis procedure was chosen to perform the analysis and to obtain results efficiently.

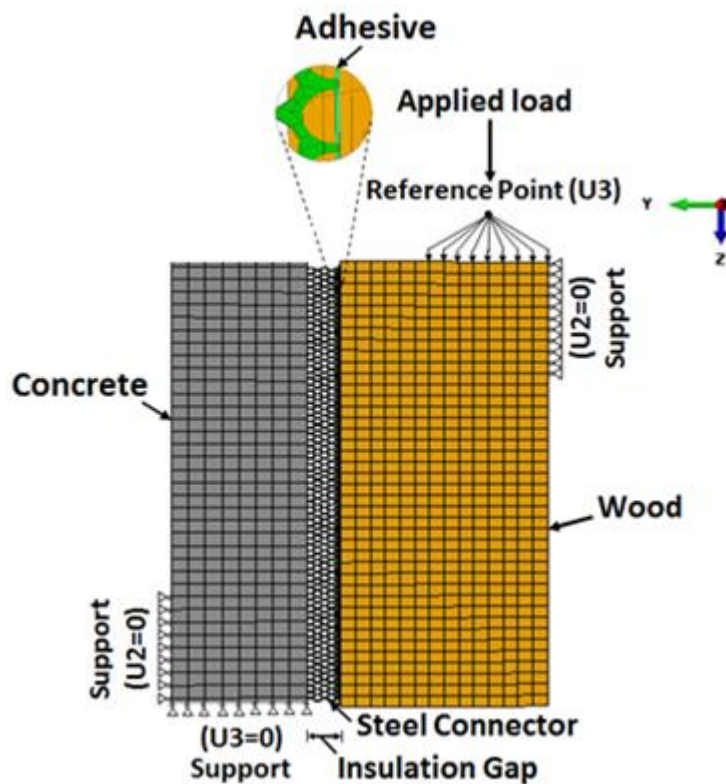


**Figure 7.3: Model with mesh and boundary conditions**

### 7.3.1 Constitutive model for concrete

Concrete was represented using the concrete damage plasticity model proposed by Lubliner et al. (1989) and implemented in ABAQUS™ finite element software. This model represents the behavior of concrete under tension and compression. For the tensile stress state, two regions are identified: elastic and softening regions. For the compressive stress state, three regions are identified: elastic, hardening, and softening regions. The multiaxial behavior of concrete is assumed isotropic.

The general three-dimensional stress-strain relationship under tension is represented by (Simulia Abaqus documentation 2016):

$$\sigma_t = (1 - d_t)D_O(\varepsilon_t - \varepsilon_t^P) \quad (7.1)$$

Where  $d_t$  is a damage parameter determined using the dissipated energy density of concrete under tension,  $D_O$  is the stiffness,  $\varepsilon_t$  is the tensile strain, and  $\varepsilon_t^P$  is the plastic tensile strain.

Similarly, the general three-dimensional compressive stress-strain relationship is defined by (Simulia Abaqus documentation 2016):

$$\sigma_c = (1 - d_c)D_O(\varepsilon_c - \varepsilon_c^P) \quad (7.2)$$

Where  $d_c$  is the damage parameter determined from the dissipated energy density of concrete under compression,  $D_O$  is the stiffness,  $\varepsilon_c$  is the compressive strain, and  $\varepsilon_c^P$  is the plastic compressive strain.

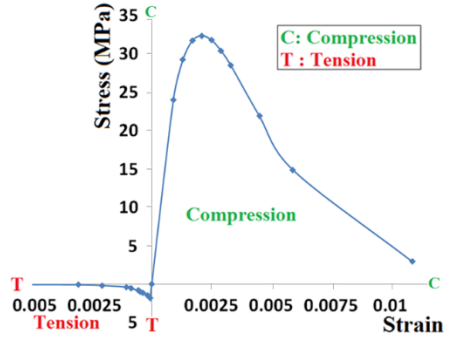
The concrete used in the test was class B25 with a minimum compressive strength of 30 MPa (Clouston et al. 2005). Properties of the concrete material used in the FE model were obtained from ABAQUS™ verification manual (see part (a) of Figure 7.4 and section A4 of the Appendix for input data used in the model).

### **7.3.2 Constitutive model for wood**

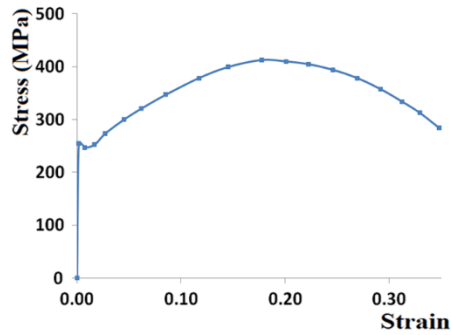
The properties of the experimentally tested wood material were those of German Spruce glulam, grade BS11 (comparable to North American glulam stress-class 16F-1.3E), with characteristic (5<sup>th</sup> percentile) tensile and compressive strength of 17 MPa and 24 MPa, respectively (Clouston et al. 2005). The constitutive behavior of the wood was simulated as an elastic-orthotropic material as no failure in the wood was observed during the tests. The different stiffness properties in each of the principal material directions were obtained from NDS® (2015) and adopted in the FE model (see section A4 of the Appendix for wood material input data).

### **7.3.3 Constitutive model for steel**

The constitutive behavior of the perforated steel plate was modeled using the metal plasticity model available in the ABAQUS software. This model uses the von Mises yield criterion to define the yield surface of metals that exhibit isotropic yielding. The steel used in the laboratory test and the FE model satisfies ASTM A36 steel with a minimum yield strength of 248 MPa (ASM International 2002) and ultimate tensile strength of 412 MPa (see part (b) of Figure 7.4 and section A4 of the Appendix for the material input data).



(a)



(b)

**Figure 7.4: Stress-strain relationships adopted for (a) concrete and (b) steel materials (see section A4 of the Appendix for values)**

### 7.3.4 Constitutive model for adhesive

The adhesive material was simulated considering three stages of material behavior: (1) elastic, (2) damage initiation, and (3) damage evolution. Shear stiffness of the adhesive was assumed negligible (Simulia Abaqus documentation 2016):

$$\begin{Bmatrix} \sigma_1 \\ \sigma_2 \\ \sigma_3 \end{Bmatrix} = \begin{bmatrix} E_{11} & 0 & 0 \\ 0 & E_{22} & 0 \\ 0 & 0 & E_{33} \end{bmatrix} \begin{Bmatrix} \varepsilon_1 \\ \varepsilon_2 \\ \varepsilon_3 \end{Bmatrix} \quad (7.3)$$

Where  $\sigma_1$ ,  $\sigma_2$ ,  $\sigma_3$  are the stresses in the three principal directions;  $E_1$ ,  $E_2$ ,  $E_3$  are Young's moduli in the three principal directions; and  $\varepsilon_1$ ,  $\varepsilon_2$ ,  $\varepsilon_3$  are the strains in the three principal directions.

The quadratic nominal strain criterion was used to model the damage initiation of the adhesive envelope between the wood and the steel connector. This model assumes initiation of damage when the quadratic function of the nominal strain ratios reaches a value of one (Simulia Abaqus documentation 2016), as given in Equation 7.4:

$$\left\{\frac{\varepsilon_1}{\varepsilon_1^o}\right\}^2 + \left\{\frac{\varepsilon_2}{\varepsilon_2^o}\right\}^2 + \left\{\frac{\varepsilon_3}{\varepsilon_3^o}\right\}^2 = 1 \quad (7.4)$$

where  $\varepsilon_1^o$  is the maximum nominal strain normal to the interface,  $\varepsilon_2^o$  is the maximum nominal strain in the longitudinal direction, and  $\varepsilon_3^o$  is the maximum nominal strain in the transverse direction. Laboratory tests on structural adhesives conducted by Tomblin et al. (2002) show that damage initiation of several types of adhesives occur at a strain of 0.05. Therefore, this value was used for the maximum nominal strains in all principal material directions (see section A4 of the Appendix).

For the damage evolution stage, a damage variable,  $D$ , is introduced to the stress-strain relationship. The value of this parameter varies between zero and 1 for no damage and complete damage, respectively.

$$D = \frac{\delta_m^f(\delta_m^{max} - \delta_m^o)}{\delta_m^{max}(\delta_m^f - \delta_m^o)} \quad (7.5)$$

where  $\delta_m^o$  is the displacement corresponding to maximum stress,  $\delta_m^f$  is the final displacement before complete loss of strength, and  $\delta_m^{max}$  is the maximum value of the effective displacement. The general value of  $\delta_m$  can be computed by:

$$\delta_m = \sqrt{\delta_1^2 + \delta_2^2 + \delta_3^2} \quad (7.6)$$

where  $\delta_1$  is the displacement normal to the interface,  $\delta_2$  is the displacement in the longitudinal direction, and  $\delta_3$  is the displacement in the transverse direction.



The final stress values are determined using:

$$\sigma_1 = (1 - D)\overline{\sigma}_1$$

$$\sigma_2 = (1 - D)\overline{\sigma}_2 \tag{7.7}$$

$$\sigma_3 = (1 - D)\overline{\sigma}_3$$

where  $\overline{\sigma}_1$ ,  $\overline{\sigma}_2$ , and  $\overline{\sigma}_3$  are the stress components before damage.

#### 7.4 Finite element model validation

The FE modeling approach was verified by replicating the measured response of the push-out shear tests reported in Clouston et al. (2005). As seen in Figure 7.5, the simulated load-displacement response was in good agreement with the experimental results as the predicted initial stiffness, yield point, and ductility are all well within the range of the experimental data.

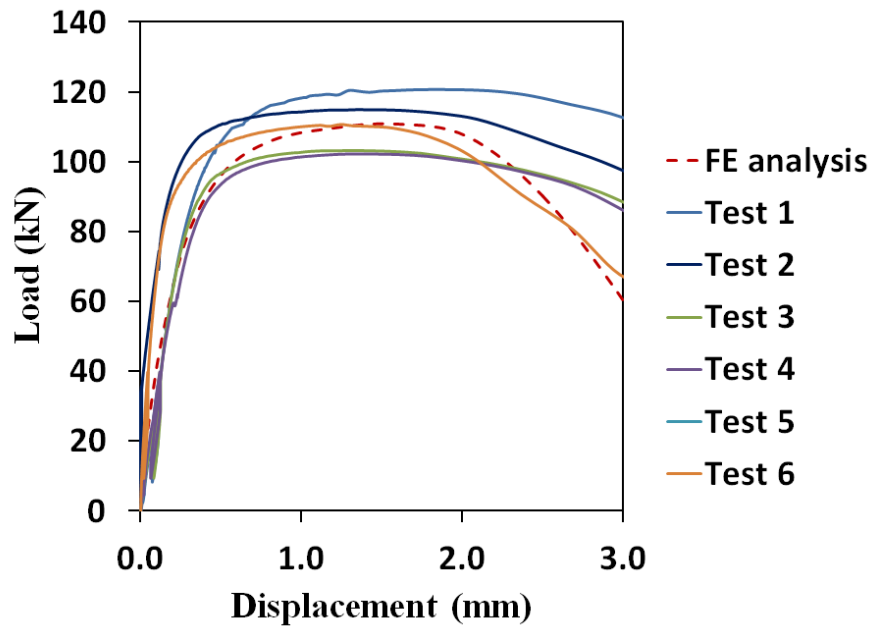


**Figure 7.5: Load-displacement curves obtained from finite element model and experimental tests reported by Clouston et al. (2005)**

Table 7.1 compares results for the values of peak load, peak load deformation, maximum shear stress, and slip modulus between FE modeling and laboratory tests. The percentage difference for peak load values (0.73%), and shear stress values (0.14%) are close. While the percentage difference for peak load deformation (10%) and slip modulus (3.35%) are larger, they also lie within acceptable levels. Given the high variation that exists in elastic modulus of wood, it is not surprising that higher discrepancies were found for quantities that are dependent on the stiffness of the connection.

**Table 7.1: Test and FEM results**

Test	Peak load (kN)	Deformation at peak (mm)	Maximum Shear stress (N/mm <sup>2</sup> )	Slip modulus (kN/mm)
Test 1	120.97	1.743	3.02	353.87
Test 2	114.89	1.402	2.87	367.65
Test 3	103.53	1.339	2.59	371.75
Test 4	102.53	1.404	2.56	331.13
Test 5	116.88	1.519	2.92	410.96
Test 6	110.96	1.246	2.77	657.42
Test average	111.62	1.442	2.79	415.46
Standard deviation	7.41	0.172	0.18	121.38
FEM	110.80	1.587	2.77	401.54
Percentage difference *	0.73	10.0	0.14	3.35

\* Percentage difference = |FEM-Test average| / Test average

In addition to these parameters, the model was able to capture the failure mode observed during the tests. Clouston et al. (2005) reported that shear failure for each specimen occurred along the midline of the steel connector. This observation is in agreement with the distribution of von Mises stresses at yield computed from the finite element model and presented in Figure 7.6. A band of von Mises stress with values exceeding the yield strength of 250 MPa along the midline of the connector is shown in

Figure 7.6. The favorable comparisons between the response obtained with the FE model and the laboratory tests generated confidence in the ability of the model to capture, in a reliable manner, the response of systems with parameters different from those tested in the laboratory.

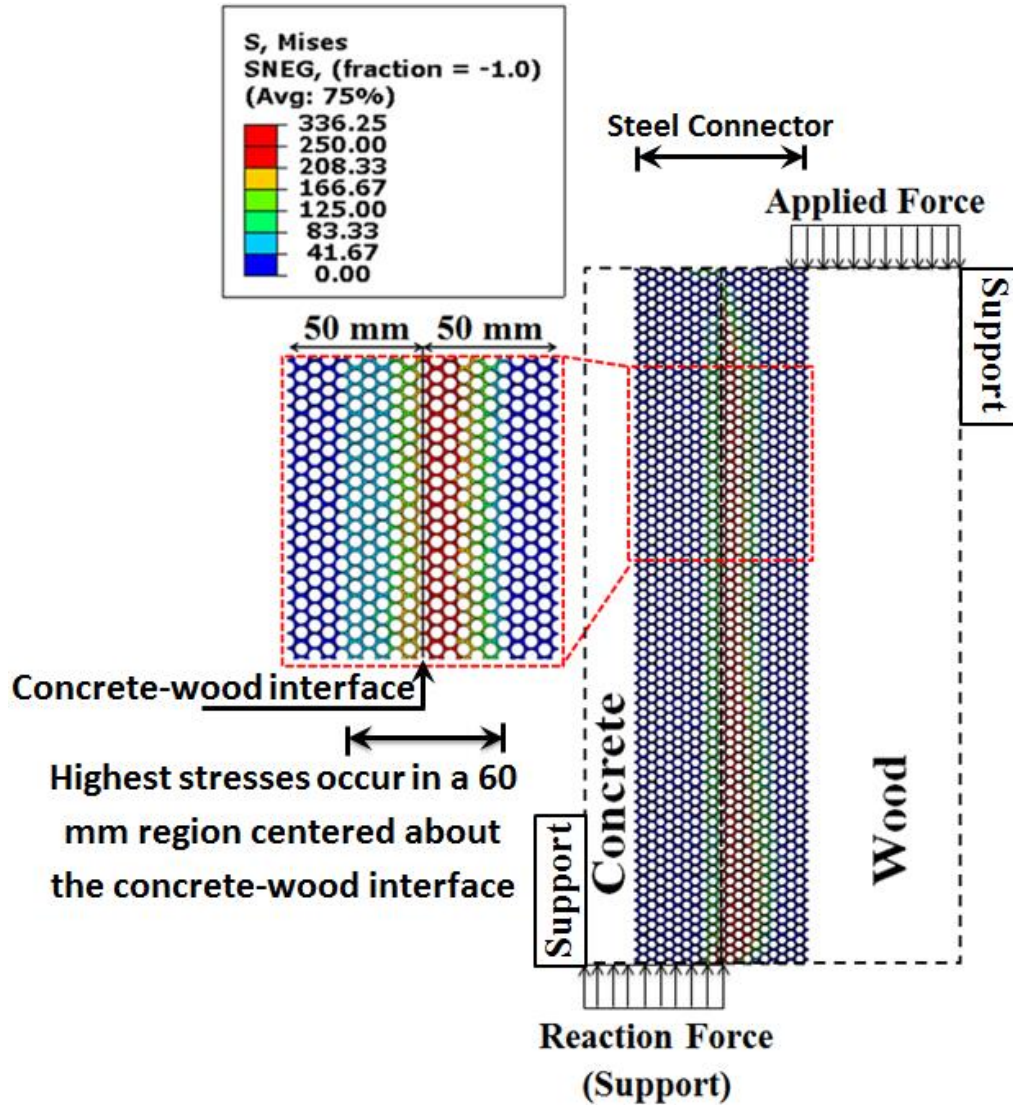


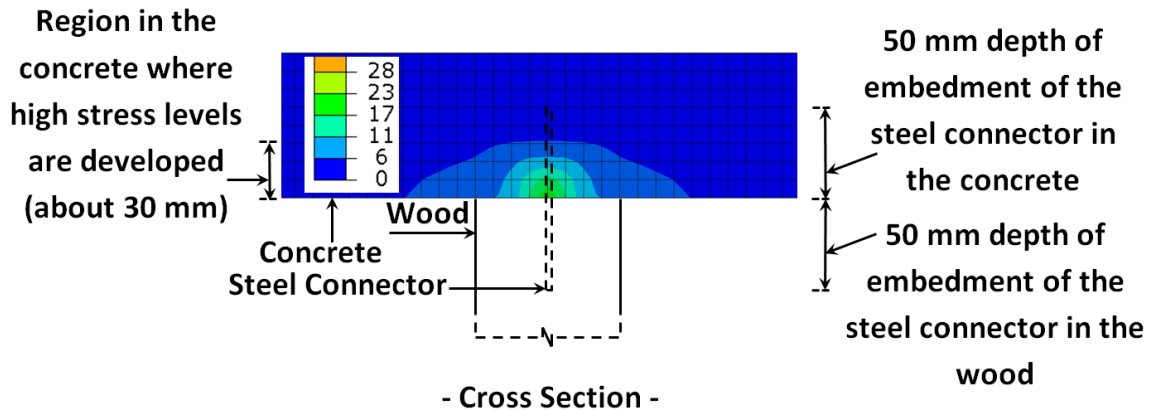
Figure 7.6: Von Mises stress distribution in the steel connector

## **7.5 Parametric Study**

The validated FE model was subsequently used to investigate the mechanical behavior of the concrete-wood system when the following key parameters are varied: (1) the depth of embedment of the steel connector in the concrete and the wood; (2) the thickness of the perforated steel plate; and (3) the thickness of the insulation gap between the concrete and the wood. The influence of these key parameters on the response of the system is discussed in this section.

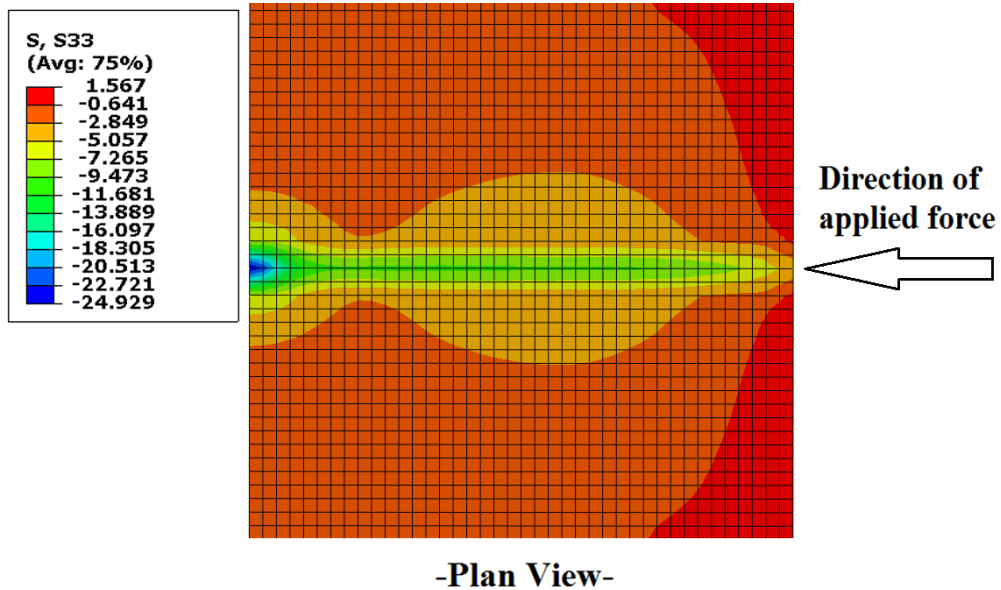
### **7.5.1 Effect of embedment depth of steel connector**

The FE model was implemented to study the stress state surrounding the interface of the materials to provide insight into the importance of embedment depth of the connector, both into the concrete and into the wood. The stress state studied was at incipient yield of the steel connector or just after yield had initiated. As expected, stresses were found to develop only within a limited region of the connector. In the steel connector, shown in Figure 7.6, stresses were predominantly within about 30 mm of the depth of embedment in both the concrete and wood indicating a possible lower limit on the required embedment of the steel connector to be slightly greater than 60 mm. The actual minimum embedment recommended for design should be verified, however, through additional experimental testing supported by further FE modeling. Figure 7.7 maps the stress distribution in the concrete in cross-section view. The interfacial stress in the direction of the applied load is predictably symmetric about the steel plate.



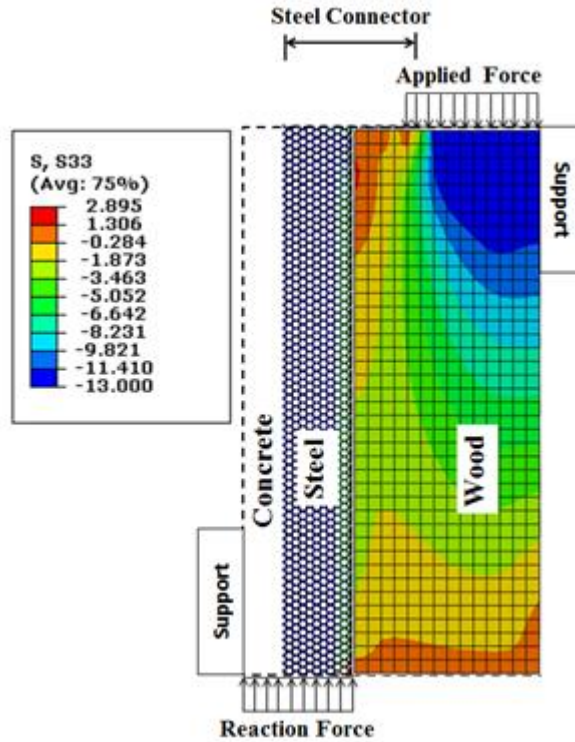
**Figure 7.7: Interfacial stresses developed in concrete cross section around the steel connector, MPa**

Figure 7.8 plots stress distribution in the direction of the applied force developed at the surface of concrete (around the steel connector). It is roughly uniform in the immediate proximity of the steel plate, where the stresses are highest, reaching a maximum tensile stress of 1.6 MPa and a maximum compressive stress of 24.9 MPa. These values are lower than the corresponding tensile and compressive strength of the concrete (3 MPa and 30 MPa, respectively). The computed stresses show that concrete did not reach failure when yielding of the steel connector occurred, which ensures a ductile performance of the system.



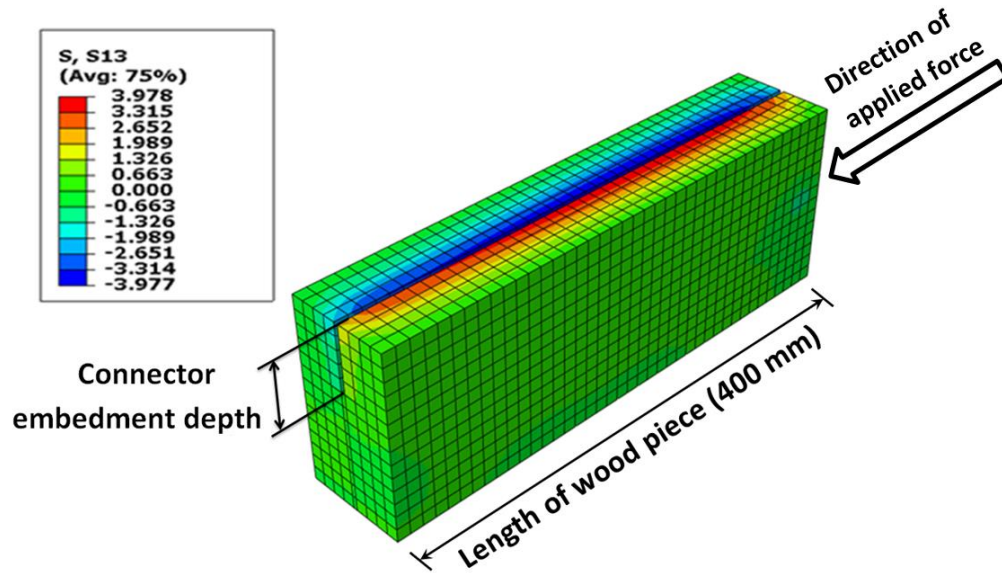
**Figure 7.8: Stress distribution in the direction of the applied force developed at the surface of concrete around the steel connector, MPa**

The stress distribution, shown in Figure 7.6, indicates that steel yielding initiates in the region of the connector that is embedded in the wood member (or adhesive) close to the surface. Correspondingly, Figure 7.9 shows the distribution of longitudinal stresses (parallel to the applied force) developed in the wood. Stresses in the wood at yielding of the steel connector varied between 2.9 MPa in tension and 13 MPa in compression near the loaded end. Similarly, to the concrete material, these calculated stresses are lower than the characteristic tensile and compressive strength of wood parallel-to-grain (17 MPa and 24 MPa, respectively). Therefore, no failure in the wood is anticipated to occur at the yield of the steel connector.



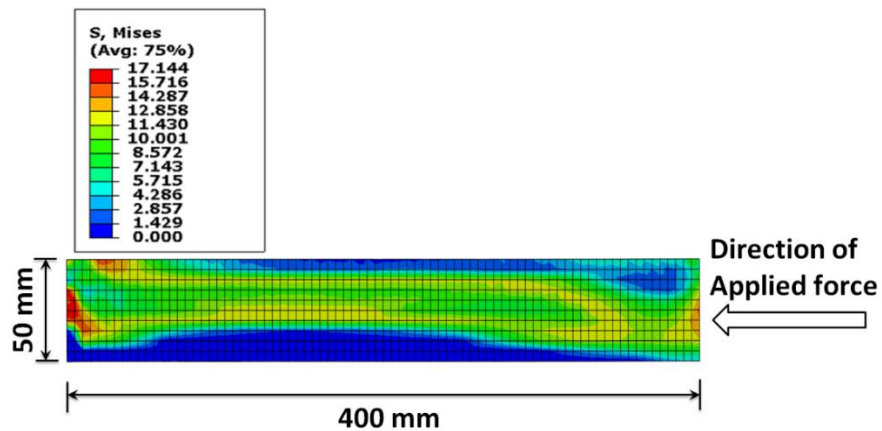
**Figure 7.9: Distribution of longitudinal stresses in the direction of the applied force developed in the wood, MPa**

Figure 7.10 shows the shear stress distribution around the connector in the wood. At yielding of the connector, the maximum shear stress in the wood was 3.9 MPa. An average uniform shear stress distribution determined by dividing the ultimate applied force by the gross contact area of the steel to the wood was equal to 2.77 MPa as shown in Table 7.1. This value compares extremely well with the 2.79 MPa average shear stress reported by Clouston et al. (2005) from their tests. Here, stress distribution obtained from FE analysis and presented in Figure 7.10 reflects the distribution of shear stresses better in comparison with the assumption of uniform shear stress.



**Figure 7.10: Shear stress distribution around the connector in the wood, MPa**

Figure 7.11 shows interfacial von Mises stresses developed in the adhesive. The maximum stress value in the adhesive was 17 MPa at the yield of the connector compared to a strength of approximately 43 MPa for the epoxy adhesive. This result again indicates that the ductile component of the system, the steel plate, is the one that dominates the mechanical response.



**Figure 7.11: Interfacial von Mises stresses developed in the adhesive, MPa**



### **7.5.2 Effect of steel plate thickness**

In modeling the different steel plate thicknesses, it was assumed that the adhesive layer thickness remained the same for each run such that the slot thickness in the wood changed. Figure 7.12 illustrates the predicted load-displacement behavior of wood-concrete systems with connector plate thicknesses ranging from 1.0 mm to 3.0 mm. This figure indicates that connector strength improves significantly - by 180 % - over the range of thicknesses studied. In reality, this increase in shear strength of the connector would be limited by the capacities of the other components of the composite system. For example, the FE simulation indicated that when the thickness of the steel connector is increased, higher stresses are developed in the wood member, in which case wood failure could become a concern. To this point, connector shear strength is only one of several failure mechanisms that can occur in the overall composite system. In addition to shear failure, the floor system needs to be designed against wood tensile-bending failure or concrete compressive-bending failure. The design methodology for concrete-wood systems is discussed in detail in the literature (Ceccotti 2002, Clouston et al. 2005, Fragiacommo 2006).

Connector stiffness (or slip modulus,  $K$ ) is one of the key parameters in the design of wood-concrete composite systems because it influences the degree of composite action developed in the system under service loading. As the value of the slip modulus increases, the total deflection of the wood-concrete system decreases. Often, serviceability is the controlling design criterion in these systems and a high slip modulus is necessary to achieve high floor rigidity. Increasing steel plate thickness from 1mm to 3mm is shown to improve slip modulus by 130 % as shown in Figure 7.12. It is noted,

however, that the benefits of composite action on the overall performance of the floor decay asymptotically when approaching full composite action (Clouston et al. 2005).

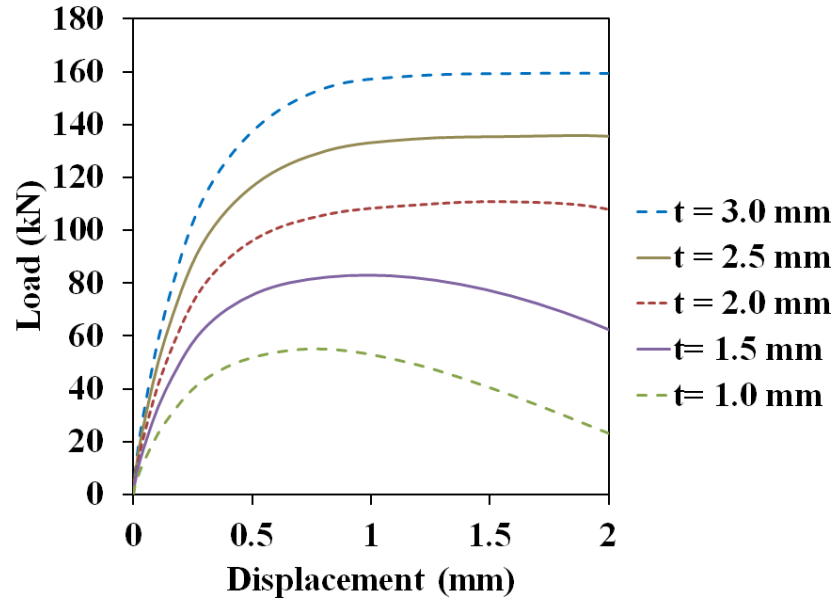


**Figure 7.12: Load-displacement curves of the HBV shear connector corresponding to different steel connector thicknesses (t)**

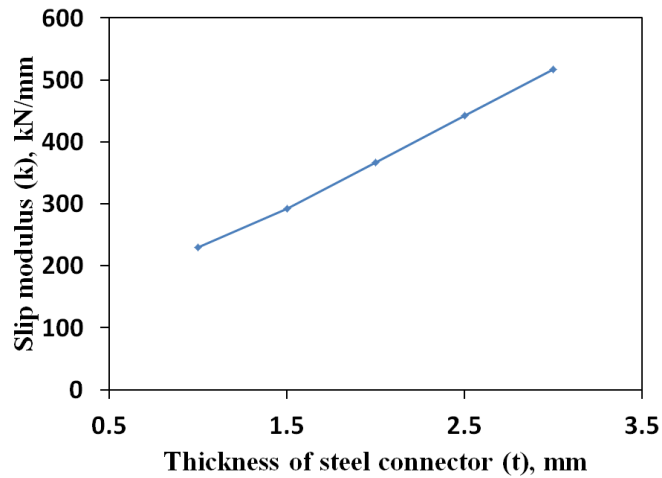


**Figure 7.13: Variation in slip modulus with change in steel connector thickness**

### **7.5.3 Effect of the gap between concrete and wood**

The FE results presented in Figure 7.14 indicate that any gap (up to 25mm thick) between the concrete and the wood has no influence on slip modulus, defined as the initial slope of the load-displacement curves. This information is very useful in practice, as it allows room in the floor system for sound insulation or permanent formwork without compromising floor rigidity. Introducing a gap does, however, seem to have an impact on connector strength. A gap of 5 mm reduced the strength by about 11% and by about 15% if a 25 mm gap is formed. The observed failure mechanism was governed by steel yielding caused by stresses generated from the force-couple moment between connected elements (concrete and wood). Introducing a larger gap increases the force-couple moment and may promote local buckling of the steel plate due to increase in the unsupported length of the steel connector (see Figure 7.15). Similar behavior was observed in laboratory tests conducted by Rafsanjani and Bertoldi (2017) in perforated plates loaded in uniaxial tension. Figure 7.14 shows that the rate of strength reduction decreases with increasing gap height, particularly after the gap is increased past 10 mm.

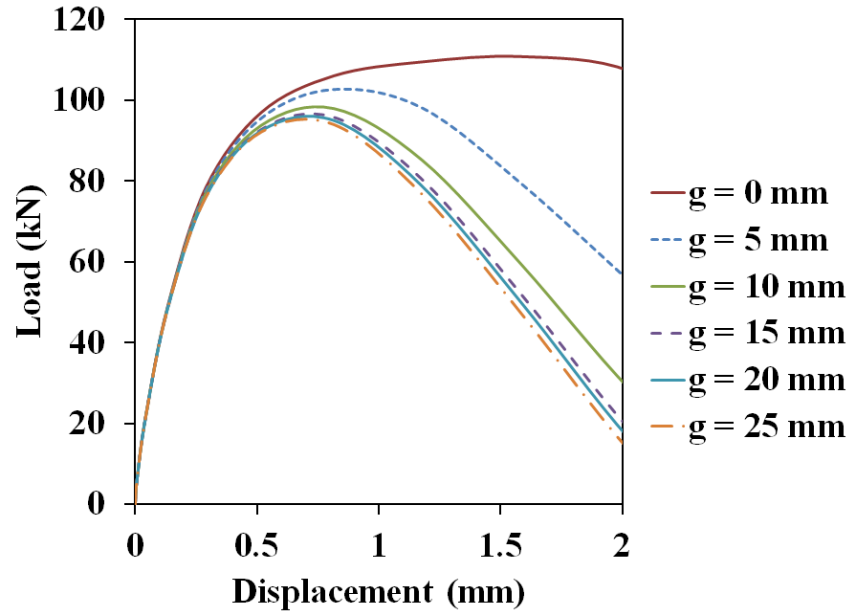


Figure 7.14: Effect of the insulation gap (g) between concrete and wood

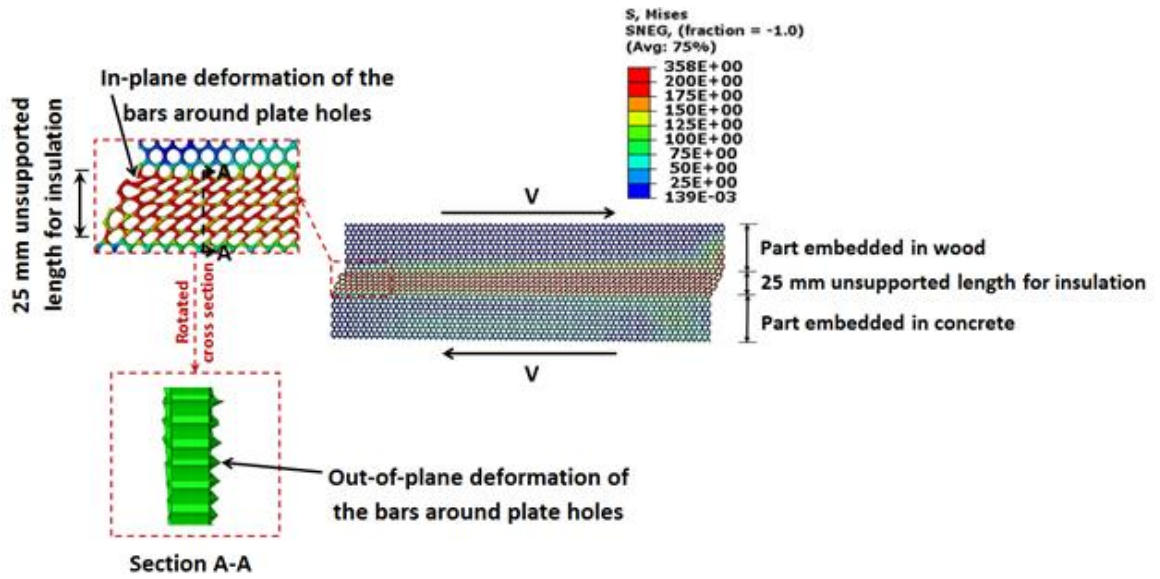


Figure 7.15: Deformed shape of the plate with 25 mm insulation gap

## CHAPTER 8

### CONCLUSIONS AND DESIGN RECOMMENDATIONS

#### 8.1 Bonded and mechanically anchored externally applied FRP to concrete

A parametric study was conducted by varying key properties of CFRP anchors to examine their influence on FRP sheets bonded to the surface of concrete. Based on the findings of the extensive number of simulations conducted that are reported in this dissertation, the following conclusions may be drawn:

1. The analysis of stress data obtained from finite element modeling showed that only 62 % of the carbon fiber strength (2350 MPa [340 ksi]) of a single CFRP sheet was reached at peak load if anchors are not used (bonded only joint). In contrast, the fiber strength in the sheet (3600 MPa [522 ksi]) was reached when CFRP anchors are used. Adding anchors to CFRP sheets along the debonding path increases the strength of the joint by more than 100%. However, a diminishing contribution of the anchors to strength was observed when spacing between anchor rows increases, particularly if they are placed at a spacing that exceeds the stress transfer zone.
2. Strength gain of the anchored system achieved by adding shallow anchors is more pronounced than further strength gains obtained by increasing anchor depth. Further increases in system strength were not observed for anchor depths beyond 90 mm (3.5 in.). However, joints with shallow anchors (30 mm [1.2 in.] or less) fail by anchor pullout and concrete cover separation before reaching the strength of the CFRP sheet, so the use of shallow anchors should not be encouraged.
3. The width of FRP sheet should be fully covered by the anchor splay(s) on the loaded side of the FRP sheet to obtain the maximum strength of the system.

Furthermore, the anchor splay can be formed in a butterfly shape within a circular sector that sweeps at least 90° for maximum anchor efficiency.

4. The maximum tensile force developed in the FRP sheet increases approximately linearly with a corresponding increase in thickness of the FRP sheet.

## **8.2 Development of strain efficiency factor for anchored FRP sheets**

A proposed modification to existing strain equations (ACI 440.2R-17) to incorporate the beneficial effect of using FRP anchors on externally bonded applications of FRP sheets to strengthen reinforced concrete elements was developed. The modification was developed in a format that could be easily incorporated into the framework of design guides such as ACI 440.2R-17. The proposed method is based on finite element analysis and a parametric study conducted to examine the increase in strength of externally bonded applications of FRP laminates due to the incorporation of FRP spike anchors. The strength of the anchored FRP-concrete system obtained from the parametric study was normalized to the strength of the unanchored FRP-concrete system. Because the relationship between stress and strain of FRP laminates is linear, the proposed modification focuses on using an anchorage strain efficiency factor  $K_{\epsilon a}$  that increases the debonding strain limit presented in the ACI 440.2R-17 Guide.

The formulation of the anchorage strain efficiency factor has been verified by comparing the calculated results with values determined by several laboratory tests reported from three research groups. The value of  $K_{\epsilon a}$  obtained from equations derived using nonlinear regression analysis were found to lie within +/-15% accuracy bands when compared with experimental data. A simplified version of these equations was proposed,

which results in more conservative values with little loss of accuracy in the average results. Further laboratory tests of FRP anchored sheets are needed to validate the formulas developed in this research.

### **8.3 Bonded and mechanically anchored wood-concrete composites**

A three-dimensional finite element (FE) model was constructed and analyzed to investigate the influence of several key parameters on shear stresses and strains of perforated steel plate wood-concrete composite connectors. The parameters studied were: (1) thickness of plate; (2) insulation gap between concrete and wood; (3) depth of embedment in concrete; and (4) depth of embedment in wood.

The following conclusions can be drawn based on the parametric study conducted in this research:

1. Thickness of the perforated steel plate (in the range of 1mm to 3mm) correlates directly with shear stiffness and strength of the connector system: thicker plates lead to higher values. This finding is limited in a practical sense, however, because using thicker steel plates could shift the reliable and ductile steel failure to a less desirable wood tensile-bending failure or concrete compressive-bending failure in the overall composite floor system.
2. A gap between the concrete and the wood (for insulation or permanent formwork) of up to 25mm was predicted to have no impact on slip modulus of the connector system. This finding is important because the slip modulus determines the level of composite action of the composite floor. The more rigid the shear connector is, the

higher the overall stiffness and strength of the wood-concrete composite floor system for resisting gravity loads.

3. Reductions in strength were predicted when an insulation gap is created between the concrete and the wood. A gap of 5 mm reduced the strength by about 11% and by about 15% if a 25 mm gap is formed. This reduction is due to yielding of the connector because of the additional stresses generated by changing the location of the neutral axis and the lack of lateral support that permits local buckling of the perforated steel connector.
4. FE modeling showed that stresses are predominantly developed within a limited region of the connector in the concrete slab on both sides of the connection. This finding led to the conclusion that the embedment depth of the perforated steel connector in concrete should not be less than 30 mm.
5. Similarly, the depth of embedment in the wood (or the adhesive) should not be less than 30 mm measured from the surface of the wood member. The FE modeling predicted that the yield of the steel connector starts at the region embedded in the wood member close to the surface.
6. At the yield of the steel connector, FE simulation showed that no failure was experienced in the other materials of the connector system. This observation is in agreement with previous experimental results and with the design philosophy of promoting a ductile failure of the connector.



## APPENDIX

### SUPPLEMENTAL INFORMATION

#### A.1 Example Applications of Anchor Efficiency Factor

##### A.1.1 Example 1.1– Calculation of Anchorage Efficiency Factor

A CFRP-concrete specimen tested by Niemitz et al. (2010) is considered to examine the proposed formula of the anchorage efficiency factor. The specimen was remarked BI-13-0.6-5 is referring to group type B (anchored sheets), anchor pattern I (two anchors are used and configured as shown below), FRP sheet width = 127 mm, anchor shaft diameter = 6 mm, and FRP anchor splay diameter = 50 mm. In addition to the previous properties, the dry FRP sheet thickness is 0.22 mm, the distance between anchors is 254 mm, the anchor shaft length is 50 mm, the anchor splay angle is 360 degrees, and the anchor splay diameter / FRP sheet width is 0.4.

The ultimate tensile force is 45.4 kN. For the unanchored specimen of the same properties, the ultimate tensile load is 35.6 kN, the experimental FRP strain value is 0.0045,  $f'_c$  for concrete = 28.6 MPa, the cured FRP sheet thickness is 1 mm, the number of plies = 1, the modulus of elasticity of a one-ply cured FRP sheet is 228 GPa.

Determine the anchorage efficiency factor?

Solution:

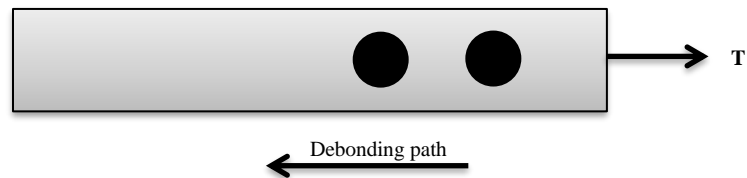


Figure A1: Anchored FRP sheet

From Equation 6.15

$$K_{\varepsilon a} = 1.617 \cdot (0.72(t_f)^{-0.2})^{-1} \cdot (0.52(a_d)^{0.24})^1 \cdot (0.5(f_d) + 0.52)^{0.1} \geq 1.0 \text{ Here,}$$

Two anchors are used and spaced more than 200 mm from each other.

The dry FRP sheet thickness is 0.22 mm. Therefore,  $S_t = 0.975$

The anchor shaft diameter is 6 mm. Therefore,  $S_{ad} = 0.799$

The anchor splay diameter / FRP sheet width is about 0.4. Therefore,  $S_{fd} = 0.72$

Therefore, the anchorage efficiency factor:

$$\therefore K_{\varepsilon a} = 1.617 \cdot 0.975^{-1} \cdot 0.799^1 \cdot 0.72^{0.1} = 1.283 \geq 1.0 \quad \therefore \text{OK (compare to}$$

1.275 from the experimental test, see Table 6.3).

Now, multiply the resulted anchorage efficiency factor by the ultimate tensile force and/or the FRP strain of unanchored specimen. The result should be close to the ultimate tensile force and/or the average FRP strain of the anchored specimen to verify the solution.

Therefore;

The ultimate tensile force of the anchored specimen =  $K_{\varepsilon a}$  x the ultimate tensile force of the unanchored specimen =  $1.283 \times 35.6 \text{ kN} = 45.675 \text{ kN}$  (compare to the experimental value of 45.4 kN)

### **A.1.2 Example 1.2– Flexural Strengthening of RC Beam with FRP Anchored Sheets**

A design example from the ACI 440.2R-17 design guide is modified by applying FRP anchors and considering the proposed anchorage efficiency factor (design example 16.3 of the ACI 440.2R-17). In this example, the flexural strength of an interior reinforced concrete beam with FRP laminates is determined. This beam is a simply supported

concrete beam reinforced with three No.9 bars and is subjected to a 50% increase in its live load carrying requirements. The other details of the beam are reported in the ACI 440.2R-17 design guide (see Figure A2).

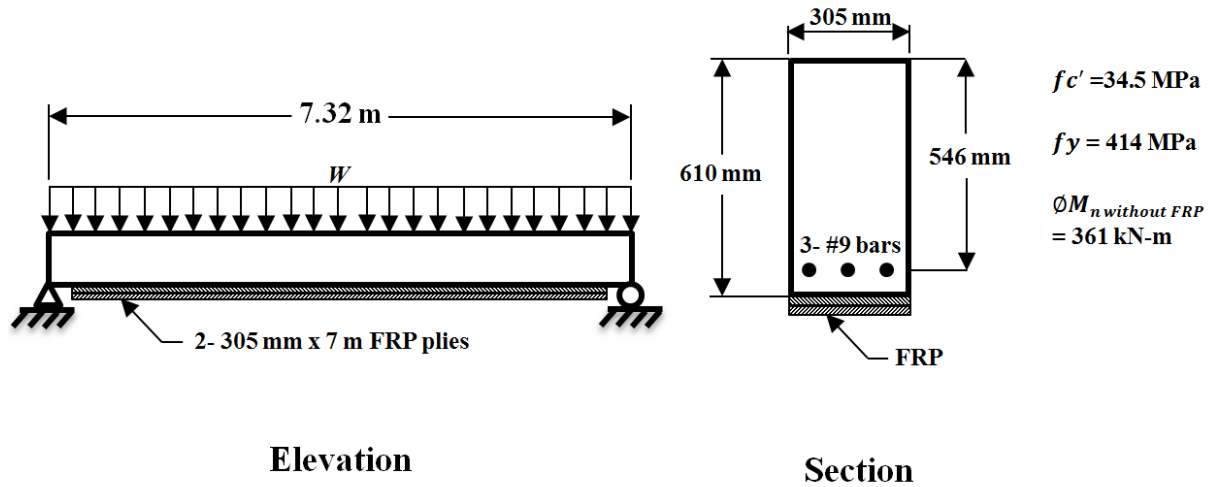


**Figure A2: A simply supported beam with external FRP reinforcement**

Several experimental tests have reported that maximum measured strains were close to the mid-span of the tested beams (Guadagnini et al. 2006; Teng et al. 2009; Loo et al. 2012). Therefore, two debonding regions around the mid-span has been assumed (see Figure A3). In addition to debonding, FRP end peeling (cover delamination) may occur. Here, it should be noted that this example focuses on debonding regions while end-peeling region can be detected by following the procedure stated in section 14.1.2 of the ACI 440.2R-17.

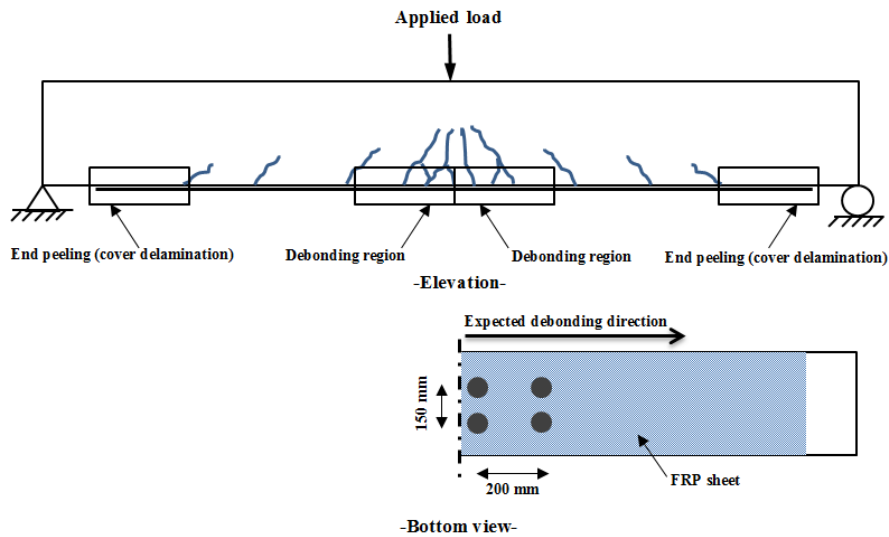


**Figure A3: Proposed application of the anchors (dimensions are not to scale)**

Four anchors have been applied for each debonding region (2 along the width of the FRP sheet by 2 along debonding path). Therefore,  $n_a = 2$  anchors,  $t_f = 0.24 \times 2$  layers = 0.48 mm (dry thickness = 1.02 mm - 0.78 mm assumed adhesive thickness = 0.24 mm),  $s_a = 200$  mm,  $a_d = 13$  mm,  $f_d = 60 \text{ mm} / (300 \text{ mm} / 2) = 0.4$ .

Consequently, the design strain of the FRP system (step 4 of the design example 16.3 of the ACI 440.2R-17 design guide) should be modified as following to consider the effect of the anchors;

First, determine the anchorage efficiency factor from Equation 6.14

$$\begin{aligned}
 K_{\epsilon a} &= (0.007(2)^3 - 0.13(2)^2 + 0.74(2) \\
 &+ 1)^{1.6} \cdot (0.72(0.48)^{-0.2})^{-1} \cdot (1.7(200)^{-0.15})^{2.35} \cdot (0.52(13)^{0.24})^1 \cdot (0.5(0.4) \\
 &+ 0.52)^{0.1} = 1.843 \geq 1.0
 \end{aligned}$$

Second, determine the design strain from Equation 6.21 (the design strain formula is updated by considering the anchorage efficiency factor);

$$\begin{aligned}\varepsilon_{fd(anchored)} &= K_{\varepsilon a} \times 0.41 \sqrt{\frac{f'_c}{nE_f t_f}} \leq 0.9 \varepsilon_{f\mu} \\ &= 1.843 \times 0.009 = 0.0165 \text{ should be } \leq 0.9 (0.0142) = 0.0128\end{aligned}$$

Therefore,  $\varepsilon_{fd(anchored)} = 0.0128$

Here, the design strain obtained due to the effect of anchorage is much more than that of the unanchored FRP reinforcement (0.0128 for the anchored FRP reinforcement compared to 0.009 for the unanchored FRP reinforcement, see example 16.3 ACI 440.2R-17 for the unanchored design strain value). This difference is very significant in design. Therefore, the modified strain value should be considered in the following steps of the design example if anchors are applied.

The effective level of strain in the FRP reinforcement will be (Modify step 6 of the design example 16.3 of the ACI 440.2R-17 design guide);

$$\begin{aligned}\varepsilon_{fe} &= \varepsilon_{c\mu} \left( \frac{d_f - c}{c} \right) - \varepsilon_{bi} \leq \varepsilon_{fd} \\ \varepsilon_{fe} &= 0.003 \left( \frac{609.6 \text{ mm} - 109.2 \text{ mm}}{109.2 \text{ mm}} \right) - 0.00061 \leq 0.0128\end{aligned}$$

$\varepsilon_{fe} = 0.0131$  should be  $\leq 0.0128$

Use

$$\varepsilon_{fe} = \varepsilon_{fd(anchored)} = 0.0128$$

Based on the new strain level of the anchored FRP sheet and by completing the rest of this step and the following steps as reported in the ACI 440.2R-17, the obtained flexural strength of the anchored beam was about 455 kN.m compared to 443 kN.m of the

unanchored beam. The resulted value is also compared with the analytical procedure reported in Research Report 1776-1 (Breña et al. 2001) that determines the moment-curvature of beams with external FRP sheet reinforcement assuming a perfect bond. The obtained moment value assuming a perfect bond was 458 kN.m. This value is satisfactory since with the perfect bond assumption the full strength of the FRP sheet is reached as in the case of the anchored sheet. However, the resulted strengthening level should also be verified through further experimental tests.

If only two anchors are used along the width of the FRP sheet, Equation 16 should be used to determine the anchorage efficiency factor rather than Equation 15.

$$K_{\varepsilon a} = 1.617 \cdot (0.72(0.48)^{-0.2})^{-1} \cdot (0.52(13)^{0.24})^1 \cdot (0.5(0.4) + 0.52)^{0.1} = 1.8$$

$$\geq 1.0$$

Again,

$\varepsilon_{fd(anchored)} = 1.8 \times 0.009 = 0.0162$  should be  $\leq 0.9 (0.0142) = 0.0128$ . While almost the same level of debonding strain is achieved (that is limited by a rupture strain of 0.0128), only two anchors along the width of the sheet at each debonding region are required to achieve the previously obtained level of flexural strength. This example illustrates FE simulation results presented in Figure 6.7 that anchors placed at about 200 mm or more from each other (along the debonding path) have no significant effect on debonding strength. However, it is recommended to add more anchors along the debonding path to achieve more ductility.

The contribution of the FRP reinforcement in bending strength after applying the anchors is more than the contribution of the unanchored sheet. However, it should be

noted that the allowable rupture strain governs the solution when the strain determined based on the proposed anchorage efficiency factor is more than the allowable rupture strain of the FRP reinforcement (  $0.9 \varepsilon_{f\mu}$  ). In this case, the times of contribution of the FRP reinforcement in bending strength after applying the anchors compared to the unanchored FRP reinforcement will be less than the anchorage efficiency factor.

## **A.2 Main user interface**

The main user interface includes a menu bar that shows several options for controlling the application. The main menu item is FRP Estimator. This command includes three options:

- 1- Estimate flexural strength of FRP reinforced beams**
- 2- Estimate required anchorage length**
- 3- Estimate flexural strength of anchored FRP reinforced beams**

These options perform three types of calculations: flexural strength due to the use of FRP reinforcement, required anchorage length, and flexural strength due to adding FRP anchors to the system. File, windows, and help are other menu items that are included to assist in controlling the application.

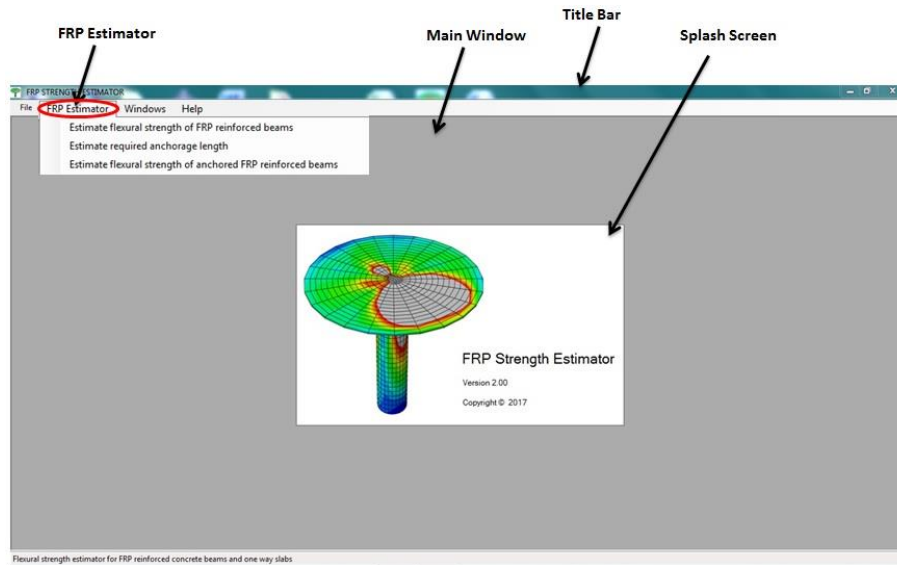


**Figure A4: User interface**

### **A.2.1 Estimate flexural strength of FRP reinforced beams**

This option performs cracked section analysis, Moment capacity check, Service stress check, creep rupture check, and allow the optimization of the thickness of the FRP plate. The formulation that is conducted within this option is based on the solution procedure that is reported in the ACI 440.2R-17. A step-by-step input-output interface is used to describe the solution procedure adopted by the ACI 440 committee. It should be noted that default values in textboxes are based on the example reported in section 16.3 of the ACI 440 report.



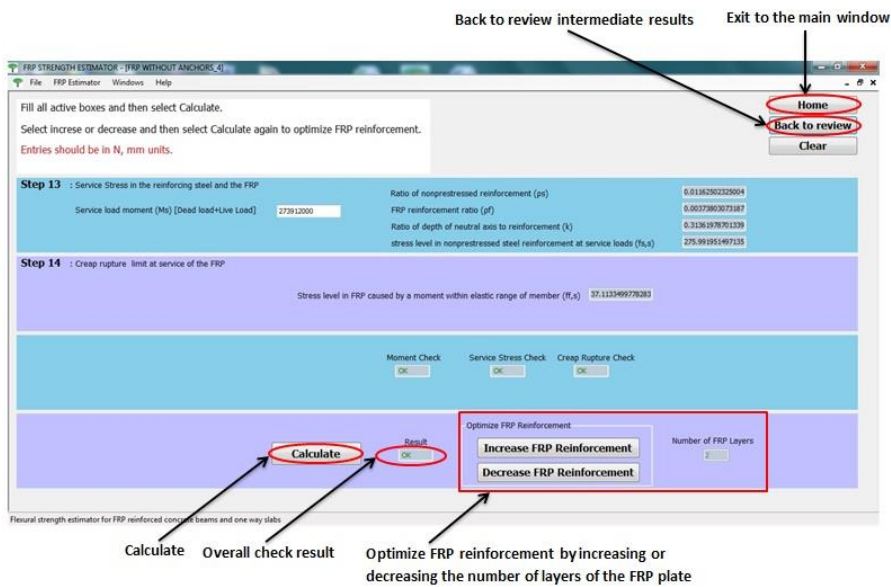
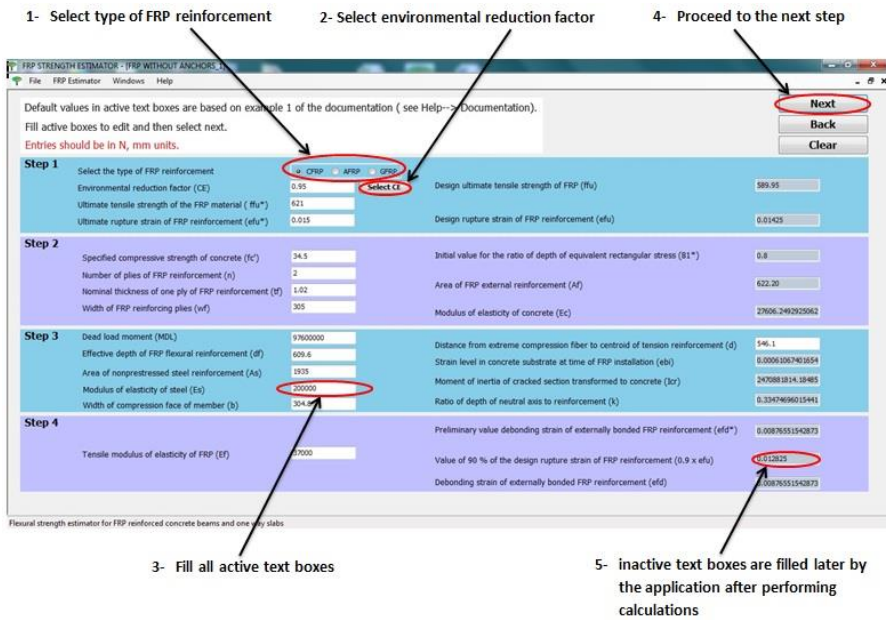
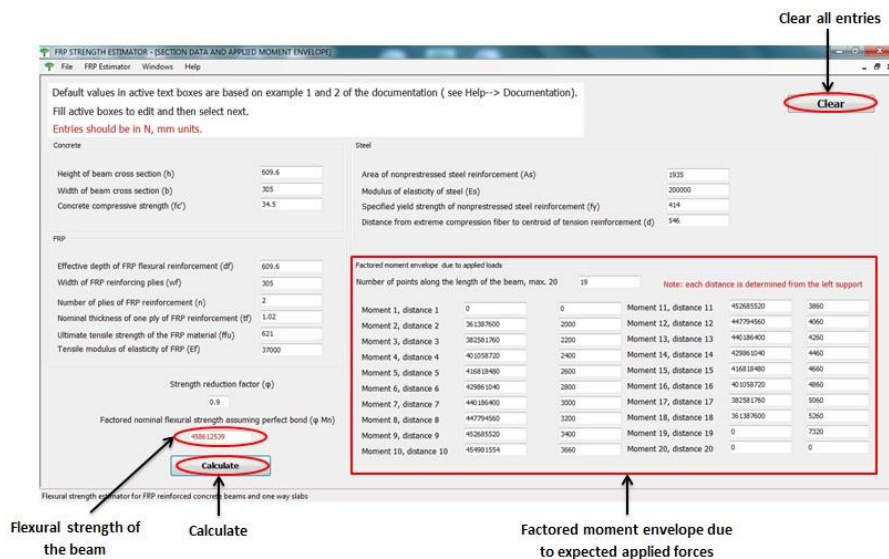


**Figure A5: Estimation of flexural strength**

### A.2.2 Estimate required anchorage length

If the goal strength has not been achieved based on moment capacity check, Service stress check, or creep rupture check performed in the first option in FRP Estimator. Users have the option to either optimizing the thickness of the FRP plate by increasing the

number of layers or adding FRP anchors to the system. If the second option is considered, users should first determine anchored length of the FRP plate along the length of the beam. This option is performed by determining FRP strain assuming perfect bond between FRP plate and concrete substrate (this could be reached by adding FRP anchors). Then, the resulted strains along the length of the beam are compared with the debonding strain limit determined from Equation 6.4. If the FRP strain exceeds the debonding strain limit at a specific station along the length of the beam, FRP anchors are required at that station to overcome debonding of the FRP plate (FRP anchors should be applied at the station before the first and after the last stations where debonding strain is exceeded).



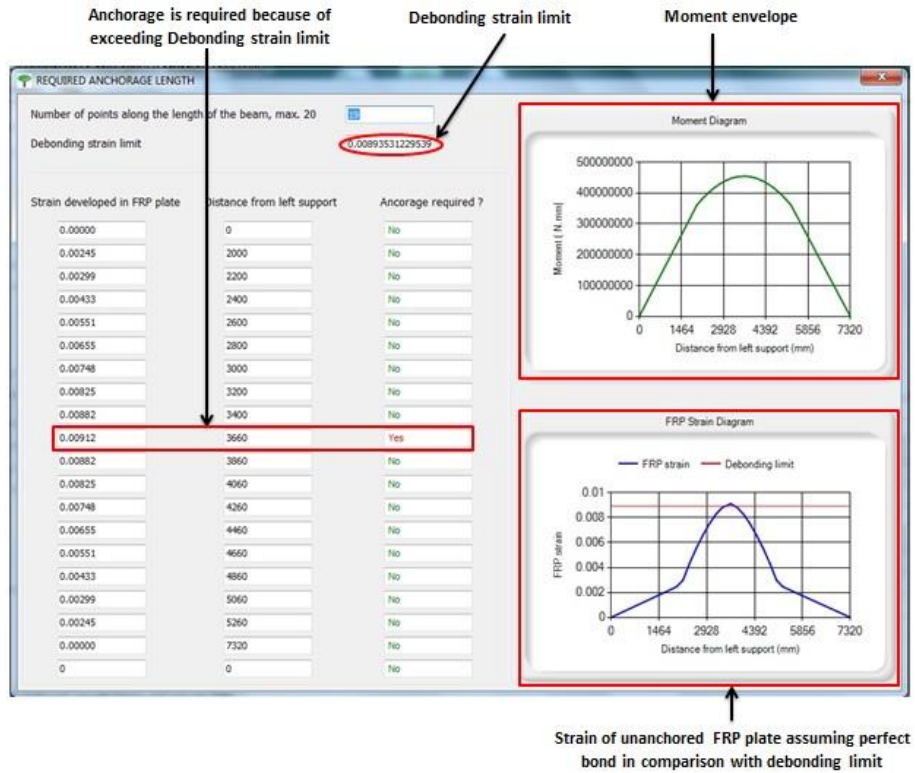


**Figure A6: Estimating required anchorage length**

### A.2.3 Estimate flexural strength of anchored FRP reinforced beams

After determining the required anchorage length, the number of anchors, the spacing between anchors and dimensions of the anchors can be introduced to the application to estimate flexural strength. If the goal flexural strength of the beam has not been achieved, anchorage properties can be changed until reaching the required strength.

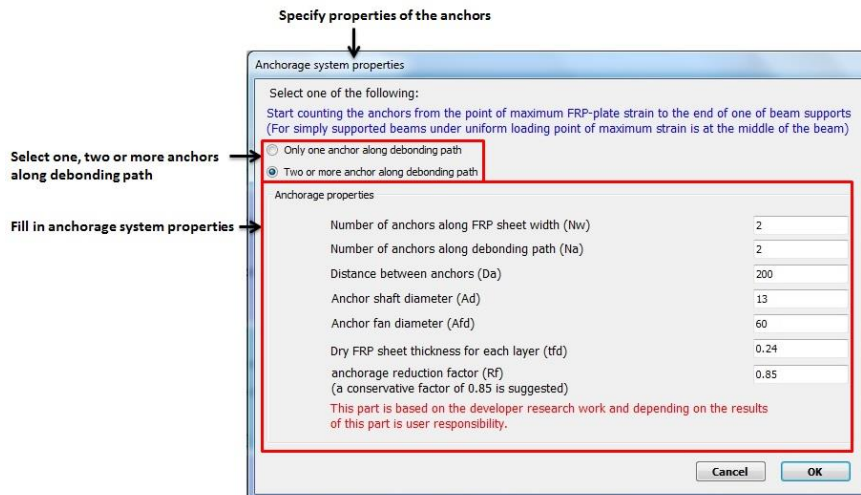
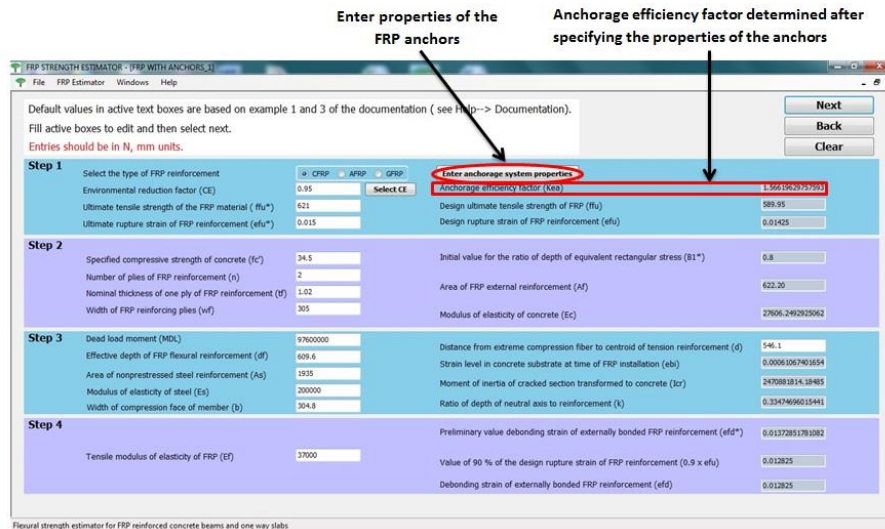


**Figure A7: Assigning anchorage system properties**

## A.3 Examples solved using the software tool developed

### A.3.1 Example 3.1

This example is reported in the ACI 440.2R-17 design guide (design example 16.3 of the ACI 440.2R-08). In this example, the flexural strength of an interior reinforced concrete beam with FRP laminates is determined. This beam is a simply supported

concrete beam reinforced with three No.9 bars and is subjected to a 50% increase in its live load carrying requirements. The other details of the beam are shown in Figure A2.

After selecting estimate flexural strength of FRP reinforced beams from the menu bar, the input values are introduced to the application as needed for each step following the solution procedure that is reported in the ACI 440. Default values in active text boxes represent input values of this example. Then, the application performs cracked section analysis, moment capacity check, service stress check, creep rupture check, and optimize the thickness of the FRP plate if required by the user.

### **A.3.2 Example 3.2**

If a goal flexural strength has not been achieved after performing calculations as in example 2.1, the user has the option either to increase the number of layers of the FRP plate or to apply FRP anchors to reduce or prevent the effect of FRP plate debonding. If the second option is chosen, the user should determine the required anchorage length by selecting required anchorage length from the menu item FRP Estimator. The default values are the same values from example 2.1; however, the user can change them by introducing new values in active text boxes. Moment envelop of the beam should be introduced to the application so that FRP strain level is determined.

Proceeding to the determination stage by clicking on Calculate, a new window appears and shows the locations where anchorage is required. If the FRP strain exceeds the debonding strain limit at a specific station along the length of the beam, FRP anchors are required at that station to overcome debonding of the FRP plate (FRP anchors should be applied at the station before the first and after the last stations where debonding strain is

exceeded). This window also shows introduced moment diagram and FRP strain diagram that compares FRP strain with debonding strain limit.

### **A.3.3 Example 3.3**

In this example, FRP anchors are applied to the beam in example 2.1. Example 2.2 shows that FRP strain exceeds debonding strain at the center of the beam. In addition, experimental tests in the literature have reported that maximum measured strains were close to the mid-span of the tested beams (Guadagnini et al. 2006, Loo et al. 2012). Therefore, two debonding regions around the mid-span have been assumed (see Figure A.3).

Therefore, four anchors are assumed to be applied for each debonding region (two along the width of the FRP sheet by two along the debonding path). Other required information are; dry FRP thickness = 1.02 mm -0.78 mm (assumed adhesive thickness) = 0.24 mm, distance between anchors =200 mm, anchor shaft diameter = 13 mm, anchor fan diameter =60mm.

By introducing all the above data (in addition to the data of example 2.1), the application updates the design strain of the FRP system to consider the effect of the anchors. Then, the application performs cracked section analysis; moment capacity check, service stress check, and creep rupture check as in example 2.1.

### **A.3.4 Example 3.4**

The specimen examined in this example was tested experimentally and reported in Smith et al. 2011. The experimental work included several reinforced concrete slabs externally reinforced with carbon fiber reinforced polymer (CFRP). The slabs were simply supported and they were tested in 4-point bending. The length of each slab was



#### A.4 Material input data of the HBV-shear connector

The following are input data for the concrete damage plasticity model (Units N, mm):

Young's modulus,  $E = 26480$

Poisson's ratio,  $= 0.167$

Plasticity

Dilation angle = 15.0

Flow potential eccentricity = 0.1

Biaxial/uniaxial compression plastic strain ratio = 1.16

Invariant stress ratio = 0.6667

Viscosity = 0.0

Compression behavior:

Stress	Inelastic strain
24.019	0.0000
29.208	0.0004
31.709	0.0008
32.358	0.0012
31.768	0.0016
30.379	0.0020
28.507	0.0024
21.907	0.0036
14.897	0.0050
2.953	0.0100

Tension behavior:

Stress,	Cracking strain
1.780	0.0000
1.457	0.0001
1.113	0.0003
0.960	0.0004
0.800	0.0005
0.536	0.0008
0.359	0.0010
0.161	0.0020
0.073	0.0030
0.040	0.0050

The following are input data for the elastic-orthotropic wood model (Units N, mm):

E1	E2	E3	Nu12	Nu13	Nu23	G12	G13	G23
8963	8963	7584	0.39	0.39	0.39	650	650	650

The following are input data for the steel material model (Units N, mm):

Elastic

Young's Modulus    Poisson's ratio

200000                      0.26

Plastic

Yield strain	Plastic strain	Yield strain	Plastic strain
248.0000	0.00000	412.0000	0.17547
245.9705	0.00563	409.866	0.19893
252.2252	0.01501	404.6113	0.22051
273.244	0.02534	394.1019	0.24397
299.5174	0.04316	378.3378	0.26743
320.5362	0.06005	357.319	0.28995
346.8097	0.08351	333.6729	0.31059
378.3378	0.11542	312.6542	0.32748
399.3566	0.14357	283.7534	0.34625

The following are input data for the adhesive material model (Units N, mm):

Elastic

E1                      E2                      E3



3160                    1200                    1200

Quad Damage

Nominal strain (Normal –only mode)    0.05

Nominal strain (Shear –only mode) First direction    0.05

Nominal strain (Shear –only mode) Second direction    0.05

## A.5 Source codes

### A.5.1 Sample of a Python code used to create an input data file, an output data file and an execution command file

```
#input data builder
#####
import os
u= 0
while u <= 20.5:
    m=u*10
    with open('Part1.txt','r') as infile1, open('Part2.txt','r') as infile2,open('Part3.txt','r') as infile3, open('Job-
Sh-nofrp'+str(m)+'.inp','w') as outfile:
        for line in infile1:
            outfile.write(line.split("<_>")[0])
# print data*****
tx1='** LOADS'
tx2='**'
tx3='** Name: Load-1   Type: Pressure'
tx4='*Dsload'
P= 0.134615 * u
u= u + 0.5
tx5= 'Surf-139, P, '+str(P)
tx6= '**'
outfile.write('\n'+tx1+'\n'+tx2+'\n'+tx3+'\n'+tx4+'\n'+tx5+'\n'+tx6+'\n')
for line in infile3:
    outfile.write(line.split("<_>")[0])
u= 0
while u <= 20.5:
    m=u*10
    os.system ('abaqus job=Job-Sh-nofrp'+str(m)+' interactive')
    u= u + 0.5
#####
#output Data Builder
#####
# -*- coding: utf-8 -*-
import xlswriter
import numpy
import math
# Create a workbook and add a worksheet.
```

```

workbook = xlswriter.Workbook('DATA.xlsx')
worksheet = workbook.add_worksheet()
col = 0
from odbAccess import openOdb
u= 0
while u <= 20.5:
    m=u*10
    row = 0
    odb = openOdb('Job-Sh-nofrp'+str(m)+'.odb')
    RP_region= odb.rootAssembly.nodeSets['RP']
    x=-1
    for frame in odb.steps['Step-1'].frames:
        x=x+1
        OD_Frame= odb.steps['Step-1'].frames[x]
        Field1=OD_Frame.fieldOutputs['U']
        Field2=OD_Frame.fieldOutputs['RF']
        FinalF1=Field1.getSubset(region=RP_region).values
        FinalF2=Field2.getSubset(region=RP_region).values
        for v1 in FinalF1:
            xu= v1.data[0]
            worksheet.write_number(row,col, xu)
        for v2 in FinalF2:
            mc=col+1
            yrf=v2.data[0]
            worksheet.write(row,mc,yrf)
            row=row+1
        col=col+2
    u= u + 0.5
workbook.close()
#####
Shell execution
#####

import subprocess

process = subprocess.call('abaqus cae noGUI=Outpdata.py',shell=True)

#####

```

## A.5.2 VB code of the developed software

```

<?xml version="2.00" encoding="utf-8" ?>0
<configuration>
  <system.diagnostics>
    <sources>
      <!-- This section defines the logging configuration for
My.Application.Log -->
      <source name="DefaultSource" switchName="DefaultSwitch">
        <listeners>
          <add name="FileLog"/>
          <!-- Uncomment the below section to write to the
Application Event Log -->

```

```

        <!--<add name="EventLog"/>-->
    </listeners>
</source>
</sources>
<switches>
    <add name="DefaultSwitch" value="InFation" />
</switches>
<sharedListeners>
    <add name="FileLog"
        initializeData="FileLogWriter"/>
</sharedListeners>
</system.diagnostics>
</configuration>

```

---

```

Public Class F2_4

    Private Sub B2_Click(ByVal sender As System.Object, ByVal e As
System.EventArgs) Handles B2.Click
        F2_3.Show()
        F2_3.WindowState = FWindowState.Maximized
        Me.WindowState = FWindowState.Minimized
    End Sub

    Private Sub F2_4_Load(ByVal sender As System.Object, ByVal e As
System.EventArgs) Handles MyBase.Load
        Me.CenterToScreen()
    End Sub

    Private Sub B3_Click(ByVal sender As System.Object, ByVal e As
System.EventArgs) Handles B3.Click
        Dim B As DialogResult = MessageBox.Show("You will be
transferred to the homepage!", "Please Notice:", MessageBoxButtons.OKCancel)
        If B = DialogResult.OK Then
            F1.Show()
            Me.Hide()
            F2.Hide()
            F2_2.Hide()
            F2_3.Hide()
        End If
    End Sub

    Private Sub B5_Click(ByVal sender As System.Object, ByVal e As
System.EventArgs) Handles B5.Click
        Dim n As Decimal
        Try
            n = CDec(Me.Textns.Text)
            n = n - 1
            If n <= 0 Then
                n = 1
                MessageBox.Show("Number of FRP layers should not be
zero.", "Warning")
            End If
            Me.Textns.Text = CStr(n)
        End Try
    End Sub

```

```

        F2.Textn.Text = CStr(n)
    Catch
        MessageBox.Show("Please check your entries.", "Entry
error")
    End Try
End Sub

Public Sub B1_Click(ByVal sender As System.Object, ByVal e As
System.EventArgs) Handles B1.Click
    Dim CE, ffus, efus, ffu, efu, fc, Ass, n, tf, wf, Bls, Af, Ec
As Decimal
    Dim MDL, df, d, Icr, k, ebi, Ef, efds, nefu, efd, Cl, efe,
ecs, es As Decimal
    Dim Esm, fy, fs, ffe, b, ecp, B1, Alpha1, C2, Mns, Mnf As
Decimal
    Dim C1s, C2s, C, PHI, PSI, Mu, PHIMN, Rhos, Rhof, Ks, fss, Ms,
ffs, ne, j, esy, fch As Decimal
    Dim chm, chs, chc As Integer
    Dim Atx As Control
    Try

        ' step 1 -----
        CE = CDec(F2.TextCE.Text)
        ffus = CDec(F2.Textffus.Text)
        efus = CDec(F2.Textefus.Text)
        ffu = CE * ffus
        efu = CE * efus
        F2.Textffu.Text = CStr(ffu)
        F2.Textefu.Text = CStr(efu)
        ' step 2 -----
        fc = CDec(F2.Textfc.Text)
        Ass = CDec(F2.TextAs.Text)
        n = CDec(F2.Textn.Text)
        tf = CDec(F2.Texttf.Text)
        wf = CDec(F2.Textwf.Text)
        Bls = 1.05 - 0.05 * (fc / 6.9)
        Af = n * tf * wf
        Ec = 4700 * (fc) ^ 0.5
        F2.TextBls.Text = CStr(Bls)
        F2.TextAf.Text = CStr(Af)
        F2.TextEc.Text = CStr(Ec)
        ' step 3 -----
        b = CDec(F2.Textb.Text)
        Esm = CDec(F2.TextEsm.Text)
        ne = Esm / Ec
        MDL = CDec(F2.TextMDL.Text)
        df = CDec(F2.Textdf.Text)
        d = CDec(F2.Textd.Text)
        Rhos = Ass / (b * d)
        k = ((Rhos * ne) ^ 2 + 2 * Rhos * ne) ^ 0.5 - Rhos * ne
        F2.Textk.Text = CStr(k)
        j = 1 - (k / 3)
        Icr = b * (k ^ 2) * j * (d ^ 3) / 2
        F2.TextIcr.Text = CStr(Icr)
    
```

```

ebi = MDL * (df - k * d) / (Icr * Ec)
F2.Textebi.Text = CStr(ebi)
' step 4 -----
Ef = CDec(F2.TextEf.Text)
efds = 0.41 * (fc / (n * Ef * tf)) ^ 0.5
nefu = 0.9 * efu
If efds > nefu Then
    efd = nefu
Else
    efd = efds
End If
F2.Textefds.Text = CStr(efds)
F2.Textnefu.Text = CStr(nefu)
F2.Textefd.Text = CStr(efd)
' step 5 -----
C1 = 0.2 * d
F2_2.TextC1.Text = CStr(C1)
' step 6 -----
efe = 0.003 * ((df - C1) / C1) - ebi
If efe > efd Then
    efe = efd
End If
ecs = (efe + ebi) * (C1 / (df - C1))
F2_2.Textefe.Text = CStr(efe)
F2_2.Textecs.Text = CStr(ecs)
' step 7 -----
es = (efe + ebi) * ((d - C1) / (df - C1))
F2_2.Textes.Text = CStr(es)
' step 8 -----

fy = CDec(F2_2.Textfy.Text)
fs = Esm * es
If fs > fy Then
    fs = fy
End If
ffe = Ef * efe
F2_2.Textfs.Text = CStr(fs)
F2_2.Textffe.Text = CStr(ffe)
' step 9 -----

ecp = 1.7 * fc / Ec
B1 = ((4 * ecp - ecs) / (6 * ecp - 2 * ecs))
Alpha1 = (3 * ecp * ecs - ecs * ecs) / (3 * B1 * ecp *
ecp)

C2 = (Ass * fs + Af * ffe) / (Alpha1 * fc * B1 * b)
F2_3.Textecp.Text = CStr(ecp)
F2_3.TextB1.Text = CStr(B1)
F2_3.TextAlpha1.Text = CStr(Alpha1)
F2_3.TextC2.Text = CStr(C2)
' step 10 -----
F2_3.TextBox1.Text = F2_2.TextC1.Text
F2_3.TextBox2.Text = F2_3.TextC2.Text
C1s = C1
C2s = C2

```

```

10:      If (C1s / C2s) > 1.00001 Then
          C1s = C1s - 0.1
          ' step 10-6-1 -----
          efe = 0.003 * ((df - C1s) / C1s) - ebi
          If efe > efd Then
              efe = efd
          End If
          ecs = (efe + ebi) * (C1s / (df - C1s))

          ' step 10-7-1 -----
          es = (efe + ebi) * ((d - C1s) / (df - C1s))

          ' step 10-8-1 -----

          fs = Esm * es
          If fs > fy Then
              fs = fy
          End If
          ffe = Ef * efe
          ' step 10-9-1 -----
          ecp = 1.7 * fc / Ec
          B1 = ((4 * ecp - ecs) / (6 * ecp - 2 * ecs))
          Alpha1 = (3 * ecp * ecs - ecs * ecs) / (3 * B1 * ecp *
ecp)

          C2s = (Ass * fs + Af * ffe) / (Alpha1 * fc * B1 * b)
          GoTo 10
      End If

20:      If (C1s / C2s) < 0.99999 Then
          C1s = C1s + 0.1
          ' step 10-6-2 -----
          efe = 0.003 * ((df - C1s) / C1s) - ebi
          If efe > efd Then
              efe = efd
          End If
          ecs = (efe + ebi) * (C1s / (df - C1s))

          ' step 10-7-2 -----
          es = (efe + ebi) * ((d - C1s) / (df - C1s))

          ' step 10-8-2 -----

          fs = Esm * es
          If fs > fy Then
              fs = fy
          End If
          ffe = Ef * efe
          ' step 10-9-2 -----
          ecp = 1.7 * fc / Ec
          B1 = ((4 * ecp - ecs) / (6 * ecp - 2 * ecs))
          Alpha1 = (3 * ecp * ecs - ecs * ecs) / (3 * B1 * ecp *
ecp)

          C2s = (Ass * fs + Af * ffe) / (Alpha1 * fc * B1 * b)
          GoTo 20

```

```

End If
C = C1s
F2_3.TextC.Text = CStr(C)
F2_3.Textes2.Text = CStr(es)
F2_3.Textfs2.Text = CStr(fs)
F2_3.TextB12.Text = CStr(B1)
F2_3.TextAlpha12.Text = CStr(Alpha1)
F2_3.Textffd2.Text = CStr(ffe)
' step 11 -----
Mns = Ass * fs * (d - ((B1 * C) / 2))
Mnf = Af * ffe * (df - ((B1 * C) / 2))
F2_3.TextMns.Text = CStr(Mns)
F2_3.TextMnf.Text = CStr(Mnf)
' step 12 -----

esy = fy / Esm
If es >= 0.005 Then
    PHI = CDec(F2_3.TextPHI.Text)
ElseIf es > esy And es < 0.005 Then
    PHI = 0.65 + (0.25 * (es - esy)) / (0.005 - esy)
ElseIf es <= esy Then
    PHI = 0.65
End If

PSI = CDec(F2_3.TextPSI.Text)
Mu = CDec(F2_3.TextMu.Text)
PHIMN = PHI * (Mns + PSI * Mnf)
F2_3.TextPHIMN.Text = CStr(PHIMN)
' step 13 -----

Ms = CDec(Me.TextMs.Text)
Rhos = Ass / (b * d)
Rhof = Af / (b * d)
Ks = ((Rhos * (Esm / Ec) + Rhof * (Ef / Ec)) ^ 2 + 2 *
(Rhos * (Esm / Ec) + Rhof * (Ef / Ec) * (df / d)) - (Rhos * (Esm / Ec)
+ Rhof * (Ef / Ec))) ^ 0.5
fss = ((Ms + ebi * Af * Ef * (df - (Ks * d / 3))) * (d -
Ks * d) * Esm) / (Ass * Esm * (d - (Ks * d / 3)) * (d - Ks * d) + Af *
Ef * (df - (Ks * d / 3)) * (df - (Ks * d)))
Me.TextRhos.Text = CStr(Rhos)
Me.TextRhof.Text = CStr(Rhof)
Me.TextKs.Text = CStr(Ks)
Me.Textfss.Text = CStr(fss)

' step 14 -----
ffs = fss * (Ef / Esm) * (df - Ks * d) / (d - Ks * d) -
ebi * Ef

Me.Textffs.Text = CStr(ffs)
' step check -----
If F2.RadioB3.Checked Then
    fch = 0.2 * ffu
ElseIf F2.RadioB2.Checked Then
    fch = 0.3 * ffu
Else

```

```

        fch = 0.55 * ffu
End If
chm = 0
chs = 0
chc = 0
If PHIMN >= Mu Then
    Me.TextChm.Text = " OK "
    Me.TextChm.ForeColor = Color.Green
    chm = 1
Else
    Me.TextChm.Text = " No check "
    Me.TextChm.ForeColor = Color.Red
    chm = 2
End If
If fss <= 0.8 * fy Then
    Me.TextChs.Text = " OK "
    Me.TextChs.ForeColor = Color.Green
    chs = 1
Else
    Me.TextChs.Text = " No check "
    Me.TextChs.ForeColor = Color.Red
    chs = 2
End If
If ffs <= fch Then
    Me.TextChc.Text = " OK "
    chc = 1
    Me.TextChc.ForeColor = Color.Green
Else
    Me.TextChc.Text = " No check "
    Me.TextChc.ForeColor = Color.Red
    chc = 2
End If
' Results check -----
Me.Textns.Text = CStr(n)
If chm = 1 And chs = 1 And chc = 1 Then
    Me.TextR.Text = " OK "
    Me.TextR.ForeColor = Color.Green
Else
    Me.TextR.Text = " No check "
    Me.TextR.ForeColor = Color.Red
End If

' enable -----

For Each Atx In Me.Panel2.Controls

    If TypeOf Atx Is TextBox Then

        Atx.Enabled = True

    End If
Next

For Each Atx In Me.Panel3.Controls

```



```

        If TypeOf Atx Is TextBox Then
            Atx.Enabled = True
        End If
    Next

    For Each Atx In Me.Panel4.Controls

        If TypeOf Atx Is TextBox Then
            Atx.Enabled = True
        End If
    Next

    For Each Atx In Me.Panel5.Controls

        If TypeOf Atx Is TextBox Then
            Atx.Enabled = True
        End If

        Textns.Enabled = False

    Next

    ' error -----
    Catch
        MessageBox.Show("Please enter valid values.", "Entry
error")
    End Try

End Sub

Private Sub B4_Click(ByVal sender As System.Object, ByVal e As
System.EventArgs) Handles B4.Click
    Dim n As Decimal
    Try
        n = CDec(Me.Textns.Text)
        n = n + 1
        Me.Textns.Text = CStr(n)
        F2.Textn.Text = CStr(n)
    Catch
        MessageBox.Show("Please check your entries.", "Entry
error")
    End Try

End Sub

```

```

    Private Sub btnClear_Click(ByVal sender As System.Object, ByVal e
As System.EventArgs) Handles btnClear.Click
        Dim Atx As Control
        Dim B As DialogResult = MessageBox.Show("This option will
clear all data!", "Please Notice:", MessageBoxButtons.OKCancel)
        If B = DialogResult.OK Then

            For Each Atx In Me.Panel2.Controls

                If TypeOf Atx Is TextBox Then

                    Atx.Text = Nothing

                End If
            Next

            For Each Atx In Me.Panel3.Controls

                If TypeOf Atx Is TextBox Then

                    Atx.Text = Nothing

                End If
            Next

            For Each Atx In Me.Panel4.Controls

                If TypeOf Atx Is TextBox Then

                    Atx.Text = Nothing

                End If
            Next

            For Each Atx In Me.Panel5.Controls

                If TypeOf Atx Is TextBox Then

                    Atx.Text = Nothing

                End If
            Next
        Next
    End If
End Sub

Private Sub Textns_TextChanged(ByVal sender As System.Object,
ByVal e As System.EventArgs) Handles Textns.TextChanged

End Sub

Private Sub Label20_Click(ByVal sender As System.Object, ByVal e
As System.EventArgs) Handles Label20.Click

```

```

    End Sub

    Private Sub Panell_Paint(ByVal sender As System.Object, ByVal e As
System.Windows.Fs.PaintEventArgs) Handles Panell.Paint

        End Sub
    End Class

```

---

```

Public Class F1

    Private Sub B1_Click(ByVal sender As System.Object, ByVal e As
System.EventArgs)
        F2.Show()
        Me.Hide()
    End Sub

    Private Sub B2_Click(ByVal sender As System.Object, ByVal e As
System.EventArgs)
        F3.Show()
        Me.Hide()
    End Sub

    Private Sub F1_Load(ByVal sender As System.Object, ByVal e As
System.EventArgs) Handles MyBase.Load
        Me.CenterToScreen()
    End Sub

    Private Sub B3_Click(ByVal sender As System.Object, ByVal e As
System.EventArgs)
        Me.Close()
    End Sub

    Private Sub ExitToolStripMenuItem_Click(ByVal sender As
System.Object, ByVal e As System.EventArgs) Handles
ExitToolStripMenuItem.Click
        Me.Close()
    End Sub

    Private Sub AboutToolStripMenuItem_Click(ByVal sender As
System.Object, ByVal e As System.EventArgs) Handles
AboutToolStripMenuItem.Click
        AboutBox1.Show()
    End Sub

    Private Sub GroupBox1_Enter(ByVal sender As System.Object, ByVal e
As System.EventArgs)

        End Sub

    Private Sub HelpToolStripMenuItem_Click(ByVal sender As
System.Object, ByVal e As System.EventArgs) Handles
HelpToolStripMenuItem.Click

        End Sub

```

```

        Private Sub B3_Click_1(ByVal sender As System.Object, ByVal e As
System.EventArgs)
            F4.Show()
            Me.Hide()
        End Sub

        Private Sub
EstimateFlexuralStrengthForFRPReinforcedBeamsToolStripMenuItem_Click(By
Val sender As System.Object, ByVal e As System.EventArgs) Handles
EstimateFlexuralStrengthForFRPReinforcedBeamsToolStripMenuItem.Click
            F2.MdiParent = Me
            F2.Show()
            F2.WindowState = FWindowState.Maximized
        End Sub

        Private Sub
EstimateRequiredAnchorageLengthToolStripMenuItem_Click(ByVal sender As
System.Object, ByVal e As System.EventArgs) Handles
EstimateRequiredAnchorageLengthToolStripMenuItem.Click
            F4.MdiParent = Me
            F4.Show()
            F4.WindowState = FWindowState.Maximized
        End Sub

        Private Sub
EstimateFlexuralStrengthOfFRPReinforcedBeamsToolStripMenuItem_Click(ByV
al sender As System.Object, ByVal e As System.EventArgs) Handles
EstimateFlexuralStrengthOfFRPReinforcedBeamsToolStripMenuItem.Click
            F3.MdiParent = Me
            F3.Show()
            F3.WindowState = FWindowState.Maximized
        End Sub

        Private Sub FRPEstimatorToolStripMenuItem_Click(ByVal sender As
System.Object, ByVal e As System.EventArgs) Handles
FRPEstimatorToolStripMenuItem.Click

        End Sub
        Private Sub ToolStripMenuItem2_Click(ByVal sender As Object, ByVal
e As EventArgs) Handles ToolStripMenuItem2.Click
            Me.LayoutMdi (MdiLayout.Cascade)
        End Sub

        Private Sub ToolStripMenuItem3_Click(ByVal sender As Object, ByVal
e As EventArgs) Handles ToolStripMenuItem3.Click
            Me.LayoutMdi (MdiLayout.TileVertical)
        End Sub

        Private Sub ToolStripMenuItem4_Click(ByVal sender As Object, ByVal
e As EventArgs) Handles ToolStripMenuItem4.Click
            Me.LayoutMdi (MdiLayout.TileHorizontal)
        End Sub

```

```

    Private Sub ToolStripMenuItem5_Click(ByVal sender As Object, ByVal
e As EventArgs) Handles ToolStripMenuItem5.Click
        For Each ChildF As F In Me.MdiChildren
            ChildF.Close()
        Next
    End Sub

```

```

    Private Sub DocumentationToolStripMenuItem_Click(ByVal sender As
System.Object, ByVal e As System.EventArgs) Handles
DocumentationToolStripMenuItem.Click
        DimRetVal
        RetVal = Shell("hh.exe " & "C:\Practical Engineering
Software\FRP Strength Estimator\Documentation.chm", vbNormalFocus)

    End Sub
End Class

```

---

```

Public Class F2

```

```

    Private Sub B1_Click(ByVal sender As System.Object, ByVal e As
System.EventArgs) Handles B1.Click
        ' enable -----
        Dim Atx As Control
        For Each Atx In Me.Panel2.Controls

            If TypeOf Atx Is TextBox Then

                Atx.Enabled = True

            End If
        Next

        For Each Atx In Me.Panel3.Controls

            If TypeOf Atx Is TextBox Then

                Atx.Enabled = True

            End If
        Next

        For Each Atx In Me.Panel4.Controls

            If TypeOf Atx Is TextBox Then

                Atx.Enabled = True
            End If
        Next

        For Each Atx In Me.Panel5.Controls

            If TypeOf Atx Is TextBox Then

                Atx.Enabled = True
            End If
        Next
    End Sub

```

```

        End If

    Next
    F2_2.MdiParent = F1
    F2_2.Show()
    F2_2.WindowState = FWindowState.Maximized
    Me.WindowState = FWindowState.Minimized
End Sub

Private Sub B2_Click(ByVal sender As System.Object, ByVal e As
System.EventArgs) Handles B2.Click
    Dim B As DialogResult = MessageBox.Show("You will be
transferred to the homepage!", "Please Notice:", MessageBoxButtons.OKCancel)
    If B = DialogResult.OK Then
        F1.Show()
        Me.Hide()
        F2_2.Hide()
        F2_3.Hide()
        F2_4.Hide()
    End If
End Sub

Private Sub F2_Load(ByVal sender As System.Object, ByVal e As
System.EventArgs) Handles MyBase.Load
    Me.CenterToScreen()
End Sub

Private Sub btnClear_Click(ByVal sender As System.Object, ByVal e
As System.EventArgs) Handles btnClear.Click
    Dim Atx As Control
    Dim B As DialogResult = MessageBox.Show("This option will
clear all data!", "Please Notice:", MessageBoxButtons.OKCancel)
    If B = DialogResult.OK Then

        For Each Atx In Me.Panel2.Controls

            If TypeOf Atx Is TextBox Then

                Atx.Text = Nothing

            End If
        Next

        For Each Atx In Me.Panel3.Controls

            If TypeOf Atx Is TextBox Then

                Atx.Text = Nothing

            End If
        Next
    End If
Next

```

```

        For Each Atx In Me.Panel4.Controls
            If TypeOf Atx Is TextBox Then
                Atx.Text = Nothing
            End If
        Next

        For Each Atx In Me.Panel5.Controls
            If TypeOf Atx Is TextBox Then
                Atx.Text = Nothing
            End If
        Next
    End If
End Sub

Private Sub TextEsm_TextChanged(ByVal sender As System.Object,
ByVal e As System.EventArgs) Handles TextEsm.TextChanged

    End Sub

Private Sub Label25_Click(ByVal sender As System.Object, ByVal e As
As System.EventArgs) Handles Label25.Click

    End Sub

Private Sub B3_Click(ByVal sender As System.Object, ByVal e As
System.EventArgs) Handles B3.Click
    F2_1.Show()
    Me.Enabled = False
End Sub
End Class

```

---

```

Public Class F2_1

    Private Sub F2_1_Load(ByVal sender As System.Object, ByVal e As
System.EventArgs) Handles MyBase.Load

        End Sub

        Private Sub PictureBox1_Click(ByVal sender As System.Object, ByVal
e As System.EventArgs) Handles PictureBox1.Click

            End Sub

            Private Sub B1_Click(ByVal sender As System.Object, ByVal e As
System.EventArgs) Handles B1.Click
                Dim CE As Decimal
                If Me.RadioB1.Checked Then
                    CE = 0.95
                End If
            End Sub
        End Sub
    End Class

```

```

ElseIf Me.RadioB2.Checked Then
    CE = 0.75
ElseIf Me.RadioB3.Checked Then
    CE = 0.85
ElseIf Me.RadioB4.Checked Then
    CE = 0.85
ElseIf Me.RadioB5.Checked Then
    CE = 0.65
ElseIf Me.RadioB6.Checked Then
    CE = 0.75
ElseIf Me.RadioB7.Checked Then
    CE = 0.85
ElseIf Me.RadioB8.Checked Then
    CE = 0.5
ElseIf Me.RadioB9.Checked Then
    CE = 0.7
End If
F2.TextCE.Text = CStr(CE)
Me.Hide()
F2.Enabled = True
End Sub

Private Sub B2_Click(ByVal sender As System.Object, ByVal e As
System.EventArgs) Handles B2.Click
    Me.Hide()
    F2.Enabled = True
End Sub
End Class

```

---

```

Public Class F2_2

Private Sub B1_Click(ByVal sender As System.Object, ByVal e As
System.EventArgs) Handles B1.Click
    Dim Atx As Control
    For Each Atx In Me.Panel2.Controls

        If TypeOf Atx Is TextBox Then

            Atx.Enabled = True

        End If
    Next

    For Each Atx In Me.Panel3.Controls

        If TypeOf Atx Is TextBox Then

            Atx.Enabled = True

        End If
    Next

    For Each Atx In Me.Panel4.Controls

```



```

        If TypeOf Atx Is TextBox Then
            Atx.Enabled = True
        End If
    Next

    For Each Atx In Me.Panel5.Controls

        If TypeOf Atx Is TextBox Then

            Atx.Enabled = True

        End If

    Next
    F2_3.MdiParent = F1
    F2_3.Show()
    F2_3.WindowState = FWindowState.Maximized
    Me.WindowState = FWindowState.Minimized

End Sub

Private Sub B2_Click(ByVal sender As System.Object, ByVal e As
System.EventArgs) Handles B2.Click
    F2.Show()
    F2.WindowState = FWindowState.Maximized
    Me.WindowState = FWindowState.Minimized
End Sub

Private Sub F2_2_Load(ByVal sender As System.Object, ByVal e As
System.EventArgs) Handles MyBase.Load
    Me.CenterToScreen()
End Sub

Private Sub C1_TextChanged(ByVal sender As System.Object, ByVal e
As System.EventArgs) Handles TextC1.TextChanged

End Sub

Private Sub btnClear_Click(ByVal sender As System.Object, ByVal e
As System.EventArgs) Handles btnClear.Click
    Dim Atx As Control
    Dim B As DialogResult = MessageBox.Show("This option will
clear all data!", "Please Notice:", MessageBoxButtons.OKCancel)
    If B = DialogResult.OK Then

        For Each Atx In Me.Panel2.Controls

            If TypeOf Atx Is TextBox Then

                Atx.Text = Nothing

            End If

        Next
    End If
End Sub

```

```

        For Each Atx In Me.Panel3.Controls
            If TypeOf Atx Is TextBox Then
                Atx.Text = Nothing
            End If
        Next

        For Each Atx In Me.Panel4.Controls
            If TypeOf Atx Is TextBox Then
                Atx.Text = Nothing
            End If
        Next

        For Each Atx In Me.Panel5.Controls
            If TypeOf Atx Is TextBox Then
                Atx.Text = Nothing
            End If
        Next
    End If
End Sub

Private Sub Textfy_TextChanged(ByVal sender As System.Object,
ByVal e As System.EventArgs) Handles Textfy.TextChanged

    End Sub
End Class

```

---

```

Public Class F2_3

    Private Sub Label33_Click(ByVal sender As System.Object, ByVal e
As System.EventArgs) Handles Label33.Click

        End Sub

        Private Sub B1_Click(ByVal sender As System.Object, ByVal e As
System.EventArgs) Handles B1.Click
            Dim Atx As Control
            For Each Atx In Me.Panel2.Controls

                If TypeOf Atx Is TextBox Then

                    Atx.Enabled = True

                End If
            End For
        End Sub
    End Class

```

```

Next
For Each Atx In Me.Panel3.Controls
    If TypeOf Atx Is TextBox Then
        Atx.Enabled = True
    End If
Next
For Each Atx In Me.GroupBox1.Controls
    If TypeOf Atx Is TextBox Then
        Atx.Enabled = True
    End If
Next
For Each Atx In Me.Panel4.Controls
    If TypeOf Atx Is TextBox Then
        Atx.Enabled = True
    End If
Next
For Each Atx In Me.Panel5.Controls
    If TypeOf Atx Is TextBox Then
        Atx.Enabled = True
    End If
Next
F2_4.MdiParent = F1
F2_4.Show()
F2_4.WindowState = FWindowState.Maximized
Me.WindowState = FWindowState.Minimized

End Sub

Private Sub Panel3_Paint(ByVal sender As System.Object, ByVal e As
System.Windows.Fs.PaintEventArgs) Handles Panel3.Paint

End Sub

Private Sub B2_Click(ByVal sender As System.Object, ByVal e As
System.EventArgs) Handles B2.Click
    F2_2.Show()
    F2_2.WindowState = FWindowState.Maximized
    Me.WindowState = FWindowState.Minimized
End Sub

```

```

        Private Sub F2_3_Load(ByVal sender As System.Object, ByVal e As
System.EventArgs) Handles MyBase.Load
            Me.CenterToScreen()
        End Sub

        Private Sub Label13_Click(ByVal sender As System.Object, ByVal e
As System.EventArgs) Handles Label13.Click

        End Sub

        Private Sub Textes2_TextChanged(ByVal sender As System.Object,
ByVal e As System.EventArgs) Handles Textes2.TextChanged

        End Sub

        Private Sub TextBox41_TextChanged(ByVal sender As System.Object,
ByVal e As System.EventArgs) Handles TextPHI.TextChanged

        End Sub

        Private Sub btnClear_Click(ByVal sender As System.Object, ByVal e
As System.EventArgs) Handles btnClear.Click
            Dim Atx As Control
            Dim B As DialogResult = MessageBox.Show("This option will
clear all data!", "Please Notice:", MessageBoxButtons.OKCancel)
            If B = DialogResult.OK Then

                For Each Atx In Me.Panel2.Controls

                    If TypeOf Atx Is TextBox Then

                        Atx.Text = Nothing

                    End If
                Next

                For Each Atx In Me.Panel3.Controls

                    If TypeOf Atx Is TextBox Then

                        Atx.Text = Nothing

                    End If
                Next

                For Each Atx In Me.GroupBox1.Controls
                    If TypeOf Atx Is TextBox Then

                        Atx.Text = Nothing

                    End If
                Next

                For Each Atx In Me.Panel4.Controls

```

```

        If TypeOf Atx Is TextBox Then
            Atx.Text = Nothing
        End If
    Next

    For Each Atx In Me.Panel5.Controls

        If TypeOf Atx Is TextBox Then

            Atx.Text = Nothing

        End If

    Next
End If
End Sub
End Class

```

---

```

Public Class F3

    Private Sub B1_Click(ByVal sender As System.Object, ByVal e As
System.EventArgs) Handles B1.Click
        ' enable -----
        Dim Atx As Control
        For Each Atx In Me.Panel2.Controls

            If TypeOf Atx Is TextBox Then

                Atx.Enabled = True

            End If

        Next

        For Each Atx In Me.Panel3.Controls

            If TypeOf Atx Is TextBox Then

                Atx.Enabled = True

            End If

        Next

        For Each Atx In Me.Panel4.Controls

            If TypeOf Atx Is TextBox Then

                Atx.Enabled = True

            End If

        Next

        For Each Atx In Me.Panel5.Controls

```

```

        If TypeOf Atx Is TextBox Then

            Atx.Enabled = True

        End If

    Next
    F3_2.MdiParent = F1
    F3_2.Show()
    F3_2.WindowState = FWindowState.Maximized
    Me.WindowState = FWindowState.Minimized
End Sub

Private Sub B2_Click(ByVal sender As System.Object, ByVal e As
System.EventArgs) Handles B2.Click
    Dim B As DialogResult = MessageBox.Show("You will be
transferred to the homepage!", "Please Notice:", MessageBoxButtons.OKCancel)
    If B = DialogResult.OK Then
        F1.Show()
        Me.Hide()
        F3_2.Hide()
        F3_3.Hide()
        F3_4.Hide()
    End If
End Sub

Private Sub btnClear_Click(ByVal sender As System.Object, ByVal e
As System.EventArgs) Handles btnClear.Click
    Dim Atx As Control
    Dim B As DialogResult = MessageBox.Show("This option will
clear all data!", "Please Notice:", MessageBoxButtons.OKCancel)
    If B = DialogResult.OK Then

        For Each Atx In Me.Panel2.Controls

            If TypeOf Atx Is TextBox Then

                Atx.Text = Nothing

            End If
        Next

        For Each Atx In Me.Panel3.Controls

            If TypeOf Atx Is TextBox Then

                Atx.Text = Nothing

            End If
        Next

        For Each Atx In Me.Panel4.Controls

```

```

        If TypeOf Atx Is TextBox Then
            Atx.Text = Nothing
        End If
    Next

    For Each Atx In Me.Panel5.Controls

        If TypeOf Atx Is TextBox Then

            Atx.Text = Nothing

        End If

    Next
End If
End Sub

Private Sub B3_Click(ByVal sender As System.Object, ByVal e As
System.EventArgs) Handles B3.Click
    F3_1.Show()
    Me.Enabled = False
End Sub

Private Sub B4_Click(ByVal sender As System.Object, ByVal e As
System.EventArgs) Handles B4.Click
    F3_0.Show()
    Me.Enabled = False
End Sub
End Class

```

---

```

Public Class F3_0

    Private Sub Label2_Click(ByVal sender As System.Object, ByVal e As
System.EventArgs) Handles Label2.Click

        End Sub

    Private Sub Label25_Click(ByVal sender As System.Object, ByVal e
As System.EventArgs) Handles Label25.Click

        End Sub

    Private Sub B1_Click(ByVal sender As System.Object, ByVal e As
System.EventArgs) Handles B1.Click
        Dim Nw, Na, Da, Ad, Afd, Rf, tfd
        Try
            Na = CDec(Me.TextNa.Text)
            Da = CDec(Me.TextDa.Text)
            Nw = CDec(Me.TextNw.Text)
            Ad = CDec(Me.TextAd.Text)
            Afd = CDec(Me.TextAfd.Text)

```

```

tfd = CDec(Me.Texttfd.Text)
Rf = CDec(Me.TextRf.Text)

If Da <= 0 And Na > 1 Then
    MessageBox.Show("Please enter valid values for Na and
Da! Na value will be set to 1.", "Entry error")
    Me.TextNa.Text = CStr(1)
    RadioB1.Checked = True
ElseIf Da > 200 Then
    MessageBox.Show("Anchors placed more than 200 mm of
each other are ineffective in achieving more strength. A single anchor
along debonding path will be assumed.", "Please note:")
    Me.TextNa.Text = CStr(1)
    RadioB1.Checked = True
ElseIf Da < 0 Then
    MessageBox.Show("Please enter valid value for Da ",
"Entry error")
ElseIf Na <= 0 Then
    MessageBox.Show("Please enter valid value for Na ",
"Entry error")
ElseIf (Na - Int(Na)) <> 0 Then
    MessageBox.Show("Please enter valid value for Na ",
"Entry error")
ElseIf Nw <= 0 Then
    MessageBox.Show("Please enter valid value for Nw ",
"Entry error")
ElseIf (Nw - Int(Nw)) <> 0 Then
    MessageBox.Show("Please enter valid value for Nw ",
"Entry error")
ElseIf Ad <= 0 Then
    MessageBox.Show("Please enter valid value for Ad ",
"Entry error")
ElseIf Afd <= 0 Then
    MessageBox.Show("Please enter valid value for Afd ",
"Entry error")
ElseIf tfd <= 0 Then
    MessageBox.Show("Please enter valid value for tfd ",
"Entry error")
ElseIf Rf <= 0 Or Rf > 1 Then
    MessageBox.Show("Please enter valid value for Rf ",
"Entry error")
Else
    Me.Hide()
    F3.Enabled = True
End If
Catch
    MessageBox.Show("Please enter valid values.", "Entry
error")
End Try

End Sub

Private Sub RadioB1_CheckedChanged(ByVal sender As System.Object,
ByVal e As System.EventArgs) Handles RadioB1.CheckedChanged

```



```

TextNw.Enabled = True
TextNa.Enabled = False
TextNa.Text = " 1 "
TextDa.Enabled = False
TextDa.Text = " 0 "
TextAd.Enabled = True
TextAfd.Enabled = True
Textttfd.Enabled = True
TextRf.Enabled = True
End Sub

Private Sub Textdf_TextChanged(ByVal sender As System.Object,
ByVal e As System.EventArgs) Handles TextDa.TextChanged

End Sub

Private Sub RadioB2_CheckedChanged(ByVal sender As System.Object,
ByVal e As System.EventArgs) Handles RadioB2.CheckedChanged
TextNw.Enabled = True
TextNa.Enabled = True
TextNa.Text = ""
TextDa.Enabled = True
TextDa.Text = ""
TextAd.Enabled = True
TextAfd.Enabled = True
Textttfd.Enabled = True
TextRf.Enabled = True
End Sub

Private Sub B2_Click(ByVal sender As System.Object, ByVal e As
System.EventArgs) Handles B2.Click

Dim B As DialogResult = MessageBox.Show("Anchorage system
properties will be deleted!", "Entry Cancelation", MessageBoxButtons.YesNo)
If B = DialogResult.Yes Then

Me.RadioB1.Checked = False
Me.RadioB2.Checked = False
Me.TextNw.Text = ""
Me.TextNa.Text = ""
Me.TextDa.Text = ""
Me.TextAd.Text = ""
Me.TextAfd.Text = ""
Me.Textttfd.Text = ""
Me.TextRf.Text = ""
Me.TextNw.Enabled = False
Me.TextNa.Enabled = False
Me.TextDa.Enabled = False
Me.TextAd.Enabled = False
Me.TextAfd.Enabled = False
Me.Textttfd.Enabled = False
Me.TextRf.Enabled = False
Me.Hide()
F3.Enabled = True

```

```

        End If

    End Sub

End Class

```

---

```

Public Class F3_1

    Private Sub F3_1_Load(ByVal sender As System.Object, ByVal e As
System.EventArgs) Handles MyBase.Load

        End Sub

        Private Sub PictureBox1_Click(ByVal sender As System.Object, ByVal
e As System.EventArgs) Handles PictureBox1.Click

            End Sub

            Private Sub B1_Click(ByVal sender As System.Object, ByVal e As
System.EventArgs) Handles B1.Click
                Dim CE As Decimal
                If Me.RadioButton1.Checked Then
                    CE = 0.95
                ElseIf Me.RadioButton2.Checked Then
                    CE = 0.75
                ElseIf Me.RadioButton3.Checked Then
                    CE = 0.85
                ElseIf Me.RadioButton4.Checked Then
                    CE = 0.85
                ElseIf Me.RadioButton5.Checked Then
                    CE = 0.65
                ElseIf Me.RadioButton6.Checked Then
                    CE = 0.75
                ElseIf Me.RadioButton7.Checked Then
                    CE = 0.85
                ElseIf Me.RadioButton8.Checked Then
                    CE = 0.5
                ElseIf Me.RadioButton9.Checked Then
                    CE = 0.7
                End If
                F3.TextCE.Text = CStr(CE)
                Me.Hide()
                F3.Enabled = True
            End Sub

            Private Sub B2_Click(ByVal sender As System.Object, ByVal e As
System.EventArgs) Handles B2.Click
                Me.Hide()
                F3.Enabled = True
            End Sub
        End Class

```

---

```

Public Class F3_2

    Private Sub Label6_Click(ByVal sender As System.Object, ByVal e As
System.EventArgs) Handles Label6.Click

```

```

End Sub

Private Sub TextBox20_TextChanged(ByVal sender As System.Object,
ByVal e As System.EventArgs) Handles Textes.TextChanged

End Sub

Private Sub Label20_Click(ByVal sender As System.Object, ByVal e As
As System.EventArgs) Handles Label20.Click

End Sub

Private Sub B1_Click(ByVal sender As System.Object, ByVal e As
System.EventArgs) Handles B1.Click
    Dim Atx As Control
    For Each Atx In Me.Panel2.Controls

        If TypeOf Atx Is TextBox Then

            Atx.Enabled = True

        End If
    Next

    For Each Atx In Me.Panel3.Controls

        If TypeOf Atx Is TextBox Then

            Atx.Enabled = True

        End If
    Next

    For Each Atx In Me.Panel4.Controls

        If TypeOf Atx Is TextBox Then

            Atx.Enabled = True
        End If
    Next

    For Each Atx In Me.Panel5.Controls

        If TypeOf Atx Is TextBox Then

            Atx.Enabled = True

        End If

    Next
    F3_3.MdiParent = F1
    F3_3.Show()
    F3_3.WindowState = FWindowState.Maximized

```

```

        Me.WindowState = FWindowState.Minimized
    End Sub

    Private Sub B2_Click(ByVal sender As System.Object, ByVal e As
System.EventArgs) Handles B2.Click
        F3.Show()
        F3.WindowState = FWindowState.Maximized
        Me.WindowState = FWindowState.Minimized
    End Sub

    Private Sub F3_2_Load(ByVal sender As System.Object, ByVal e As
System.EventArgs) Handles MyBase.Load
        Me.CenterToScreen()
    End Sub

    Private Sub C1_TextChanged(ByVal sender As System.Object, ByVal e
As System.EventArgs) Handles TextC1.TextChanged

    End Sub

    Private Sub btnClear_Click(ByVal sender As System.Object, ByVal e
As System.EventArgs) Handles btnClear.Click
        Dim Atx As Control
        Dim B As DialogResult = MessageBox.Show("This option will
clear all data!", "Please Notice:", MessageBoxButtons.OKCancel)
        If B = DialogResult.OK Then
            For Each Atx In Me.Panel2.Controls

                If TypeOf Atx Is TextBox Then

                    Atx.Text = Nothing

                End If
            Next

            For Each Atx In Me.Panel3.Controls

                If TypeOf Atx Is TextBox Then

                    Atx.Text = Nothing

                End If
            Next

            For Each Atx In Me.Panel4.Controls

                If TypeOf Atx Is TextBox Then

                    Atx.Text = Nothing

                End If
            Next

            For Each Atx In Me.Panel5.Controls

```

```

        If TypeOf Atx Is TextBox Then
            Atx.Text = Nothing
        End If
    Next
End If

End Sub

Private Sub Textfy_TextChanged(ByVal sender As System.Object,
ByVal e As System.EventArgs) Handles Textfy.TextChanged

    End Sub
End Class

```

---

```

Public Class F3_3

    Private Sub Label33_Click(ByVal sender As System.Object, ByVal e
As System.EventArgs) Handles Label33.Click

        End Sub

    Private Sub B1_Click(ByVal sender As System.Object, ByVal e As
System.EventArgs) Handles B1.Click
        Dim Atx As Control
        For Each Atx In Me.Panel2.Controls

            If TypeOf Atx Is TextBox Then

                Atx.Enabled = True

            End If
        Next

        For Each Atx In Me.Panel3.Controls

            If TypeOf Atx Is TextBox Then

                Atx.Enabled = True

            End If
        Next
        For Each Atx In Me.GroupBox1.Controls
            If TypeOf Atx Is TextBox Then

                Atx.Enabled = True

            End If
        Next

        For Each Atx In Me.Panel4.Controls

```

```

        If TypeOf Atx Is TextBox Then
            Atx.Enabled = True
        End If
    Next

    For Each Atx In Me.Panel5.Controls

        If TypeOf Atx Is TextBox Then

            Atx.Enabled = True

        End If

    Next
    F3_4.MdiParent = F1
    F3_4.Show()
    F3_4.WindowState = FWindowState.Maximized
    Me.WindowState = FWindowState.Minimized
End Sub

Private Sub Panel3_Paint(ByVal sender As System.Object, ByVal e As
System.Windows.Forms.PaintEventArgs) Handles Panel3.Paint

End Sub

Private Sub B2_Click(ByVal sender As System.Object, ByVal e As
System.EventArgs) Handles B2.Click

    F3_2.Show()
    F3_2.WindowState = FWindowState.Maximized
    Me.WindowState = FWindowState.Minimized
End Sub

Private Sub F3_3_Load(ByVal sender As System.Object, ByVal e As
System.EventArgs) Handles MyBase.Load
    Me.CenterToScreen()
End Sub

Private Sub Label13_Click(ByVal sender As System.Object, ByVal e
As System.EventArgs) Handles Label13.Click

End Sub

Private Sub Textes2_TextChanged(ByVal sender As System.Object,
ByVal e As System.EventArgs) Handles Textes2.TextChanged

End Sub

Private Sub TextBox41_TextChanged(ByVal sender As System.Object,
ByVal e As System.EventArgs) Handles TextPHI.TextChanged

End Sub

```

```

    Private Sub btnClear_Click(ByVal sender As System.Object, ByVal e
As System.EventArgs) Handles btnClear.Click
        Dim Atx As Control
        Dim B As DialogResult = MessageBox.Show("This option will
clear all data!", "Please Notice:", MessageBoxButtons.OKCancel)
        If B = DialogResult.OK Then

            For Each Atx In Me.Panel2.Controls

                If TypeOf Atx Is TextBox Then

                    Atx.Text = Nothing

                End If
            Next

            For Each Atx In Me.Panel3.Controls

                If TypeOf Atx Is TextBox Then

                    Atx.Text = Nothing

                End If
            Next

            For Each Atx In Me.GroupBox1.Controls
                If TypeOf Atx Is TextBox Then

                    Atx.Text = Nothing

                End If
            Next

            For Each Atx In Me.Panel4.Controls

                If TypeOf Atx Is TextBox Then

                    Atx.Text = Nothing

                End If
            Next

            For Each Atx In Me.Panel5.Controls

                If TypeOf Atx Is TextBox Then

                    Atx.Text = Nothing

                End If
            Next

        End If
    End Sub
End Class

```

---

```
Public Class F3_4
```

```

    Private Sub Label10_Click(ByVal sender As System.Object, ByVal e
As System.EventArgs) Handles Label10.Click

        End Sub

    Private Sub Panel3_Paint(ByVal sender As System.Object, ByVal e As
System.Windows.Forms.PaintEventArgs) Handles Panel3.Paint

        End Sub

    Private Sub Mcheck_TextChanged(ByVal sender As System.Object,
ByVal e As System.EventArgs) Handles TextChm.TextChanged

        End Sub

    Private Sub B2_Click(ByVal sender As System.Object, ByVal e As
System.EventArgs) Handles B2.Click
        F3_3.Show()
        F3_3.WindowState = FWindowState.Maximized
        Me.WindowState = FWindowState.Minimized

        End Sub

    Private Sub F3_4_Load(ByVal sender As System.Object, ByVal e As
System.EventArgs) Handles MyBase.Load
        Me.CenterToScreen()
        End Sub

    Private Sub B3_Click(ByVal sender As System.Object, ByVal e As
System.EventArgs) Handles B3.Click
        Dim B As DialogResult = MessageBox.Show("You will be
transferred to the homepage!", "Please Notice:", MessageBoxButtons.OKCancel)
        If B = DialogResult.OK Then
            F1.Show()
            Me.Hide()
            F3.Hide()
            F3_2.Hide()
            F3_3.Hide()
        End If
        End Sub

    Private Sub B5_Click(ByVal sender As System.Object, ByVal e As
System.EventArgs) Handles B5.Click
        Dim n As Decimal
        Try
            n = CDec(Me.Textns.Text)
            n = n - 1
            If n <= 0 Then
                n = 1
                MessageBox.Show("Number of FRP layers should not be
zero.", "Warning")
            End If
        End If
    End Sub

```



```

        Me.Textns.Text = CStr(n)
        F3.Textn.Text = CStr(n)
    Catch
        MessageBox.Show("Please check your entries.", "Entry
error")
    End Try
End Sub

Public Sub B1_Click(ByVal sender As System.Object, ByVal e As
System.EventArgs) Handles B1.Click
    Dim CE, ffus, efus, ffu, efu, fc, Ass, n, tf, wf, Bls, Af, Ec
As Decimal
    Dim MDL, df, d, Icr, k, ebi, Ef, efds, nefu, efd, Cl, efe,
ecs, es As Decimal
    Dim Esm, fy, fs, ffe, b, ecp, B1, Alpha1, C2, Mns, Mnf As
Decimal
    Dim C1s, C2s, C, PHI, PSI, Mu, PHIMN, Rhos, Rhof, Ks, fss, Ms,
ffs, ne, j, esy, fch As Decimal
    Dim chm, chs, chc As Integer
    Dim Atx As Control
    Dim Nw, Na As Integer
    Dim Da, Ad, Afd, Asd, tfd, Rf, Kea

    Try

        ' step 1 -----
        CE = CDec(F3.TextCE.Text)
        ffus = CDec(F3.Textffus.Text)
        efus = CDec(F3.Textefus.Text)
        ffu = CE * ffus
        efu = CE * efus
        F3.Textffu.Text = CStr(ffu)
        F3.Textefu.Text = CStr(efu)
        ' step 2 -----
        fc = CDec(F3.Textfc.Text)
        Ass = CDec(F3.TextAs.Text)
        n = CDec(F3.Textn.Text)
        tf = CDec(F3.Texttf.Text)
        wf = CDec(F3.Textwf.Text)
        Bls = 1.05 - 0.05 * (fc / 6.9)
        Af = n * tf * wf
        Ec = 4700 * (fc) ^ 0.5
        F3.TextBls.Text = CStr(Bls)
        F3.TextAf.Text = CStr(Af)
        F3.TextEc.Text = CStr(Ec)
        ' step 3 -----
        b = CDec(F3.Textb.Text)
        Esm = CDec(F3.TextEsm.Text)
        ne = Esm / Ec
        MDL = CDec(F3.TextMDL.Text)
        df = CDec(F3.Textdf.Text)
        d = CDec(F3.Textd.Text)
        Rhos = Ass / (b * d)
        k = ((Rhos * ne) ^ 2 + 2 * Rhos * ne) ^ 0.5 - Rhos * ne

```

```

F3.Textk.Text = CStr(k)
j = 1 - (k / 3)
Icr = b * (k ^ 2) * j * (d ^ 3) / 2
F3.TextIcr.Text = CStr(Icr)
ebi = MDL * (df - k * d) / (Icr * Ec)
F3.Textebi.Text = CStr(ebi)
' step 4 -----
Ef = CDec(F3.TextEf.Text)
Nw = CInt(F3_0.TextNw.Text)
Na = CInt(F3_0.TextNa.Text)
Da = CDec(F3_0.TextDa.Text)
Ad = CDec(F3_0.TextAd.Text)
Afd = CDec(F3_0.TextAfd.Text)
tfd = CDec(F3_0.Texttfd.Text)
Rf = CDec(F3_0.TextRf.Text)
Asd = Afd / (wf / Nw)

If Da = 0 Then
    Kea = Rf * 0.75 * ((0.007 * Na ^ 3 - 0.13 * Na ^ 2 +
0.74 * Na + 1) ^ 1.6) * ((0.72 * (n * tfd) ^ (-0.2)) ^ (-1)) * (0.52 *
Ad ^ 0.24) * ((0.5 * Asd + 0.52) ^ 0.1)
Else
    Kea = Rf * ((0.007 * Na ^ 3 - 0.13 * Na ^ 2 + 0.74 *
Na + 1) ^ 1.6) * ((0.72 * (n * tfd) ^ (-0.2)) ^ (-1)) * ((1.7 * Da ^ -
0.15) ^ 2.35) * (0.52 * Ad ^ 0.24) * ((0.5 * Asd + 0.52) ^ 0.1)
End If

efds = Kea * 0.41 * (fc / (n * Ef * tf)) ^ 0.5
nefu = 0.9 * efu
If efds > nefu Then
    efd = nefu
Else
    efd = efds
End If
F3.Textefds.Text = CStr(efds)
F3.Textnefu.Text = CStr(nefu)
F3.Textefd.Text = CStr(efd)
F3.TextKea.Text = CStr(Kea)
' step 5 -----
C1 = 0.2 * d
F3_2.TextC1.Text = CStr(C1)
' step 6 -----
efe = 0.003 * ((df - C1) / C1) - ebi
If efe > efd Then
    efe = efd
End If
ecs = (efe + ebi) * (C1 / (df - C1))
F3_2.Textefe.Text = CStr(efe)
F3_2.Textecs.Text = CStr(ecs)
' step 7 -----
es = (efe + ebi) * ((d - C1) / (df - C1))
F3_2.Textes.Text = CStr(es)
' step 8 -----

```

```

fy = CDec(F3_2.Textfy.Text)
fs = Esm * es
If fs > fy Then
    fs = fy
End If
ffe = Ef * efe
F3_2.Textfs.Text = CStr(fs)
F3_2.Textffe.Text = CStr(ffe)
' step 9 -----

ecp)
ecp = 1.7 * fc / Ec
B1 = ((4 * ecp - ecs) / (6 * ecp - 2 * ecs))
Alpha = (3 * ecp * ecs - ecs * ecs) / (3 * B1 * ecp *

C2 = (Ass * fs + Af * ffe) / (Alpha * fc * B1 * b)
F3_3.Textecp.Text = CStr(ecp)
F3_3.TextB1.Text = CStr(B1)
F3_3.TextAlpha.Text = CStr(Alpha)
F3_3.TextC2.Text = CStr(C2)
' step 10 -----
F3_3.TextBox1.Text = F3_2.TextC1.Text
F3_3.TextBox2.Text = F3_3.TextC2.Text
C1s = C1
C2s = C2
10: If (C1s / C2s) > 1.00001 Then
    C1s = C1s - 0.1
    ' step 10-6-1 -----
    efe = 0.003 * ((df - C1s) / C1s) - ebi
    If efe > efd Then
        efe = efd
    End If
    ecs = (efe + ebi) * (C1s / (df - C1s))

    ' step 10-7-1 -----
    es = (efe + ebi) * ((d - C1s) / (df - C1s))

    ' step 10-8-1 -----

    fs = Esm * es
    If fs > fy Then
        fs = fy
    End If
    ffe = Ef * efe
    ' step 10-9-1 -----
    ecp = 1.7 * fc / Ec
    B1 = ((4 * ecp - ecs) / (6 * ecp - 2 * ecs))
    Alpha = (3 * ecp * ecs - ecs * ecs) / (3 * B1 * ecp *

ecp)
    C2s = (Ass * fs + Af * ffe) / (Alpha * fc * B1 * b)
    GoTo 10
End If

20: If (C1s / C2s) < 0.99999 Then
    C1s = C1s + 0.1

```

```

' step 10-6-2 -----
efe = 0.003 * ((df - C1s) / C1s) - ebi
If efe > efd Then
    efe = efd
End If
ecs = (efe + ebi) * (C1s / (df - C1s))

' step 10-7-2 -----
es = (efe + ebi) * ((d - C1s) / (df - C1s))

' step 10-8-2 -----

fs = Esm * es
If fs > fy Then
    fs = fy
End If
ffe = Ef * efe
' step 10-9-2 -----
ecp = 1.7 * fc / Ec
B1 = ((4 * ecp - ecs) / (6 * ecp - 2 * ecs))
Alphal = (3 * ecp * ecs - ecs * ecs) / (3 * B1 * ecp *
ecp)

C2s = (Ass * fs + Af * ffe) / (Alphal * fc * B1 * b)
GoTo 20
End If
C = C1s
F3_3.TextC.Text = CStr(C)
F3_3.Textes2.Text = CStr(es)
F3_3.Textfs2.Text = CStr(fs)
F3_3.TextB12.Text = CStr(B1)
F3_3.TextAlphal2.Text = CStr(Alphal)
F3_3.Textffd2.Text = CStr(ffe)
' step 11 -----
Mns = Ass * fs * (d - ((B1 * C) / 2))
Mnf = Af * ffe * (df - ((B1 * C) / 2))
F3_3.TextMns.Text = CStr(Mns)
F3_3.TextMnf.Text = CStr(Mnf)
' step 12 -----

esy = fy / Esm
If es >= 0.005 Then
    PHI = CDec(F3_3.TextPHI.Text)
ElseIf es > esy And es < 0.005 Then
    PHI = 0.65 + (0.25 * (es - esy)) / (0.005 - esy)
ElseIf es <= esy Then
    PHI = 0.65
End If

PSI = CDec(F3_3.TextPSI.Text)
Mu = CDec(F3_3.TextMu.Text)
PHIMN = PHI * (Mns + PSI * Mnf)
F3_3.TextPHIMN.Text = CStr(PHIMN)
' step 13 -----

```

```

Ms = CDec(Me.TextMs.Text)
Rhos = Ass / (b * d)
Rhof = Af / (b * d)
Ks = ((Rhos * (Esm / Ec) + Rhof * (Ef / Ec)) ^ 2 + 2 *
(Rhos * (Esm / Ec) + Rhof * (Ef / Ec) * (df / d)) - (Rhos * (Esm / Ec)
+ Rhof * (Ef / Ec))) ^ 0.5
fss = ((Ms + ebi * Af * Ef * (df - (Ks * d / 3))) * (d -
Ks * d) * Esm) / (Ass * Esm * (d - (Ks * d / 3)) * (d - Ks * d) + Af *
Ef * (df - (Ks * d / 3)) * (df - (Ks * d)))
Me.TextRhos.Text = CStr(Rhos)
Me.TextRhof.Text = CStr(Rhof)
Me.TextKs.Text = CStr(Ks)
Me.Textfss.Text = CStr(fss)

' step 14 -----
fss = fss * (Ef / Esm) * (df - Ks * d) / (d - Ks * d) -
ebi * Ef
Me.Textfss.Text = CStr(fss)
' step check -----
If F3.RadioB3.Checked Then
    fch = 0.2 * ffu
ElseIf F3.RadioB2.Checked Then
    fch = 0.3 * ffu
Else
    fch = 0.55 * ffu
End If
chm = 0
chs = 0
chc = 0
If PHIMN >= Mu Then
    Me.TextChm.Text = " OK "
    Me.TextChm.ForeColor = Color.Green
    chm = 1
Else
    Me.TextChm.Text = " No check "
    Me.TextChm.ForeColor = Color.Red
    chm = 2
End If
If fss <= 0.8 * fy Then
    Me.TextChs.Text = " OK "
    Me.TextChs.ForeColor = Color.Green
    chs = 1
Else
    Me.TextChs.Text = " No check "
    Me.TextChs.ForeColor = Color.Red
    chs = 2
End If
If ffs <= fch Then
    Me.TextChc.Text = " OK "
    chc = 1
    Me.TextChc.ForeColor = Color.Green
Else
    Me.TextChc.Text = " No check "
    Me.TextChc.ForeColor = Color.Red

```

```

        chc = 2
    End If
    ' Results check -----
    Me.Textns.Text = CStr(n)
    If chm = 1 And chs = 1 And chc = 1 Then
        Me.TextR.Text = " OK "
        Me.TextR.ForeColor = Color.Green
    Else
        Me.TextR.Text = " No check "
        Me.TextR.ForeColor = Color.Red
    End If

    ' enable -----

    For Each Atx In Me.Panel2.Controls

        If TypeOf Atx Is TextBox Then

            Atx.Enabled = True

        End If
    Next

    For Each Atx In Me.Panel3.Controls

        If TypeOf Atx Is TextBox Then

            Atx.Enabled = True

        End If
    Next

    For Each Atx In Me.Panel4.Controls

        If TypeOf Atx Is TextBox Then

            Atx.Enabled = True
        End If
    Next

    For Each Atx In Me.Panel5.Controls

        If TypeOf Atx Is TextBox Then

            Atx.Enabled = True

        End If

        Textns.Enabled = False

    Next

    ' error -----
Catch

```

```

        MessageBox.Show("Please enter valid values.", "Entry
error")
    End Try

End Sub

Private Sub TextRhos_TextChanged(ByVal sender As System.Object,
ByVal e As System.EventArgs) Handles TextRhos.TextChanged

End Sub

Private Sub Textffs_TextChanged(ByVal sender As System.Object,
ByVal e As System.EventArgs) Handles Textffs.TextChanged

End Sub

Private Sub TextBox53_TextChanged(ByVal sender As System.Object,
ByVal e As System.EventArgs) Handles TextR.TextChanged

End Sub

Private Sub Label15_Click(ByVal sender As System.Object, ByVal e
As System.EventArgs) Handles Label15.Click

End Sub

Private Sub TextChs_TextChanged(ByVal sender As System.Object,
ByVal e As System.EventArgs) Handles TextChs.TextChanged

End Sub

Private Sub B4_Click(ByVal sender As System.Object, ByVal e As
System.EventArgs) Handles B4.Click
    Dim n As Decimal
    Try
        n = CDec(Me.Textns.Text)
        n = n + 1
        Me.Textns.Text = CStr(n)
        F3.Textn.Text = CStr(n)
    Catch
        MessageBox.Show("Please check your entries.", "Entry
error")
    End Try

End Sub

Private Sub btnClear_Click(ByVal sender As System.Object, ByVal e
As System.EventArgs) Handles btnClear.Click
    Dim Atx As Control
    Dim B As DialogResult = MessageBox.Show("This option will
clear all data!", "Please Notice:", MessageBoxButtons.OKCancel)
    If B = DialogResult.OK Then

```

```

        For Each Atx In Me.Panel2.Controls
            If TypeOf Atx Is TextBox Then
                Atx.Text = Nothing
            End If
        Next

        For Each Atx In Me.Panel3.Controls
            If TypeOf Atx Is TextBox Then
                Atx.Text = Nothing
            End If
        Next

        For Each Atx In Me.Panel4.Controls
            If TypeOf Atx Is TextBox Then
                Atx.Text = Nothing
            End If
        Next

        For Each Atx In Me.Panel5.Controls
            If TypeOf Atx Is TextBox Then
                Atx.Text = Nothing
            End If
        Next
    End If
End Sub
End Class
Imports System.IO

Public Class F4

    Private Sub Panell_Paint(ByVal sender As System.Object, ByVal e As
System.Windows.Fs.PaintEventArgs) Handles Panell.Paint

        End Sub

    Private Sub Textwf_TextChanged(ByVal sender As System.Object,
ByVal e As System.EventArgs) Handles Texth1.TextChanged

        End Sub

```



```

Private Sub Label15_Click(ByVal sender As System.Object, ByVal e
As System.EventArgs) Handles Label15.Click

End Sub

Private Sub TextBox16_TextChanged(ByVal sender As System.Object,
ByVal e As System.EventArgs) Handles Textnp.TextChanged

End Sub

Private Sub B1_Click(ByVal sender As System.Object, ByVal e As
System.EventArgs) Handles B1.Click

Try
    B1.Cursor = Cursors.WaitCursor
    Dim h1, b1, fc1, as1, es1, fy1, dd1, df1, wf1, n1, tf1,
ffu1, elfu1, m(30), d(30), elash, esh, fr, epl(30), dm(30), ecu As
Decimal
    Dim h12, b12, fc12, as12, es12, fy12, dd12, df12, wf12,
n12, tf12, ffu12, elfu12, tfs, efl, Mmax, MM(30), mc, PHI, Mmax1 As
Decimal
    Dim i, np, npm, k As Integer
    Const dir As String = "C:\Practical Engineering
Software\FRP Strength Estimator\"
    Const path As String = dir & "estlaa.dat"
    Dim textout As New StreamWriter(New FileStream(path,
FileMode.Create, FileAccess.Write))

    h12 = CDec(Texth1.Text)
    b12 = CDec(Textb1.Text)
    fc12 = CDec(Textfc1.Text)
    ecu = 0.003
    as12 = CDec(Textas1.Text)
    es12 = CDec(Textes1.Text)
    fy12 = CDec(Textfy1.Text)
    dd12 = CDec(Textddl.Text)
    df12 = CDec(Textdf1.Text)
    wf12 = CDec(Textwf1.Text)
    n12 = CDec(Textn1.Text)
    tf12 = CDec(Texttf1.Text)
    ffu12 = CDec(Textfful.Text)
    elfu12 = CDec(Texteful.Text)
    'units are changed from (N, mm) to (kips , in) inside the
program for the input file
    h1 = h12 * 0.0393701
    h1 = FatNumber(h1, 2)
    b1 = b12 * 0.0393701
    b1 = FatNumber(b1, 2)
    fc1 = fc12 * 0.1450377
    fc1 = FatNumber(fc1, 2)
    as1 = as12 * 0.00155
    as1 = FatNumber(as1, 3)
    es1 = es12 * 0.1450377
    es1 = FatNumber(es1)

```

```

fy1 = fy12 * 0.1450377
fy1 = FatNumber(fy1)
ddl = ddl2 * 0.0393701
ddl = FatNumber(ddl, 2)
df1 = df12 * 0.0393701
df1 = FatNumber(df1, 2)
wf1 = wf12 * 0.0393701
wf1 = FatNumber(wf1, 2)
n1 = n12 * 1
n1 = FatNumber(n1)
tf1 = tf12 * 0.0393701
tf1 = FatNumber(tf1, 4)
fful = fful2 * 0.1450377
fful = FatNumber(fful)
elful = elful2 * 0.1450377
elful = FatNumber(elful)
np = CDec(Textnp.Text)
'   npm = CDec(Textnpm.Text)
npm = 20
textout.Write(npm & " ")
textout.WriteLine(0.05)
textout.Write(h1 & " ")
textout.WriteLine(b1)
textout.Write(l & " ")
textout.Write(es1 & " ")
textout.Write(fy1 & " ")
elash = es1 * 0.069
elash = FatNumber(elash)
esh = 0.015
textout.Write(elash & " ")
textout.WriteLine(esh)
textout.Write(ddl & " ")
textout.WriteLine(as1)
textout.Write(fc1 & " ")
textout.Write(0.002 & " ")
textout.Write(ecu & " ")
fr = (-7.5 * Math.Sqrt(fc1 * 1000)) / 1000
fr = FatNumber(fr, 2)
textout.Write(fr & " ")
textout.WriteLine(0.94)
textout.Write(df1 & " ")
textout.Write(wf1 & " ")
tfs = n1 * tf1
textout.Write(tfs & " ")
textout.Write(elful & " ")
textout.WriteLine(fful)
textout.Close()
Const path1 As String = dir & "estlapm.dat"
Dim textout1 As New StreamWriter(New FileStream(path1,
FileMode.Create, FileAccess.Write))
m(1) = CDec(Textm1.Text)
m(2) = CDec(Textm2.Text)
m(3) = CDec(Textm3.Text)
m(4) = CDec(Textm4.Text)

```

```

m(5) = CDec(Textm5.Text)
m(6) = CDec(Textm6.Text)
m(7) = CDec(Textm7.Text)
m(8) = CDec(Textm8.Text)
m(9) = CDec(Textm9.Text)
m(10) = CDec(Textm10.Text)
m(11) = CDec(Textm11.Text)
m(12) = CDec(Textm12.Text)
m(13) = CDec(Textm13.Text)
m(14) = CDec(Textm14.Text)
m(15) = CDec(Textm15.Text)
m(16) = CDec(Textm16.Text)
m(17) = CDec(Textm17.Text)
m(18) = CDec(Textm18.Text)
m(19) = CDec(Textm19.Text)
m(20) = CDec(Textm20.Text)
d(1) = CDec(Textd1.Text)
d(2) = CDec(Textd2.Text)
d(3) = CDec(Textd3.Text)
d(4) = CDec(Textd4.Text)
d(5) = CDec(Textd5.Text)
d(6) = CDec(Textd6.Text)
d(7) = CDec(Textd7.Text)
d(8) = CDec(Textd8.Text)
d(9) = CDec(Textd9.Text)
d(10) = CDec(Textd10.Text)
d(11) = CDec(Textd11.Text)
d(12) = CDec(Textd12.Text)
d(13) = CDec(Textd13.Text)
d(14) = CDec(Textd14.Text)
d(15) = CDec(Textd15.Text)
d(16) = CDec(Textd16.Text)
d(17) = CDec(Textd17.Text)
d(18) = CDec(Textd18.Text)
d(19) = CDec(Textd19.Text)
d(20) = CDec(Textd20.Text)
For i = 1 To np
    dm(i) = d(i)
Next

'Add chart Moment-distance
F4_1.Chart1.Series(0).ChartType =
DataVisualization.Charting.SeriesChartType.Line
F4_1.Chart1.Series(0).BorderWidth = 2
F4_1.Chart1.ChartAreas(0).AxisX.Minimum = dm(1)
F4_1.Chart1.ChartAreas(0).AxisX.Maximum = dm(np)
F4_1.Chart1.ChartAreas(0).RecalculateAxesScale()
For i = 1 To np
    F4_1.Chart1.Series("Series1").Points.AddXY(dm(i),
m(i))
Next
'end of chart 1

textout1.WriteLine(np)

```

```

PHI = CDec(TextPHI.Text)
For i = 1 To np
    d(i) = d(i) * 0.0393701
    d(i) = FatNumber(d(i))
    m(i) = (m(i) * 0.000008850745454036) / PHI
    m(i) = FatNumber(m(i))
    textout1.Write(d(i) & " ")
    textout1.WriteLine(m(i))
Next
textout1.Close()

Shell("C:\Practical Engineering Software\FRP Strength
Estimator\est1.exe", , True, -1)
Mmax = 0
Const path3 As String = dir & "estlout2.dat"
Dim textin3 As New StreamReader(New FileStream(path3,
FileMode.Open, FileAccess.Read))
For i = 1 To npm + 1
    'For i = 1 To npm + 1
    Dim row As String = textin3.ReadLine
    Dim column() As String = row.Split(CChar("/"))
    MM(i) = CDec(column(1))
    If Mmax < MM(i) Then
        Mmax = MM(i)
    End If
Next
textin3.Close()
Mmax = Mmax * 112984.828917
Mmax1 = PHI * Mmax
Mmax1 = FatNumber(Mmax1)
Textmmax.Text = CStr(Mmax1)
Textmmax.ForeColor = Color.Red
k = 0

For i = 1 To np
    mc = m(i) * 112984.828917
    If Mmax < mc Then
        k = 1
    End If
Next

If k = 1 Then
    MessageBox.Show("Applied bending moment exceeds moment
capacity of the section!", "Please Notice:")
    B1.Cursor = Cursors.Default
    Exit Sub
End If

Const path2 As String = dir & "estlapmout3.dat"
Dim textin As New StreamReader(New FileStream(path2,
FileMode.Open, FileAccess.Read))
For i = 1 To np
    Dim row As String = textin.ReadLine

```

```

        Dim column() As String = row.Split(CChar("/"))
        epl(i) = CDec(column(4))
    Next
    textin.Close()
    efl = 0.083 * Math.Sqrt(fc1 / (n1 * tf1 * elful))

    'Add chart FRP-strain
    F4_1.Chart2.Series(0).ChartType =
DataVisualization.Charting.SeriesChartType.Line
    F4_1.Chart2.Series(0).BorderWidth = 2
    F4_1.Chart2.ChartAreas(0).AxisX.Minimum = dm(1)
    F4_1.Chart2.ChartAreas(0).AxisX.Maximum = dm(np)
    F4_1.Chart2.ChartAreas(0).RecalculateAxesScale()
    For i = 1 To np
        F4_1.Chart2.Series("FRP strain").Points.AddXY(dm(i),
epl(i))
    Next
    F4_1.Chart2.Series("Debonding limit").Points.AddXY(dm(i),
efl)
    F4_1.Chart2.Series("Debonding limit").Points.AddXY(dm(np),
efl)
    'end of chart 1

    F4_1.Textnp1.Text = Textnp.Text
    F4_1.Textefl.Text = CStr(efl)
    F4_1.TextBd1.Text = Textd1.Text
    F4_1.TextBd2.Text = Textd2.Text
    F4_1.TextBd3.Text = Textd3.Text
    F4_1.TextBd4.Text = Textd4.Text
    F4_1.TextBd5.Text = Textd5.Text
    F4_1.TextBd6.Text = Textd6.Text
    F4_1.TextBd7.Text = Textd7.Text
    F4_1.TextBd8.Text = Textd8.Text
    F4_1.TextBd9.Text = Textd9.Text
    F4_1.TextBd10.Text = Textd10.Text
    F4_1.TextBd11.Text = Textd11.Text
    F4_1.TextBd12.Text = Textd12.Text
    F4_1.TextBd13.Text = Textd13.Text
    F4_1.TextBd14.Text = Textd14.Text
    F4_1.TextBd15.Text = Textd15.Text
    F4_1.TextBd16.Text = Textd16.Text
    F4_1.TextBd17.Text = Textd17.Text
    F4_1.TextBd18.Text = Textd18.Text
    F4_1.TextBd19.Text = Textd19.Text
    F4_1.TextBd20.Text = Textd20.Text
    F4_1.Textst1.Text = CStr(epl(1))
    F4_1.Textst2.Text = CStr(epl(2))
    F4_1.Textst3.Text = CStr(epl(3))
    F4_1.Textst4.Text = CStr(epl(4))
    F4_1.Textst5.Text = CStr(epl(5))
    F4_1.Textst6.Text = CStr(epl(6))
    F4_1.Textst7.Text = CStr(epl(7))
    F4_1.Textst8.Text = CStr(epl(8))

```

```

F4_1.Textst9.Text = CStr(ep1(9))
F4_1.Textst10.Text = CStr(ep1(10))
F4_1.Textst11.Text = CStr(ep1(11))
F4_1.Textst12.Text = CStr(ep1(12))
F4_1.Textst13.Text = CStr(ep1(13))
F4_1.Textst14.Text = CStr(ep1(14))
F4_1.Textst15.Text = CStr(ep1(15))
F4_1.Textst16.Text = CStr(ep1(16))
F4_1.Textst17.Text = CStr(ep1(17))
F4_1.Textst18.Text = CStr(ep1(18))
F4_1.Textst19.Text = CStr(ep1(19))
F4_1.Textst20.Text = CStr(ep1(20))

If ep1(1) < efl Then
    F4_1.TextA1.Text = " No "
    F4_1.TextA1.ForeColor = Color.Green
Else
    F4_1.TextA1.Text = " Yes "
    F4_1.TextA1.ForeColor = Color.Red
End If

If ep1(2) < efl Then
    F4_1.TextA2.Text = " No "
    F4_1.TextA2.ForeColor = Color.Green
Else
    F4_1.TextA2.Text = " Yes "
    F4_1.TextA2.ForeColor = Color.Red
End If
If ep1(3) < efl Then
    F4_1.TextA3.Text = " No "
    F4_1.TextA3.ForeColor = Color.Green
Else
    F4_1.TextA3.Text = " Yes "
    F4_1.TextA3.ForeColor = Color.Red
End If
If ep1(4) < efl Then
    F4_1.TextA4.Text = " No "
    F4_1.TextA4.ForeColor = Color.Green
Else
    F4_1.TextA4.Text = " Yes "
    F4_1.TextA4.ForeColor = Color.Red
End If
If ep1(5) < efl Then
    F4_1.TextA5.Text = " No "
    F4_1.TextA5.ForeColor = Color.Green
Else
    F4_1.TextA5.Text = " Yes "
    F4_1.TextA5.ForeColor = Color.Red
End If
If ep1(6) < efl Then
    F4_1.TextA6.Text = " No "
    F4_1.TextA6.ForeColor = Color.Green
Else
    F4_1.TextA6.Text = " Yes "

```

```

        F4_1.TextA6.ForeColor = Color.Red
    End If
    If epl(7) < efl Then
        F4_1.TextA7.Text = " No "
        F4_1.TextA7.ForeColor = Color.Green
    Else
        F4_1.TextA7.Text = " Yes "
        F4_1.TextA7.ForeColor = Color.Red
    End If
    If epl(8) < efl Then
        F4_1.TextA8.Text = " No "
        F4_1.TextA8.ForeColor = Color.Green
    Else
        F4_1.TextA8.Text = " Yes "
        F4_1.TextA8.ForeColor = Color.Red
    End If
    If epl(9) < efl Then
        F4_1.TextA9.Text = " No "
        F4_1.TextA9.ForeColor = Color.Green
    Else
        F4_1.TextA9.Text = " Yes "
        F4_1.TextA9.ForeColor = Color.Red
    End If
    If epl(10) < efl Then
        F4_1.TextA10.Text = " No "
        F4_1.TextA10.ForeColor = Color.Green
    Else
        F4_1.TextA10.Text = " Yes "
        F4_1.TextA10.ForeColor = Color.Red
    End If
    If epl(11) < efl Then
        F4_1.TextA11.Text = " No "
        F4_1.TextA11.ForeColor = Color.Green
    Else
        F4_1.TextA11.Text = " Yes "
        F4_1.TextA11.ForeColor = Color.Red
    End If
    If epl(12) < efl Then
        F4_1.TextA12.Text = " No "
        F4_1.TextA12.ForeColor = Color.Green
    Else
        F4_1.TextA12.Text = " Yes "
        F4_1.TextA12.ForeColor = Color.Red
    End If
    If epl(13) < efl Then
        F4_1.TextA13.Text = " No "
        F4_1.TextA13.ForeColor = Color.Green
    Else
        F4_1.TextA13.Text = " Yes "
        F4_1.TextA13.ForeColor = Color.Red
    End If
    If epl(14) < efl Then
        F4_1.TextA14.Text = " No "
        F4_1.TextA14.ForeColor = Color.Green
    End If

```

```

Else
    F4_1.TextA14.Text = " Yes "
    F4_1.TextA14.ForeColor = Color.Red
End If
If epl(15) < efl Then
    F4_1.TextA15.Text = " No "
    F4_1.TextA15.ForeColor = Color.Green
Else
    F4_1.TextA15.Text = " Yes "
    F4_1.TextA15.ForeColor = Color.Red
End If
If epl(16) < efl Then
    F4_1.TextA16.Text = " No "
    F4_1.TextA16.ForeColor = Color.Green
Else
    F4_1.TextA16.Text = " Yes "
    F4_1.TextA16.ForeColor = Color.Red
End If
If epl(17) < efl Then
    F4_1.TextA17.Text = " No "
    F4_1.TextA17.ForeColor = Color.Green
Else
    F4_1.TextA17.Text = " Yes "
    F4_1.TextA17.ForeColor = Color.Red
End If
If epl(18) < efl Then
    F4_1.TextA18.Text = " No "
    F4_1.TextA18.ForeColor = Color.Green
Else
    F4_1.TextA18.Text = " Yes "
    F4_1.TextA18.ForeColor = Color.Red
End If
If epl(19) < efl Then
    F4_1.TextA19.Text = " No "
    F4_1.TextA19.ForeColor = Color.Green
Else
    F4_1.TextA19.Text = " Yes "
    F4_1.TextA19.ForeColor = Color.Red
End If
If epl(20) < efl Then
    F4_1.TextA20.Text = " No "
    F4_1.TextA20.ForeColor = Color.Green
Else
    F4_1.TextA20.Text = " Yes "
    F4_1.TextA20.ForeColor = Color.Red
End If

Me.Enabled = False
Threading.Thread.Sleep(500)
'My.Application.DoEvents()
F4_1.Show()
F4_1.Activate()
Bl.Cursor = Cursors.Default

```



```

        Catch
            MessageBox.Show("Please Check for the following: invalid
entries, file does not exist, or/and missing directory.", "Error")
            Bl.Cursor = Cursors.Default
        End Try

    End Sub

    Private Sub TextAs_TextChanged(ByVal sender As System.Object,
ByVal e As System.EventArgs) Handles Textas1.TextChanged

    End Sub

    Private Sub TextEsm_TextChanged(ByVal sender As System.Object,
ByVal e As System.EventArgs) Handles Textes1.TextChanged

    End Sub

    Private Sub Textfy_TextChanged(ByVal sender As System.Object,
ByVal e As System.EventArgs) Handles Textfy1.TextChanged

    End Sub

    Private Sub Textddl_TextChanged(ByVal sender As System.Object,
ByVal e As System.EventArgs)

    End Sub

    Private Sub Textml_TextChanged(ByVal sender As System.Object,
ByVal e As System.EventArgs) Handles Textml.TextChanged

    End Sub

    Private Sub Textdf1_TextChanged(ByVal sender As System.Object,
ByVal e As System.EventArgs) Handles Textdf1.TextChanged

    End Sub

    Private Sub btnClear_Click(ByVal sender As System.Object, ByVal e
As System.EventArgs) Handles btnClear.Click
        Dim Atx As Control
        Dim B As DialogResult = MessageBox.Show("This option will
clear all data!", "Please Notice:", MessageBoxButtons.OKCancel)
        If B = DialogResult.OK Then

            For Each Atx In Me.GroupBox1.Controls

                If TypeOf Atx Is TextBox Then

                    Atx.Text = Nothing

                End If
            Next
            For Each Atx In Me.GroupBox2.Controls

```

```

        If TypeOf Atx Is TextBox Then
            Atx.Text = Nothing
        End If
    Next
    For Each Atx In Me.GroupBox3.Controls
        If TypeOf Atx Is TextBox Then
            Atx.Text = Nothing
        End If
    Next
    For Each Atx In Me.Panel2.Controls
        If TypeOf Atx Is TextBox Then
            Atx.Text = "0"
        End If
    Next
    Textnp.Text = "0"
    Textmmax.Text = ""
    TextPHI.Text = ""
End If
End Sub

Private Sub B3_Click(ByVal sender As System.Object, ByVal e As
System.EventArgs)
    Dim B As DialogResult = MessageBox.Show("You will be
transferred to the homepage!", "Please Notice:", MessageBoxButtons.OKCancel)
    If B = DialogResult.OK Then
        F1.Show()
        Me.Hide()
        F4_1.Hide()
    End If
End Sub
Function FileExists(ByVal FileToTest As String) As Boolean
    FileExists = (Dir(FileToTest) <> "")
End Function

Private Sub F4_Load(ByVal sender As System.Object, ByVal e As
System.EventArgs) Handles MyBase.Load

End Sub

Private Sub Textmmax_TextChanged(ByVal sender As System.Object,
ByVal e As System.EventArgs) Handles Textmmax.TextChanged

End Sub

```

```

        Private Sub Label8_Click(ByVal sender As System.Object, ByVal e As
System.EventArgs) Handles Label8.Click

            End Sub
        End Class
    
```

---

```

Imports System.Windows.Fs.DataVisualization.Charting

Public Class F4_1

    Private Sub frmProgramma_FClosing(ByVal sender As Object, ByVal e
As System.Windows.Fs.FClosingEventArgs) Handles Me.FClosing
        If e.CloseReason Then
            F4.Enabled = True
            F4.Bl.Cursor = Cursors.Default
        End If
    End Sub

End Class
    
```

---

```

Public NotInheritable Class SplashScreen2

    Private Sub SplashScreen2_Load(ByVal sender As Object, ByVal e
As System.EventArgs) Handles Me.Load

        If My.Application.Info.Title <> "" Then
            ApplicationTitle.Text = My.Application.Info.Title
        Else
            ApplicationTitle.Text =
System.IO.Path.GetFileNameWithoutExtension(My.Application.Info.Assembly
Name)
        End If

        Version.Text = System.String.Fat(Version.Text,
My.Application.Info.Version.Major, My.Application.Info.Version.Minor)

        Copyright.Text = My.Application.Info.Copyright
    End Sub

    Private Sub DetailsLayoutPanel_Paint(ByVal sender As
System.Object, ByVal e As System.Windows.Fs.PaintEventArgs) Handles
DetailsLayoutPanel.Paint

        End Sub
    End Class
    
```

---

## REFERENCES

- AASHTO, 2012. *Guide Specifications for Design of Bonded FRP Systems for Repair and Strengthening of Concrete Bridge Elements* 1st Edition.
- Abdel Baky H.M., 2008. *Nonlinear micromechanics-based finite element analysis of the interfacial behavior of FRP-strengthened reinforced concrete beams*. Quebec, Canada: University of Shearbrooke.
- Abdel Baky, H., Ebead, U. A., and Neale, K.W., 2012. *Nonlinear micromechanics-based bond–slip model for FRP/concrete interfaces*. *Engineering Structures*, 39, pp.11–23.
- ACI Committee 440, 2017. *Guide for the Design and Construction of Externally Bonded FRP Systems for Strengthening Concrete Structures (ACI 440.2R-17)*. Farmington Hills, MI: American Concrete Institute.
- AFGC, 2011. *Reparation et Renforcement des Structures en Beton au Moyen des Materiaux Composites*, The French Association of Civil Engineers.
- ASM International, 2002. *Atlas of stress-strain curves*. Materials Park, OH: ASM International.
- Bathon, L., and Bletz-Mühldorfer, O., 2014. *Fatigue performance of single span wood-concrete-composite bridges*. In: *Materials and Joints in Timber Structures*, Netherlands, pp.493-497.
- Bathon, L., Bletz, O. and Bahmer, R., 2006. *Long term performance of continuous wood-concrete composite systems*. In: *Proc. of the 9th World Conference on Timber Engineering*.
- Bedon, C., and Fragiacomio, M., 2017. *Three-Dimensional Modelling of Notched Connections for Timber–Concrete Composite Beams*. *Structural Engineering International*, 27(2), pp.184-196.
- Bizindavyi, L., and Neale, K.W.K., 1999. *Transfer Lengths and bond strengths for composites bonded to concrete*. *Journal of composites for construction*, 3, pp.153-160.
- Breña, S. F., and McGuirk, G., 2013. *Advances on the Behavior Characterization of FRP-Anchored Carbon Fiber-Reinforced Polymer (CFRP) Sheets Used to Strengthen Concrete Elements*. *International Journal of Concrete Structures and Materials*, 7(1), pp.3-16.
- Breña, S. F., Bramblett, R. M., and Benouaich M. A., Wood S. L., Kreger M. E., 2001. *Research Report 1776-1, Use of Carbon Fiber Reinforced Polymer Composites to Increase the Flexural Capacity of Reinforced Concrete Beams*. Center for Transportation Research, the University of Texas at Austin.
- Brena, S. F., Bramblett, R. M., Wood, S. L., and Kreger, M. E., 2003. *Increasing flexural capacity of reinforced concrete beams using carbon fiber-reinforced polymer composites*. *Structural Journal*, 100(1), pp. 36-46.

Camanho, P.P., and Dávila, C.G., 2002. *NASA Technical Memorandum: Mixed-mode decohesion finite elements for the simulation of delamination in composite materials*. NASA/TM-2002–211737, pp.1–37.

Camata, G., Spacone, E., and Zarnic, R., 2007. *Experimental and nonlinear finite element studies of RC beams strengthened with FRP plates*. *Composites Part B: Engineering*, 38(2), pp.277–288.

Ceccotti, A., 2002. *Composite concrete-timber structures*. *Progress in Structural Engineering and Materials*, 4(3), pp.264-275.

Chajes, M.J., Januszka, T.F., Mertz, D.R., Thomson, T.A., and Finch, W.W., 1995. *Shear strengthening of reinforced concrete beams using externally applied composite fabrics*. *Structural Journal*, 92(3), pp.295-303

Chen, J.F., Yang, Z.J., and Holt, G.D., 2001. *FRP or steel plate-to-concrete bonded joints: Effect of test methods on experimental bond strength*. *Steel and Composite Structures*, 1(2), pp.231–244.

Clouston P., Bathon LA, and Schreyer A., 2005. *Shear and Bending Performance of a Novel Wood – Concrete Composite System*. *J Struct Eng*, 131(9), pp.1404-1412.

Clouston, P., and Schreyer, A., 2008. *Design and use of wood–concrete composites*, *Practice Periodical on Structural Design and Construction*, 13(4), pp.167-174.

Clouston, P., and Schreyer, A., 2016. *UMass Design Building: A Catalyst for Regional Change*. World Conference of Timber Engineering, Vienna, Austria, August 22-26. IMWS and ITI, Vienna University of Technology.

CNR-DT 200., 2013. *Guide for the Design and Construction of Externally Bonded FRP Systems for strengthening Existing Structures*. Italian Advisory Committee on Technical Recommendations for Constructions, Rome, Italy.

Cornetti, P., and Carpinteri, A., 2011. *Modelling the FRP-concrete delamination by means of an exponential softening law*. *Engineering Structures*, 33(6), pp.1988–2001.

Czaderski, C., Soudki, K., and Motavalli, M., 2010. *Front and side view image correlation measurements on FRP to concrete pull-off bond tests*. *Journal of composites for construction*, pp.451–463.

Dai, J., Ueda, T., and Sato, Y., 2005. *Development of the Nonlinear Bond Stress–Slip Model of Fiber Reinforced Plastics Sheet–Concrete Interfaces with a Simple Method*. *Journal of Composites for Construction*, 9(1), pp.52–62.

Deutsches Institut für Bautechnik e. V. DIBT, *Allgemeine bauaufsichtliche Zulassung. Holz-Beton-Verbundsystem mit eingelebten HBV-Schubverbindem*. DIBT Z-9.1-557, Berlin in German.

Dias, A., Skinner, J., Crews, K., and Tannert, T., 2016. *Timber-concrete-composites increasing the use of timber in construction*. *European Journal of Wood and Wood Products*, 74(3), pp.443-451.

*fib* technical report bulletin 14., 2001. *Externally bonded FRP reinforcement for RC structures*. The International Federation for Structural Concrete, Département Génie Civil, Switzerland.

Fragiacomo, M., 2006. *Long-term behavior of timber–concrete composite beams*. II: Numerical analysis and simplified evaluation.” *Journal of structural engineering*, 132(1), pp.23-33.

Gao, Y.F., and Bower, A.F., 2004. *A simple technique for avoiding convergence problems in finite element simulations of crack nucleation and growth on cohesive interfaces*. *Modelling and Simulation in Materials Science and Engineering*, 12(3), pp.453–463.

Garden, H.N., Quantrill, R.J., Hollaway, L.C., Thorne, A.M. and Parke, G.A.R., 1998. *An experimental study of the anchorage length of carbon fibre composite plates used to strengthen reinforced concrete beams*. *Construction and Building Materials*, 12(4), pp.203-219.

Guadagnini, M., Pilakoutas, K., and Waldron, P., 2006. *Shear Resistance of FRP RC Beams: Experimental Study*. *Journal of Composites for Construction*, 10(6), pp.464–473.

Gutkowski, R., Brown, K., Shigidi, A., and Natterer, J., 2008. *Laboratory tests of composite wood–concrete beams*. *Construction and Building Materials*, 22(6), pp.1059-1066.

Hahn, H.T., and Williams, G.J., 1984. *Compression failure mechanisms in unidirectional composites-NASA Technical Memorandum*. Nasa Technical Memorandum 85834.

Hashin, Z., 1980. *Failure Criteria for Unidirectional Fibre Composites*. *J. Appl. Mech.* 47(2): 329-334.

Hashin, Z., and Rotem, A., 1973a. *A Fatigue Failure Criterion for Fiber Reinforced Materials*. *Journal of Composite Materials*, 7(4), pp.448–464.

Hashin, Z., and Rotem, A., 1973b. *Failure Criteria for Unidirectional Fiber Composites*. *Journal of Composite Materials*, 7, pp.448–464.

Hillerborg, A., Modéer, M., and Petersson, P. E., 1976. *Analysis of crack formation and crack growth in concrete by means of fracture mechanics and finite elements*. *Cement and Concrete Research*, 6, pp.773–781.

IBM Corp. Released 2017. *IBM SPSS Statistics for Windows*. Version 25.0.: IBM Corp.

ISIS Canada Design Manuals, 2007. *Strengthening Reinforced Concrete Structures with Externally-Bonded Fiber-Reinforced Polymers*, Winnipeg, Manitoba: ISIS.

JSCE., 2001. *Recommendations for Upgrading of Concrete Structures with Use of Continuous Fiber Sheets*. Japan Society of Civil Engineering.

Lee, J. and Fenves, G.L., 1998. *Plastic-Damage Model for Cyclic Loading of Concrete Structures*. Journal of Engineering Mechanics, 124, pp.892–900.

Liu, Y., Zwingmann, B. and Schlaich, M., 2014. *Nonlinear Progressive Damage Analysis of Notched or Bolted Fibre-Reinforced Polymer (FRP) Laminates Based on a Three-Dimensional Strain Failure Criterion*. Polymers, 6(Cdm), pp.949–976.

Loo, K., Foster, S., and Smith, S., 2012. *Fatigue Behavior of Carbon Fiber-Reinforced Polymer-Repaired Corroded Reinforced Concrete Beams*. ACI Structural Journal, 109, pp.795–804.

Lu, X.Z., Teng, J.G., Ye, L.P., and Jiang, J.J., 2005. *Bond–slip models for FRP sheets/plates bonded to concrete*. Engineering structures, 27(6), pp.920-937.

Lu, X.Z., Ye, L.P., Teng, J.G., and Jiang, J.J., 2005. *Meso-scale finite element model for FRP sheets/plates bonded to concrete*. Engineering structures, 27(4), pp.564-575.

Lubliner, J., Oliver, J., Oller, S., and Onate, E., 1989. *A plastic-damage model for concrete*. International Journal of solids and structures, 25(3), pp.299-326.

Martinelli, E., Czaderski, C., and Motavalli, M., 2011. *Modeling in-plane and out-of-plane displacement fields in pull-off tests on FRP strips*. Engineering Structures, 33(12), pp.3715-3725.

Matouš, K., and Maniatty, A.M., 2004. *Finite element formulation for modelling large deformations in elasto-viscoplastic polycrystals*. International Journal for Numerical Methods in Engineering, 60(14), pp.2313–2333.

Matzenmiller, A., Lubliner, J., and Taylor, R.L., 1995. *A constitutive model for anisotropic damage in fiber-composites*. Mechanics of Materials, 20, pp.125–152.

Mazzotti, C., Savoia, M. and Ferracuti, B., 2008. *An experimental study on delamination of FRP plates bonded to concrete*. Construction and Building Materials, 22, pp.1409–1421.

Mcguirk, G.N., 2011. *Development of Anchorage System for Frp Strengthening*. University of Massachusetts Amherst.

McKnight, J. 2017. *Leers Weinzapfel completes America's first cross-laminated timber academic building*. Retrieved from: <https://www.dezeen.com/2017/04/28/leers-weinzapfel-completes-first-cross-laminated-timber-clt-academic-building-university-massachusetts-amherst>

Minh, N.D., Khuan, C.T., and Kiat, C.H., 2001. *Brittle Failure and Bond Development Length of CFRP-Concrete Beams*. Journal of Composites for Construction, 5(1), pp.12–17.

Miotto, J. L., and Dias, A. A., 2012. *Evaluation of perforated steel plates as connection in glulam–concrete composite structures*. Construction and Building Materials, 28(1), pp.216-223.

National Design Specification® (NDS®) for Wood Construction – 2015

Neale, K.W., Ebead, U.A., Baky, H.A., Elsayed, W.E., and Godat, A., 2006. *Analysis of the load-deformation behaviour and debonding for FRP-strengthened concrete structures*. Advances in Structural Engineering, 9(6), pp.751-763.

Nguyen, D. M., Chan, T. K., and Cheong, H. K., 2001., *Brittle failure and bond development length of CFRP-concrete beams*. J. of Compos Constr. 5 (1): 12-17.

Niemitz, C.W., James, R., and Breña, S.F., 2010. *Experimental Behavior of Carbon Fiber-Reinforced Polymer (CFRP) Sheets Attached to Concrete Surfaces Using CFRP Anchors*. Journal of Composites for Construction, 14(2), pp.185-194.

Obaidat, Y. T., Heyden, S., and Dahlblom, O., 2013. *Evaluation of parameters of bond action between FRP and concrete*. Journal of Composites for construction, 17(5), pp.626-635.

Oliver, C. D., Nassar, N. T., Lippke, B. R., and McCarter, J. B., 2014. *Carbon, fossil fuel, and biodiversity mitigation with wood and forests*. Journal of Sustainable Forestry, 33(3), pp.248-275.

Orton, S. L., Jirsa, J. O., and Bayrak., O., 2008. *Design Considerations of Carbon Fiber Anchors*. J Compos Constr. 12 (6):608-616.

Rafsanjani, A., and Bertoldi, K., 2017. *Buckling-Induced Kirigami*. Physical Review Letters, 118(8), 084301.

Riks, E., 1979. *An incremental approach to the solution of snapping and buckling problems*. International Journal of Solids and Structures, 15(7), pp.529-551.

Sebastian, W.W.M., 2001. *Significance of midspan debonding failure in FRP-plated concrete beams*. Journal of Structural Engineering, 127, pp.792-798.

Simulia ABAQUS software and documentation 6.13., 2014.

Smith, S. T., 2009. *Frp Anchors: Recent Advances in Research and Understanding*. Asia-Pacific Conference on FRP in Structures, pp.35-44.

Smith, S. T., 2011. *Strengthening of Concrete, Metallic, and Timber Construction Materials with FRP Composites*. In The 5th International Conference on FRP Composites in Civil Engineering (CICE 2010). pp. 13-19.

Smith, S. T., S. Hu, Kim, S. J., and Seracino., R., 2011. "FRP-Strengthened RC Slabs Anchored with FRP Anchors." Engineering Structures 33 (4): 1075-1087.

Tannert, T., Endacott, B., Brunner, M., and Vallée, T., 2017. *Long-term performance of adhesively bonded timber-concrete composites*. International Journal of Adhesion and Adhesives, 72, pp.51-61.

Technical Dossier HBV-Systems, 2014. *Load Bearing Constructions using Wood-Concrete-Composite Technique with glued-in HBV® - Shear Connectors*. TiComTec GmbH.

Ten Thijsse, R. H. W., Akkerman, R., and Huétink, J., 2007. *Large deformation simulation of anisotropic material using an updated Lagrangian finite element method*. Computer Methods in Applied Mechanics and Engineering, 196(33-34),



pp.3141–3150.

Teng, J. G., Chen, G. M., Chen, J. F., Rosenboom, O. A., and Lam. L., 2009. *Behavior of RC beams shear strengthened with bonded or unbonded FRP wraps*. Journal of composites for construction, 13 (5), pp.394-404.

Teng, J. G., Lu, X. Z., Ye, L. P., and Jiang., J. J., 2004. *Recent Research on Intermediate Crack Induced Debonding in FRP Strengthened Beams*. In the 4th International Conference on Advanced Composite Materials for Bridges and Structures. Canada.

Teng, J. G., Smith, S. T., Yao, J., and Chen., J. F., 2003. *Intermediate Crack Induced Debonding in RC Beams and Slabs*. Construction and Building Materials, 17 (6-7), 447-462.

Tomblin, John, Waruna Seneviratne, Paulo Escobar, and Yap Yoon-Khian, 2002. *Shear stress-strain data for structural adhesives*. No. DOT/FAA/AR-02/97. Wichita State Univ KS Dept Of Aeronautical Engineering.

Ueda, T., Sato, Y., and Asano, Y., 1999. *Experimental Study on Bond Strength of Continuous Carbon Fiber Sheet*. In 4th int. sym. on fiber reinforced polymer reinforcement for reinforced concrete structures. pp. 407–16.

Wang, J., 2006. *Cohesive zone model of intermediate crack-induced debonding of FRP-plated concrete beam*. International Journal of Solids and Structures, 43(21), pp.6630–6648.

Wu, Y., and Jiang, C., 2013. *Quantification of bond-slip relationship for externally bonded FRP-to-concrete joints*. Journal of Composites for Construction, pp.673–686.

Wu, Y., Zhou, Z., Yang, Q., and Chen, W., 2010. *On shear bond strength of FRP-concrete structures*. Engineering Structures, 32(3), pp.897-905.

Yao, J., Teng, J.G., and Chen, J.F., 2005. *Experimental study on FRP-to-concrete bonded joints*. Composites Part B: Engineering, 36(2), pp.99-113.

Yeoh, D., Fragiacomio, M., De Franceschi, M., and Buchanan, A. H., 2010a. *Experimental tests of notched and plate connectors for LVL-concrete composite beams*. Journal of Structural Engineering, 137(2), 261-269.

Yeoh, D., Fragiacomio, M., De Franceschi, M., and Heng Boon, K., 2010b. *State of the art on timber-concrete composite structures: Literature review*. Journal of structural engineering, 137(10), pp.1085-1095.

Yuan, H., Teng, J.G., Seracino, R., Wu, Z.S., and Yao, J., 2004. *Full-range behavior of FRP-to-concrete bonded joints*. Engineering structures, 26(5), pp.553-565.

Zhang, H. W., and S. T. Smith. 2012. *FRP-to-concrete joint assemblages anchored with multiple FRP anchors*. Composite Structures 94 (2), pp.403-414.

Zhang, H., Smith, S.T., Gravina, R.J., and Wang, Z., 2017. *Modelling of FRP-*

*concrete bonded interfaces containing FRP anchors.* Construction and Building Materials, 139, pp.394-402.